University of Nottingham
UK | CHINA | MALAYSIA

Department of Architecture and Built Environment

Faculty of Engineering

Energy Performance Study of A Self-cooled Membrane-based Liquid Desiccant Dehumidification System

Thesis by

Lingze Lin, BEng, MSc.

30th September 2023

Thesis submitted to the University of Nottingham
for the Degree of Doctor of Philosophy in Building Technology

Table of contents

Table of contents i

Abstract viii

Acknowledgements x

List of Figures xi

List of Table xviii

Nomenclature xix

Section 1: Introduction 1

1.1. Background 1

1.2. Aim and objectives 5

1.3. Thesis structure 7

Section 2: Literature Review 8

2.1. Introduction 8

2.2. Liquid desiccant dehumidifier 9

2.2.1. Adiabatic-type dehumidifier 9

2.2.2. Internally-cooled dehumidifier 12

2.2.3. Self-cooled dehumidifier 20

2.2.4. Membrane-based dehumidifier 23

2.2.5. Membrane-based internally-cooled dehumidifier 31

2.3. Liquid desiccant regenerator 35

2.3.1. Direct contact regenerator 35

2.3.2. Membrane-based regenerator 41

2.4. Completed liquid desiccant dehumidification system 45

2.5. Numerical modelling methods 51

2.5.1. Simplified method 53

2.5.2. Effectiveness $\boldsymbol{NTU}$ ($\boldsymbol{\varepsilon - NTU}$) method 57

2.5.3. Finite difference method 62

2.6. Summary 71

Section 3: Numerical and experimental analysis of a self-cooled membrane-based liquid desiccant dehumidifier 76

3.1. Introduction 76

3.2. Numerical modelling 77

3.2.1. Model description and assumptions 77

3.2.2. Governing equations 80

3.2.3. Boundary conditions 90

3.2.4. Normalization of governing equations 91

3.2.5. Discretization of governing equations 94

3.2.6. Heat and mass transfer coefficient 95

3.2.7. Thermodynamic parameters of air and desiccant solution 96

3.2.8. Numerical solving scheme 101

3.2.9. Mesh independent test 104

3.3. Experiment set-up 105
3.3.1. Experimental system describe 105
3.3.2. Preparation of self-cooled desiccant solution 108
3.3.3. Data collection instrument 109
3.3.4. Uncertainty analysis 112
3.4. Performance evaluation 113
3.5. Model validation 114
3.6. Results and discussion 116
3.6.1. Equilibrium specific humidity of self-cooled desiccant solution ……116
3.6.2. Temperature and humidity field 120
3.6.3. Effect of process air conditions 124
3.6.3.1. Effect of process air temperature 124
3.6.3.2. Effect of process air humidity ratio 126
3.6.3.3. Effect of process air flow rate 129
3.6.4. Effect of solution properties 131
3.6.4.1. Effect of solution temperature 131
3.6.4.2. Effect of LiCl concentration 133
3.6.4.3. Effect of solution flow rate 136
3.6.5. Effect of circulated air conditions 138
3.6.5.1. Effect of circulated air temperature 138

3.6.5.2. Effect of circulated air flow rate 140

3.7. Summary 142

Section 4: Numerical and experimental analysis of a membrane-based liquid desiccant regenerator 145

4.1. Introduction 145

4.2. Numerical modelling 146

4.2.1. Model description and assumptions 146

4.2.2. Governing equations 147

4.2.3. Boundary conditions 150

4.2.4. Normalization of governing equations 150

4.2.5. Discretization of governing equations 151

4.2.6. Thermodynamic parameters of air and desiccant solution 151

4.2.7. Numerical solving scheme 153

4.2.8. Mesh independent test 156

4.3. Experiment set-up 157

4.4. Performance evaluation 157

4.5. Model validation 158

4.6. Results and discussion 160

4.6.1. Temperature and humidity field 160

4.6.2. Effect of air conditions 163

4.6.2.1. Effect of air temperature 163

4.6.2.2. Effect of air relative humidity 165

4.6.2.3. Effect of air flow rate 167

4.6.3. Effect of solution properties 169

4.6.3.1. Effect of solution temperature 169

4.6.3.2. Effect of LiCl concentration 171

4.6.3.3. Effect of solution flow rate 173

4.7. Summary 175

Section 5: Performance assessment of a complete self-cooled membrane-based liquid desiccant dehumidification system 178

5.1. Introduction 178

5.2. 5.2 Numerical modelling 179

5.2.1. Model description and assumptions 179

5.2.2. 5.2.2 Dehumidifier and regenerator 181

5.2.2.1. Governing equations 181

5.2.2.2. Boundary conditions 182

5.2.2.3. Normalization of governing equations 183

5.2.2.4. Discretization of governing equations 184

5.2.3. Heat exchanger 185

5.2.4. Numerical solving scheme 186

5.3. Experimental set-up 188

5.4. Performance evaluation 191

5.4.1. Effectiveness of the complete system 191
5.4.2. Total cooling output 191
5.4.3. Coefficient of performance 192
5.5. Model validation 193
5.6. Results and discussion 195
5.6.1. Effect of evaporative coolant 195
5.6.2. Effect of dehumidifier air flow rate 199
5.6.3. Effect of regenerator air flow rate 203
5.6.4. Effect of solution flow rate 206
5.6.5. Effect of solution concentration 210
5.7. Summary 214
Section 6: Conclusion and future work 216
6.1. Main conclusion 216
6.2. Recommendation for future work 220
Reference list 223
Appendices 236
Appendix A: Normalization procedures for governing equations 236
Appendix B: Matlab code for air humidity and solution equilibrium humidity 241
Appendix C: Matlab code for the self-cooled membrane-based liquid desiccant dehumidifier 243

Appendix D: Matlab code for the membrane-based liquid desiccant regenerator 249

Appendix E: Matlab code for the complete self-cooled membrane-based liquid desiccant dehumidification system 254

Appendix F: Calculation of Re number 236

Abstract

The pandemic outbreak of COVID-19 has led to a significant impact on global human activity, economic and energy consumption. More researches have focused on novel technologies with higher energy efficiencies to provide comfort indoor environment. Among them, membrane-based liquid desiccant dehumidification system is regarded as an efficient method for air humidity control due to its feasibility without desiccant carry-over problem. Besides, self-cooled liquid desiccant is selected to improve the dehumidification performance.

The aim of this study is to develop a novel self-cooled membrane-based liquid desiccant dehumidification system by combining the membrane-based air-liquid contactors with self-cooled liquid desiccant solution. Numerical models for single dehumidifier, regenerator and the complete dehumidification system have been developed based on steady-state heat and mass transfer process using finite difference method. Moreover, experimental works have been conducted to validate the numerical results.

It is found that the addition of ethanol into desiccant solution can improve the moisture removal rate (MRR) and dehumidification effectiveness (ε_{deh}) of the dehumidifier up to 44.7% and 21.8%, respectively. However, the system regeneration ability is reduced compared to pure LiCl aqueous solution. From the complete dehumidification system perspective, the latent cooling output and COP can be increased by 19.57% and 21.98% respectively. The dehumidifier can operate under high effectiveness in different weather conditions, and air flow rate has the most significant influence on its performance. The dehumidification

performance benefits from lower inlet solution temperature and higher desiccant concentration. The increase gradient of dehumidifier performance hardly changes when mass flow rate ratio is higher than 1, and effects of the circulate air temperature and flow are negligible. Cooler and drier air can enhance reconcentration ability of the regenerator. The regeneration performance can be improved with higher inlet solution temperature and lower LiCl concentration, and a critical value of mass flow rate ratio m^* = 3 is obtained. For the complete system, the increase of dehumidifier air flow rate will reduce the dehumidification effectiveness but improve the total cooling output and COP, while the effect of regenerator air flow rate is less significant. The performance of the complete dehumidification system can be enhanced by increasing the solution concentration, and the highest COP reaches to 1.2676.

Acknowledgements

First and foremost, I wish to express my deepest gratitude to my supervisors, Dr. Zhu Jie and Dr. Guohui Gan, for their unwavering guidance, invaluable feedback, and steadfast mentorship throughout my PhD journey. Their wisdom and insights have been instrumental in shaping the course and outcomes of this research. I really looking forward to collaborating with them again.

I would also like to extend my appreciation to Marmont Laboratory for their technical assistance. Special mention goes to technicians Carson Cheng and Tony Gospel, whose expertise and hands-on help proved invaluable at critical stages of my research. To my colleagues and friends, Dr. Ke Qu, Mr. Yuhao Wang, Mr. Shaofan Wang, Mr. Yuhan Zhang, Dr. Xin Wang, Mr. Yingrui Li, Dr. Tianhong Zheng, Dr. Ziwei Chen and Dr. Hongyu Bai. Your camaraderie, feedback, and constant encouragement have enriched this journey immeasurably. The collaboration, insights, and moments of levity we shared have been a valuable source of both personal and academic growth.

I am immensely thankful to my dearest parents, Mr. Bin Lin and Mrs. Xinhong Zhang, for their unwavering love, support, and belief in my abilities. Their sacrifices and teaching have been the foundation upon which all my achievements stand.

Lastly, to my dearest girlfriend Ms. Man Luo, your love, patience, and understanding have been a beacon of light during the challenging times. Thank you for being my rock and for sharing this journey with me. You are the apple of my eye.

List of Figures

Figure 1-1. Hourly electricity demand changes for homes in Britain [12]..... 2

Figure 2-1 Celdek packing [40]..... 11

Figure 2-2 Celdek packing [40]..... 13

Figure 2-3 (a) Schematic diagram of plate absorber (b) Single piece of plate absorber [44]..... 14

Figure 2-4 Internally-cooled dehumidifier (a) Sold view (b) inner view [45] .. 15

Figure 2-5 Parallel plate internally-cooled dehumidifier with fins: (a) plan view (b) schematic diagram (c) detailed geometry [46]..... 15

Figure 2-6 Schematic of fin-coil type internally cooled dehumidifier: (a) photo and (b) schematic [47] 16

Figure 2-7 Internally-cooled packing tower dehumidifier [51]..... 18

Figure 2-8 Outside evaporative cooling dehumidifier [53] 19

Figure 2-9 Experimental setup of self-cooled dehumidifier (a) schematic, and (b) photo [60]..... 22

Figure 2-10 Structure of a parallel-plate membrane dehumidifier [62] 25

Figure 2-11 Prototype hollow fibre air-liquid contactor [70]..... 28

Figure 2-12 Structure of the counter flow hollow fibre membrane dehumidifier [71, 72]..... 29

Figure 2-13 Cross-flow hollow fibre contactor (a) schematic (b) photo [74] ... 30

Figure 2-14 The structure of a cross flow internally-cooled membrane-based liquid desiccant dehumidifier [76]..... 32

Figure 2-15 3-fluid internally-cooled membrane-based dehumidifier (a) schematic diagram (b) solution channel with cooling coil [77] 33

Figure 2-16 Schematic diagram of the IHPMC [78] 34
Figure 2-17 Experimental test rig of packed column regenerator [80] 36
Figure 2-18 Experimental test rig of the Celdek cross-flow regenerator [82]... 38
Figure 2-19 Solar thermal powered regenerator [86] 40
Figure 2-20 Experimental test rig of electrodialysis regenerator [87]..... 41
Figure 2-21 Schematic diagram of the membrane-based regenerator unit [90] 43
Figure 2-22 Laboratory rig of the membrane-based parallel-plate regenerator [92]..... 44
Figure 2-23 Schematic diagram of a close loop heat and mass recovery system [95]..... 46
Figure 2-24 Schematics of (A) air-liquid membrane-based exchanger (B) close loop membrane-based system [96] 47
Figure 2-25 Test rig of the complete dehumidification system [97] 48
Figure 2-26 Heat pump liquid desiccant dehumidification system [99]..... 50
Figure 2-27 Heat and mass transfer in counter-flow arrangement [123]..... 62
Figure 2-28 Solving scheme of finite difference method for dehumidifier [124] 64
Figure 2-29 2-D schematic of cross-flow computational domain [127]..... 65
Figure 2-30 Numerical model of internally-cooled dehumidifier [129]..... 67
Figure 2-31 Control element for internally-cooled dehumidifier [130] 67
Figure 2-32 Schematic of a counter-flow small-scale single panel LAMEE [131]..... 69
Figure 3-1 Structure of numerical modelling 77
Figure 3-2 The interrelationship between heat and mass transfer processes..... 79
Figure 3-3 2D flow direction of the dehumidifier 81

Figure 3-4 Control volume for heat transfer of process air in air channel 83
Figure 3-5 Control volume for mass transfer of water in air channel 84
Figure 3-6 Control volume for energy transfer of desiccant solution 85
Figure 3-7 Control volume for mass transfer of water in solution channel..... 86
Figure 3-8 Control volume for mass transfer of ethanol in desiccant solution . 87
Figure 3-9 Control volume for heat transfer of circulated air in solution channel 88
Figure 3-10 Control volume for mass transfer of ethanol in circulated air 89
Figure 3-11 Flow chart of the solving procedure 103
Figure 3-12 Schematic diagram of the experiment rigs..... 106
Figure 3-13 Experimental rigs of the self-cooled membrane-based dehumidification system. 107
Figure 3-14 Comparison of moisture removal rate between numerical and experimental data..... 115
Figure 3-15 Comparison of dehumidification effectiveness between numerical and experimental data 116
Figure 3-16 Specific humidity of desiccant solution at (a) $Ceth = 0\%$; (b) $Ceth = 5\%$; and (c) $Ceth = 10\%$ 118
Figure 3-17 (a) Air temperature field; (b) Air specific humidity field; (c) Solution temperature field; (d) LiCl concentration field; (e) Ethanol concentration field; (f) Circulated air temperature field. 123
Figure 3-18 LiCl concentration field with 0% ethanol..... 124
Figure 3-19 (a) Effect of inlet air temperature on moisture removal rate. (b) Effect of inlet air temperature on dehumidification effectiveness..... 126

Figure 3-20 (a) Effect of inlet air relative humidity on moisture removal rate. (b) Effect of inlet air relative humidity on dehumidification effectiveness..... 128
Figure 3-21 (a) Effect of process air flow rate on moisture removal rate. (b) Effect of inlet air flow rate on dehumidification effectiveness 130
Figure 3-22 (a) Effect of inlet solution temperature on moisture removal rate. (b) Effect of inlet solution temperature on dehumidification effectiveness 133
Figure 3-23 (a) Effect of inlet LiCl concentration on moisture removal rate. (b) Effect of inlet LiCl concentration on dehumidification effectiveness. 135
Figure 3-24 (a) Effect of solution mass flow rate on moisture removal rate. (b) Effect of solution mass flow rate on dehumidification effectiveness..... 138
Figure 3-25 (a) Effect of inlet circulated air temperature on moisture removal rate. (b) Effect of inlet circulated air temperature on dehumidification effectiveness. 139
Figure 3-26 (a) Effect of circulated air flow rate on moisture removal rate. (b) Effect of circulated air flow rate on dehumidification effectiveness..... 141
Figure 4-1 Structure of numerical modelling of regenerator..... 146
Figure 4-2 2D flow direction of the regenerator..... 148
Figure 4-3 Specific humidity of desiccant solution for regenerator at (a) $Ceth = 0\%$; (b) $Ceth = 5\%$; and (c) $Ceth = 10\%$..... 153
Figure 4-4 Flow chart of the solving procedure for regenerator 155
Figure 4-5 Comparison of moisture removal addition between numerical and experimental data..... 159
Figure 4-6 Comparison of regeneration effectiveness between numerical and experimental data..... 160

Figure 4-7(a) Air temperature field; (b) Air specific humidity field; (c) Solution temperature field; (d) LiCl concentration field. 162
Figure 4-8 (a) Effect of inlet air temperature on moisture addition rate. (b) Effect of inlet air temperature on regeneration effectiveness 164
Figure 4-9 (a) Effect of inlet air relative humidity on moisture addition rate. (b) Effect of inlet air relative humidity on regeneration effectiveness 166
Figure 4-10 (a) Effect of inlet air flow rate on moisture addition rate. (b) Effect of inlet air flow rate on regeneration effectiveness 168
Figure 4-11 (a) Effect of solution temperature on moisture addition rate. (b) Effect of solution temperature on regeneration effectiveness 170
Figure 4-12 (a) Effect of LiCl concentration on moisture addition rate. (b) Effect of LiCl concentration on regeneration effectiveness 172
Figure 4-13 (a) Effect of solution flow rate on moisture addition rate. (b) Effect of solution flow rate on regeneration effectiveness 175
Figure 5-1 Modelling concept of the complete dehumidification system 180
Figure 5-2 Flow chart of the solving procedure for the complete dehumidification system 188
Figure 5-3 Schematic diagram of the dehumidification system 189
Figure 5-4 Comparison of sensible effectiveness between numerical and experimental data 194
Figure 5-5 Comparison of latent effectiveness between numerical and experimental data 195
Figure 5-6 System effectiveness variations under different ethanol concentrations 197

Figure 5-7 Total cooling output variations under different ethanol concentrations 198
Figure 5-8 COP variations under different ethanol concentrations 198
Figure 5-9 Sensible effectiveness variations under different dehumidifier air flow rates 201
Figure 5-10 Latent effectiveness variations under different dehumidifier air flow rates 201
Figure 5-11 Total cooling output variations under different dehumidifier air flow rates 202
Figure 5-12 COP variations under different dehumidifier air flow rates 202
Figure 5-13 Sensible effectiveness variations under different regenerator air flow rates 204
Figure 5-14 Latent effectiveness variations under different regenerator air flow rates 205
Figure 5-15 Total cooling output variations under different regenerator air flow rates 205
Figure 5-16 COP variations under different regenerator air flow rates 206
Figure 5-17 Sensible effectiveness variations under different solution flow rates 208
Figure 5-18 Latent effectiveness variations under different solution flow rates 209
Figure 5-19 Total cooling output variations under different solution flow rates 209
Figure 5-20 COP variations under different solution flow rates 210

Figure 5-21 Sensible effectiveness variations under different solution concentrations 212
Figure 5-22 Latent effectiveness variations under different solution concentrations 212
Figure 5-23 Total cooling output variations under different solution concentrations 213
Figure 5-24 COP variations under different solution flow rates 213

List of Table

Table 3-1. Binary parameters for the mixed desiccant solution 100

Table 3-2. Thermal properties of air and desiccant solution 101

Table 3-3. Mesh independent test 104

Table 3-4. Membrane physical properties of the dehumidifier 107

Table 3-5. Specifications of the chemical compound 108

Table 3-6. Specifications of experimental instruments 111

Table 3-7. Specifications of measurement instruments with associated accuracies 112

Table 4-1. Mesh independent test for regenerator 156

Table 5-1 Physical properties of dehumidifier and regenerator 190

Nomenclature

a	activity
A	surface area (m^2)
C	concentration (%); constant number
COP	coefficient of performance
c_p	specific heat capacity (J/kgK)
Cr	thermal capacity (W/K)
D	mass diffusivity (m^2/s)
d_h	hydraulic diameter of the fluid channel (m)
f_s	activity coefficient of solvent
h	specific enthalpy (J/kg)
h^*	operating factor
H	height of the membrane unit(m)
k	thermal conductivity (W/mK)
L	length of the dehumidifier (m)
LC	short range contribution
m	mass flow rate (kg/s); constant number
MAR	moisture addition rate (kg/s)
MFR	moisture flux rate (kg/s)
MRR	moisture removal rate (kg/s)
$NTRL$	non-random two-liquid method
NTU	number of heat transfer units
NTU_m	number of mass transfer units

Nu	Nusselt number
P	pressure (Pa)
PDH	long range contribution
Pr	Prandtl number
Q	energy power (kW)
r	condensation heat (J/kg)
Re	Reynolds number
RH	relative humidity (%)
Sc	Schmidt number
Sh	Sherwood number
SMR	Simple mixing rule
T	temperature (℃)
U	the overall heat transfer coefficient (W/m^2K)
u	velocity (m/s)
U_m	the overall mass transfer coefficient (kg/m^2s)
v	kinematic viscosity (m^2/s)
W	humidity ratio (kg/kg); power consumption (kW); width (m)
x	mole concentration
X	solution mass fraction

Greek letters

α	convective heat transfer coefficient (W/m^2K)
δ	thickness (m)
ε	effectiveness

ρ	density (kg/m^3)
τ	binary parameter
η	efficiency

Subscripts

air	air flow
atm	atmosphere
c	cold fluid
ca	circulated air
d	duct
deh	dehumidification
$desi$	desiccant
eth	ethanol
exp	experimental
fan	fan
$float$	float state
h	hot fluid
in	inlet
lat	latent
max	maximum
mem	membrane
$moisture$	moisture of mass transfer
num	numerical
out	outlet

$pump$	pump
reg	regeneration
s	solvent
sen	sensible
sol	solution flow
tot	total
w	water

Superscripts

$*$	dimensionless

Section 1: Introduction

Section 1 provides a brief introduction of this thesis and is structured in the following sections: Section 1.1 presents the background of this research; Section 1.2 shows the aim and objectives of this research; Section 1.3 is the summary of the thesis structure.

1.1. Background

The outbreak of COVID-19 has caused significant impact on human society all over the world. Until 2023, there are over 651 million confirmed cases for COVID-19 and the death number over 6.66 million [1]. The WHO (World Health Organization) has found that the domestic violence increased by 50% due to the mental issue caused by the long-term quarantine [2]. Further problems such as medical treatment [3], education [4], travelling [5], global GDP [6], unemployment [7] and energy [8] have also been reported. Among these influences, the energy consumption is considered to be one of the critical factors due to the quarantine policy during the pandemic. Based on the World Energy Outlook published by International Energy Agency [9], during the COVID-19 pandemic in 2020, the global coal demand has decreased by 7%, the electricity consumption has reduced by 2% and the total energy consumption went down by 6%. However, situations are different for building energy consumptions, especially residential buildings. Before the outbreak of COVID, around 38% to 42% of total UK energy demand was from building consumption [10]. For the US, the Department of Energy reported that buildings consumed 41% of total primary energy source, among these energy consumptions, 22% are for

residential buildings and 19% are for commercial buildings [11]. During the lockdown period, although the total electricity in the United Kingdom has decreased by 15%, the household electricity demand has increased by 17%, based on the data collected from 2000 smart meters [12]. The energy demand of residential buildings in Ireland has reported to be 11% to 20% higher than before [13]. In California, the increase of residential electricity demand is around 8.9% to 12.4% during the pandemic [14]. The changes in hourly electricity demand for homes in Britain before and during the pandemic period have been presented in Fig. 1-1 [12]. As it can be seen, there has been a significant increase of electricity demand during daytime. Due to the lockdown policies, people's daily activities have been completely changed, such as working from home, attending school remotely or indoor isolation.

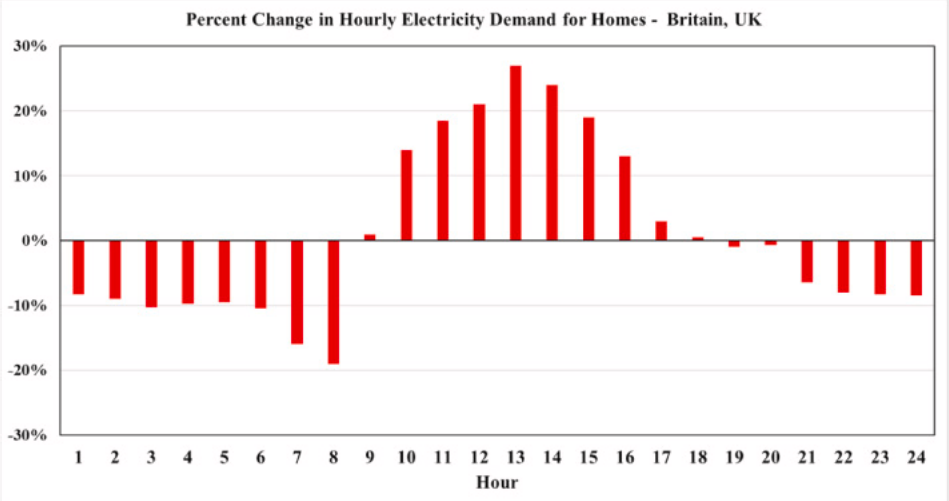

Figure 1-1. Hourly electricity demand changes for homes in Britain [12]

In 1902, the first modern electrical air conditioning system was developed by Willis H. Carrier in New York [15]. With the COVID-19 pandemic, the current design and operation guidelines are facing series challenges never met before. Inappropriate air conditioning or ventilation could lead to further infection to the

population in the enclosed environments, especially hospitals [16], due to the airborne transmission of COVID-19. On the contrary, suitable operation conditions for air conditioning system can reduce the spread of SARS-CoV-2, however, significant growth of energy consumption has been obtained. As a result, new guidelines on operation and management of HVAC system have been proposed by many countries around the world such as EU [17], USA [18], China [19], Japan [20] and Canada [21]. To sum up, these guidelines have emphasized the importance of increasing fresh air volume, adjusting operation conditions and developing novel technologies. The trade-off between indoor comfort and energy consumption have drawn more and more attentions by governments, scientists and researchers. The outbreak of COVID-19 should not just be considered as challenges, but also a good opportunity for the development of air conditioning system.

It is important for building service engineers to find balance between indoor thermal comfort and energy consumption. With the development of modern society, people spend more and more of their time within indoor environments [22]. Therefore, indoor thermal comfort, which significantly influences occupants' health, well-being and productivity, has become a critical issue. Temperature is the most important environmental factor influencing thermal comfort [23], while relative humidity within the range of 40%-70% is normally acceptable [24]. However, if indoor environment is operating under high humidity condition (over 70%), it is likely to suffer from the problem of mould, fungi, bacteria, viruses and dust mites, which can cause series damages on occupants' health and well-being such as infectious disease, allergic reactions and

mycotoxicosis especially for hot weather conditions [25]. To provide a better indoor environment, a maximum room air humidity not exceeding 60% during summer cooling season has been proposed by CIBSE Guide [26].

For traditional air humidity control approach, it is commonly to dehumidify the moisture air by using cooling coils to reduce the air temperature below its dew point. However, further energy for heating is required since the air temperature after dehumidification is too low for indoor thermal comfort. Moreover, it lead to the problems of mould and bacteria due to the condensation of water [27]. Such design concept for humidity control is only suitable for air dehumidification but not for humidification. As a result, alternative dehumidification techniques have been developed such as electrochemical dehumidification, solid dehumidification and liquid desiccant dehumidification [28]. Among them, liquid desiccant dehumidification has drawn more attentions due to the feasibility, effectively and no condensation problem. However, due to the corrosion problem of liquid desiccant solution such as calcium chloride, lithium bromide and lithium chloride aqueous solution, liquid desiccant dehumidification has not been widely used in practice until the end of the 20^{th} century [29].

With the development of corrosion resistance materials especially plastic in recent years, the liquid desiccant dehumidification has become more attractive due to the high efficiency in air humidity control by applying low grade energy sources, such as solar power, geothermal energy and industrial waste energy [30]. Although the relationship between COVID-19 and liquid desiccant dehumidification system has been reported, similar tests were conducted for the airborne SARS virus by the Chinese CDC Virus Disease Institute in 2004 [31].

Further studies have focused on whether the mixture of LiBr and LiCl solution can kill the SARS virus [32]. The results have shown that the mixed solution can chemically damage the SARS virus and destroy it particles. In the post-pandemic era, liquid desiccant dehumidification is highly likely to become a novel and promising technology with great potential to enhance indoor thermal comfort while reducing energy consumption of air conditioning systems. Current research trends of liquid desiccant dehumidification have focused on how to avoid the desiccant carry-over problem, optimize the design structure, adjust the operating conditions and improve the dehumidification performance [33]. Recent studies on liquid desiccant dehumidification technologies are focused on membrane-based internally-cooled dehumidifier since it can restrain the temperature rise during dehumidification process and prevent the carry-over problem at the same time. Although the latent heat caused by the condensation of moisture during the dehumidification process can be removed with the application of heat exchangers, adding cooling coils inside the membrane structure would make the dehumidifier structure complex and increase the maintenance cost. A novel working hypothesis for the self-cooled liquid desiccant solution combining with membrane-based dehumidifier has been proposed in this study.

1.2. Aim and objectives

The research aim of this thesis is to establish a novel dehumidification system with better performance of humidity control and lower energy consumption in hot and humid weather condition. Therefore, a self-cooled membrane-based liquid desiccant dehumidification system has been developed by using the

desiccant solution and evaporative coolant. The scopes of work include: design of the dehumidification system, numerical modelling, experimental test and performance evaluation under various operating conditions. To be more specific, individual unit such as dehumidifier and regenerator have been investigated thoughtfully as well as the whole dehumidification system. In order to achieve the research aim of this thesis, several objectives are listed:

1) Literature review on previous studies and researches related to liquid desiccant dehumidification technologies are conducted. The working principles of different types of dehumidification systems can be inspired for developing the heat and mass conservation equations and setting-up the experiment rigs. Research gaps in existing literatures of liquid desiccant dehumidification have to be identified.
2) Numerical and experimental analyses of the self-cooled membrane-based dehumidifier are carried out under different operating conditions and performance evaluation based on simulation and experimental results.
3) Numerical and experimental analyses of the membrane-based regenerator are achieved under different operating conditions and performance evaluation based on simulation and experimental results.
4) A complete self-cooled membrane-based dehumidification system is developed by combining the dehumidifier, regenerator and external heating and cooling medium, and investigating the system performance based on numerical and experimental results.
5) Conclusions and recommendations for future work are presented at end.

1.3. Thesis structure

This thesis is structured into six sections and five additional appendices to achieve the thesis aim and objectives,

Chapter 1 is the introduction to this thesis, by presenting a brief research background, research aim and objectives, and the thesis structure.

Chapter 2 presents a comprehensive literature review on current researches related to liquid desiccant dehumidification technologies. The research gaps between published literatures and current research are highlighted.

Chapter 3 displays the numerical and experimental studies of a novel self-cooled membrane-based liquid desiccant dehumidifier.

Chapter 4 shows the numerical and experimental studies of a membrane-based liquid desiccant regenerator.

Chapter 5 presents the numerical and experimental studies of a complete self-cooled membrane-based liquid desiccant dehumidification system, which includes a dehumidifier, a regenerator and external cold and hot water supply systems.

Chapter 6 concludes the main findings of this research and provides recommendations for future work.

Last but not least, the normalization methods for governing equations and Matlab scripts are presented in Appendices.

Section 2: Literature Review

2.1. Introduction

This section provides an extensive literature review of liquid desiccant dehumidification techniques. The main aim of this section is to present a comprehensive background and current progress of liquid desiccant dehumidification. More importantly, the research gap and suitable methodology for this research need to be identified based on published literatures. To achieve these purposes, a comprehensive review is conducted including the single unit of liquid desiccant dehumidifier and regenerator, the complete dehumidification system and the numerical modelling methods.

The structures of **Section 2** are: **Section 2.2** shows different types of dehumidifier including adiabatic-type, internally-cooled, self-cooled, membrane-based and membrane-based internally-cooled; **Section 2.3** presents different types of regenerator including direct contacted type and membrane-based; **Section 2.4** introduces the complete liquid desiccant dehumidification systems; **Section 2.5** presents different numerical modelling approaches including simplified method, effectiveness NTU method and finite difference method; **Section 2.6** summaries the main finding of the literature review and identify the research gap between previous studies and current research.

2.2. Liquid desiccant dehumidifier

2.2.1. Adiabatic-type dehumidifier

The adiabatic type dehumidifier is widely used in industrial and residential applications. The contacting area between air and liquid desiccant solution was relatively large by using simple geometric configurations, therefore, adiabatic dehumidifier can provide high efficiency of heat and mass transfer. Still, it had potential disadvantages by causing too much pressure drop on the dehumidification air while it passed through the packed beds. Current investigations of adiabatic dehumidifier were focused on refining the structure and adjusting operation conditions of the dehumidifier to improve the moisture removal performance.

For adiabatic type dehumidifier, the heat transfer only occurred between the process air and liquid desiccant, which means no additional cooling sources. Zurigat et al [34] conducted an experiment test of packed bed column dehumidifier by using triethylene glycol (TEG) under low packing density. Two different packing structures (wood and aluminium) were tested as control groups. A more accurate correlation was given in the paper compared with Chung correlation [35], which was shown to be over-predicted the effectiveness. The results have shown that the dehumidification rate can be improved by increasing inlet liquid desiccant concentration, liquid desiccant flow rate and air flow rate for both wood and aluminium packings. However, with the increasing of the process air temperature, the moisture removal rate can only be increased for aluminium packed bed. Babakhani and Soleymani [36] have developed an

advanced analytical solution of heat and mass transfer processes within an adiabatic packed bed liquid desiccant dehumidifier. Under several suitable assumptions, the correlation of dehumidification effectiveness and moisture removal rate were shown to have very good agreement with experiment data. The analytical results have presented that the desiccant concentration, liquid desiccant solution temperature, air-flow rate and relative humidity have significant influences on dehumidification performance while the liquid desiccant flow rate and the process air temperature did not have an obvious impact. Longo and Gasparella [37] presented experiment tests of a chemical dehumidification of air by a liquid desiccant regeneration in an absorption tower using random packing. The new liquid desiccant solution (H_2O, $KCOOH$) was compared with traditional hygroscopic solution (H_2O, $LiBr$) under typical operative condition of air conditioning system. A one-dimensional simulation result of the packed tower was compared with the experiment data to verify the accuracy of the result. The new liquid desiccant solution was suggested for air conditioning systems or drying process since it could provide consistent reduction in humidity level and with less corrosively. An advanced liquid desiccant cooling system has been designed by Pietruschka et al [38], which shifts the humidification and dehumidification process completely to the returning air and adding an efficient heat exchanger to cool the supply air in order to avoid hygienic problems. The testing results showed that the new system can provide 18.8℃ air temperature for the indoor environment under the summer design conditions of 32℃ and 40% relative humidity. The experiment results was also validated by the developed numerical models, good agreement was found between experiments and simulation. Zhang et al. [39] experimentally investigated the mass-transfer

process of a structured packing liquid desiccant dehumidifier using LiCl aqueous solution. The deviations between numerical model and experimental results were proved to be within ±20%. The testing dehumidifier were made by a 500mm long and 270mm wide transparent plastic rectangular parallelepiped, which was installed in a 250mm depth structured packing. The results presented that the mass transfer coefficient were improved from 4.0 to 8.5 g/m^2s by increasing the air velocities from 0.5 to 1.5 m/s. Gao et al. [40] established a cross-flow liquid desiccant dehumidifier using LiCl solution and Celdek structured packing which was shown in Fig. 2-1. Based on the experiment results, the moisture efficiency is mainly influenced by air flow rate and liquid desiccant flow rate, while the enthalpy efficiency is mainly affected by air flow, air temperature, air moisture content and solution flow. The efficiency of this adiabatic cross-flow liquid desiccant dehumidifier can be improved by increasing the thickness, width or height without higher pressure loss.

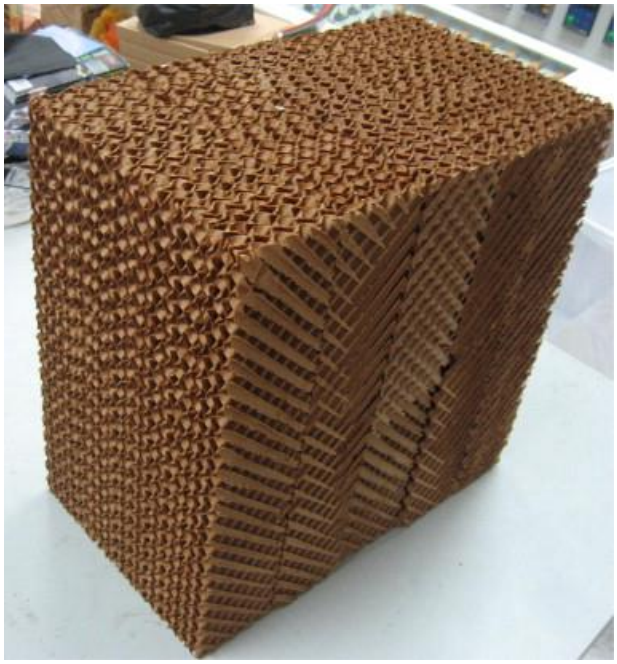

Figure 2-1 Celdek packing [40]

The previous studies of adiabatic liquid desiccant dehumidifiers have presented several methods for both experiment and modelling. The improvement of the dehumidifier performance was mainly focused on adjusting the operating conditions and structure optimizations. To sum up, the adiabatic type dehumidifier has been widely used in real applications, since it has high heat and mass transfer efficiency, simple structure and low maintenance cost [41]. However, the increase of the performance is limited since the desiccant temperature will be increased during the dehumidifier process which caused by the absorption of water vapour. To solve such problem, internally cooled liquid desiccant dehumidifier was applied and introduced in the following section.

2.2.2. Internally-cooled dehumidifier

As an adiabatic dehumidifier, the temperature of liquid desiccant solution continuously increased among its flow direction during the dehumidification process. The increase of desiccant temperature would have a negative impact on the potential of desiccant solution to absorb water vapour from the process air [42]. To ensure the dehumidifier can work under high efficiency for both temperature and humidity control, internally cooled type dehumidifier was conducted by installing cooling coil inside the dehumidifier.

A commonly used internally cooled type dehumidifier was shown in Fig. 2-2 [43], the cooling coil using cold water was installed inside the dehumidifier to remove the latent heat caused by water vapour absorption. Outside the dehumidifier, it was covered with insulation layer to avoid heat transfer from the environment. Inside, the process air and desiccant solution were in cross-flow arrangement,

which can be replaced by parallel or counter-flow structures. However, it is relatively difficult to install the cooling coil inside the dehumidifier, and more importantly, such dehumidifier type required high mass flow rate of the liquid desiccant to achieve better dehumidification performance.

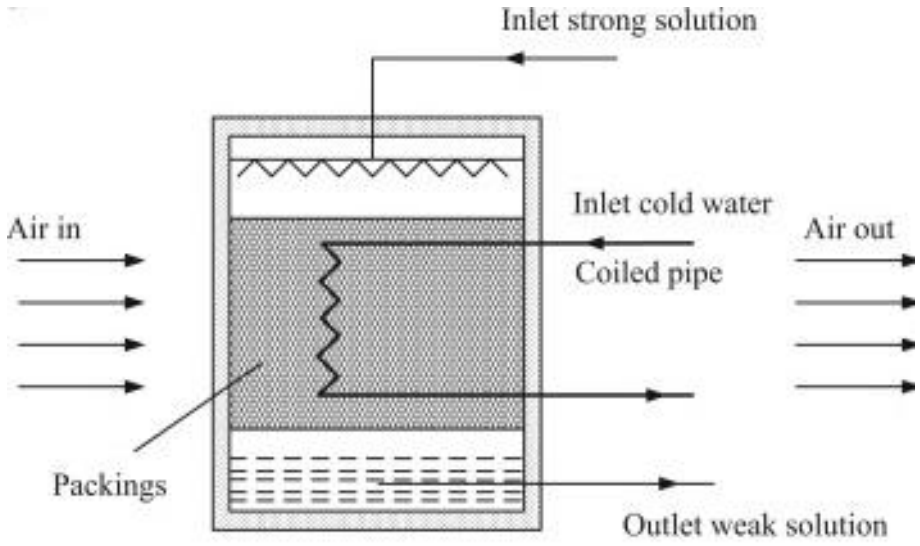

Figure 2-2 Celdek packing [40]

Another internally-cooled dehumidifier shown in Fig. 2-3 were investigated by Yoon et al. [44] through numerical study. Inside the dehumidifier, vertical plated were separated with equal distance. The strong desiccant solution flowed down at both sides of the plate and was cooled by cold water inside the plates. These parallel plates can be replaced by corrugated plates to increase the contact area between process air and desiccant solution, so that the performance of moisture removal rate can be improved. This type of internally cooled dehumidifier has been proved to be more promising since the desiccant solution was able to be cooled efficiently by the cold water in the neighbouring channel.

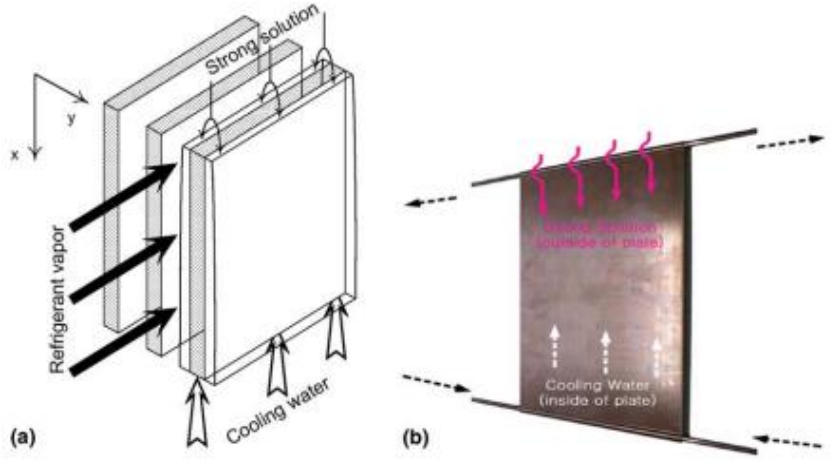

Figure 2-3 (a) Schematic diagram of plate absorber (b) Single piece of plate absorber [44]

Further numerical and experimental investigations of internally-cooled dehumidifier has been conducted by Kessling et al. [45], as illustrated in Fig. 2-4. The proposed dehumidifier was made of conductive plastic to avoid the corrosion problem caused by the desiccant solution (LiCl aqueous solution). A comprehensive parametric test has been conducted to achieve a higher dehumidification performance. Meanwhile, mass transfer coefficients were obtained from experimental works and they were used in numerical model by applying finite difference method.

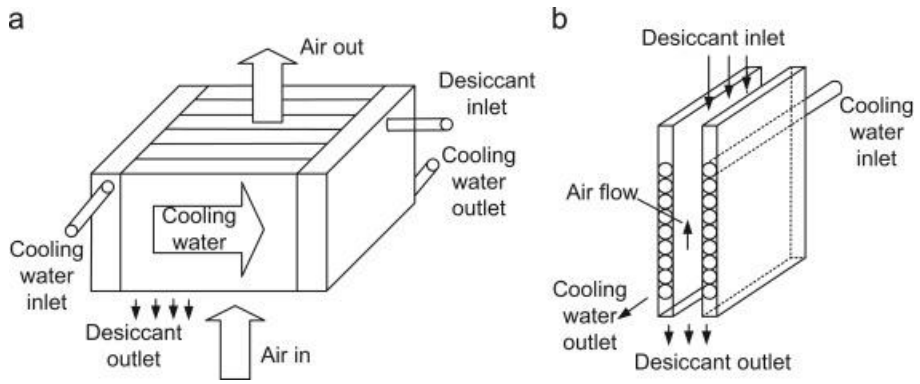

Figure 2-4 Internally-cooled dehumidifier (a) Sold view (b) inner view [45]

Yin et al. [46] developed an internally-cooled dehumidifier using parallel plate with fins. As presented in Fig. 2-5, fin coils made of stainless steel intersecting next to two neighbouring plates are proposed to increase the contact area between the desiccant solution and cooling water to enhance the heat transfer efficiency. The results have shown that the cooling efficiency increases with the decrease of inlet cold water temperature, thus the dehumidifier can operate under the condition with relatively low solution temperature and enhance the moisture removal ability.

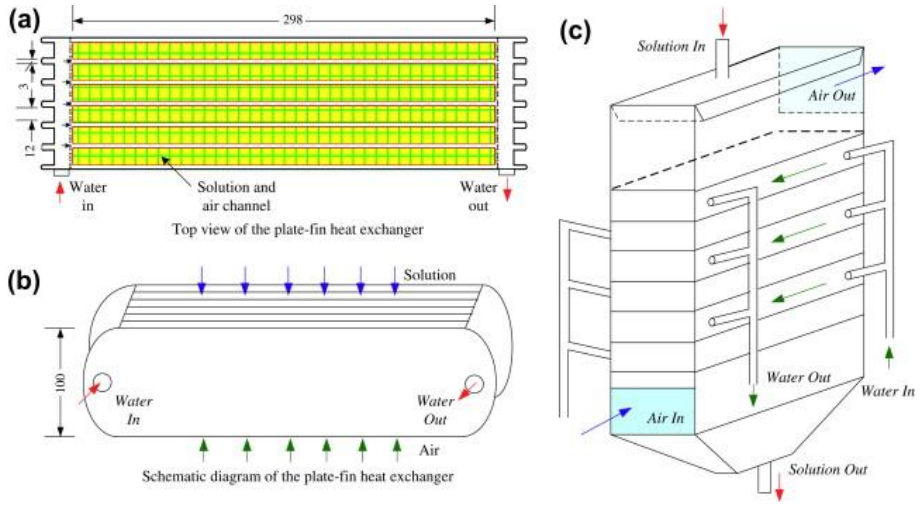

Figure 2-5 Parallel plate internally-cooled dehumidifier with fins: (a) plan view (b) schematic diagram (c) detailed geometry [46]

In Fig. 2-6 [47], an internally-cooled type dehumidifier which is called fin-coil dehumidifier has been presented. The cooling water flowed inside the cooling coil from the bottom to the top of the dehumidifier, and the process air was brought in direct contact with the liquid desiccant solution for cooling and dehumidification. Tubes with fins were installed inside the dehumidifier to increase the contact area between the process air and cooling coils. The cooling water flows into the bottom of the dehumidifier from a water separator, and then collected at the top of the unit. Both experimental and simulation investigation has been conducted. The results showed that the moisture removal rate can be improved by increasing the solution flow rate.

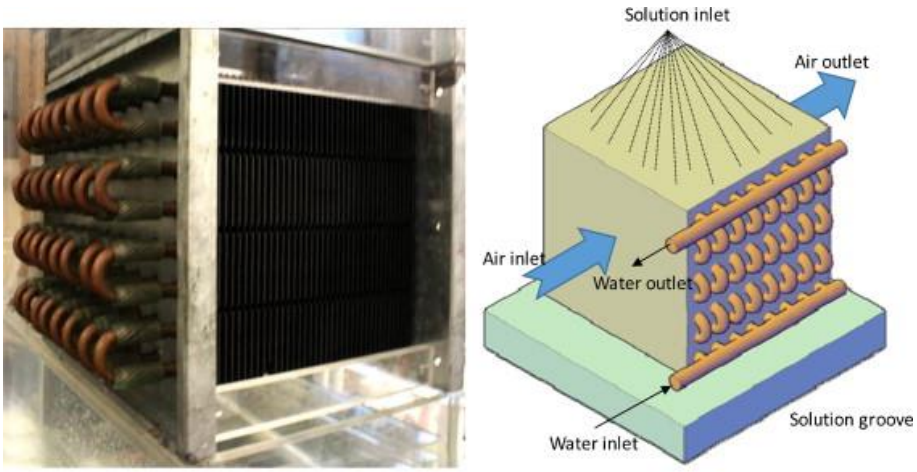

Figure 2-6 Schematic of fin-coil type internally cooled dehumidifier: (a) photo and (b) schematic [47]

Further studies on fin coil type internally-cooled dehumidifier have been conducted by many researchers. Chen et al. [48] experimentally investigated a plastic finned-tube dehumidifier, with emphasis on material thermal conductivity. For the heat exchanger proposed in this study, when the thermal conductivity

reaches a certain critical value (15 W/mK), the improvement of thermal conductivity became less significant to increase the dehumidification performance. Zhang et al. [49] proposed an internally-cooled exchanger with fin coils which is made of stainless steel to improve the contact area. A comprehensive parametric study was conducted experimentally by using LiBr as desiccant solution. The performance of the internally-cooled dehumidifier was evaluated by several performance indicators, such as moisture removal rate, dehumidification effectiveness and volume mass transfer coefficient. Giannetti et al. [50] characterized the wetting behaviour of desiccant solution films on the internally-cooled dehumidifier, and the results showed that the falling film wettability is critical for the fin-coil internally-cooled desiccant exchanger. A good agreement has been obtained between experimental and numerical results.

Another commonly used type of internally-cooled dehumidifier is the packed tower with cooling tubes. As presented in Fig. 2-7, an internally cooled packed-bed structured dehumidifier is developed by Bansal et al. [51]. This research presents the dehumidification performance of a novel packed tower structure with the provision for internally-cooled dehumidifier and compared to an adiabatic dehumidifier with identical structure. The proposed packing tower with rigid media pads is built up by cellulose paper. It is designed to be in cross-flow arrangement in order to simplify the structure and reduce the maintenance cost because it reduces the height of the tower and make it easy to be connected with the duct system. However, it tends to be less effectiveness for the heat and mass transfer since the cellulose packing has cooling tubes built inside the dehumidifier.

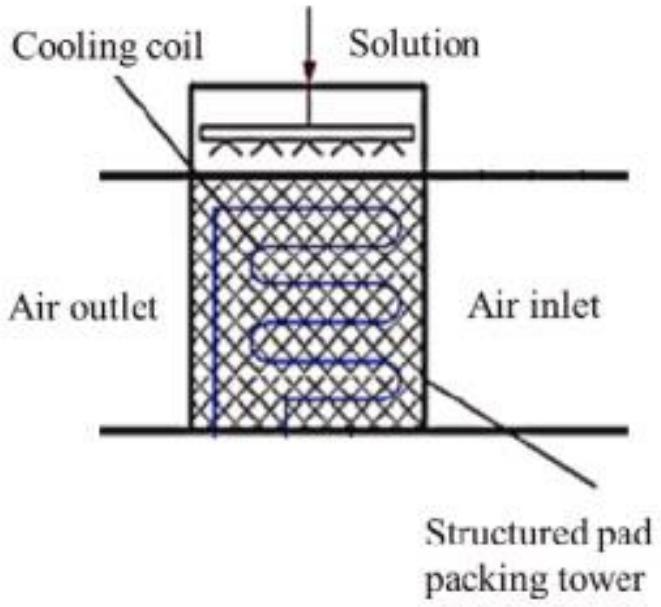

Figure 2-7 Internally-cooled packing tower dehumidifier [51]

Despite from the structure of the internally-cooled dehumidifier, cooling medium is another factor that draws significant interest from many researchers. The pre-mentioned studies are all using cooling water as the cooling medium to reduce the solution temperature. Evaporative air and refrigerant are also selected as the internal cooling medium. Saman and Alizadeh [52] developed a novel internally-cooled dehumidifier using evaporative air as cooling medium. Flat plate is used to separate the air and solution channels, where the process air can be chilled and dehumidified while the solution can be cooled. The hot and humid air is driven in one flow channel to meet the desiccant solution, while on the other side of the plate, evaporative air (normally return air from indoor environment) is in contact with cold water. Thus the latent heat released to the desiccant solution can be removed by the evaporative air. Cheng et al. [53] presented the experimental study and performance evaluation of a novel dehumidifier with outside evaporative cooling as shown in Fig. 2-8. Several operation conditions has been

tested to evaluate the effect on the performance, include the inlet air conditions, solution mass flow rate and concentration, spray water mass flow rate and its temperature. The experimental results have proved that the dehumidification performance can be improved by around 25% compared to the adiabatic dehumidifier.

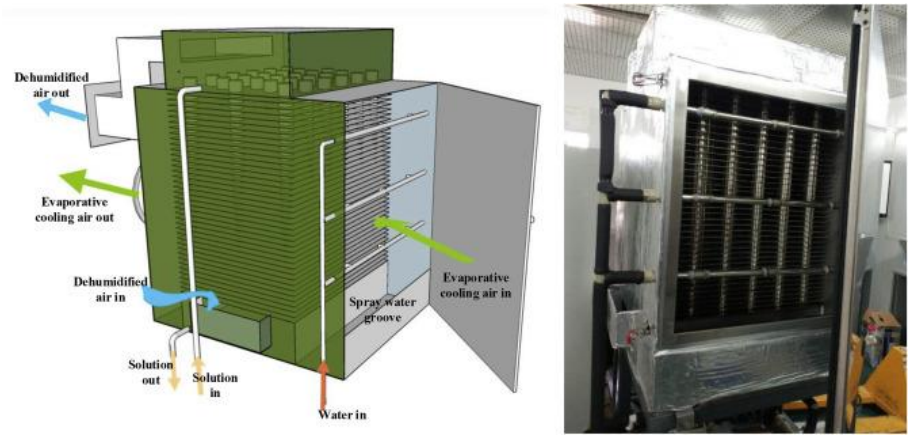

Figure 2-8 Outside evaporative cooling dehumidifier [53]

Yamaguchi et al. [54] developed a hybrid liquid desiccant air-dehumidification system and it is evaluated by experiments and simulations. During their study, lithium chloride is selected as desiccant solution while refrigerant R407C is used to restrain the temperature rise of desiccant solution. Based on the results, the dehumidification performance of 5.9 g/kg moisture removal rate can be achieved under the summer conditions of Tokyo, Japan. Liu et al. [55] developed a numerical model to investigate the performance of an internally-cooled dehumidifier using refrigerant in Matlab Simulink platform. Within the dehumidifier, the process air and desiccant solution are in direct contact with each other, while the desiccant solution is cooled by the refrigerant flow through tubes. The simulation results show that the dehumidification performance can be

enhanced by reducing the solution flow rate and increasing the solution heat exchanger efficiency.

The temperature rise of the desiccant solution during dehumidification process can be restrained by indirectly contacting cooling mediums such as cold water, air or refrigerant. The results have shown that the internally-cooled dehumidifiers provide better dehumidification performance compared to the adiabatic type [51, 56]. The internally cooled dehumidifiers provided promising improvement of liquid desiccant dehumidification systems. However, all of the internally-cooled type dehumidifiers suffered the problem of liquid desiccant droplets cross over. Thus, membrane-based modules were introduced in the following section.

2.2.3. Self-cooled dehumidifier

As mentioned before, the internally-cooled liquid desiccant dehumidifiers have several problems such as liquid droplets cross over, complex configurations and high maintenance costs. To solve these problems, a new method of liquid desiccant dehumidifiers was conducted in the past few years by adding phase change materials or evaporative coolant into the liquid desiccant solution. Thus, the desiccant solution was formed into 'self-cooled' liquid desiccant and the dehumidifier could work under low temperature conditions without using cooling coils, which lead to a better structure design.

Ren et al. [57] proposed a new phase change enhanced liquid desiccant by adding micro-encapsulated phase change materials (MPCMs) into lithium chloride (LiCl) solution. Critical properties of the new solution such as density, enthalpy-temperature relationship, thermal conductivity and vapour pressure were

evaluated by either experiment test or theoretical analyzation. The characterisations of the desiccant solution using different types of MPCMs were also investigated. The results indicated that the new solution has lower vapour pressure and higher thermal capacity compared with original desiccant solution (LiCl-water solution), therefore, it is convinced that the dehumidification performance can be improved by using MPCM enhanced liquid desiccant solutions in future works. Lu et al. [58] investigated the surface vapour pressure of a microencapsulated phase change materials solution under the temperature range of 293.2K – 353.2K for a typical dehumidification system. The experimental results represent that the surface vapour pressure can be reduced by adding MicroPCMs compared with pure LiCl desiccant solution. When mass concentration of LiCl and MicroPCMs reach 40% and 2% respectively, the vapour pressure drop can be up to 17%. It comes to a conclusion that the addition of phase change materials can enhance the dehumidification process, however, may have a negative impact on regeneration performance.

After assessing the thermal properties of the adding PCM into liquid desiccant solution, an experimental study has been conducted on the liquid desiccant dehumidification performance of microencapsulated phase change materials slurry [59]. The experimental results showed that with the addition of 2% MicroPCMs, the improvement of moisture removal rate and dehumidification effectiveness can be up to 24.0% and 23.1%, respectively. It has also found that even by considering the reduction of surface vapour pressure of the desiccant solution, the enhancement of dehumidification was about 50-60% due to the phased change endothermic impact of MicroPCMs. The idea of using self-cooled

liquid desiccant solution has been proved to have a positive influence on the dehumidification process.

Lun et al. [60] conducted an experimental analysis of a liquid desiccant dehumidifier with self-cooled liquid desiccant. Ethanol was added into lithium chloride solution as an evaporative coolant to suppress the increase of desiccant solution temperature. The experimental setup of his study was shown in Fig. 2-9, including dehumidifier, desiccant solution regenerator, ethanol recovery device, glycerol absorbing device and ethanol absorbing device. The self-cooled desiccant solution was driven to the nozzles on top of dehumidifier and sprayed on the surface of the packed bed in dehumidifier. Latent heat from moisture content can be removed by the evaporation of ethanol during dehumidification process. The result showed that a decreased temperature, increased flow rate and increased concentration of the desiccant solution were capable of providing the optimal performance of the dehumidifier using self-cooled liquid desiccant. Compared with conventional LiCl solution under the same experiment condition, the dehumidification performance of using self-cooled liquid desiccant was improved by more than 40%, which is quite impressive.

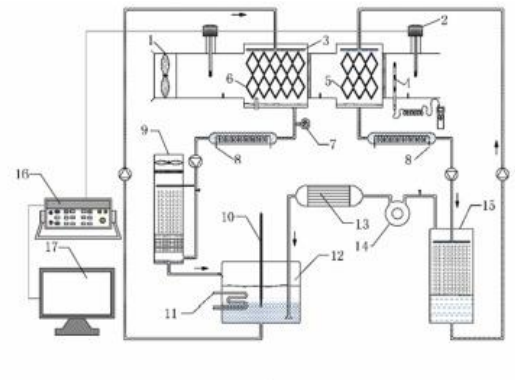

Figure 2-9 Experimental setup of self-cooled dehumidifier [60]

Since the conventional packed bed structure was used for the dehumidifier, the process air had direct contact with the desiccant solution. It is a great risk for letting the evaporative ethanol being exposed to the air which will be transferred inside buildings. A complex ethanol recovery system has to be installed for preventing the leakage of ethanol vapour into the indoor environment. The design of this self-cooled liquid desiccant dehumidification system seems to fail the original proposes of improving internally-cooled type dehumidifier, which were to simplify the structure and reduce the maintenance cost.

2.2.4. Membrane-based dehumidifier

Semi-permeable membranes have been employed in the air dehumidification process to avoid the occurrence of crossover droplets between desiccant solution and process air. This technology is commonly referred to as membrane-based liquid desiccant air dehumidification. Selective permeable membranes which only allow moisture content to pass through, can be created in the form of parallel-plates or hollow fibres. The solution flowed on one side of the membranes while the air flowed on the other. Effective heat and moisture exchange occurred through the membrane. Other potentially harmful gases or liquid solutions were prevented from passing through the membranes [61]. The semi-permeable membranes were encased in plastic casings to create parallel-plates membrane modules or hollow fibre membrane modules, respectively. Both the parallel-plates and hollow fibre membrane designs provide distinct advantages and limitations. The parallel plate was simpler and easier to build, with smaller pressure losses in the channels. The second was more complicated and challenging to build, particularly in relation to the sealing of its two ends and

the pressure loss was greater in the channels. Nevertheless, the hollow fibre membrane module packing densities were higher and the dehumidification efficiency was greater. For component design and system optimisation, it was important to use the fundamental transport data within the membrane modules. As a result, in recent years, the investigations have mostly focused on fluid flow and conjugate heat and mass transfer during the dehumidification process.

Huang et al. [62] created a mathematical model for the cross-flow parallel-plate membrane module to demonstrate the characteristics of heat and mass transport in membrane-based liquid desiccant air dehumidification. The air and solution flows were regarded to be fully developed hydrodynamically, as well as thermally and in concentration. The momentum, heat, and mass transfer governing equations for air and solution streams have been established, solved, and experimentally validated. The structure was constructed by stacking the membranes as depicted in Fig. 2-10 Flow channels were created by maintaining equal spacings between adjacent membranes. In order to facilitate duct sealing, the solution stream and air stream alternately flowed through the parallel channels in a cross-flow configuration. Other flow arrangement made it difficult to seal the liquid fluid channels. The liquid desiccant was utilised to dehumidify the process air, while absorbing moisture from the air via the membranes. The experimental results revealed that the Nusselt number on the air side, under the conjugate heat and mass transfer condition ($Nu_{C,a}$), was between the Nusselt number under uniform temperature condition (Nu_T) and that under heat flux condition (Nu_H). The Nusselt number on the solution side under the conjugate heat and mass

transfer condition ($Nu_{C,s}$) was found to be roughly 15% more than that on the air side ($Nu_{C,a}$).

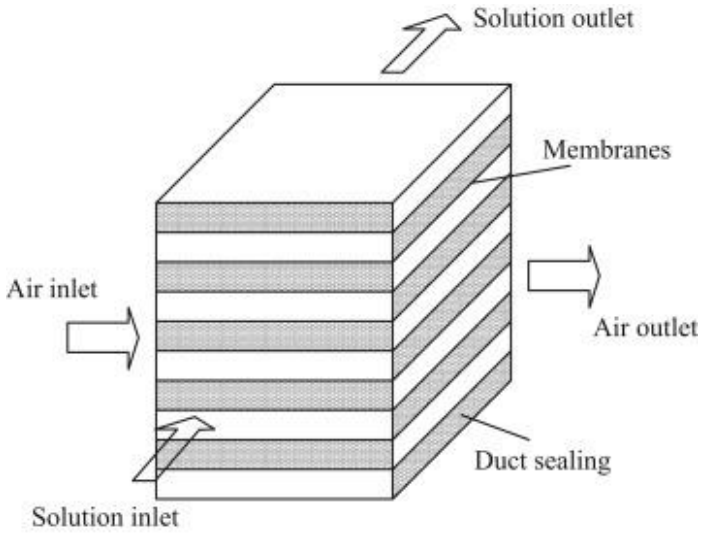

Figure 2-10 Structure of a parallel-plate membrane dehumidifier [62]

The membrane modules with parallel plates had been employed as air-to-air heat and mass exchangers [63]. This module was also employed in air dehumidification system due to its simple structure and easy production of parallel-plate membranes. Mahmud et al. [64] presented a RAMEE (run-around membrane energy exchanger) system with two quasi-counter flow membrane-based energy exchangers. Within each exchanger, the micro-porous membrane served as a barrier between the air and desiccant solution streams. The membrane only facilitated the exchange of heat and water vapour between the two streams. It was discovered that raising the desiccant flow rate led to an increase in the overall system effectiveness, whereas increasing the airflow rate led to a drop in overall dehumidification performance. Vail et al. [65] created a steady-state model to investigate heat transfer in a RAMEE system with two parallel-plate quasi-counterflow membrane modules. The effectiveness of the run-around heat

exchanger was found to be between the effectiveness of similar run-around systems with two cross-flow exchangers or two counter-flow exchangers. Larson et al. [66] investigated the elastic and moisture transfer characteristics of membrane materials in the context of developing air-to-liquid energy exchangers. These energy exchangers were comprised of a series of pressurised membrane channels. The impact of membrane orientation, strain rate, and relative humidity on elastic properties were investigated, as well as the influence of humidity on water vapour resistance. Seyed-Ahmadi et al. [67] investigated the coupled heat and moisture transfer in a run-round heat and moisture exchanger using a liquid desiccant numerically and experimentally. In their research, they created a two-dimensional transient model for the coupled heat and moisture transfer in the membrane exchanger. A comparison of numerical modelling findings and experimental data acquired from laboratory testing for both sensible and latent efficacy for the simultaneous heat and moisture transmission in the RAMEE revealed good agreement at varied operating conditions. A further numerical study [68] was conducted to examine the transient behaviour of the RAMEE under various initial and operational conditions such as number of heat transfer unit, thermal capacity ratio, storage volume ratio and desiccant concentration. The simulation results have shown that the storage volume ratio and the desiccant concentration are the most important parameters that affect the heat and mass transfer within the RAMEE.

The parallel-plate membrane-based dehumidifier is widely used because the structure is simple. However, packing density of parallel-plate structure is about 500 m^2/m^3, which means the heat and mass transfer processes between air and

desiccant solution are limited [61]. For a hollow fibre membrane-based liquid desiccant dehumidifier, the air and desiccant solution are able to flow through either inside or outside the fibres. In real applications, it is preferred to let the air flow through the outside while solution flows through inside the fibres in order to reduce the pressure drop of air and enhance the dehumidification performance [69]. In 2001, the first hollow fibre air-liquid contactor is built by Bergero and Chiari [70], as shown in Fig 2-11. A rectangular arrangement consisting of 800 polypropylene fibres was employed for the purpose of both air humidification and dehumidification. LiCl aqueous solution is chosen as the working desiccant. The total contact area of the proposed hollow fibre contactor is 1.2 m^2 and the polypropylene capillaries are structured in staggered arrangement. The mass transfer area per unit volume of the prototype is up to 593 m^2/m^3. Based on the experimental and empirical investigations, it has been determined that the performance of the proposed hollow fibre contactor can be improved by decreasing the air flow rate.

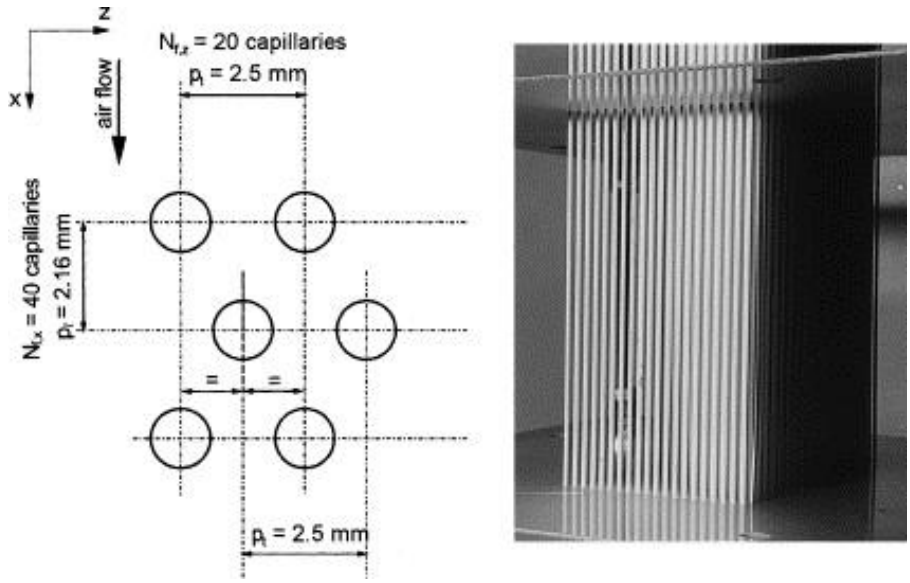

Figure 2-11 Prototype hollow fibre air-liquid contactor [70]

Zhang [71, 72] has developed both experimental study and numerical model for a counter-flow hollow fibre air-liquid contactor, as illustrated in Fig. 2-12. There are 200 hollow fibres being installed inside the proposed hollow fire dehumidifier. The hollow fibre is designed to have an inner diameter of 600 μm and outer diameter of 750 μm. By conducting a simple analytical solution at first, the conjugate heat and mass transfer process within the hollow fibre dehumidifier has been analysed by applying the free surface method. As a result, the velocity, temperature and concentration fields for air and desiccant solution are solved by using finite volume method. Moreover, the local and mean Nusselt and Sherwood number have been determined as well.

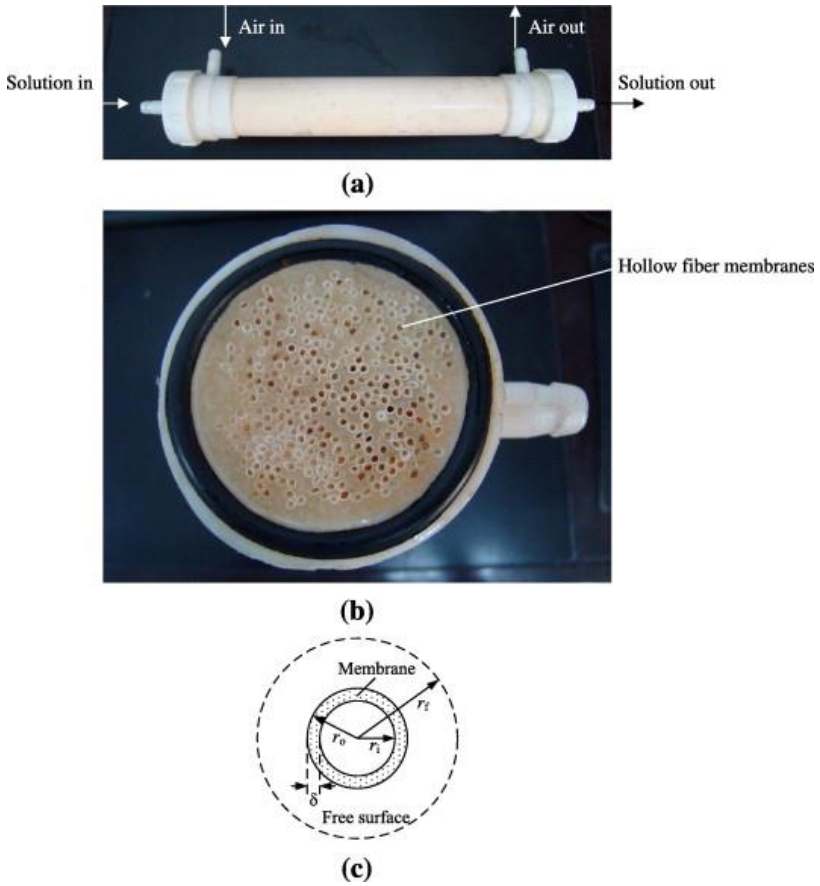

Figure 2-12 Structure of the counter flow hollow fibre membrane dehumidifier [71, 72]

Moreover, counter-flow hollow fibre dehumidifiers are also investigated by many studies. Huang et al. [73] proposed a hollow fibre dehumidifier in counter-flow arrangement. There were 600 fibres installed inside the rectangular shell container. First, the flow inside was assumed to be laminar and the heat and mass transfer process were assessed by free surface approach. Subsequently, a more complex and realistic numerical model has been developed by assuming the air flow to be turbulent within the hollow fibre dehumidifier. The $k-\varepsilon$ turbulent model was selected to simulate the turbulent air flow, while the desiccant solution was still treated as laminar flow. The Nusselt and Sherwood number were obtained from experimental works. As shown in Fig 2-13, another cross-flow

hollow fibre contactor is evaluated by Chen et al. [74]. Experimental tests have also been conducted to validate with simulation results, and a good agreement has been achieved. The numerical model was developed based on the governing partial difference equations for the heat and moisture transfer processes in the proposed hollow fibre dehumidifier. The finite difference iteration were solved in Matlab unit it converged. A grid size of 60 × 60 has been proved to be sufficient for the dehumidifier cross section diameter of 0.2m and height of 0.6m.

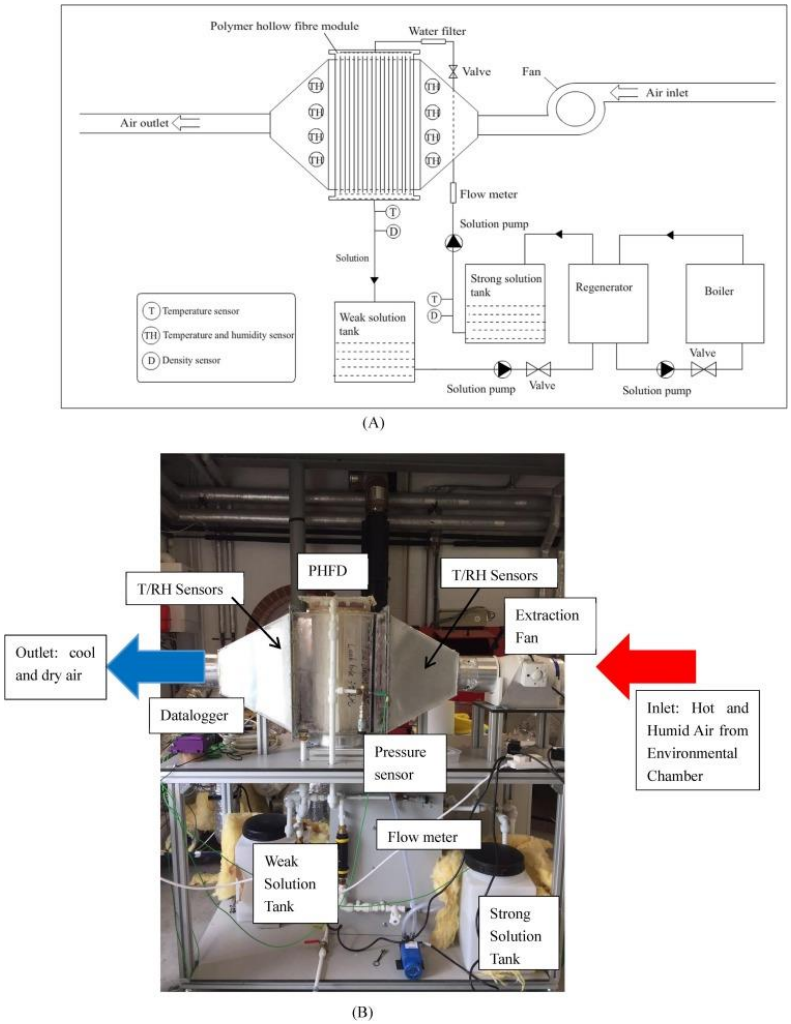

Figure 2-13 Cross-flow hollow fibre contactor (a) schematic (b) photo [74]

In conclusion, the hollow fibre membrane dehumidifier generally provide higher packing density to enhance the dehumidification performance compared to flat

plate membrane dehumidifier. Unfortunately, the complex structure design and high pressure drop within the fibre tube are two major drawback during real applications in practice. Thus, the parallel-plate dehumidifier are far more widely used for air dehumidification. All the parallel-plat and hollow fibre membrane-based dehumidifiers mentioned above are adiabatic types, the solution temperature will increase during the dehumidification process with the phase change of moisture. To enhance the dehumidification performance, similar to direct contact internally-cooled dehumidifier, the membrane-based internally cooled dehumidifier have drawn more attention to studies and researches in recent years.

2.2.5. Membrane-based internally-cooled dehumidifier

The previous review of membrane-based dehumidifiers were adiabatic types, similar to internally-cooled direct contact dehumidifiers, internally-cooled membrane-based liquid desiccant dehumidifier have been developed and evaluated to remove latent heat absorbed by the desiccant solution. In 2008, the first membrane-based contactor with cooling coil inside was proposed by Conde et al. [75]. Huang et al. [76] conducted both numerical and experimental works for an internally-cooled membrane-based liquid desiccant dehumidifier to improve dehumidification process. The geometry of the proposed cross-flow internally-cooled dehumidifier is shown in Fig. 2-14. The air and solution channels were built by membranes and the plastic plates being stacked together. The process air and liquid desiccant were divided by membranes in cross-flow configuration. The cooling water flows vertically along the plastic plates to for the water falling films in the water channel. One cooling water channel next to

one desiccant solution channel is separated by parallel plastic plates. The sweep air flows over water falling films, in a co-current configuration. When the heat is released to the solution channel, they can be removed by the falling water through plastic plates, and thus the latent heat can be removed by the evaporative sweep air.

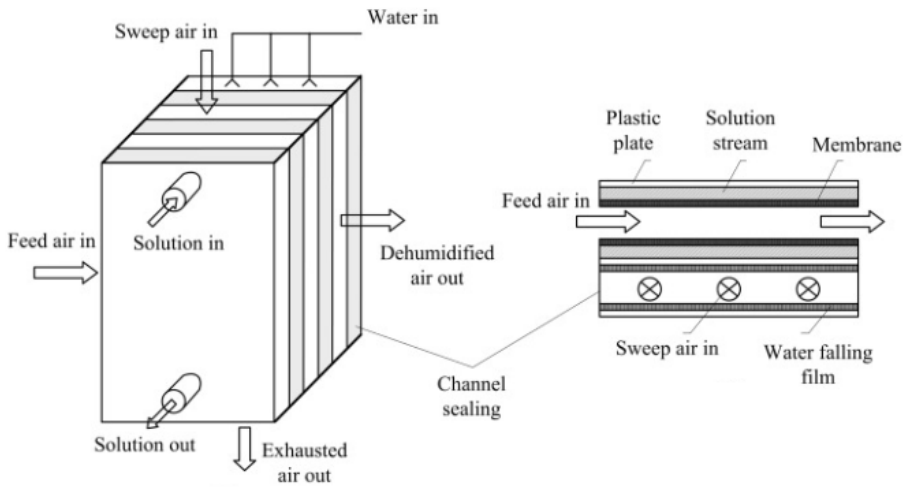

Figure 2-14 The structure of a cross flow internally-cooled membrane-based liquid desiccant dehumidifier [76]

Abdel-Salam et al. [77] developed and tested a novel 3-fluid liquid-to-air membrane energy exchanger as depicted in Fig. 2-15. The prototype is built by micro-porous semi-permeable membranes and the heat and mass transfer are indirect between air and desiccant solution. Meanwhile, the refrigeration tubes are installed inside the solution channel to restrain the temperature rise of desiccant solution during the dehumidification process. Cold water is selected as the cooling medium since the high heat capacity, high boiling point, low freezing point and low cost. Comparison between membrane-based internally-cooled

dehumidifier and adiabatic membrane-based dehumidifier under the same structure has been conducted. The results show that under the same operation conditions, the moisture removal rate and sensible cooling output can be improved up to 54% and 140%, respectively, by using water as refrigerant.

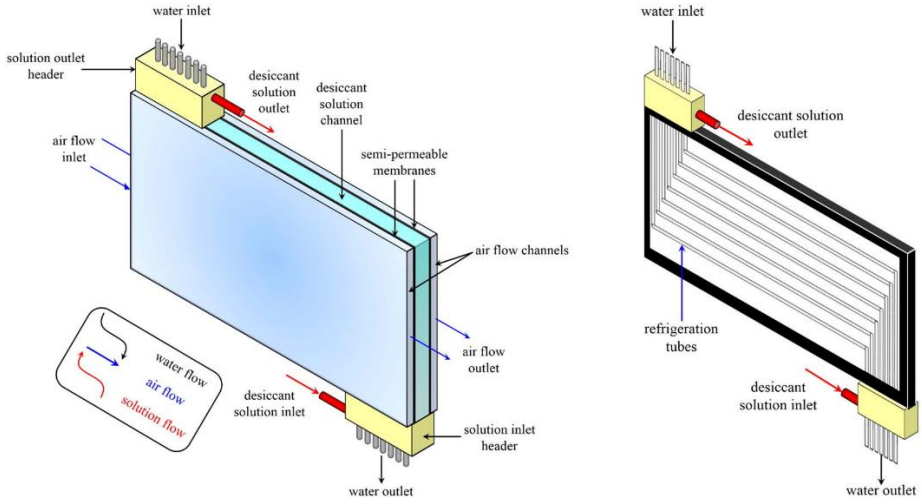

Figure 2-15 3-fluid internally-cooled membrane-based dehumidifier (a) schematic diagram (b) solution channel with cooling coil [77]

Qiu et al. [78] conducted a new internally-cooled hexagonal parallel-plate membrane-based channel (IHPMC). The schematic diagram of the proposed dehumidifier is presented in Figure 2-16. A hexagonal structure has been proposed for air, desiccant solution and cooling medium to flow through the membrane channels. The pressure drop can be improved with the hexagonal structure compared to the membrane-based internally-cooled dehumidifier in counter flow arrangement [79]. By applying cooling coils inside the solution channel, the condensation heat can be removed. The impact of dehumidifier structure on the product of several dimensionless parameters includes Reynolds number and Nusselt number are evaluated instead of the heat and moisture transfer. The air and solution flow are assumed to be laminar and the numerical

model was developed between two neighbouring channels. The energy and momentum governing equations were proposed together with a uniform temperature boundary conditions, and finite volume method is applied to solve the equations in CFD software Fluent. The results have shown that under the tube outer diameter equal to 2mm, the Reynolds number increases with the increase of tube numbers, while the Nusselt number will decrease. It provided valuable information for further performance analysis, structure design of the internally-cooled membrane-based dehumidifiers used for liquid desiccant air dehumidification.

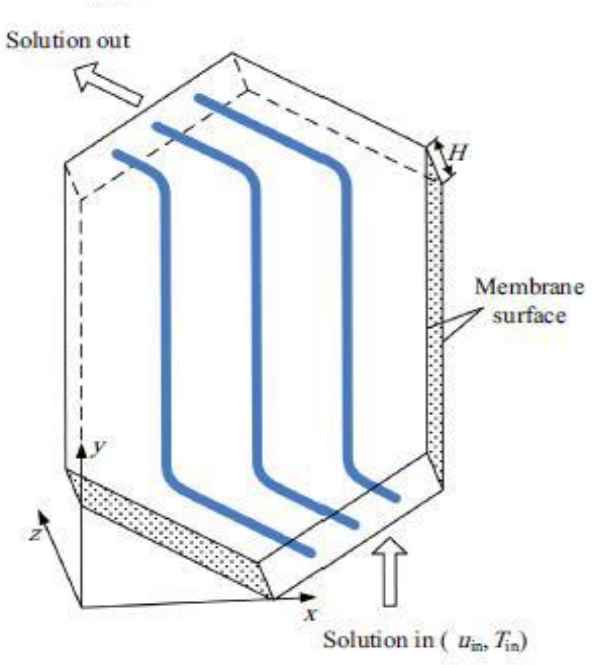

Figure 2-16 Schematic diagram of the IHPMC [78]

To sum up, the membrane-based internally-cooled dehumidifier is able to avoid droplet carry over problem and restrain the temperature rise during the dehumidification process. However, by installing cooling coil inside solution channels built up by membranes, the structure of the proposed dehumidifier

become extremely complex which lead to high maintenance cost. The combination of using self-cooled liquid desiccant solution inside membrane-based dehumidifier is proposed in this research, since it can not only simplify the design structure, but also prevent the leakage of ethanol vapour. More importantly, the dehumidification performance can be enhanced with the removal of condensation heat during the dehumidification process by the evaporation of ethanol.

2.3. Liquid desiccant regenerator

2.3.1. Direct contact regenerator

The design concept of regenerator was similar to the dehumidifier, however, instead of absorbing moisture from humid air, water will be removed by the return air to reconcentrate the dilute desiccant solution. Fumo and Goswami [42] conducted an investigation on a cross flow packed bed regenerator, in which LiCl was selected as the desiccant solution. The regenerator tower is packed with polypropylene Rauschert Hiflow rings that were 2.54 cm long and with a specific surface area of 210 m^2/m^3. Three spray heads were evenly positioned in an equilateral triangle at the top of the regenerator tower to spread the diluted solution. The regenerator tower operates with a counter-flow arrangement, facilitating direct contact between the desiccant solution and the air. The moisture in the weak solution is transported by air flows as a result of the surface vapour pressure difference. According to their findings, desiccant inlet temperature, concentration, and air mass flow rate all have the most significant impacts on regeneration performance.

Longo and Gasparella [80] used LiBr solution to conduct a counter flow packed column regenerator with structured and random packing. Two structures were tested: a random column with one Pall Ring element and a structured column Mellapack 250Y with cylindrical elements composed of perforated and corrugated sheets. In this study, a one-dimensional simulation model was developed to evaluate the regenerator, and there were good matches between experimental and numerical results. The regeneration temperature was reported to be approximately 50 °C, which may be obtained using solar energy or other recovered heat, and the regeneration performance of a random packed column is 20-25% higher than that of a structured packed column. The diagram of experimental test rig for the packed column counter flow regenerator are presented in Fig. 2-17.

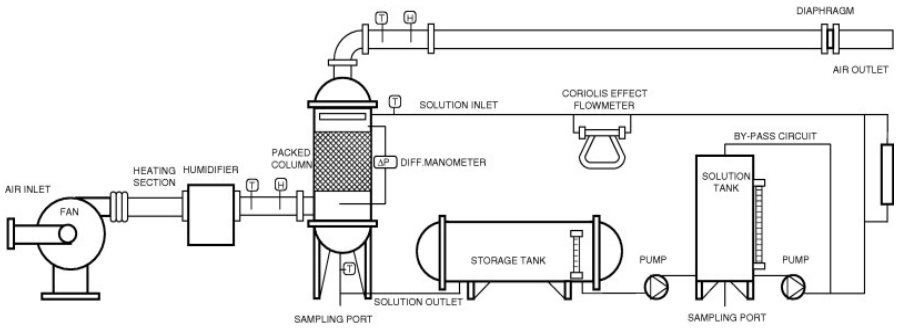

Figure 2-17 Experimental test rig of packed column regenerator [80]

Although counter flow packed beds offer the benefit of high heat and mass transfer efficiency, the construction of this type is highly complex and difficult to fabricate. In contrast, the duct arrangement and installation of cross flow packed beds are comparatively more convenient and simpler as compared to counter flow configurations. By combining multiple cross flow packed beds

together, the heat and mass transfer potential of the regenerator can be improved [81].

Liu et al [82] constructed a regenerator utilising Celdek structured packings and conducted the experiments by LiBr solution as the liquid desiccant. The schematic diagram of the experimental test rig for the Celdek cross-flow regenerator is shown in Fig. 2-18. In the regenerator, solution and air come into direct contact and form a cross flow pattern. The dimensions of the regenerator are 0.55 metres in height, 0.40 metres in length, and 0.35 metres in width. The packing material used was Celdek structured packing, which has a specific surface area of 396 m^2/m^3 and a flute height of 7 mm. Corrugated cellulose paper sheets with varying flute angles were used to make the packings. One steep and one flat sheet of paper were attached together. They came to the conclusion that regeneration effectiveness would be enhanced by increasing the mass flow rate and concentration of the solution, while it would be diminished by increasing the mass flow rate of air and the temperature of the solution. A dimensionless mass transfer correlation was also constructed and validated using experimental data.

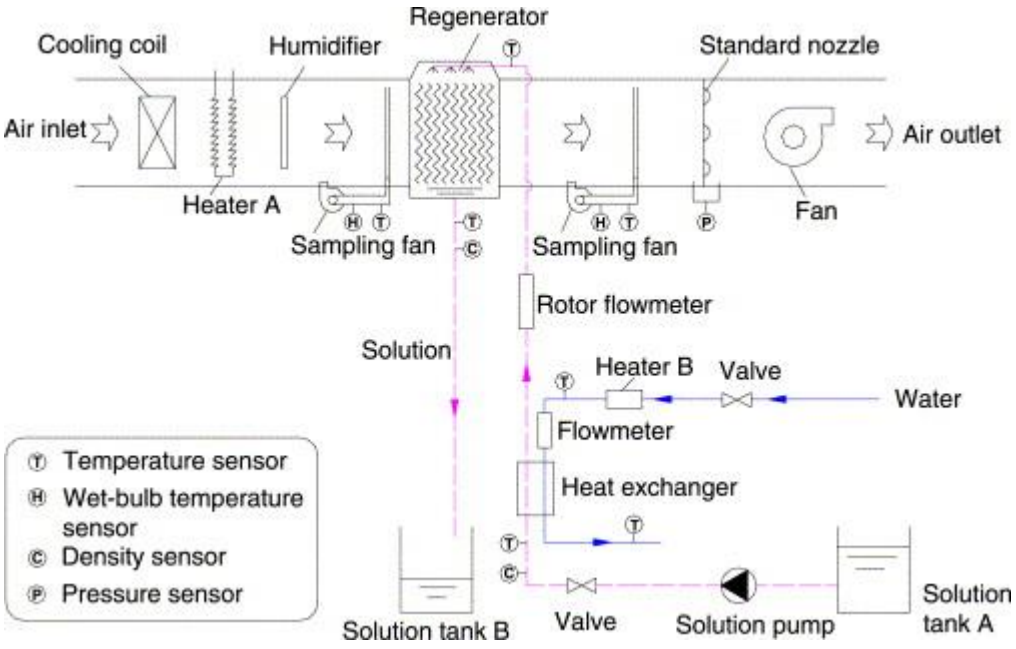

Figure 2-18 Experimental test rig of the Celdek cross-flow regenerator [82]

Shen et al. [83] studied a liquid desiccant regenerator with a heat recovery heat pipe system that used lithium chloride as the desiccant solution. Heat mass transfer occurs concurrently between the air and solution flows in the regenerator tower where the upwind air flow and liquid desiccant make direct contact on the surface of the structured packing in a counter-flow arrangement. Their use of a heat pipe heat exchanger for the regeneration air heat recovery makes their research distinct from others. The temperature difference between the air and the solution in the regenerator is reduced as a result of this preheating process, allowing the solution to maintain a relatively higher temperature and vapour pressure. Therefore, the mass transfer ability from solution to air can be improved. Further study of a heat recovery system combining with fixed-plate heat exchanger has been carried out [84]. The regenerator tower still has the same structure, but a fixed plate heat exchanger has been installed as the heat recovery unit. The results have been compared with the performance of regenerating with

and without a heat recovery system. It has found that the fixed-plate heat exchanger system recovered a maximum of 25% and 26.5% of waste heat, resulting in energy savings of 26.5% and 27% for 4 and 8 rows arrangement, respectively. Maximum 16–19% of waste heat was collected for the fixed-plate heat recovery system, reducing the energy consumption by 14–18%.

The regeneration of liquid desiccant solution can also be accomplished through low-grade energy sources, such as solar energy. Recent innovations in this field have mostly focused around the application of solar thermal regeneration and solar electrodialysis technology. The solar thermal regeneration system involves the utilisation of a solar collector to heat a weak solution for absorbing solar thermal energy. The regenerator in the electro-dialysis system is essentially an electro-dialysis stack made up of many cells arranged in parallel between two electrodes. This technique is powered by photovoltaic cells and operates on the principle of ion transport under the effect of an electrical field. Cheng and Zhang [85] conducted a detailed comparison of the two aforementioned types. They concluded that the solar electro-dialysis regeneration system exhibits superior energy efficiency, but at a higher cost compared to the solar thermal regeneration system.

Both numerical and experimental researches were conducted by Alosaimy and Hamed [86] on a packed column regenerator that was powered by a solar heating system. As shown in Fig. 2-19, the regenerator was a honeycomb-packed column, and water heated by a solar heating system was circulated through a finned-tube air heater to raise the temperature of the air. Then, in the packed column regenerator, heated air was in direct contact with weak solution. The results

demonstrated that when a storage tank is combined with a solar collector, the system can operate in almost steady-state conditions.

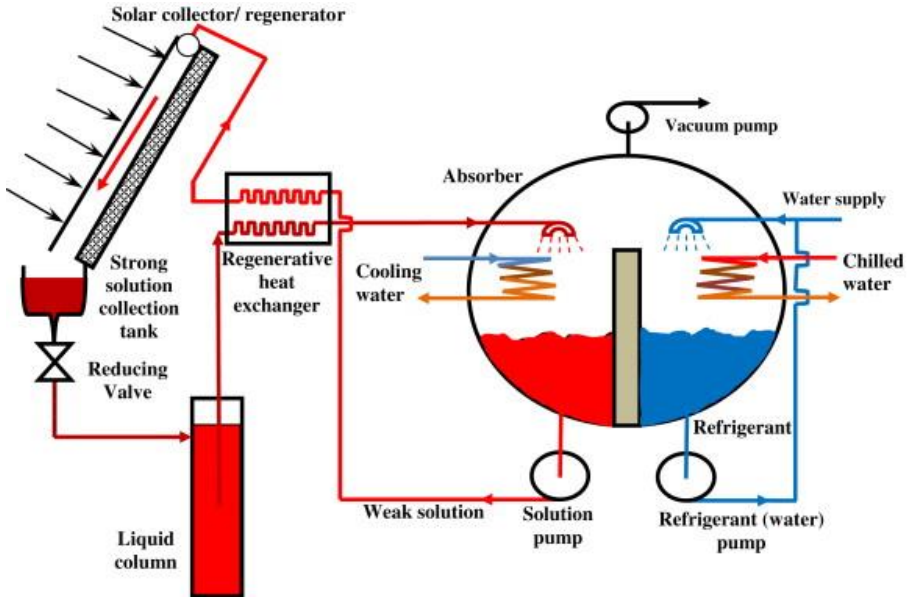

Figure 2-19 Solar thermal powered regenerator [86]

Cheng et al. [87] presented a photovoltaic-electrodialysis (PV-ED) regeneration technique. The regenerator can be described as an electrodialysis (ED) stack consisting of many parallel cells positioned between two electrodes. The desiccant solution is concentrated and diluted in alternating cells, which means the weak solution enters the concentrate cells and the diluted solution enters the diluted cells. As a result, the weak solution can be concentrated and the diluted solution can be diluted in the ED stack. The concentrated solution can thus be used to remove moisture from the air. The primary investigation revealed that despite the low PV efficiency, the regeneration performance of a PV-ED system can be twice greater than that of a traditional solar thermal system.

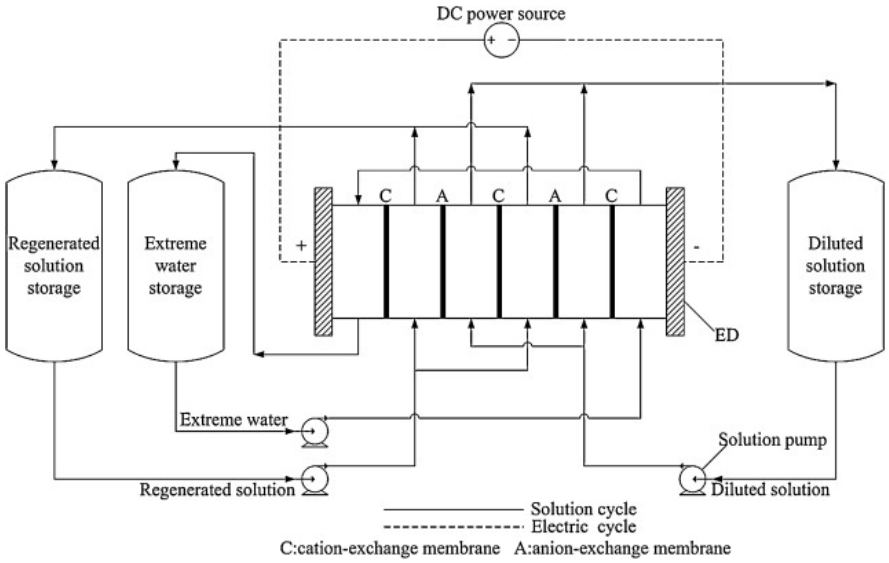

Figure 2-20 Experimental test rig of electrodialysis regenerator [87]

To sum up, all regenerators mentioned before are in direct-contact arrangement, which lead to the underlying issue of desiccant carry-over. Previous literatures have also investigated the use of membrane-based regenerators as a potential solution to eliminate carry-over problems and will be introduced in the following section.

2.3.2. Membrane-based regenerator

To address the desiccant droplet carry-over issue, a membrane-based regenerator provides an alternative to a direct-contact regenerator. Ge et al. [88] conducted a comparison between experimental and numerical data for heat and mass transfer of a flat-plate membrane-based heat mass transfer contractor used for regeneration. A single-panel regenerator on a small scale was used, and the solution and air were in a counter-cross flow arrangement. The structure of the regenerator is comparable to the dehumidifier in [89]. The length of the regenerator is 0.99 m, the solution and air channel thicknesses are 1.2 mm and 5

mm, respectively, and the membrane thickness is 0.265 mm. Then, they studied the effects of various operating factors, including NTU, Cr^*, humidity ratio and air inlet temperature, solution inlet temperature and concentration, on the regenerator effectiveness and moisture flux ratio. The influence of the dimensionless parameters NTU and Cr^* on regenerator performance is found to be the most significant, but the effects of solution and air characteristics are relatively lower. In their investigation, air side effectiveness was applied to evaluate regenerator performance.

Duong et al. [90] studied the regeneration of LiCl solution for air conditioning using membrane distillation, as presented in Fig. 2-21. The regenerator was a plate framed module that was made by porous membrane technology. It contained layers of flat-sheet polytetrafluoroethylene (PTFE) membranes. The membranes utilised in the study had a nominal pore size of 0.2 μm, a porosity of 80%, and a total active surface area of 138 cm^2; their thickness was 60 μm. Stainless steel coils submerged in a hot water bath heated the diluted solution during the experiments. After entering the solution channels, heat and mass were transferred across the membranes, causing the diluted solution to be concentrated there. The regeneration performance was assessed using the regeneration capacity and the specific thermal energy consumption. The results showed that at a feed temperature of 65 °C, the system can increase the solution concentration to 29% without suffering a substantial amount of desiccant solution loss. If the feed temperature was raised, regeneration capacity would rise and specific thermal energy consumption would be reduced.

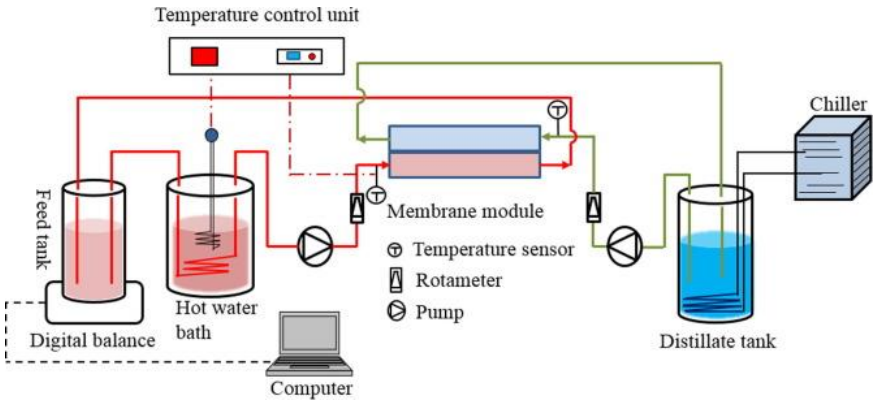

Figure 2-21 Schematic diagram of the membrane-based regenerator unit [90]

Datta et al. [91] developed and conducted an experimental investigation on a multi-effect regenerator. This regenerator employs selective membranes for the purpose of separating the solution and water vapour. The regenerator utilised the polypropylene membranes with a pore size of 0.2 μm and a thickness ranging from 0.12 to 0.2 μm. The dimensions of the regenerator were 70 cm in height, 70 cm in breadth, and 15 cm in thickness. In the experiments, LiCl served as the working solution. The system performance was evaluated using the performance ratio, which is defined as the ratio of heat generation throughout the regeneration process to the average heating energy. Based on the findings, a performance value of 2.5 was achieved at a heating water temperature of 50°C, while the inlet feed concentration was maintained at 8%. Performance ratio would be improved as the temperature of the inlet solution increased, but it would drastically drop when the concentration of the inlet solution increased.

Bai et al. [92] conducted the performance evaluation of a membrane-based flat plate heat and mass exchanger through numerical model and experimental test. The test rig of regenerator is presented in Fig. 2-22, it consists one membrane-based regenerator, two storage tanks and heat exchanger connected with external

heating source. The geometry of the regenerator is 410 mm × 230 mm × 210 mm with 11 air and solution channels. A good agreement has been obtained based on simulation and experimental results. It has found that the dimensionless parameters number of heat transfer unit and flow rate ratio have the most significant impact on the regeneration performance. The air inlet temperature and humidity have less influence on the regenerator while increasing the solution temperature was considered to be a practical approach to improve the regeneration performance.

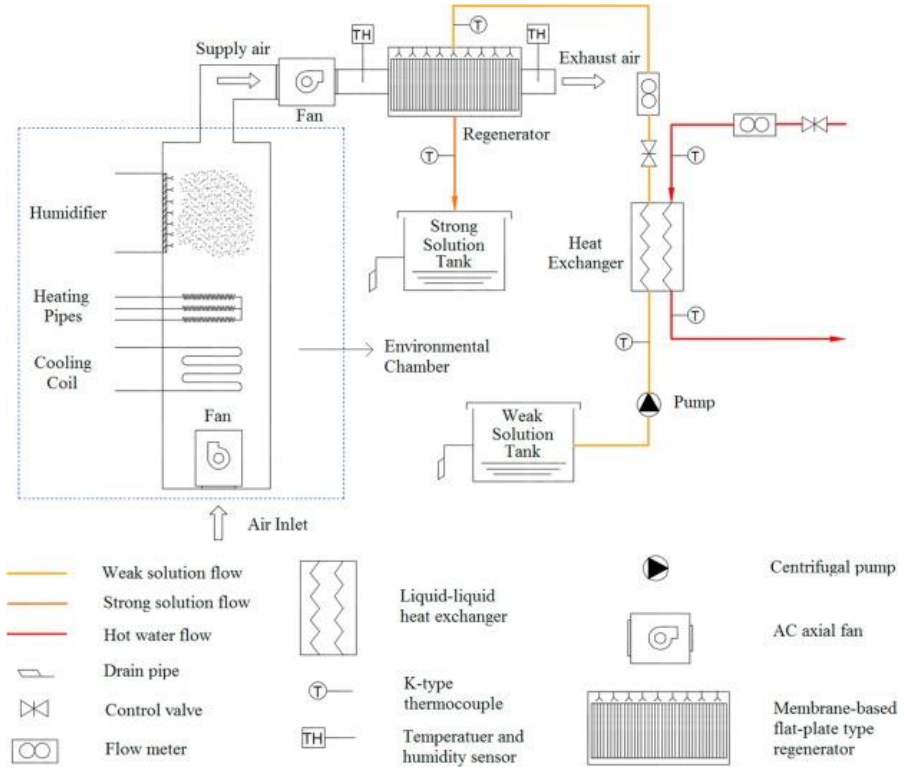

Figure 2-22 Laboratory rig of the membrane-based parallel-plate regenerator [92]

In conclusion, to reconcentrate the desiccant solution after dehumidification process, the investigations of various types of regenerator have been conducted by many researchers. Direct contact type regenerators including packed bed or

packed columns have been widely used due to its simple structure. To avoid the carry-over problem of liquid desiccant during regeneration process, membrane-based regenerators were proposed but limited studies have been conducted. To reconcentrate the proposed self-cooled liquid desiccant solution for this research, membrane-based regenerator seems to be a better option to avoid the pollution of ethanol vapour into indoor environments.

2.4. Completed liquid desiccant dehumidification system

In 1951, London and Kays [93] firstly proposed the run-around system, they investigated a liquid desiccant run-around system for gas-turbine plant. Once the air and solution heat capacity rates are the same under constant NTU values, the system's optimal performance can be attained. The performance of a run-around heat recovery system was further analysed by Forsyth and Besant [94], while glycol aqueous solution was selected as the coupling fluid and two same coil heat exchanger. A numerical model was created to predict the system performance. However, the results did not match well with the experimental results since various complicated factors in the experimental tests were not taken into account for the mass transfer correlations. Although the system effectiveness was proposed to find the optimal operation conditions of the system, it should not be treated as the only factor influencing the design, the total cost of the entire life cycle should be taken into considerations. Fan et al. [95] conducted a numerical model to evaluate the performance of a close loop heat and mass recovery system. There were two cross flow heat and mass exchangers with the same geometry,

one was working as the supply exchanger (dehumidifier) and the other as the exhaust exchanger (regenerator). LiCl was selected as the liquid desiccant solution while the solution and air are in cross flow arrangement in both dehumidifier and regenerator. The solution could reconcentrate itself through mass exchange with the exhaust air flows. Since the total heat and moisture transfer rates in the exhaust exchanger balance the rates in the supply exchanger, the operation condition of the dehumidification system can be considered to be steady-state. Therefore, neither energy nor moisture needs to be added to or removed from the system, and the only energy input is the energy required for the operation of the pump and fan. A numerical model was established to simulate the close loop system and validated with the experimental tests. The results have shown that the size of the air channel has a more significant effect on the system performance compared to the size of the solution channel. Additionally, it has found that the thermal entrance length of the two heat mass exchangers can be ignored. The system comprised two cross flow liquid-to-air heat and mass exchangers, as depicted in Fig. 2-23.

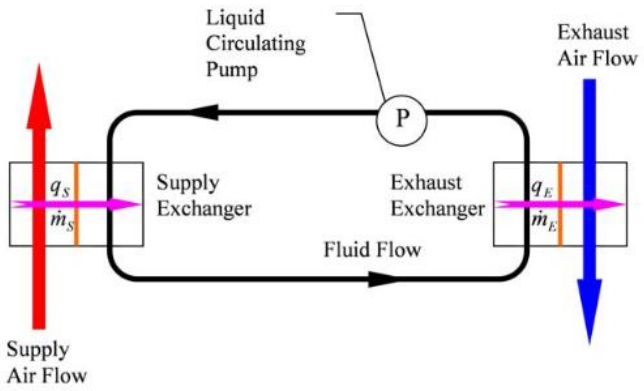

Figure 2-23 Schematic diagram of a close loop heat and mass recovery system [95]

Hemingson et al. [96] evaluated the steady-state performance of a run-around membrane-based heat and mass recovery system. This system consisted of two identical counter-flow RAMEE units and were assessed under various outdoor air conditions. The effectiveness of the run-around system was found to be highly dependent on outdoor conditions. Under certain weather conditions, the effectiveness can reach up to 100% or fell below 0%. Additionally, the latent and sensible effectiveness were respectively affected by the mass and heat transfer process. The schematic diagrams of a single membrane-based liquid-air contactor are shown in Fig. 2-24.

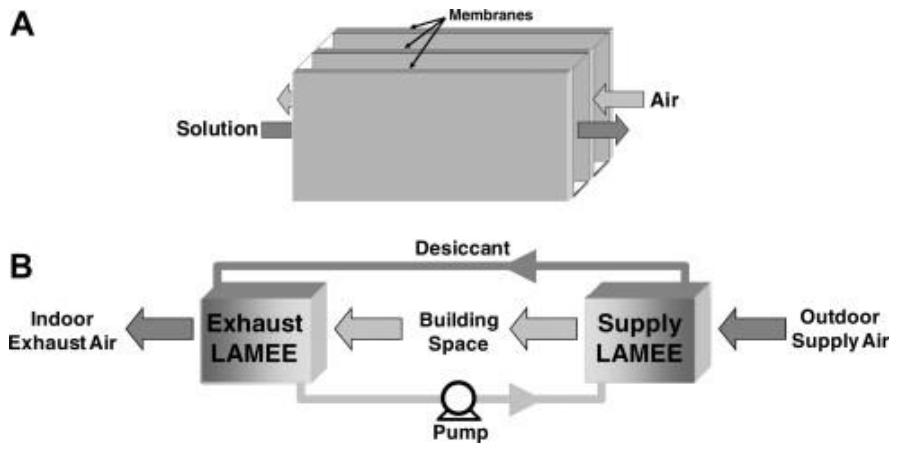

Figure 2-24 Schematics of (A) air-liquid membrane-based exchanger (B) close loop membrane-based system [96]

Vali et al. [65] conducted a study on a run-around liquid desiccant dehumidification system that included two identical counter-cross flow flat-plate heat exchangers. The two-dimensional numerical model only took into account of the heat transfer, and it assumed that the heat transfer between the solution and the supply and exhaust exchanger was balanced under steady-state operation condition. This counter-cross flow run-around system was found to be less

effective than the counter-flow system, but more effective than the cross-flow. For a constant total surface area, the most efficient heat exchangers were those having a small entry aspect ratio and short inlet and outlet lengths for solution flow. Bai et al. [97] conducted the steady-state performance evaluation and energy assessment of a complete membrane-based dehumidification system. Apart from the dehumidifier and regenerator, external hot and cold water supplies units were used to enhance the dehumidification performance. A comprehensive parametric study for the complete system was carried out experimentally and numerically. A good agreement was found between simulation and experimental results, and it was suggested that the system performance can be enhanced by operating the dehumidification system at or below the critical value of solution to air mass flow rate ratio. The test rig of the proposed dehumidification system is presented in Fig. 2-25.

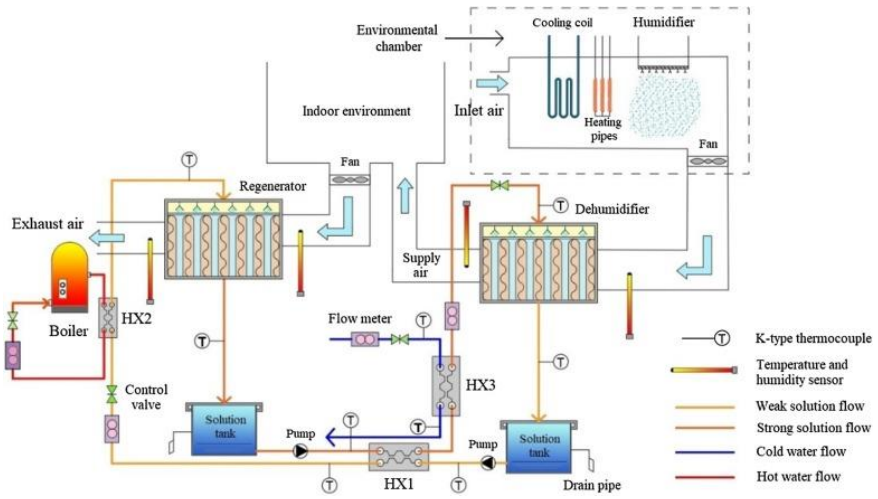

Figure 2-25 Test rig of the complete dehumidification system [97]

Apart from the steady-state evaluation of the complete dehumidification system, the transient performance has analysed by many other researchers. Seyed-Ahmadi et al. [67] investigated the transient simulation of a run-around heat and

moisture exchanger system. This system is comprised of two identical cross-flow liquid and membrane energy exchangers (LAMEEs) operating in a closed loop configuration. First, they created a theoretical model utilising the finite difference method and an implicit time discretization to study transient performance. A new definition of the so-called quasi-steady state, which was the period of time that all heat and mass lost in one airflow was taken by the other air flow, was developed to analyse the transient performance. As a result, the system was studied for a sufficient amount of time to reach a quasi-steady state. Good agreements were observed when comparing numerical results and analytical solution results and the numerical model proved beneficial for determining RAMEE's transient response time and achieving proper control of RAMEE under different practical situations.

Beyond the scope of heat and mass transfer during the dehumidification process, Patel et al. [98] examined the transfer of contaminants in run-around membrane energy exchangers. Volatile organic compounds (VOCs) in a run-around system have the potential to spread from the exhaust air side to the supply air side for a variety of reasons, which could have significant health impacts on occupants, such as headaches, drowsiness, and breathing problems. Sulphur hexafluoride served as a tracer gas in experiments to determine air leakage. Toluene and formaldehyde were utilised to examine the transfer fraction of volatile organic compounds. The findings indicated that the transfer of low water soluble VOCs between two exchangers was insignificant in a run-around dehumidification system, while a tiny detectable transfer of water soluble VOSs was traced.

For the complete liquid desiccant dehumidification system, the performance can be further improved by integrating with low grade energy such as heat pump. Zhang et al. [99] developed a liquid desiccant dehumidification system driven by heat pump. The exhaust heat from the condenser can be utilized to heat the desiccant solution before entering the regenerator. The numerical model was built based on heat and moisture transfer within the dehumidifier and regenerator, heat pump system and the heat exchangers. For air-cooled condenser, the system COP can be increased by 18% while the water-cooled condenser can improve the system COP by 35%. The schematic diagram of the heat pump driven dehumidification system is presented in Fig. 2-26.

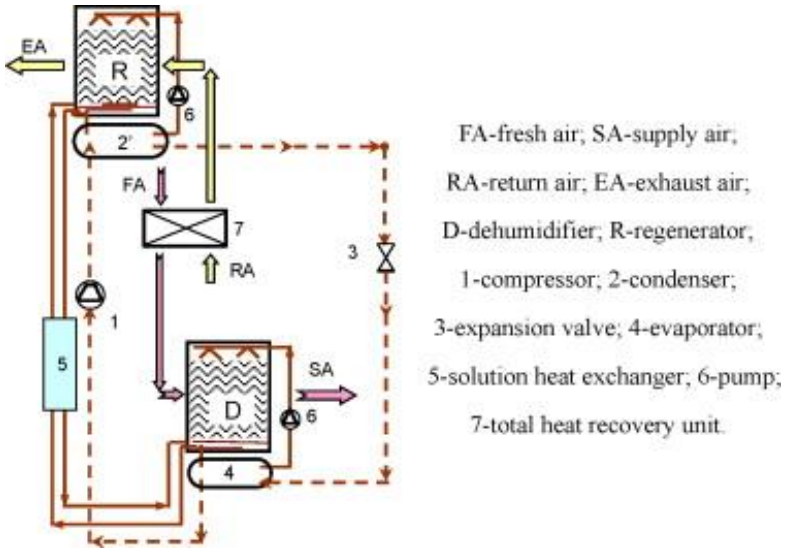

Figure 2-26 Heat pump liquid desiccant dehumidification system [99]

Further researches have also combined the heat pump with internally-cooled liquid desiccant dehumidification system. Liu et al. [100] proposed a theoretical method to investigate the energy performance of a heat pump driven internally-cooled liquid desiccant dehumidification system. The ideal operation conditions for the system were identified and analysed to fully understand the limitation of

current design for liquid desiccant dehumidification system. The results have shown that under actual working condition, the system COP is only about 10% to 35% of the maximum COP. Zhang et al. [101] evaluated the performance of a heat pump driven dehumidification system using exergy analysis instead of energy performance. Based on the exergy destruction method, the exergy destruction of the dehumidification system can be separated into exergy from evaporators, condensers, heat and mass transfer process and mixing processes. The results have shown that the exergy efficiency can be improved to 25% by reducing the heat and mass transfer uniformity coefficient.

To sum up, extensive researches on the complete close loop liquid desiccant dehumidification systems have been conducted in numerous aspects. Most of their researches were setting the heat and mass transfer rate to be the same for dehumidifier and regenerator. In recent years, combination of dehumidification system with external heating and cooling source have drawn more attentions due to its ability to improve the system performance.

2.5. Numerical modelling methods

In order to properly predict the dehumidification performance, it is important to choose the suitable method for heat and mass transfer analyzations. The mass transfer of water between the air and desiccant is generally driven by the difference in surface vapour pressure. The moisture content in the air will be transferred into the desiccant solution once the vapour pressure of air is higher than the desiccant. To begin with, several commonly used assumptions for developing the numerical models are listed below.

1) There is no heat transfer between the dehumidifier and the surrounding environment.
2) Both the air and desiccant solution are laminar and fully developed.
3) Thermal properties of all fluids inside dehumidifier are considered to be uniform.
4) The heat and mass transfer processes are in steady-state.
5) The effect of the falling film thickness of the desiccant solution is negligible.
6) The contact area between air and desiccant solution is fully and uniformly wetted.

Assumptions 1-4 are widely accepted and used by most of the numerical studies for the liquid desiccant dehumidifier. However, assumptions 5 and 6 disputed and evaluated by other studies to ensure that the proposed models become closer to the real applications. Mesquita et al. [102] proposed a numerical model by considering the variation of film thickness during the dehumidification process. By comparing with the conventional models with constant film thickness, the results have shown that without considering the film thickness of desiccant solution, the numerical results are normally lower than real situations, especially when the solution flow rate is low. In assumption 6, the heat and mass transfer area between air and desiccant solution are assumed to be equal to the total contact area. However, in reality, fully wetted condition is not easy to achieve particularly under lower solution flow rate. As a result, the actual heat and moisture transfer area is less than the designed area of dehumidifier. Jain et al. [103] defined two wetness factors for partially surface wetting that can be

integrated within the heat and mass transfer model of the dehumidifier. One factor is determined by the fraction of total contact area for heat transfer, while the other one is for mass transfer. The proposed model predictions are within 30% compared to the experimental results. Further heat and mass transfer numerical model to predict the solution film shape and vapour condensation on the unwetted area has been developed by Wen et al. [104].

After setting the assumptions, the numerical model to predict the dehumidification process can be developed. Based on previous studies, three most commonly used heat and mass transfer modelling methods: simplified, finite difference and effectiveness NTU methods have been introduced in the following sections.

2.5.1. Simplified method

To predict the outlet conditions of the dehumidifiers, a simplified analytical model has been proposed by Khan and Ball [105], which is suitable for hourly dehumidification performance evaluation. The algebraic model was developed after analysing around 1700 groups of data collected by finite difference method, which can be expressed as:

$$W_o = n_0 + n_1 W_i + n_2 T_{s,i} + n_3 T_{s,i}^2 \qquad (2-1)$$

$$W_o = m_0 + m_1 W_i + m_2 T_{a,o} + m_3 T_{a,o}^2 \qquad (2-2)$$

By applying these two equations, the outlet air temperature and relative humidity can be easily obtained. However, the simplified model is developed based on certain operating conditions which makes it inappropriate for other conditions.

Liu et al. [106] proposed a simple model to evaluate the hourly performance of a cross-flow direct contact dehumidifier. Based on the data collected from experimental works, empirical correlation for enthalpy and latent effectiveness were determined by airflow rate, solution flow rate, enthalpy and moisture difference. Good agreements were found between numerical and experimental results and the maximum discrepancy is less than 20%. Gandhidasan [107] developed a simplified method for the design of a packed bed dehumidifier in counter-flow arrangement. The numerical model was derived by dimensionless vapour pressure and temperature difference ratio. Chen et al. [108] conducted an analytical solution of adiabatic heat and mass transfer process in packed-type liquid desiccant dehumidifier. The inlet and outlet solution concentrations of the air-liquid contactor were assumed to be the same. The mathematical model was developed based on the control volume, two parameters which is similar to the air enthalpy have been defined as:

$$K_a = Le \cdot c_{p,a} \cdot T_a + \lambda \cdot W_a \qquad (2-3)$$

$$K_e = Le \cdot c_{p,a} \cdot T_l + \lambda \cdot W_e \qquad (2-4)$$

By applying these parameters into the heat and mass transfer governing equations, and the conservation of energy and mass:

$$K_e = \frac{m^* h_{a,in} - K_{e,out}}{m^* - 1} + \frac{m^*}{m^* - 1}\left(K_{e,out} - h_{a,in}\right)e^{NTU(m^*-1)\frac{L-y}{L}} \qquad (2-5)$$

$$h_a = \frac{m^* h_{a,in} - K_{e,out}}{m^* - 1} + \frac{1}{m^* - 1}\left(K_{e,out} - h_{a,in}\right)e^{NTU(m^*-1)\frac{L-y}{L}} \quad (2-6)$$

$$W_a = W_{a,in} \cdot e^{\frac{NTU(y-L)}{L}} + W^* \cdot \left(1 - e^{\frac{NTU(y-L)}{L}}\right) + \left(W_{e,in} - W^*\right) \cdot \frac{1 - e^{NTU(m^*-1)\frac{L-y}{L}}}{1 - m^* e^{NTU(m^*-1)}} \quad (2-7)$$

$$T_a = \frac{h_a - \lambda W_a}{c_{p,a}} \quad (2-8)$$

Given the above equations both temperature and humidity field of air and desiccant can be solved during the dehumidification process. Further mathematical solution of the moisture removal rate can be solved by:

$$m_{cond} = m_a\left[\left(W_{a,in} - W^*\right) + \theta \cdot \left(W^* - W_{e,in}\right)\right] \cdot \left(1 - e^{-NTU}\right) \quad (2-9)$$

Where θ can be expressed as:

$$\theta = \frac{\dfrac{1 - e^{NTU(m^*-1)}}{1 - m^* e^{NTU(m^*-1)}}}{1 - e^{-NTU}} \quad (2-10)$$

The above mentioned method to predict the moisture removal rate is similar to $\varepsilon - NTU$ method, which will be presented in next section. Ren et al. [109] developed a novel simplified analytical method based on one-dimensional differential model. By applying several new dimensionless parameters, the governing equations were derived to ordinary differential equations, which can be expressed as:

$$\Delta W_M = C_1 e^{\lambda_1 NTU_z} + C_2 e^{\lambda_2 NTU_z} \quad (2-11)$$

$$\Delta\vartheta = -K_1 e^{\lambda_1 NTU_z} + K_2 e^{\lambda_2 NTU_z} \qquad (2-12)$$

Babakhani and Soleymani [110] reported a simplified analysis of heat and mass transfer air-liquid contactor. The humidity ratio was assumed to be constant on the heat and mass transfer interface to derive the simplified model. It was found that the simulation results can provide better accuracy. Babakhani [111] further refined the application analytical model of adiabatic heat and mass transfer process in liquid desiccant dehumidifier. By validating the simulation results with experimental data, it has found that setting the Lewis number to be 1 can provide a better prediction of the outlet air and solution conditions. Wang et al. [112] developed a hybrid simplified model to predict the real-time performance of a packed-bed liquid desiccant dehumidifier. The mathematical model was derived based on the energy and mass conservation principles and constant thermodynamic coefficients. By comparing with 270 groups of experimental data, a good agreement has been found for the proposed method. Park and Jeong [113] proposed a practical correlation to evaluate the impact of operation conditions on dehumidification performance. The experimental data was analysed statistically to conduct a simplified second-order equation model.

Due to its high efficiency, simplified method is commonly selected to evaluate the annual performance of the dehumidification system, since it does not require iteration computations. However, the applications of these analytical solutions are limited because they were developed based on specific assumptions and the accuracy may varies from different types of dehumidifier.

2.5.2. Effectiveness NTU ($\varepsilon - NTU$) method

In 1989, Stevens et al. [114] proposed a numerical model to predict the heat and mass transfer process for an air-desiccant exchanger. The equations were developed based on a simple numerical effectiveness model of cooling towers [115]. Two further assumptions were made, which include that the relationship between saturation enthalpy and temperature is laminar and the moisture transfer for the solution energy balance can be negligible. As a result, an effective heat and mass transfer process within the dehumidifier was proposed. A new dimensionless parameter (number of heat transfer units), which is now well-known as NTU has firstly been observed:

$$NTU = \frac{\alpha_D A V}{G_a} \qquad (2-13)$$

By considering the similarity between heat exchangers and dehumidifiers, the dehumidification effectiveness can be calculated by:

$$\varepsilon = \frac{1 - e^{-NTU(1-m^*)}}{1 - m^* e^{-NTU(1-m^*)}} \qquad (2-14)$$

Where m^* is the capacitance ratio, which can be expressed as:

$$m^* = \frac{G_a C_{sat}}{G_{s,i} C_{p,s}} \qquad (2-15)$$

Where C_{sat} is the saturation specific heat.

Once the number of heat transfer unit and effectiveness were obtained, the air outlet enthalpy can be thus determined by:

$$h_{a,o} = h_{a,i} + \varepsilon\left(h_e - h_{a,i}\right) \qquad (2-16)$$

Based on the above $\varepsilon - NTU$ method, all the outlet conditions of the dehumidifier such as air enthalpy, temperature, and humidity can be determined by applying the inlet conditions. However, in 1992, a correction has been made by Sadasivam and Balakrishnan [116]. Since the pre-mentioned definition of NTU is not suitable when the solution flow rate is lower than air flow rate [117]. Therefore, the number of heat transfer unit should be determined by the minimum flow rate of air and desiccant solution. A good agreement has been found between the corrected $\varepsilon - NTU$ model and experimental results.

Shah and Sekulic [118] established an analytical model for the liquid desiccant dehumidifier based on pure analogy for a flat-plate heat exchanger to predict the sensible effectiveness. However, this model is unable to predict the dehumidification performance since the mass transfer of water vapour has not been taken into consideration. The latent effectiveness for cross, counter, and counter-cross flow were conducted by Nasif et al. [119], and the equations were listed below:

$$\varepsilon_{sen,cross} = 1 - exp\frac{NTU^{0.22}}{Cr}[\exp(-Cr \cdot NTU^{0.78}) - 1] \qquad (2-17)$$

$$\varepsilon_{sen,counter} = \frac{1 - \exp[-NTU(1-Cr)]}{1 - Cr \cdot \exp[-NTU(1-Cr)]} \qquad (2-18)$$

$$\varepsilon_{sen,counter-cross} = \left(\frac{A_{cross}}{A_{counter-cross}}\right)\varepsilon_{sen,cross} + \left(\frac{A_{counter}}{A_{counter-cross}}\right)\varepsilon_{sen,counter} \qquad (2-19)$$

$$\varepsilon_{lat,cross} = 1 - exp\frac{{NTU_m}^{0.22}}{m^*}\left[\exp\left(-m^* \cdot {NTU_m}^{0.78}\right) - 1\right] \qquad (2-20)$$

$$\varepsilon_{lat,counter} = \frac{1 - \exp[-NTU_m(1-Cr)]}{1 - m^* \cdot \exp[-NTU_m(1-Cr)]} \qquad (2-21)$$

$$\varepsilon_{lat,counter-cross} = \left(\frac{A_{cross}}{A_{counter-cross}}\right)\varepsilon_{lat,cross} + \left(\frac{A_{counter}}{A_{counter-cross}}\right)\varepsilon_{lat,counter} \qquad (2-22)$$

Where, A is the active area of the exchanger (m^2).

Apart from these $\varepsilon - NTU$ methods for heat and mass transfer within direct contacted dehumidifiers, further effectiveness correction has been conducted by Zhang and Niu [120] to investigate the membrane-based liquid desiccant heat and mass exchanger. Several assumptions were made before establishing the numerical model, which include: no lateral mixture between air and solution, heat conduction and vapour diffusion can be neglected, thermal properties were considered to be constant, and the heat and moisture transfer within the membrane is one-dimensional. Based on the comparison between the proposed numerical method and experimental works, a good agreement was obtain which proved that the corrections are capable for predicting the performance of parallel-plate membrane-based dehumidifier. The sensible and latent effectiveness of the membrane-based dehumidifier can be determined by:

$$\varepsilon_{sen} = 1 - exp\left(\frac{exp(-NTU^{0.78}R_1) - 1}{NTU^{-0.22}R_1}\right) \qquad (2-23)$$

$$\varepsilon_{lat} = 1 - exp\left(\frac{exp\left(-{NTU_m}^{0.78}R_1\right) - 1}{{NTU_{lat}}^{-0.22}R_1}\right) \qquad (2-24)$$

$$R_1 = \frac{(\dot{m}c_{pa})_{min}}{(\dot{m}c_{pa})_{max}} \quad (2-25)$$

$$R_2 = \frac{\dot{m}_{min}}{\dot{m}_{max}} \quad (2-26)$$

Where NTU_m is the number of mass transfer units, which can be expressed by:

$$NTU_m = \beta \cdot NTU \quad (2-27)$$

$$\beta = \frac{1}{1+\alpha} \quad (2-28)$$

$$\alpha = \frac{\gamma_m}{\gamma_c} \quad (2-29)$$

$$\gamma_c = \frac{2}{k_s} \quad (2-30)$$

Where α is the ratio of diffusive resistance to convective membrane resistance, γ_c is the convective moisture transfer resistance.

After that, the heat and mass transfer process within the hollow fibre membrane-based dehumidifier was analysed by Zhang [121], and the numerical model has been developed. By comparing with the experimental results, the maximum discrepancies in outlet air temperature and humidity were less than 3% and 10%, respectively. The proposed $\varepsilon - NTU$ model was developed according to the heat and mass transfer between air and desiccant solution, the sensible and latent effectiveness can be determined by:

$$\varepsilon_{sen} = \frac{1-\exp[-NTU(1-C_{sen})]}{1-C_{sen}\exp[-NTU(1-C_{sen})]} \quad (2-31)$$

$$\varepsilon_{lat} = \frac{1 - \exp[-NTU_m(1 - C_{lat})]}{1 - C_{lat}\exp[-NTU_m(1 - C_{lat})]} \qquad (2-32)$$

Where C_{sen} and C_{lat} are the heat and mass capacity ratio, respectively, which can be expressed by:

$$C_{sen} = \frac{(mc_p)_{min}}{(mc_p)_{max}} \qquad (2-33)$$

$$C_{sen} = \frac{m_{min}}{m_{max}} \qquad (2-34)$$

As it can be seen that the $\varepsilon - NTU$ method can solved the heat and mass transfer by purely algebraic correlations with relative high accuracy and more importantly, easy for engineers to predict the dehumidification effectiveness. Further analytical solution has also been developed by Ge et al. [122] for a parallel-plate counter-cross-flow energy exchanger. The numerical model was conducted based on Zhang's analytical equations, and the solution flow rate and desiccant concentration are assumed to be constant during the dehumidification process. The validation between analytical solution and experimental data has been made and the results show that the maximum difference was within 10%.

To sum up, the $\varepsilon - NTU$ method has more accuracy and wider acceptance in real applications than simplified method. Although iteration is inevitable, it has been widely used since it is less time consuming, high accuracy and simple to apply by engineers.

2.5.3. Finite difference method

In finite volume model, the dehumidifier unit was divided into small control volume, and the heat and mass transfer balance will be solved within each control volume. In 1980, Factor and Grossman [123] developed an one-dimensional numerical model for a counter-flow packed bed air to liquid contactor, as presented in Fig. 2-27.

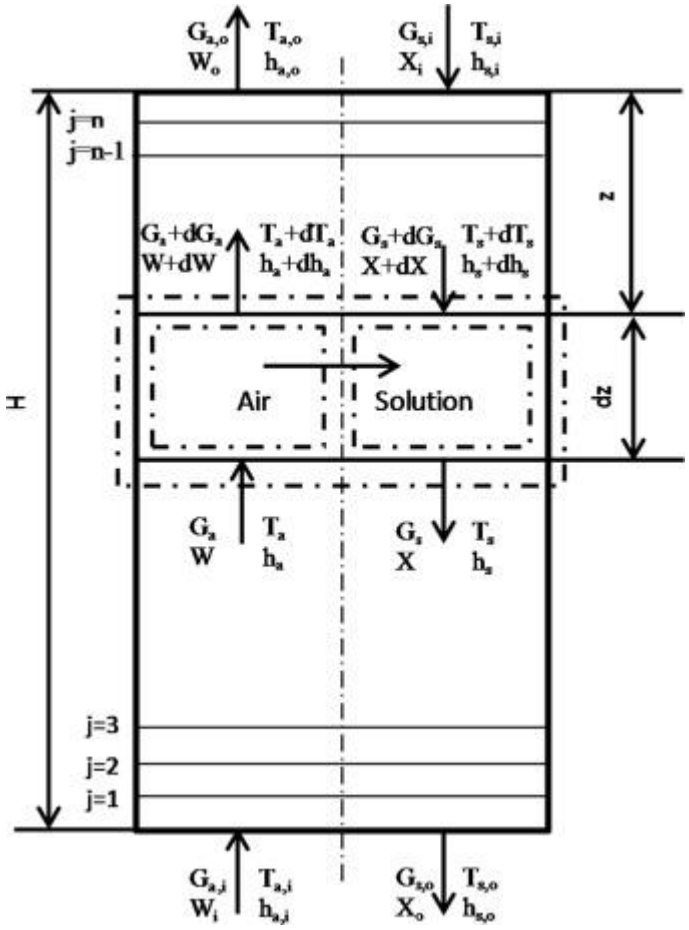

Figure 2-27 Heat and mass transfer in counter-flow arrangement [123]

As it can be seen the entire dehumidifier is divided into n parts along the air flow direction. The governing equations are developed based on the mass balance in control volume, and the interface sensible heat and mass transfer rates:

$$dG_s = G_a dW \tag{2-35}$$

$$\frac{dW}{dz} = -\frac{\alpha_D M_v A}{G_a} \ln\left(\frac{1-\frac{P_s}{P_t}}{1-\frac{P_a}{P_t}}\right) \tag{2-36}$$

$$\frac{dT_a}{dz} = -\frac{\alpha_{C,a} A(T_a - T_s)}{G_a C_{p,a}} \tag{2-37}$$

Where $\alpha_{C,a}$ and α_D are the heat and mass transfer coefficient, respectively.

In order to solve the above mentioned governing equations, the numerical integration among the flow direction of the dehumidifier is used. To start with, the outlet conditions of air and solution are presumed and the equations can be solved along the axis. By applying the boundary conditions of the model based on the inlet conditions, the calculation can be continued until the results are converged. The solving scheme flow chart of using finite difference method to analyse the heat and mass transfer within the dehumidifier is presented in Fig. 2-28 below.

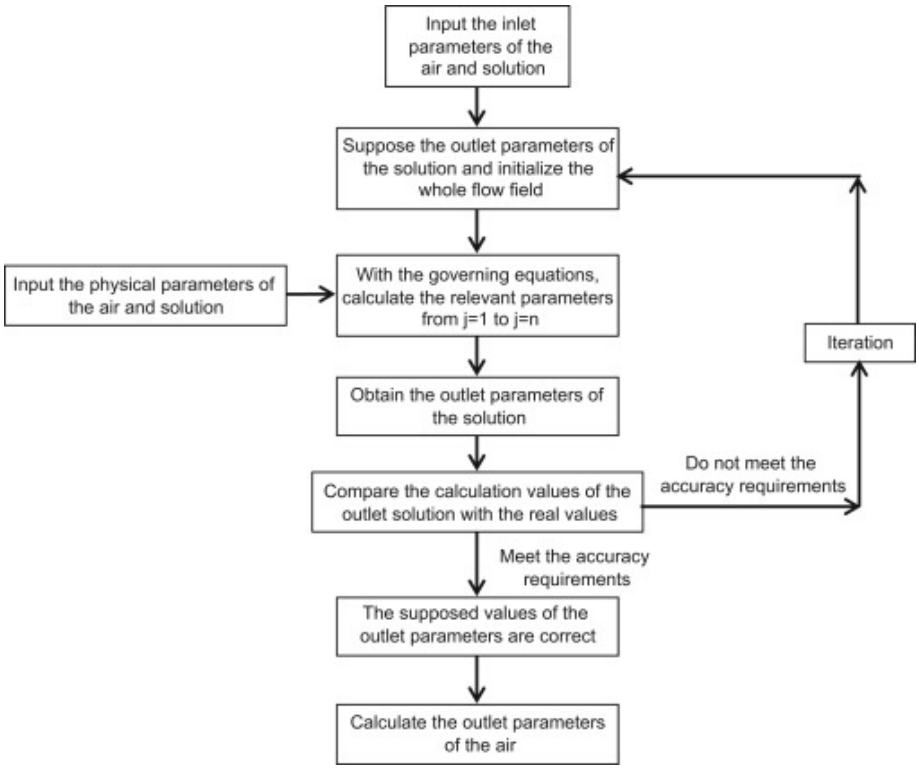

Figure 2-28 Solving scheme of finite difference method for dehumidifier [124]

Further studies for direct contact type dehumidifier were conducted based on the finite difference method. Gandhidasan et al. [125] developed a numerical model to study the heat and mass transfer process of a packed tower air-desiccant dehumidifier using finite difference method. A comprehensive parametric investigation was conducted to assess the dehumidification performance, including air inlet temperature, humidity and mass flow rate, solution inlet temperature, desiccant concentration and flow rate. Oberg and Goswami [126] evaluated the performance of a liquid desiccant air dehumidifier using finite difference method based on Factor and Grossman's model. When considering the incomplete wetting of the packing surface, necessary adjustments has been made by converting K-type mass transfer coefficient to F-type coefficient. Fumo and Goswami [42] modified the Oberg and Goswami's numerical model by applying

a new correction factor of the heat and mass transfer area. The numerical results were validated with the experimental data, and a good agreement has been obtained.

For the air and desiccant solution in cross-flow arrangement, it has also drawn a lot of interests by many researchers. Liu et al. [127] developed a two-dimensional finite difference method to predict the heat and mass transfer process within a cross-flow adiabatic liquid desiccant dehumidifier, as shown in Fig. 2-29.

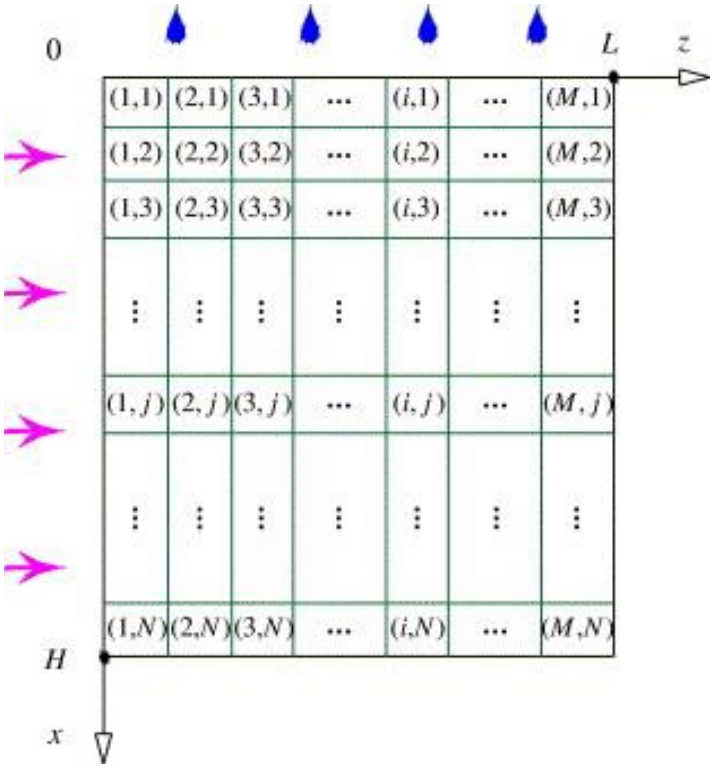

Figure 2-29 2-D schematic of cross-flow computational domain [127]

As it can be seen that the calculating domain of the x-z plane of the numerical model, and the governing equations can be discretized into this $M \times N$ grids. The discretization of governing equations can be expressed as:

$$m_a\left(h_{a,i+1,j} - h_{a,i,j}\right) = \frac{N}{M}\left(m_{s,i,j}h_{s,i,j} - m_{s,i,j+1}h_{s,i,j+1}\right) \quad (2-38)$$

$$m_a\left(W_{a,i,j} - W_{a,i+1,j}\right) = \frac{N}{M}\left(m_{s,i,j} - m_{s,i,j+1}\right) \quad (2-39)$$

$$m_{s,i,j+1} \cdot \xi_{i,j+1} = m_{s,i,j} \cdot \xi_{i,j} \quad (2-40)$$

$$h_{a,i+1,j} - h_{a,i,j} = \frac{NTU}{M}\left(h_{e,i,j} - h_{a,i,j}\right) \quad (2-41)$$

$$W_{a,i+1,j} - W_{a,i,j} = \frac{NTU}{M}\left(W_{e,i,j} - W_{a,i,j}\right) \quad (2-42)$$

Based on these equations and the inlet conditions of air and desiccant solution, the outlet conditions of the dehumidifier can be obtained. By comparing with the experimental tests, the average absolute discrepancies for enthalpy and latent effectiveness were 5.8% and 6.9%, respectively, which indicate a good agreement between experimental and numerical results.

Apart from adiabatic dehumidifier, finite difference method has also been commonly used to develop mathematical models for internally-cooled dehumidifiers. In 1998, Khan and Martinez [128] proposed the modelling method and parametric analysis of heat and moisture transfer performance of a liquid desiccant absorber, and the solution film thickness was ignored. The air and desiccant solution are in counter-flow arrangement while the desiccant and cooling water are in parallel flow direction. Ren et al. [129] developed a mathematical model as presented in Fig. 2-30. The heat and mass transfer performances during the dehumidification process have been analysed to improve the design of internally-cooled dehumidifier.

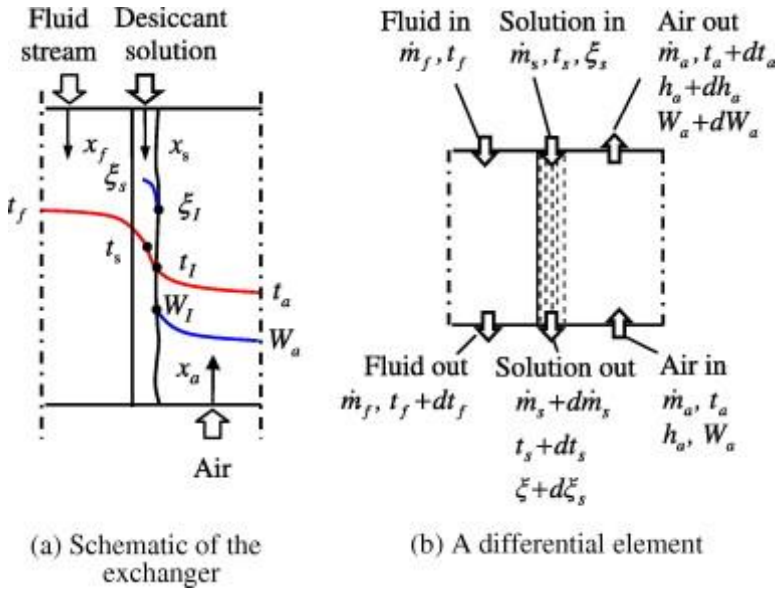

(a) Schematic of the exchanger

(b) A differential element

Figure 2-30 Numerical model of internally-cooled dehumidifier [129]

Liu et al. [130] numerically investigated an internally-cooled dehumidifier with the air and desiccant solution in counter-flow arrangement while the cooling water and solution are in cross-flow arrangement. The heat and mass transfer process for a single control element $dx \cdot dy$ is presented in Fig. 2-31.

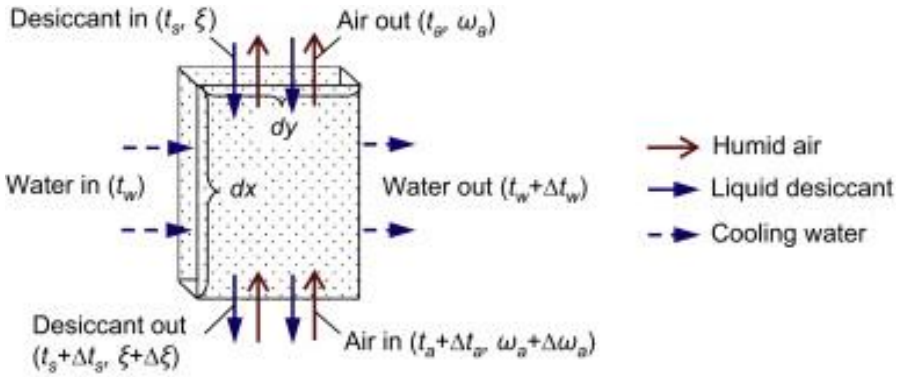

Figure 2-31 Control element for internally-cooled dehumidifier [130]

The energy and moisture conservation equations of the internally-cooled dehumidifier are:

$$m_a \frac{\partial h_a}{\partial x} = \frac{\partial (m_s h_s)}{\partial x} + C_{p,w} m_w \frac{L}{H} \cdot \frac{\partial t_w}{\partial y} \qquad (2-43)$$

$$\frac{\partial m_s}{\partial x} = m_a \frac{\partial W_a}{\partial x} \qquad (2-44)$$

$$\frac{\partial (m_s \xi)}{\partial x} = 0 \qquad (2-45)$$

The heat and mass exchange between air and desiccant solution can be expressed as:

$$\frac{\partial h_a}{\partial x} = \frac{NTU_m \cdot Le}{H} \left[(h_a - h_e) + r \cdot \left(\frac{1}{Le} - 1 \right) (W_a - W_e) \right] \qquad (2-46)$$

$$\frac{\partial W_a}{\partial x} = \frac{NTU_m}{H} (W_a - W_e) \qquad (2-47)$$

And the heat transfer between the desiccant solution and the cooling medium is:

$$\frac{\partial t_w}{\partial y} = \frac{NTU_t}{L} (t_s - t_w) \qquad (2-48)$$

Where Le is the Lewis number and NTU_t is the number of heat transfer between solution and cooling water.

The numerical modelling of membrane-based dehumidifiers using finite difference method were also conducted by many researchers. Moghaddam et al. [131] numerically investigated the steady state effectiveness of a counter flow membrane-based liquid desiccant dehumidifier. The air and solution channels are separated by semi-permeable membranes. A good agreement has been found between experimental and numerical tests. The results showed that the difference

between experiment and simulation are closer under summer cooling conditions. The schematic of his model is shown in Fig. 2-32 below:

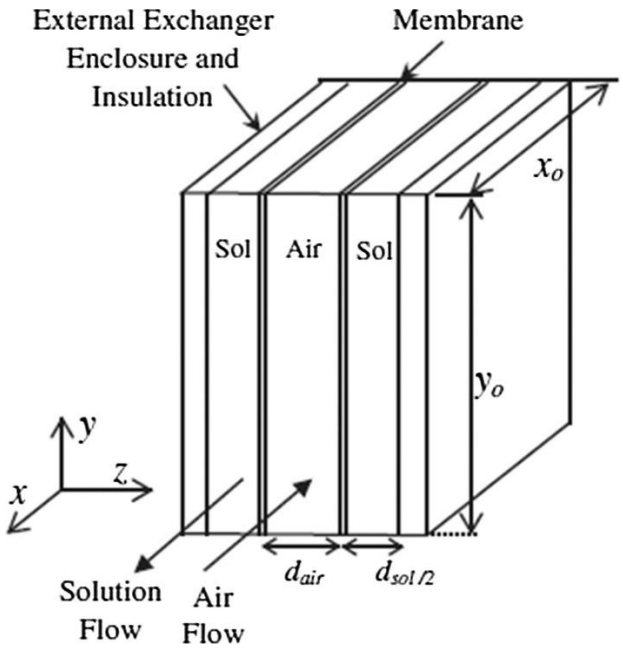

Figure 2-32 Schematic of a counter-flow small-scale single panel LAMEE [131]

Vali et al. [132] further improved the numerical model by combining the heat and mass transfer process together. The governing equations were similar to previous researches, the heat and mass transfer coefficients were assumed to be uniformed on the membrane surface. The correlation between Nusselt number and heat transfer coefficient can be expressed as:

$$Nu = \frac{\alpha d_h}{k} \qquad (2-49)$$

Similarly, mass transfer coefficient can be determined by [133]:

$$Sh = Nu \cdot Le^{-\frac{1}{3}} \qquad (2-50)$$

$$Sh = \frac{\alpha_m d_h}{D} \qquad (2-51)$$

Recently, the mathematical model for a hollow fibre membrane-based dehumidifier has been developed by Qu et al. [134] using finite difference method. The proposed model was developed by the heat and mass transfer between air and desiccant solution, the governing equations can be expressed as:

Air side energy conservation equation:

$$\frac{m_a}{n_{eq} d_h} c_{p,a} \left(\frac{\partial T_a}{\partial x}\right) = h_{ov}(T_s - T_a) \qquad (2-52)$$

Air side mass conservation equation:

$$\frac{m_a}{n_{eq} d_h} \left(\frac{\partial W_a}{\partial x}\right) = k_{ov}(W_s - W_a) \qquad (2-53)$$

Solution side energy conservation equation:

$$\frac{m_s}{n_{eq} d_h} c_{p,s} \left(\frac{\partial T_s}{\partial x}\right) = h_{ov}(T_a - T_s) + h_{cw}\rho_a k_{ov}(W_s - W_a) \qquad (2-54)$$

Solution side mass conservation equation:

$$\frac{m_s}{n_{eq} d_h} \left(\frac{\partial X_s}{\partial x}\right) = k_{ov}\rho_a(W_s - W_a) \qquad (2-55)$$

In conclusion, finite difference method has a wider range of applications compared with simplified method and $\varepsilon - NTU$ methods, and it can be adopted to almost all type of dehumidifiers. The governing equations can be discretised and solved by iteration method. Although it is time consuming, finite difference method has drawn lots of interests by many studies of liquid desiccant dehumidification process due to its high accuracy.

2.6. Summary

In this section, a comprehensive literature review focused on the liquid desiccant dehumidification technique has been conducted. The main findings from the literature review are summarized below:

- For liquid desiccant dehumidification technologies, the dehumidifier has been defined as the most critical unit and carried out by many studies. Depending on whether there is cooling medium inside the dehumidifier to restrain the temperature rise during the dehumidification process, the dehumidifier can be categorized as adiabatic type and internally-cooled type. More recently, self-cooled liquid desiccant dehumidifier has been developed to simplify the structure of internally-cooled dehumidifier.
- Membrane-based dehumidifier has been developed to overcome the desiccant carry-over problem. There are mainly two types of indirect contact type dehumidifiers, one is the parallel-plate type dehumidifier and the other is the hollow fibre type dehumidifier. Parallel-plate type has lower pressure drop for air and desiccant, while its structure is easy to construct. The design of hollow fibre dehumidifier is more complicated but it has higher heat and mass transfer potential. There were limited studies on membrane-based internally-cooled dehumidifiers due to the complexity of the configurations.
- Regenerator is considered to be another important unit for liquid desiccant dehumidification to reconcentrate the diluted solution coming out from dehumidifier. Opposite to the dehumidifier, the moisture content inside

desiccant solution can be removed by the return air. The regenerators can also be categorized into direct contact type and membrane-based type based on the heat and moisture transfer process. In order to achieve the regeneration process, the desiccant solution should normally be heated before entering the regenerator, and low-grade energy can be used including solar thermal and photovoltaic-electrodialysis.

- The complete liquid desiccant dehumidification system has been further developed by combining the dehumidifier and regenerator together in a close solution loop. Most of the previous researches have assumed that the heat and mass transfer are the same for dehumidifier and regenerator. The performance of the dehumidification system can be evaluated under steady-state or transient condition.
- There are three methods to develop the numerical model for liquid desiccant dehumidification, including simplified method, effectiveness NTU method and finite difference method. The simplified method is less time consuming since no iteration is required, but the accuracy is relatively low. It is more preferred for annual performance assessment. Effectiveness NTU method has drawn more attentions due to the fact that it is less time consuming, high accuracy and easy to apply by engineers. Finite difference method is the most commonly used approach to predict the heat and mass transfer process during the dehumidification process. Although the iteration process is more complicated, finite difference method is more suitable for component design and optimizing the operation conditions due to its high accuracy.

According to previous researches, the research gaps between previous studies and current research have been identified:

- As a newly proposed method, there are very few studies on self-cooled liquid desiccant solution, and these studies have all been conducted by direct contact type dehumidifier. However, by applying self-cooled liquid desiccant, the problem of desiccant carry-over becomes more serious, especially when evaporative coolant (ethanol) is added into desiccant solution.
- The performance evaluations of the dehumidifiers are mainly conducted by experimental works. Limited numerical models have been developed to predict the heat and mass transfer process, especially for internally-cooled dehumidifier. Among these numerical studies, none of the cooling mediums involve phase change during the dehumidification process.
- Although there are numerous researches on liquid desiccant dehumidifier, the investigations of regenerator are limited, especially for the proposed self-cooled liquid desiccant solution.
- Most of previous researches related to liquid desiccant dehumidification technologies were focused on single dehumidifier and regenerator. As a novel desiccant solution, it is essential to evaluate the dehumidification performance from the complete system perspective. So far the author's knowledge, no studies have been carried out to assess the feasibility of a complete self-cooled membrane-based liquid desiccant dehumidification system.

According to the current research gaps, the novelties of this research are:

- This research has firstly developed the idea of integrating the self-cooled liquid desiccant solution with the membrane-based dehumidifier. The problems of solution temperature rise during the dehumidification process and desiccant carry-over can be solved at the same time, without making the dehumidifier structure too complicated. More importantly, the equilibrium vapour pressure for the mixture solution of halide salt and ethanol has not been properly assessed. It is extremely essential to calculate the solution vapour pressure accurately since it is the main driving force for moisture transfer.
- In this thesis, the numerical model of a self-cooled liquid desiccant dehumidifier has be developed based on basic heat and mass transfer principles. Experimental works have also been conducted to validate with simulation results. The effects of different operation conditions on dehumidifier performance have been investigated under varies ethanol concentrations, including inlet air temperature, relative humidity, solution temperature, desiccant concentration, air and solution flow rate, circulated air temperature and mass flow rate. Section 3 develops a novel self-cooled membrane-based liquid desiccant dehumidifier and conducts a comprehensive parametric study, which can correspond to a competitive novel dehumidification technology.
- In order to reconcentrate the desiccant solution and to prevent desiccant carry-over problem, the performance of a membrane-based regenerator has been evaluated based on numerical model and experimental tests. The

influences of different operation conditions on regeneration performance have been investigated including ethanol concentration, inlet air temperature, relative humidity, solution temperature, desiccant concentration, air and solution flow rate.

- A complete membrane-based liquid desiccant dehumidification system using self-cooled liquid desiccant has been proposed in this thesis. The main components of the system include dehumidifier, regenerator, hot and cold water supply systems and heat exchangers. The steady-state numerical model of the complete system has been developed for the complete system and experimental works are conducted to validate the simulation results. The operation parameters such as ethanol concentration, dehumidifier and regenerator inlet air flow rate, solution flow rate and desiccant concentration have been selected to investigate their effects on the system performance. In order to assess the proposed self-cooled liquid desiccant solution from a holistic dehumidification system perspective, sensible and latent effectiveness, cooling output and COP are selected as the performance indices.

Section 3: Numerical and experimental analysis of a self-cooled membrane-based liquid desiccant dehumidifier

3.1. Introduction

To restrain the temperature rise of desiccant solution during dehumidification process, a self-cooled membrane-based liquid desiccant dehumidifier has been proposed by adding evaporative coolant (ethanol) into desiccant solution. In this section, the conjugate heat and mass transfer of the self-cooled membrane-based dehumidifier is evaluated by developing a numerical model using finite difference method. The experimental test is also conducted in the laboratory to validate the numerical model. The influence of varies operation parameters on the dehumidification performance are investigated, including: inlet air state (air temperature, relative humidity and flow rate); inlet desiccant solution state (solution temperature, LiCl concentration and flow rate); circulated air state (circulated air temperature and its mass flow rate) and ethanol concentrations.

The structures of **Section 3** are: **Section 3.2** shows the numerical modelling method of the proposed dehumidifier; **Section 3.3** introduces the experimental set-up in the laboratory; **Section 3.4** presents the dehumidification performance indices; **Section 3.5** shows the validation of numerical model using the experimental results; **Section 3.6** reveals the effect of different parameters on the performance of the dehumidifier; **Section 3.7** is the main conclusion of this section.

3.2. Numerical modelling

3.2.1. Model description and assumptions

The coordinate structure of the self-cooled membrane-based dehumidifier is shown in Fig. 3-1. The air and solution channels are separated by semi-permeable membranes, the process air and desiccant solution flows are crossflow, while the process air and circulated air are in counter-flow mode, respectively. One air channel and one neighbouring solution channel are selected as the calculating domain. During the dehumidification process, there are heat and mass transfer between the process air and desiccant solution. The driven force of the heat transfer process is the temperature difference between the air and desiccant solution, while the mass transfer is driven by the water surface vapour pressure difference.

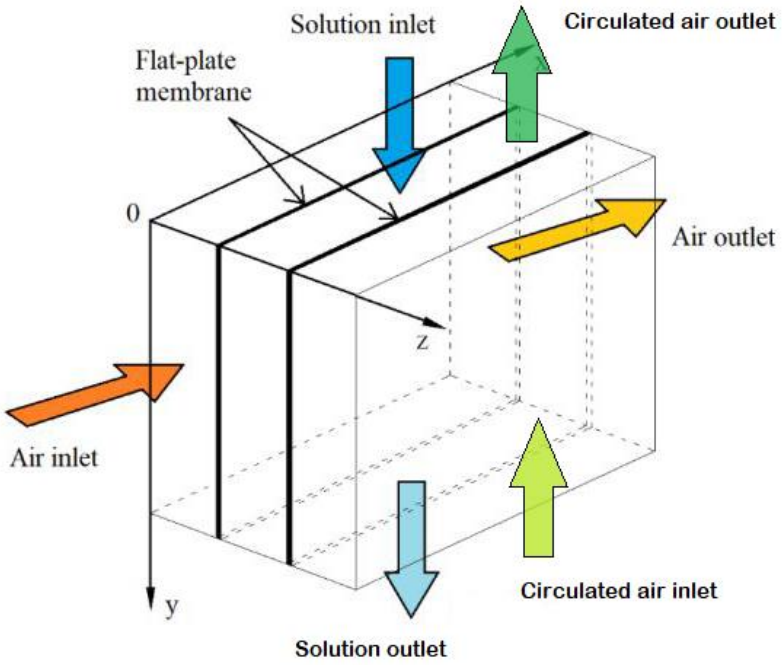

Figure 3-1 Structure of numerical modelling

The heat and mass transfer processes of the proposed self-cooled membrane-based dehumidifier are presented in Fig. 3-2. The left side of this figure shows the process of heat transfer while the right side is the mass transfer process. The temperature difference between the process air and desiccant solution leads to sensible heat transfer process ①, and the temperature difference between the circulated air and solution leads to heat transfer process ②. The mass transfer of water ③ and ethanol ④ during the dehumidification process cause the variation of solution concentration ⑤. Meanwhile, in the mass transfer process, the condensation of water vapour ⑥ and the evaporation of ethanol ⑦ lead to the change of latent heat. The conservation of energy for the self-cooled dehumidifier has to be expressed by considering both the sensible and latent heat transfer. The sensible heat transfer process ⑧ and latent heat transfer process ⑩ affect the air temperature, while the circulated air temperature is affected by heat transfer processes ⑨ and ⑪. All these heat transfer processes (⑧, ⑨, ⑩ and ⑪) have impact on the temperature of the liquid desiccant solution. The temperature change of the process air, desiccant solution and circulated air also influence the heat transfer process ① and ②. Moreover, the temperature change can affect the equilibrium specific humidity of the desiccant solution ⑫, thus affecting the driving force of mass transfer process. The mass transfer of water ⑬, ethanol ⑭ and the concentration change of solution ⑮ have also influenced the mass transfer process for both water and ethanol. As a result, the heat and mass transfer are interacted with each other, the condensation of water and evaporation of ethanol affect the temperatures of the solution, process air and circulated air. The variation of temperature can also influence the specific humidity of desiccant solution, which is the driving force for mass transfer process.

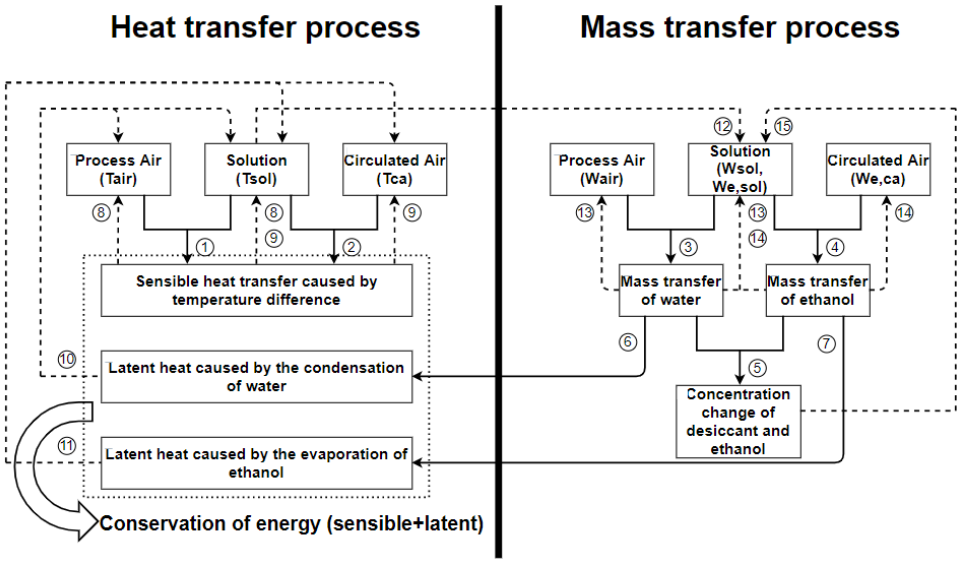

Figure 3-2 The interrelationship between heat and mass transfer processes

Several assumptions were made before establishing the numerical model, which include:

- The dehumidifier is well thermal insulated, no heat transfer between the dehumidifier and outdoor environment.
- The processes of heat and mass transfer within the dehumidifier are in steady-state.
- Mass and heat transfer only take place in z direction and axial conduction is neglected.
- The air and solution streams in both solution channels and air channels are in laminar flow mode.
- All the fluids in air and solution channels are Newtonian and they are considered to maintain constant thermophysical properties (density, thermal conductivity, and specific heat capacity).
- All of the fluids are fully developed, and the entrance effects are neglected.

- The desiccant solution is considered to be evenly sprayed in dehumidifier, the heat and mass transfer interfaces are the same.
- The mass transfer of water takes place the processed air and desiccant solution while the mass transfer of ethanol occurs between desiccant solution and circulated air only, there is no heat and mass transfer between the processed and circulated air directly.

3.2.2. Governing equations

Overall, there are three fluids inside the proposed dehumidifier which includes the process air, desiccant solution and circulated air. As a well-insulated heat and mass exchanger, the heat and mass transfer process should meet the conservation law of energy and mass, the energy conservation can be expressed as:

$$m_{air}\left(h_{air,out} - h_{air,in}\right) + m_{sol}\left(h_{sol,out} - h_{sol,in}\right) + m_{ca}\left(h_{ca,out} - h_{ca,in}\right) = 0 \qquad (3-1)$$

The mass conservation of water is:

$$m_{air}\left(W_{air,out} - W_{air,in}\right) + m_{sol}\left(X_{sol,out} - X_{sol,in}\right) = 0 \qquad (3-2)$$

The mass conservation of ethanol is:

$$m_{ca}\left(W_{eth,out} - W_{eth,in}\right) + m_{sol}\left(C_{eth,out} - C_{eth,in}\right) = 0 \qquad (3-3)$$

Where subscript air is the process air in air channel, sol is the desiccant solution and ca is the circulated air in solution channel, subscript in and out represent the inlet and outlet condition, m is the mass flow rate (kg/s), h is the specific enthalpy (J/kg), W and W_{eth} are the specific humidity of water and ethanol,

respectively, X_{sol} is the mass concentration of water in desiccant solution (kg/kg) and C_{eth} is the mass concentration of ethanol (kg/kg).

The process of heat and mass transfer in the self-cooled liquid desiccant dehumidifier can be simplified as a two-dimensional model, which is presented in Fig. 3-3. The process air flow in x direction and the desiccant solution flow in y direction. The height of the dehumidifier channel is H and the length is L. Further governing equations are generated based on the analyzation of the element $dA = dx \times dy$.

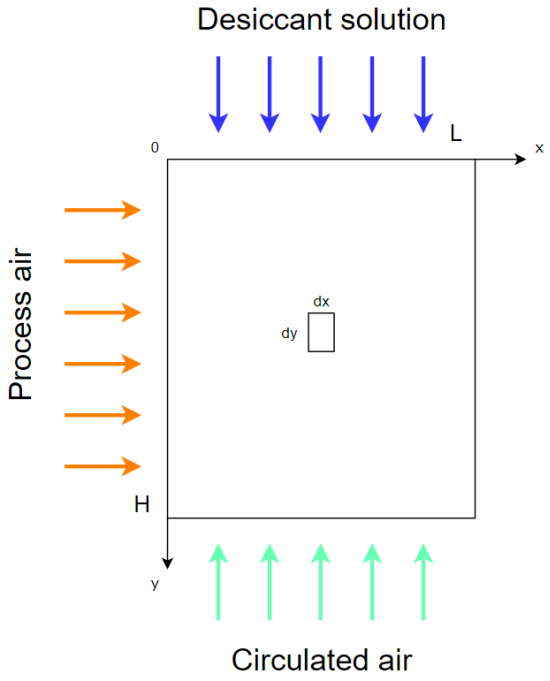

Figure 3-3 2D flow direction of the dehumidifier

Based on the conservation of energy, the energy loss of process air is equal to the energy gain of desiccant solution and circulated air, which can be expressed as:

$$\frac{m_{air}}{H}\frac{\partial h_{air}}{\partial x} + \frac{m_{sol}}{L}\frac{\partial h_{sol}}{\partial y} - \frac{m_{ca}}{L}\frac{\partial h_{ca}}{\partial y} = 0 \qquad (3-4)$$

Where H and L are the height and length of the dehumidifier (m), m is the mass flow rate (kg/s), h is the specific enthalpy (J/kg), subscript air is the process air in air channel, sol is the desiccant solution and ca is the circulated air in solution channel.

The mass conservation of water between solution and process air is:

$$\frac{m_{air}}{H}\frac{\partial W_{air}}{\partial x}+\frac{m_{sol}}{L}\frac{\partial X_{sol}}{\partial y}=0 \qquad (3-5)$$

Where X_{sol} is the mass concentration of water in desiccant solution(kg/kg), which can be calculated by:

$$X_{sol}=1-C_{sol}-C_{eth} \qquad (3-6)$$

Where C_{sol} and C_{eth} are the mass concentration of LiCl and ethanol (kg/kg), respectively.

The mass conservation of ethanol between solution and circulated air is:

$$-\frac{m_{ca}}{L}\frac{\partial W_{eth}}{\partial y}+\frac{m_{sol}}{L}\frac{\partial C_{eth}}{\partial y}=0 \qquad (3-7)$$

Where W_{eth} is the specific humidity of ethanol in circulated air (kg/kg).

For the process air in air channel, the control volume used for the heat transfer is illustrated in Fig 3-4.

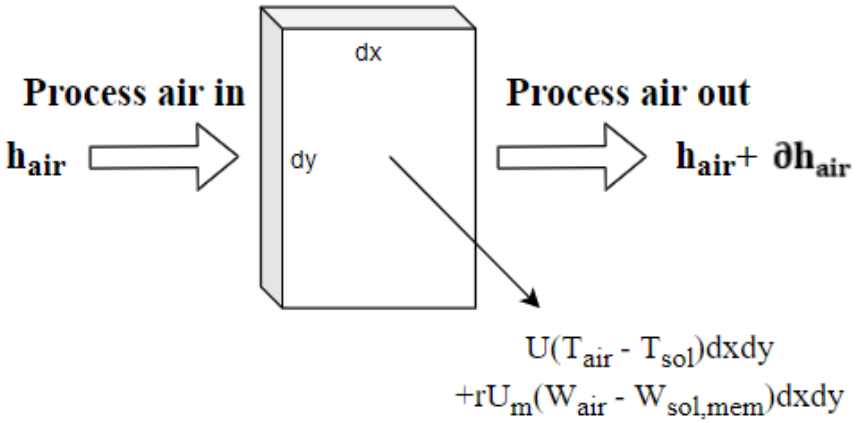

Figure 3-4 Control volume for heat transfer of process air in air channel

The heat transfer governing equation of the process air can be expressed as:

$$\frac{m_{air}}{H}\frac{\partial h_{air}}{\partial x}dxdy = -\left[U(T_{air} - T_{sol}) + r \cdot U_m\left(W_{air} - W_{sol,mem}\right)\right]dxdy \quad (3-8)$$

Where T_{air} and T_{sol} are the temperature of process air and desiccant solution, respectively, r is the condensation heat of water (J/kg), U_m (kg/m^{2}s) and U (W/m^{2}K) are the convective mass and heat transfer coefficient between air channel and solution channel, respectively, which can be defined as:

$$U_m = \left[\frac{1}{\alpha_{m,air}} + \frac{\delta_{mem}}{k_{m,mem}}\right]^{-1} \quad (3-9)$$

$$U = \left[\frac{1}{\alpha_{air}} + \frac{\delta_{mem}}{k_{mem}} + \frac{1}{\alpha_{sol}}\right]^{-1} \quad (3-10)$$

Where, δ_{mem} is the membrane thickness (m), $\alpha_{m,air}$ is the convective mass transfer coefficient of water (kg/m^{2}s), $k_{m,mem}$ is the permeability of membrane (kg/ms), k_{mem} is the thermal conductivity of membrane (W/mK), α_{air} and α_{sol}

are the convective heat transfer coefficient of air and solution (W/m^2K), respectively.

The control volume for mass transfer of water in air channel is presented in Fig. 3-5.

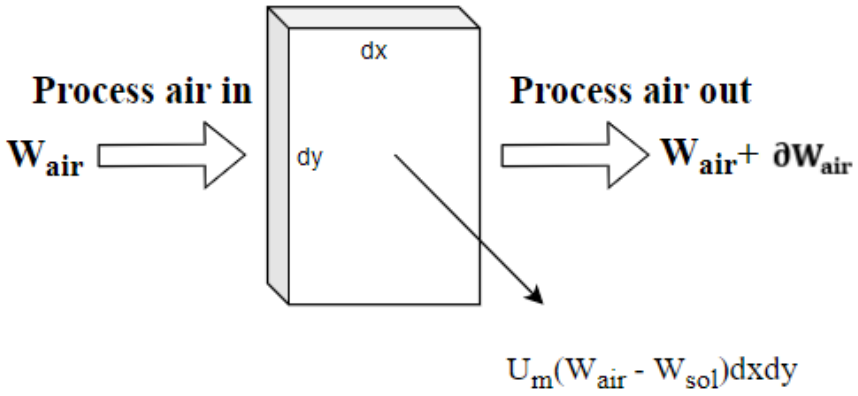

Figure 3-5 Control volume for mass transfer of water in air channel

Thus, the mass transfer governing equation of water content for process air is:

$$\frac{m_{air}}{H}\frac{\partial W_{air}}{\partial x}dxdy = -U_m\left(W_{air} - W_{sol,mem}\right)dxdy \qquad (3-11)$$

Meanwhile, the specific enthalpy of air can be expressed as:

$$h_{air} = C_{p,air}T_{air} + r \cdot W_{air} \qquad (3-12)$$

Where, $C_{p,air}$ is the specific heat capacity of air.

By combining equation $(3-8)$, $(3-11)$ and $(3-12)$, the heat transfer governing equation of process air can be converted to:

$$\frac{m_{air}}{H}\frac{\partial T_{air}}{\partial x}C_{p,air}dxdy = -U(T_{air} - T_{sol})dxdy \qquad (3-13)$$

For the self-cooled desiccant solution, the control volume used for the heat transfer is presented in Fig. 3-6.

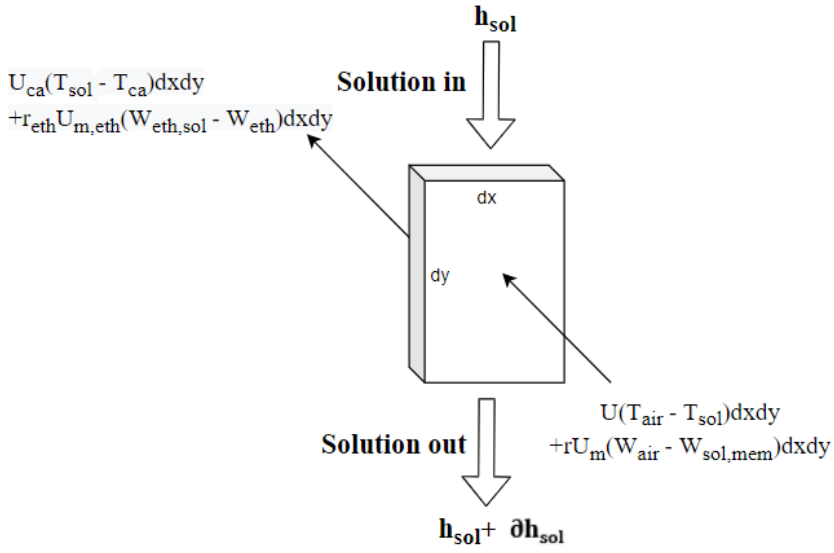

Figure 3-6 Control volume for energy transfer of desiccant solution

The energy balance of the solution stream consists the sensible heat transfer owing to temperature difference between the air channel and solution channel, as well as temperature difference between solution and circulated air; and latent heat from water vapour condensation and the evaporation of ethanol. Thus, the heat transfer governing equation of the desiccant solution can be expressed as:

$$\frac{m_{sol}}{L}\frac{\partial h_{sol}}{\partial y}dxdy = U(T_{air} - T_{sol})dxdy + r \cdot U_m\left(W_{air} - W_{sol,mem}\right)dxdy -$$

$$U_{ca}(T_{sol} - T_{ca})dxdy - r_{eth} \cdot U_{m,eth}\left(W_{eth,sol} - W_{eth}\right)dxdy \qquad (3-14)$$

Where, T_{ca} is the circulated air temperature (℃), r_{eth} is the condensation heat of ethanol (J/kg),

According to previous research, the difference of mass concentration of desiccant solution between inlet and outlet during the dehumidification process is less than

0.8% for most cases [42], which means that the relationship between specific enthalpy and temperature of the desiccant solution can be considered as:

$$\partial h_{sol} = C_{p,sol}\partial T_{sol} \qquad (3-15)$$

Where, $C_{p,sol}$ is the specific heat capacity of desiccant solution.

Therefore, the heat transfer governing equation of desiccant solution is:

$$C_{p,sol}\frac{m_{sol}}{L}\frac{\partial T_{sol}}{\partial y}dxdy = r \cdot U_m\left(W_{air} - W_{sol,mem}\right)dxdy + U(T_{air} - T_{sol})dxdy - U_{ca}(T_{sol} - T_{ca})dxdy - r_{eth} \cdot U_{m,eth}\left(W_{eth,sol} - W_{eth}\right) \quad (3-16)$$

The control volume for mass transfer of water in solution channel is presented in Fig. 3-7.

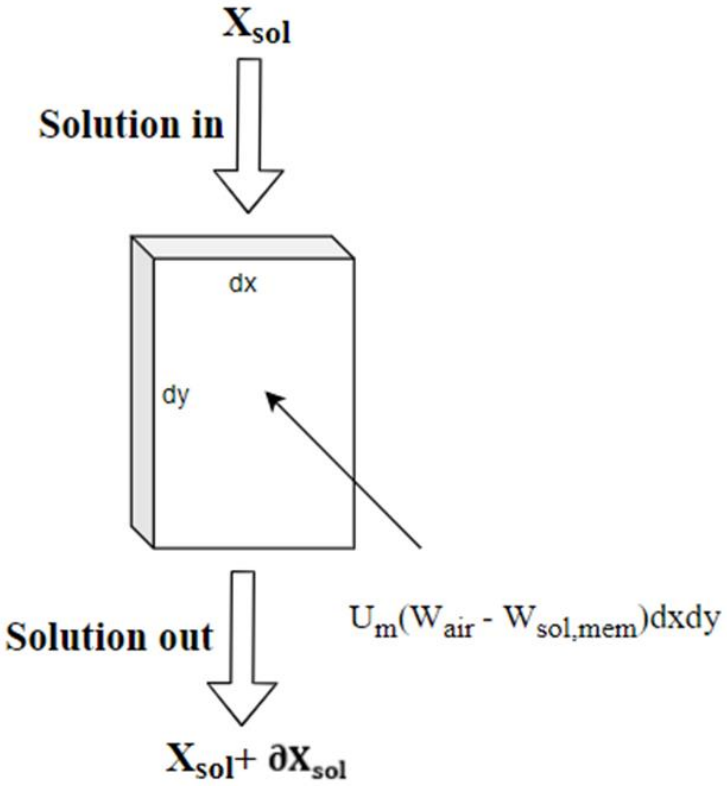

Figure 3-7 Control volume for mass transfer of water in solution channel

By combining equation $(3-5)$ and $(3-11)$, the governing equation for mass transfer of water in solution channel can be expressed as:

$$\frac{m_{sol}}{L}\frac{\partial X_{sol}}{\partial y}dxdy = U_m\left(W_{air} - W_{sol,mem}\right)dxdy \qquad (3-17)$$

The control volume for mass transfer of ethanol in desiccant solution is presented in Fig. 3-8.

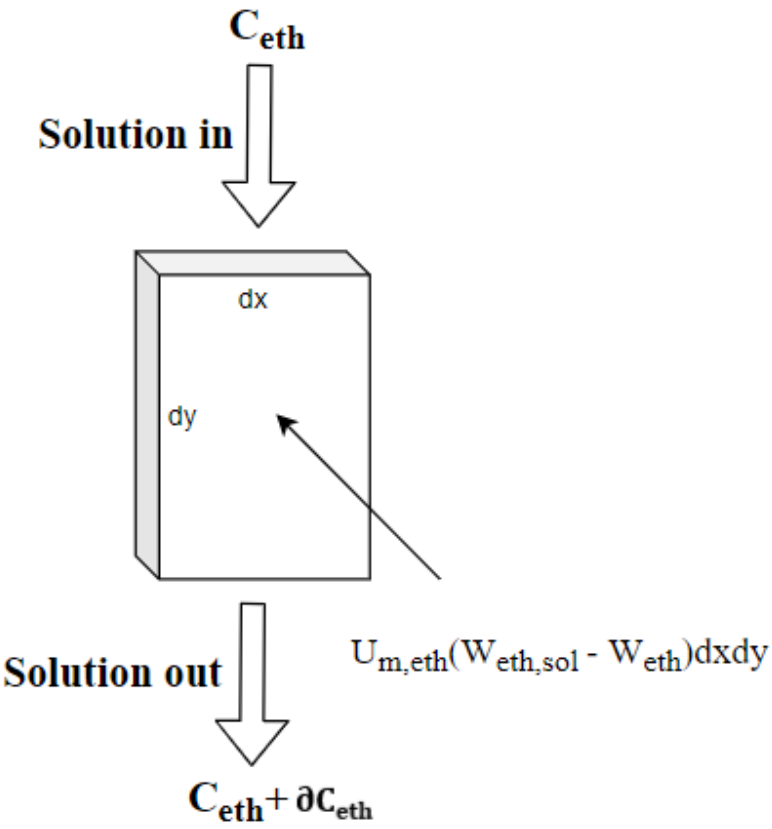

Figure 3-8 Control volume for mass transfer of ethanol in desiccant solution

For heat transfer between solution and circulated air in the solution channel, the flow directions between desiccant solution and circulated air were counter flow. The mass balance between solution and air stream was developed by the mass conservation of ethanol. The governing equations is:

$$\frac{m_{sol}}{L}\frac{\partial C_{eth}}{\partial x}dxdy = -U_{m,eth}\left(W_{eth,sol} - W_{eth}\right)dxdy \qquad (3-18)$$

Where C_{eth} is the mass concentration of ethanol in liquid desiccant.

For the circulated air in solution channel, the control volume of heat transfer is shown in figure 3-9.

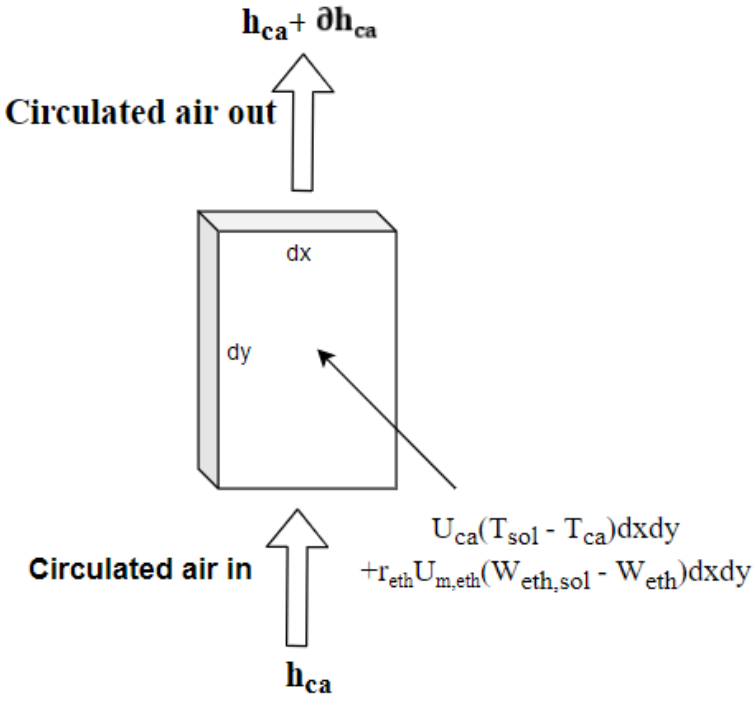

Figure 3-9 Control volume for heat transfer of circulated air in solution channel

The heat transfer governing equation of circulated air is:

$$\frac{m_{ca}}{L}\frac{\partial h_{ca}}{\partial y}dxdy = -\left[U_{ca}(T_{sol} - T_{ca}) + r_{eth}\cdot U_{m,eth}\left(W_{eth,sol} - W_{eth}\right)\right]dxdy \qquad (3-19)$$

Where r_{eth} is the condensation heat of ethanol (J/kg).

Similar to the heat transfer governing equation for process air, the governing equation can be converted to:

$$\frac{m_{ca}}{L}\frac{\partial T_{ca}}{\partial y}dxdy = -U_{ca}(T_{sol} - T_{ca})dxdy \qquad (3-20)$$

The control volume for mass transfer of ethanol in circulated air is presented in Fig 3-10.

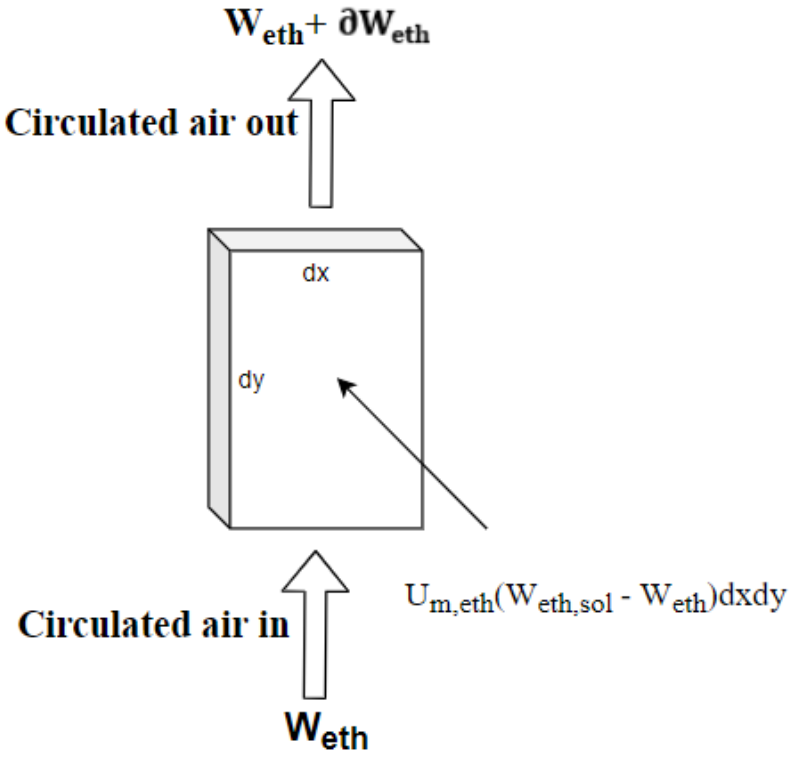

Figure 3-10 Control volume for mass transfer of ethanol in circulated air

The mass transfer governing equation of ethanol is:

$$\frac{m_{ca}}{L}\frac{\partial W_{eth}}{\partial y}dxdy = -U_{m,eth}\left(W_{eth,sol} - W_{eth}\right)dxdy \qquad (3-21)$$

To sum up, Eqs. $(3-11)$, $(3-13)$, $(3-16)$, $(3-17)$, $(3-18)$, $(3-20)$ and $(3-21)$ provide a comprehensive description of the heat and mass transfer phenomena with each elemental control volume in the proposed self-cooled

liquid desiccant dehumidifier. Further details of solving the governing equations have been presented in the following sections.

3.2.3. Boundary conditions

The boundary conditions for air channel:

$$W_{air} = W_{air,in}\ at\ x = 0 \qquad (3-22)$$

$$T_{air} = T_{air,in}\ at\ x = 0 \qquad (3-23)$$

The boundary conditions for solution channel:

$$X_{sol} = X_{sol,in}, at\ y = 0 \qquad (3-24)$$

$$T_{sol} = T_{sol.in}, at\ y = 0 \qquad (3-25)$$

$$C_{eth} = C_{eth,in}, at\ y = 0 \qquad (3-26)$$

$$W_{eth} = W_{eth,in}\ at\ y = H \qquad (3-27)$$

$$T_{ca} = T_{ca,in}, at\ y = H \qquad (3-28)$$

To solve the governing equations between air channel and solution channel, mass transfer equation on membrane surface are established:

$$U_m(W_{air} - W_{sol,mem}) = \alpha_{m,sol}(C_{sol} - C_{sol,mem}) \qquad (3-29)$$

Where, $\alpha_{m,sol}$ is the solution side mass transfer coefficient (kg/m^{2}s) and $C_{sol,mem}$ is the LiCl concentration on the membrane surface.

Heat transfer boundary equation on the membrane surface is developed as:

$$r \cdot U_m(W_{air} - W_{sol,mem}) + U(T_{air} - T_{sol,mem}) = \alpha_{sol}(T_{sol,mem} - T_{sol}) \qquad (3-30)$$

Where, α_{sol} is the convective heat transfer coefficient between air channel and solution channel .

3.2.4. Normalization of governing equations

To normalize the governing equations, several dimensionless properties have been defined.

Dimensionless length and height are defined by:

$$\mathrm{x}^{*} = \frac{\mathrm{x}}{\mathrm{L}} \qquad (3-31)$$

$$\mathrm{y}^{*} = \frac{\mathrm{y}}{\mathrm{H}} \qquad (3-32)$$

Dimensionless temperature and humidity ratio are defined by:

$$\mathrm{T}^{*} = \frac{\mathrm{T}-\mathrm{T}_{\mathrm{air,in}}}{\mathrm{T}_{\mathrm{sol,in}}-\mathrm{T}_{\mathrm{air,in}}} \qquad (3-33)$$

$$\mathrm{W}^{*} = \frac{\mathrm{W}-\mathrm{W}_{\mathrm{air,in}}}{\mathrm{W}_{\mathrm{sol,in}}-\mathrm{W}_{\mathrm{air,in}}} \qquad (3-34)$$

$$W_D = \mathrm{W}_{\mathrm{sol,in}} - \mathrm{W}_{\mathrm{air,in}} \qquad (3-35)$$

The mass flow rate ratio are defined by:

$$m^{*} = \frac{\dot{m_{sol}}}{\dot{m}_{air}} \qquad (3-36)$$

$$m_{ca}{}^{*} = \frac{\dot{m_{sol}}}{\dot{m}_{ca}} \qquad (3-37)$$

The thermal capacity ratio are defined by:

$$Cr^{*} = \frac{(\dot{m}\, c_p)_{sol}}{\dot{m}_{air} c_{p,air}} \qquad (3-38)$$

$$Cr_{ca}{}^{*} = \frac{(\dot{m}\, c_p)_{sol}}{\dot{m}_{ca} c_{p,air}} \qquad (3-39)$$

The operating factor are defined by:

$$h^{*} = \frac{\omega_{\mathrm{sol,in}} - \omega_{\mathrm{air,in}}}{\mathrm{T_{sol,in}} - \mathrm{T_{air,in}}} \times \frac{r}{c_{p,air}} \qquad (3-40)$$

$$h_e{}^{*} = \frac{\omega_{\mathrm{sol,in}} - \omega_{\mathrm{air,in}}}{\mathrm{T_{sol,in}} - \mathrm{T_{air,in}}} \times \frac{r_{eth}}{c_{p,air}} \qquad (3-41)$$

The number of mass transfer units are defined by:

$$\mathrm{NTU_m} = \frac{\mathrm{U_m A}}{\dot{\mathrm{m}}_{\mathrm{air}}} \qquad (3-42)$$

$$\mathrm{NTU_{m,ca}} = \frac{\mathrm{U_{m,eth} A}}{\dot{\mathrm{m}}_{\mathrm{ca}}} \qquad (3-43)$$

$$\mathrm{NTU_{m,sol}} = \frac{\alpha_{\mathrm{m,sol}} \mathrm{A}}{\dot{\mathrm{m}}_{\mathrm{air}}} \qquad (3-44)$$

The number of heat transfer units are defined by:

$$\mathrm{NTU} = \frac{\mathrm{UA}}{\dot{\mathrm{m}}_{\mathrm{air}} \mathrm{c_{p,air}}} \qquad (3-45)$$

$$\mathrm{NTU_{ca}} = \frac{\mathrm{U_{ca} A}}{\dot{\mathrm{m}}_{\mathrm{ca}} \mathrm{c_{p,air}}} \qquad (3-46)$$

$$\mathrm{NTU_{sol}} = \frac{\alpha_{\mathrm{sol}} \mathrm{A}}{\dot{\mathrm{m}}_{\mathrm{air}} \mathrm{c_{p,air}}} \qquad (3-47)$$

Where A is the total membrane contact area (m^2).

The normalization process of the mass transfer governing equation of process air is selected as a calculation example presented below, the rest normalization method for governing equations will be shown in Appendix A.

For mass transfer governing equation of process air:

$$\frac{m_{air}}{H}\frac{\partial W_{air}}{\partial x} = -U_m\left(W_{air} - W_{sol,mem}\right) \quad (3-48)$$

Times $\frac{LH}{m_{air}}$ for both sides:

$$\frac{\partial W_{air}}{\partial x^*} = -NTU_m\left(W_{air} - W_{sol,mem}\right) \quad (3-49)$$

Divided $(\mathrm{W_{sol,in}} - \mathrm{W_{air,in}})$ for both sides, the governing equation can be converted to:

$$\frac{\partial {W_{air}}^*}{\partial x^*} = -NTU_m\left({W_{air}}^* - {W_{sol,mem}}^*\right) \quad (3-50)$$

The normalized governing equations of the self-cooled liquid desiccant dehumidifier are listed below:

$$\frac{\partial {W_{air}}^*}{\partial x^*} = -NTU_m\left({W_{air}}^* - {W_{sol,mem}}^*\right) \quad (3-51)$$

$$\frac{\partial {T_{air}}^*}{\partial x^*} = -NTU\left({T_{air}}^* - {T_{sol}}^*\right) \quad (3-52)$$

$$\frac{\partial {T_{sol}}^*}{\partial y^*} = NTU_m h^* Cr^*\left({W_{air}}^* - {W_{sol,mem}}^*\right) + NTUCr^*\left({T_{air}}^* - {T_{sol}}^*\right) - NTU_{m,ca} {h_e}^* {Cr_{ca}}^*\left({W_{eth,sol}}^* - {W_{eth}}^*\right) - NTU_{ca} {Cr_{ca}}^*\left({T_{sol}}^* - {T_{ca}}^*\right) \quad (3-53)$$

$$\frac{\partial X_{sol}}{\partial y^*} = NTU_m W_D \frac{1}{m^*}\left({W_{air}}^* - {W_{sol,mem}}^*\right) \quad (3-54)$$

$$\frac{\partial C_{eth}}{\partial y^*} = NTU_{m,ca} W_D \frac{1}{{m_{ca}}^*}\left({W_{eth,sol}}^* - {W_{eth}}^*\right) \quad (3-55)$$

$$\frac{\partial {T_{ca}}^*}{\partial y^*} = -NTU_{ca}\left({T_{sol}}^* - {T_{ca}}^*\right) \quad (3-56)$$

$$\frac{\partial {W_{eth}}^*}{\partial y^*} = -NTU_{m,ca}\left({W_{eth,sol}}^* - {W_{eth}}^*\right) \quad (3-57)$$

The mass and heat transfer governing equations on membrane surface can be normalized as:

$$NTU_m W_D\left(W_{air}{}^* - W_{sol,mem}{}^*\right) = NTU_{m,sol}\left(C_{sol} - C_{sol,mem}\right) \quad (3-58)$$

$$NTU_m h^*\left(W_{air}{}^* - W_{sol,mem}{}^*\right) + NTU\left(T_{air}{}^* - T_{sol,mem}{}^*\right) = NTU_{sol}\left(T_{sol,mem}{}^* - T_{sol}{}^*\right) \quad (3-59)$$

3.2.5. Discretization of governing equations

Governing equations are solved by finite difference method and discretized by a backward difference scheme. Discretization equations are shown below:

$$W_{air(m,n+1)}{}^* - W_{air(m,n)}{}^* = -dx^* NTU_m\left[W_{air(m,n+1)}{}^* - W_{sol,mem(m,n+1)}{}^*\right] \quad (3-60)$$

$$T_{air(m,n+1)}{}^* - T_{air(m,n)}{}^* = -dx^* NTU\left[T_{air(m,n+1)}{}^* - T_{sol(m,n+1)}{}^*\right] \quad (3-61)$$

$$T_{sol(m+1,n)}{}^* - T_{sol(m,n)}{}^* = dy^* NTU_m h^* Cr^*\left(W_{air(m+1,n)}{}^* - W_{sol,mem(m+1,n)}{}^*\right) + dy^* NTUCr^*\left(T_{air(m+1,n)}{}^* - T_{sol(m+1,n)}{}^*\right) - dy^* NTU_{m,ca} h_e{}^* Cr_{ca}^*\left(W_{eth,sol(m+1,n)}{}^* - W_{eth(m+1,n)}{}^*\right) - dy^* NTU_{ca} Cr_{ca}^*\left(T_{sol(m+1,n)}{}^* - T_{ca(m+1,n)}{}^*\right) \quad (3-62)$$

$$X_{sol(m+1,n)} - X_{sol(m,n)} = dy^* NTU_m W_D \frac{1}{m^*}\left[W_{air(m+1,n)}{}^* - W_{sol,mem(m+1,n)}{}^*\right] \quad (3-63)$$

$$C_{eth(m+1,n)} - C_{eth(m,n)} = dy^* NTU_{m,ca} W_D \frac{1}{m^*}\left[W_{eth,sol(m+1,n)}{}^* - W_{eth(m+1,n)}{}^*\right] \quad (3-64)$$

$$T_{ca(m+1,n)}{}^* - T_{ca(m,n)}{}^* = -dy^* NTU_{ca}\left[T_{sol(m+1,n)}{}^* - T_{ca(m+1,n)}{}^*\right] \quad (3-65)$$

$$W_{eth(m+1,n)}{}^{*} - W_{eth(m,n)}{}^{*} = -dy^{*}NTU_{m,ca}\left[W_{eth,sol(m+1,n)}{}^{*} - W_{eth(m+1,n)}{}^{*}\right] \quad (3-66)$$

Where m is the number of grids in x direction, and n is number of grids in y direction.

3.2.6. Heat and mass transfer coefficients

For heat and mass transfer coefficient between desiccant solution and process air were determined based on local Nusselt and Sherwood number, which can be expressed as:

$$Nu = \frac{\alpha d_h}{k} \quad (3-67)$$

Where d_h is the hydraulic diameter and k is the thermal conductivity of desiccant solution.

$$Sh = \frac{\alpha_m d_h}{D_m} \quad (3-68)$$

Where D_m is the mass diffusivity of water.

For the Nusselt and Sherwood number within membrane-based dehumidifier, they can be obtained by presented work conducted by Huang et al [135]. Thus the overall heat and mass transfer coefficient and the number of heat and mass transfer unit between desiccant solution and processed air can be determined.

Similarly, for heat and mass transfer between circulated air and desiccant solution, the convective heat and mass transfer coefficient is also determined by Nusselt and Sherwood number, the Nusselt and Sherwood number is a universal function of Reynold, Prandtl and Schmidt number, which can be expressed as:

$$Re = \frac{ud_h}{v} \quad (3-69)$$

$$Pr = \frac{v}{D} \quad (3-70)$$

$$Sc = \frac{v}{D_m} \quad (3-71)$$

Where u is the mean fluid velocity (m/s); v is fluid kinematic viscosity (m^2/s); D is fluid thermal diffusivity (m^2/s).

The relationship between Nusselt number, Reynold number and Prandtl number is based on the empirical correlation [136]:

$$Nu = CRe^m Pr^{\frac{1}{3}} \quad (3-72)$$

In addition, the Sherwood number can be determined by:

$$Sh = CRe^m Sc^{\frac{1}{3}} \quad (3-73)$$

Where C and m are constant number which can be obtained from [136].

3.2.7. Thermodynamic parameters of air and desiccant solution

Several properties of the air and liquid desiccant solution were evaluated to establish the numerical model, which were listed in the following sections.

The air specific humidity W_{air} can be calculated by:

$$W_{air} = \frac{AH}{\rho_{air}} \quad (3-74)$$

Where, ρ_{air} is the air density (kg/m^3), AH is the air absolute humidity (kg/m^3).

The air absolute humidity can be derived from the relative humidity RH (%) by using the following correlation [137]:

$$AH = 10^{-3} \times \frac{6.112 \times e^{\left(\frac{17.67 \times T_{air}}{T_{air}+243.5}\right) \times RH \times 2.1674}}{273.15 + T_{air}} \qquad (3-75)$$

The solution equilibrium specific humidity W_{sol} can define by vapour pressure given by [138]:

$$W_{sol} = 0.622 \frac{P_{sol}}{P - P_{sol}} \qquad (3-76)$$

Where, P is the atmospheric pressure (Pa) and P_v is the vapour pressure of desiccant solution (Pa)

As a novel self-cooled desiccant by mixing ethanol with lithium chloride aqueous solution, it is critical to investigate the vapour pressure of the desiccant solution since it is the driving force for water in air to be transferred into desiccant solution in dehumidifier. Lithium chloride, water and ethanol mixture is a non-ideal solution due to presence bonding between water and ethanol molecules. Thus the vapour pressure of the desiccant solution proposed in this project is deviated from the result predicted by ideal solution theory. Therefore, a more accurate method is selected to calculate the vapour pressure using the NRTL (non-random two liquid) equation conducted by Chen et al. [139].

The vapour pressure of desiccant solution P_{sol} can be calculated by:

$$P_{sol} = a_w P_w \qquad (3-77)$$

Where a_w is the activity of water in mixture solution, P_w is the vapour pressure of pure water.

The vapour pressure of water under different temperature can be calculated by:

$$P_w = 0.61094e^{\left(\frac{17.625T_{sol}}{T_{sol}+243.04}\right)} \quad (3-78)$$

The activity of water a_w is determined by:

$$a_w = x_w f_s \quad (3-79)$$

Where x_w is the mole concentration of water, f_s is the activity coefficient of solvent.

Similarly, the equilibrium specific humidity of ethanol can be determined by the vapour pressure of ethanol in the desiccant solution:

$$W_{eth,sol} = \frac{P_{eth,sol}}{P - P_{eth,sol}} \quad (3-80)$$

The surface vapour pressure of ethanol in the desiccant solution $P_{eth,sol}$ can be calculated by:

$$P_{eth,sol} = a_{eth}P_{eth} \quad (3-81)$$

Where a_{eth} is the activity of ethanol in the mixture solution, P_{eth} is the vapour pressure of ethanol.

The vapour pressure of pure ethanol under different temperature can be determined by [140]:

$$P_{eth} = 133.322 * 10^{\left(8.04494-\frac{1554.3}{T_{sol}+222.65}\right)} \quad (3-82)$$

The activity of ethanol is calculated by:

$$a_e = x_{eth} f_s \quad (3-83)$$

Where x_{eth} is the mole concentration of ethanol.

Once the solvent activity coefficient f_s is determined, the solution vapour pressure for both water and ethanol can be calculated. The activity coefficient of water f_s is calculated by the following equation:

$$lnf_s = lnf_s^{PDH} + lnf_s^{LC} \qquad (3-84)$$

Where lnf_s^{PDH} is the long range contribution and lnf_s^{LC} is the short range contribution.

As a desiccant solution mixture with lithium chloride, water and ethanol, the long range interaction contribution lnf_s^{PDH} can be neglected [141]. The short range interaction contribution lnf_w^{LC} can be solved by:

$$\begin{aligned} & lnf_w^{LC} \\ & = \frac{2Bx_{LiCl}\tau_{LiCl,w} + Cx_e\tau_{e,w}}{(2B-2)x_{LiCl} + (C-1)x_e + 1} \\ & + \frac{2B'x_{LiCl}\left[x_{LiCl}\tau_{w,LiCl} + A'x_e\left(\tau_{w,LiCl} - \tau_{e,LiCl}\right)\right]}{[(1-2B')x_{LiCl} + (A'-B')x_e + B']^2} \\ & + \frac{(2x_{LiCl} + x_e - 1)\cdot(2Bx_{LiCl}\tau_{LiCl,w} + Cx_e\tau_{e,w})}{[(2B-2)x_{LiCl} + (C-1)x_e + 1]^2} \\ & + \frac{C'x_e\cdot[2Ax_{LiCl}\left(\tau_{w,e} - \tau_{LiCl,e}\right) + x_e\tau_{w,e}]}{[(2A-2C')x_{LiCl} + (1-C')x_e + C']^2} \end{aligned} \qquad (3-85)$$

Where x and τ represent the mole concentration and energy parameter, subscript $LiCl$, w, and e represent lithium chloride, water and ethanol, respectively.

Where:

$$A = e^{-0.053\tau_{LiCl,e}}$$

$$A' = e^{-0.053\tau_{e,LiCl}}$$

$$B = e^{-0.2\tau_{LiCl,w}}$$

$$B' = e^{-0.2\tau_{w,LiCl}}$$

$$C = e^{-0.3\tau_{e,w}}$$

$$C' = e^{-0.3\tau_{w,e}}$$

Where $\tau_{LiCl,e}$, $\tau_{e,LiCl}$, $\tau_{LiCl,w}$, $\tau_{w,LiCl}$, $\tau_{e,w}$, $\tau_{w,e}$ are the binary parameters for the mixed desiccant solution electrolyte system, which is shown in Table 3-1 [141].

Table 3-1. Binary parameters for the mixed desiccant solution

Binary Parameters	$\tau_{LiCl,e}$	$\tau_{e,LiCl}$	$\tau_{LiCl,w}$	$\tau_{w,LiCl}$	$\tau_{e,w}$	$\tau_{w,e}$
Value	-13.548	24.659	-5.902	13.592	0.4472	1.4623

Other mixed solution properties such as density and thermal conductivity are predicted by the simplest mixture rule (SMR). The SMR equation is:

$$S = S_1\emptyset_1 + S_2\emptyset_2 \qquad (3-86)$$

$$\emptyset_1 + \emptyset_2 = 1 \qquad (3-87)$$

To solve the numerical modelling in Matlab, the selected thermal properties of desiccant solution and air are shown in Table 3-2. Specific heat capacity, thermal conductivity, density and condensation heat of air, LiCl aqueous solution and ethanol are collected for heat and mass transfer reference books [137, 142], while the diffusivity of ethanol is obtained from the experimental result conducted by Lapuerta et al [143].

Table 3-2. Thermal properties of air and desiccant solution

Description	Notation	Unit	Value
Air specific heat capacity	$c_{p,air}$	KJ/kgK	1.02
Air diffusivity	$D_{m,air}$	m^2/s	2.46×10^{-5}
Specific heat capacity of LiCl	$c_{p,sol}$	KJ/kgK	3.2
Solution diffusivity	$D_{m,sol}$	m^2/s	8.92×10^{-3}
Air side heat conductivity	k_{air}	W/mK	0.03
Solution side heat conductivity	k_{sol}	W/mK	0.564
Specific heat capacity of ethanol	$c_{p,eth}$	KJ/kgK	2.46
Ethanol side heat conductivity	k_{eth}	W/mK	0.167
Diffusivity of ethanol	$D_{m,eth}$	m^2/s	1.264×10^{-5}
Air density	ρ_{air}	kg/m^3	1.29
Solution density	ρ_{sol}	kg/m^3	1254
Ethanol density	ρ_{eth}	kg/m^3	789
Water vapor latent heat	r	kJ/kg	2450
Ethanol evaporative latent heat	r_{eth}	kJ/kg	846

3.2.8. Numerical solving scheme

The aim of the numerical simulation is to solve the temperature and humidity fields of the process air in air channel; temperature, desiccant and ethanol concentration fields of the solution stream; and temperature and ethanol content fields of the circulated air in solution channel within the proposed dehumidifier, since these fields are closely linked and interacted. Therefore, the equations were

solved iteratively in Matlab until they were converged. The simulation procedures are shown below:

1) Set the inlet conditions for the process air, desiccant solution and circulated air based on the existing experiment.
2) Assume the initial specific humidity of membrane surface is identical with the inlet equilibrium specific humidity of desiccant solution.
3) Solve the discrete governing equations to obtain T_{sol}, T_{ca}, T_{air}, X_{sol}, C_{eth}, W_{eth} and W_{air} using the inlet conditions.
4) Based on the temperature and humidity fields for air and solution flows, solve the heat and mass transfer boundary conditions on the membrane surface to obtain the membrane surface temperature and concentration fields in the solution side ($T_{sol,mem}$ and $C_{sol,mem}$).
5) Calculate the membrane surface humidity field in the solution side ($W_{sol,mem}$) based on $T_{sol,mem}$ and $C_{sol,mem}$.
6) Adopt new $W_{sol,mem}$ as a default value and return to step 4 until $W_{sol,mem}$ is converged.
7) Apply the value obtained from last step and return to step 3 until the results are all converged.
8) Calculate the moisture removal rate and dehumidification effectiveness based on the outlet conditions of the dehumidifier.

For better illustration, the solution procedure used during the simulation process to solve interacted governing equation is shown below:

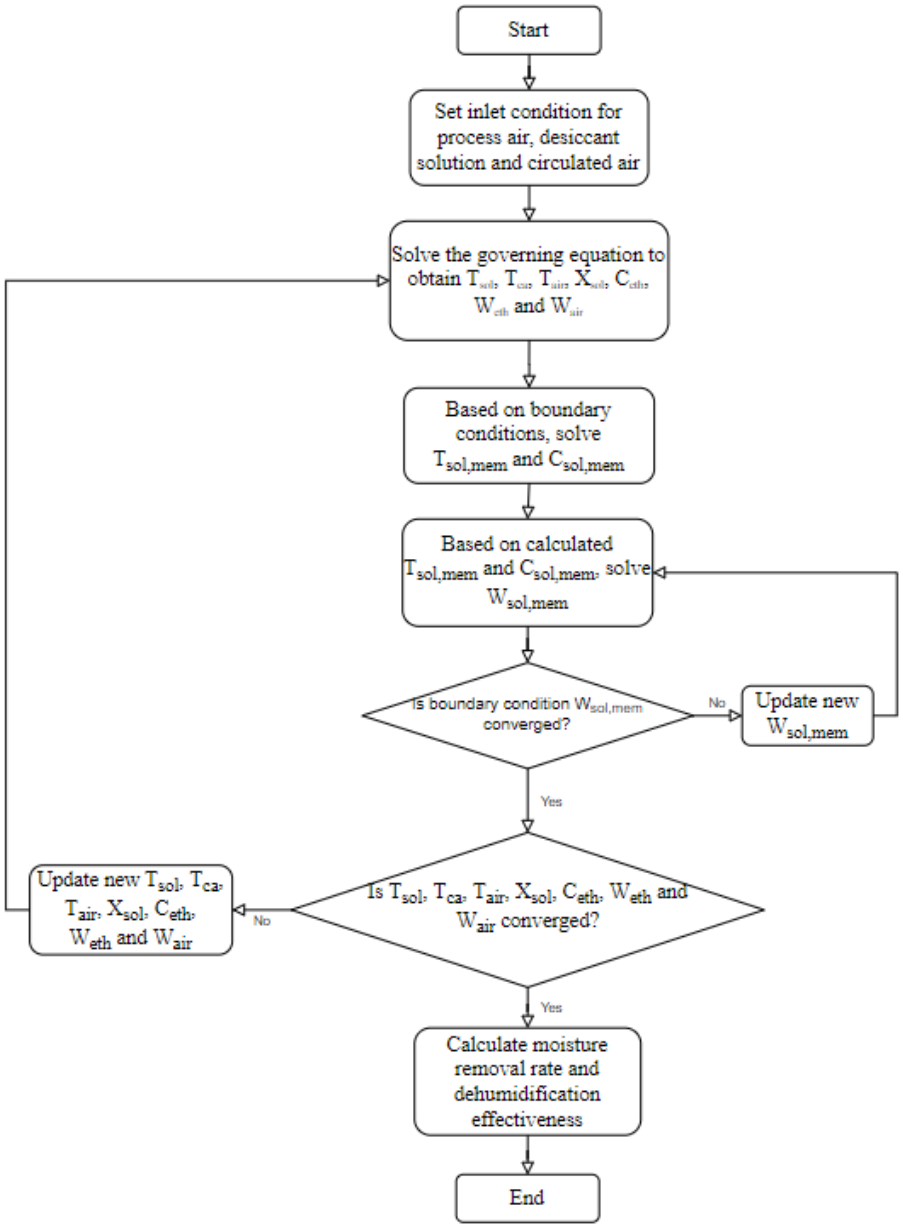

Figure 3-11 Flow chart of the solving procedure

3.2.9. Mesh independent test

In order to guarantee the accuracy of the numerical model, several tests have been conducted with the mesh size of 30×60, 50×100 and 100×200. The simulation results under different mesh size is presented in Table 3-3. The inlet conditions of process air temperature, relative humidity and mass flow rate is 28 ℃, 70% and 0.01 kg/s, respectively, while the inlet conditions of desiccant solution were set to be 20 ℃, 37% and 0.03 kg/s. The circulated air inlet temperature was 12 ℃ and mass flow rate is 0.03 kg/s. The inlet mass concentration of ethanol is set to be 10%. Since the variations of the simulation results are all less than 1%, it has been proved that the proposed numerical model to analyze the self-cooled liquid desiccant dehumidifier is independent with its mesh size. To reduce the time consumption of the simulation process, mesh size of 50×100 is selected for further evaluation.

Table 3-3. Mesh independent test

Mesh size	30×60	50×100	100×200
$T_{air,out}$ (℃)	21.331	21.319	21.310
$W_{air,out}$ (kg/kg)	0.0075	0.0075	0.0075
$T_{sol,out}$ (℃)	21.439	21.437	21.435
$C_{sol,out}$ (%)	36.98	36.98	36.98
$C_{eth,out}$ (%)	9.81	9.81	9.81
$T_{ca,out}$ (℃)	14.574	14.582	14.588

3.3. Experiment set-up

3.3.1. Experimental system description

This project is to establish a novel membrane-based self-cooled liquid desiccant solution dehumidification system. Therefore, experiment tests have to be conducted to evaluate the performance of the system under different operation conditions. Fig 3-12 below shows the experiment design of the dehumidification system. The main components are dehumidifier, regenerator, evaporative cooler, two tanks to store strong and weak desiccant solution, boiler to supply hot water, four heat exchangers, and several centrifugal pumps and AC axial fans to adjust the air and solution flow rate. The hot and humid air coming out from the environmental chamber will be driven through the dehumidifier and the liquid desiccant solution absorbs the water vapour from the process air. The evaporative coolant (ethanol) in the solution will evaporate due to the increasing of latent heat caused by water vapour condensation. Another air stream flows from the bottom side of the solution channel brings the ethanol vapour to a heat exchanger at the top of the dehumidifier. The ethanol vapour can be condensed into liquid phase by the fin coil heat exchanger and then fall back into the solution channel. After dehumidification process, the diluted solution flows to the weak solution tank, which is pumped into a plate heat exchanger where the heat transfer occurs between the weak solution and strong solution coming from the regenerator. At this stage, the weak solution is pre-heated to reduce the energy consumption of the electrical boiler. The hot and diluted desiccant solution flows to the solution channel of a membrane-based regenerator. The return air passes through the

regenerator and thus remove the water content from the solution. The strong solution comes out the regenerator will be cooled by the cold tap water, and then flow back to the dehumidifier to continue the dehumidification process.

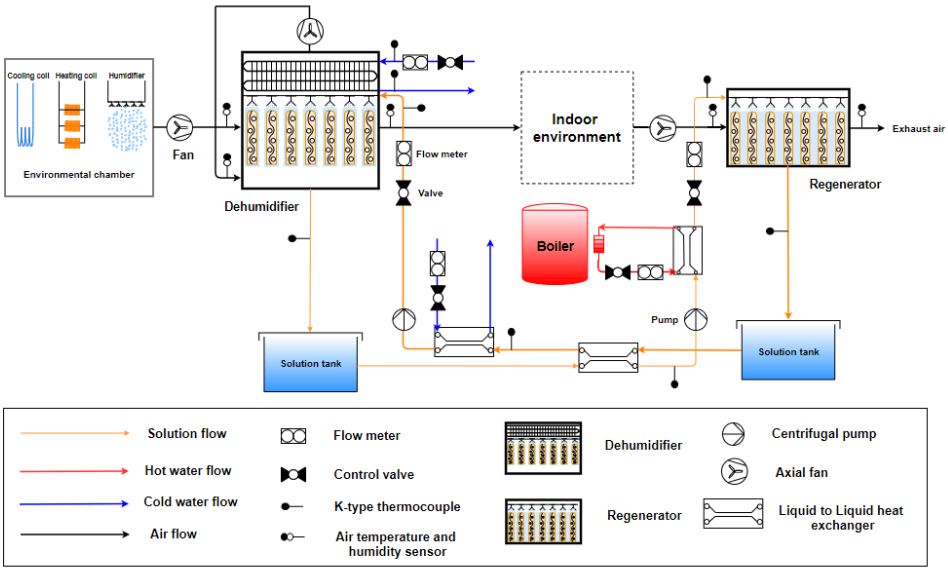

Figure 3-12 Schematic diagram of the experiment rigs

The photo of the self-cooled membrane-based liquid desiccant dehumidification system is shown in Figure 3-13. The dimension of membrane-based units for the dehumidifier and regenerator is 410mm (L) × 230mm (W) × 210mm (H) with 11 air channels and 11 solution channels. All the experimental rigs including dehumidifier, regenerator, solution tanks, heat exchangers, boiler, duct and pipes are well-insulated to minimize the influence of surrounding environment. Once the air inlet conditions met the set values, the experiment started until it achieves a steady state, the measured data can be thus collected. The specification of dehumidifier and physical properties of the membrane is presented in Table 3-4.

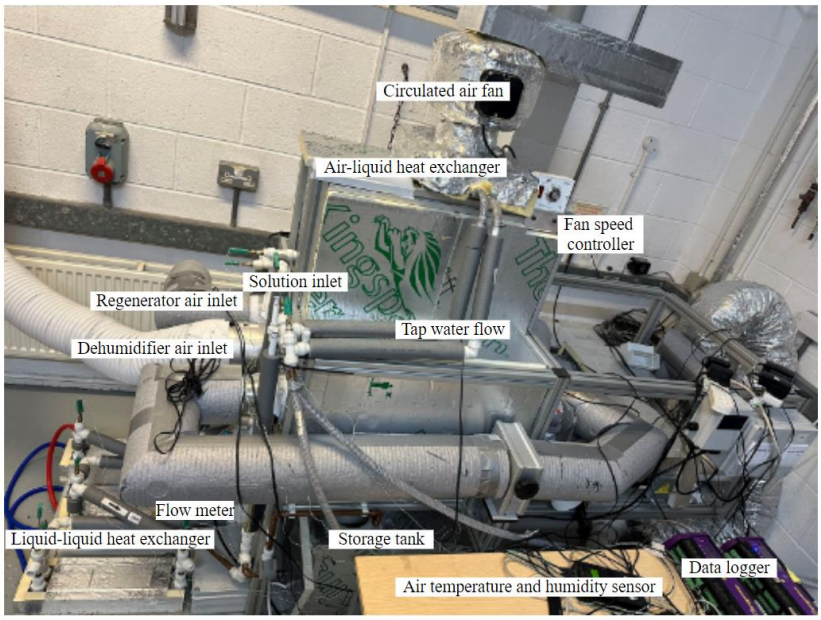

Figure 3-13 Experimental rigs of the self-cooled membrane-based dehumidification system.

Table 3-4. Membrane physical properties of the dehumidifier

Properties	Symbol	Value	Unit
Length of dehumidifier	L	0.41	m
Width of dehumidifier	W	0.23	m
Width of dehumidifier	H	0.21	m
Number of air channel	-	11	-
Number of solution channel	-	11	-
Thickness of air channel	d_{air}	0.0077	m
Thickness of solution channel	d_{sol}	0.0043	m
Thickness of membrane	δ_{mem}	0.0005	m
Membrane thermal conductivity	k_{mem}	0.3	W/mK
Membrane mass transfer conductivity	$k_{m,mem}$	3.87×10^{-6}	kg/ms

3.3.2. Preparation of self-cooled desiccant solution

Lithium bromide, lithium chloride and triethylene glycol are the most commonly used liquid desiccant in recent years due to the fact that their surface vapour pressures were lower than the humid air under low temperature and high concentration condition [144]**.** The surface vapour pressure is the most important factor for selecting liquid desiccant. Therefore, lithium chloride, as a relatively stable solution with low vapour pressure, has been selected as based desiccant solution. In order to restrain the temperature rise of the desiccant solution caused by the addition of condensation heat during the absorption of moisture, anhydrous ethanol is added to LiCl solution as an evaporative coolant. Compared with traditional internally-cooled liquid desiccant dehumidification system, the heat exchanger inside dehumidifier can be removed to simplify its structure. Detailed information about the lithium chloride and anhydrous ethanol used during the experimental tests is listed in Table 3-5.

Table 3-5. Specifications of the chemical compound

Chemical name	Purity	Supplier	Mole weight (g/mol)	Density (g/mL)
Lithium chloride	99%	Thermo Scientific Chemicals	42.38	2.06
Ethanol	99%	Fisher Chemical	46.07	0.789

3.3.3. Data collection instrument

The main testing instruments of the self-cooled liquid desiccant dehumidification system has been listed in Table 3-6, and the specifications of the measuring instruments has been presented in Table 3-7. The air flow is driven by the axial fan (Ebm-Papst Mlfingen GmbH & Co. KG) and electronic speed controller (Ductstore) is used to adjust the air flow rate. The air velocity is measured by Testo anemometer. The air temperature and humidity sensors are placed at inlet and outlet of the dehumidifier, regenerator and circulated air channel. The desiccant solution and water flow are driven by centrifugal magnetic pump (Xylem) with flow rate up to 10 L/min. The temperature of desiccant solution and water is measured by a series of K-type thermocouples and all the data are collected by DT80 data logger. Moreover, the volumetric flow rate of desiccant and water is controlled and measured by liquid flow meters (Parker). Since it is designed for measuring water flow rate at 20℃, a correlation has been applied to ensure accurate readings form the meter, which can be expressed as [145]:

$$v_{sol} = v_W \sqrt{\frac{(m_{float} - V_{float}\rho_{sol})\rho_W}{(m_{float} - V_{float}\rho_W)\rho_{sol}}} \qquad (3-88)$$

where v_{sol} and v_W are the volumetric flow rates of desiccant solution and water (L/min), respectively. ρ_{sol} and ρ_W are the solution and water densities (kg/m^3), respectively. m_{float} and V_{float} are the flow meter float weight (kg) and volume (m^3), respectively. As for the flow meter used in this study, the float weight (m_{float}) is 2.1× 10^{-3}kg and volume (V_{float}) is 0.25× 10^{-6}m^3.

It should be noted that the outlet concentration of desiccant solution has not been measured during this research project. Unlike conventional liquid desiccant dehumidification system using pure LiCl aqueous solution, the outlet solution concentration can be determined by measuring its temperature and density. However, for the proposed self-cooled liquid desiccant solution, the mass transfer contain both the condensation of water and evaporation of ethanol. The mass concentration for LiCl and ethanol at outlet of the dehumidifier cannot be determined by simply measuring its density. Moreover, ethanol vapour detector (Dragger) is installed at the outlet of dehumidifier and regenerator air channel to ensure no leakage of ethanol gas.

Table 3-6. Specifications of experimental instruments

Instruments	Properties		Supplier
Centrifugal magnetic-driven pump	Power	15 W	Xylem
	Maximum frequency	50 Hz	
	Maximum speed	2600 r/min	
	Maximum capacity	10 L/min	
AC axial fan	Power	45 W	Ebm-papst Mlfingen GmbH & Co. KG
	Nominal speed	2800/min	
Boiler	Capacity	12.87 kW	RM cylinders
	Supply temperature range	50 – 70 ℃	
	Water storage	117 L	
	Circulating pump	68 W	
	Hot water flow rate	0 - 5 L/min	
Liquid-to-liquid exchanger	Designed temperatures	-35 ℃ to 170 ℃	Xylem
	Maximum flow rate	81900 L/min	
	Maximum heat transfer area	1858 m^2	
	Designed pressure	Up to 30 bar	
Air-to-liquid exchanger	Cooling power	97 W	Advanced Thermal Solutions, Inc.
	Weight	4 kg	
	Fan size	3.15 $inches^2$	
	Maximum pressure	100psi	

Table 3-7. Specifications of measurement instruments with associated accuracies

Measurement devices	Parameter	Measurement range	Accuracy
RS K-type thermocouple probe	Liquid temperature	0-1100 ℃	±0.75%
Sensirion EK-H4 humidity sensor	Temperature and humidity	-40-125 ℃ 0-100 % RH	±3% ±2%
Testo anemometer 405	Air velocity	0-10 m/s	±5%
Brannan hydrometer 200 Series	Solution density	1.0-1.4 g/m^3	±2%
Parker liquid flow indicator	Water flow rate	1-22 L/min	±2%
Parker Easiflow Series flowmeter	Solution flow rate	1-15 L/min	±5%
Data logger DT-80 Series 2	N/A	Data acquisition	±0.15%

3.3.4. Uncertainty analysis

For an experimental investigation, it is critical to measure the errors based on the uncertainties of the measuring instruments which is provided in Table 3-7. According to a method of uncertainty measurement conducted by Bell [146], a calculated value of U_Y can be determined by the function of U_{X_i} of each variable X_i. Thus, error bars are presented in the figure of experimental data analysis.

$$U_Y = \sqrt{\sum_{i=1}^{N} \left(\frac{\partial Y}{\partial X_i}\right)^2 \cdot {U_{X_i}}^2} \qquad (3-89)$$

3.4. Performance evaluation

Moisture removal rate (MRR) and dehumidification effectiveness are the most important parameters used to evaluate the performance of a heat and mass exchanger [47]. The moisture removal rate of the process air represents the dehumidification capacity, which is related to the mass flow rate of air and the difference between inlet and outlet air specific humidity. Thus, MRR can be determined by:

$$MRR = m_{air}\left(W_{air,in} - W_{air,out}\right) \qquad (3-90)$$

Where, $W_{air,in}$ and $W_{air,out}$ are the inlet and outlet specific humidity of the process air (kg/kg).

Effectiveness is the most important parameter used to evaluate the performance of a heat and mass exchanger. Dehumidification effectiveness is defined as the ratio between the actual and the maximum possible moisture transfer rates inside the dehumidifier.

$$\varepsilon_{deh} = \frac{W_{air,in} - W_{air,out}}{W_{air,in} - W_{sol,in}} \qquad (3-91)$$

Where $W_{sol,in}$ is the inlet equilibrium specific humidity of the self-cooled liquid desiccant solution (kg/kg).

3.5. Model validation

The experimental results have been used to validate the numerical model. Overall, 59 groups of the experimental tests under different operating conditions have been conducted to validate numerical results. The mass concentration of ethanol various from 0%, 5% and 10%. If more ethanol is added to LiCl aqueous solution, the solubility of lithium chloride will be reduced, resulting in crystallization problem. The temperature of desiccant solution were varied from 17 ℃ to 29 ℃. The mass concentration of lithium chloride was within the range of 28% to 37%. The Based on the capacity of fans and solution pump, the range of mass flow rate of the process air, desiccant solution and circulated air were set to be $0.01 - 0.025$, $0.01 - 0.03$ and $0.01 - 0.025\ kg/s$, respectively. To evaluate the dehumidification performance under different weather conditions, the inlet air temperature and relative humidity of the process air before entering the self-cooled membrane-based dehumidifier were in the range of $22 - 34$ ℃ and $60 - 80\%$, respectively. The temperature of circulated air ranged from 12 ℃ to 18 ℃.

The comparison of moisture removal rate and dehumidification effectiveness between the numerical results and experimental data were present in Figure 3-14 and 3-15 below. It is clear that almost all the deviation between numerical and experimental results were within 10%, which shows that the numerical results are within the tolerance range of experimental data. The maximum discrepancies for moisture removal rate and dehumidification effectiveness are 11.2% and 11.4%, respectively. As a result, the numerical results have been proved to have a good agreement with the experimental data which indicates that the proposed

numerical model of the self-cooled membrane-based liquid desiccant dehumidifier is valid to predict the dehumidification performance.

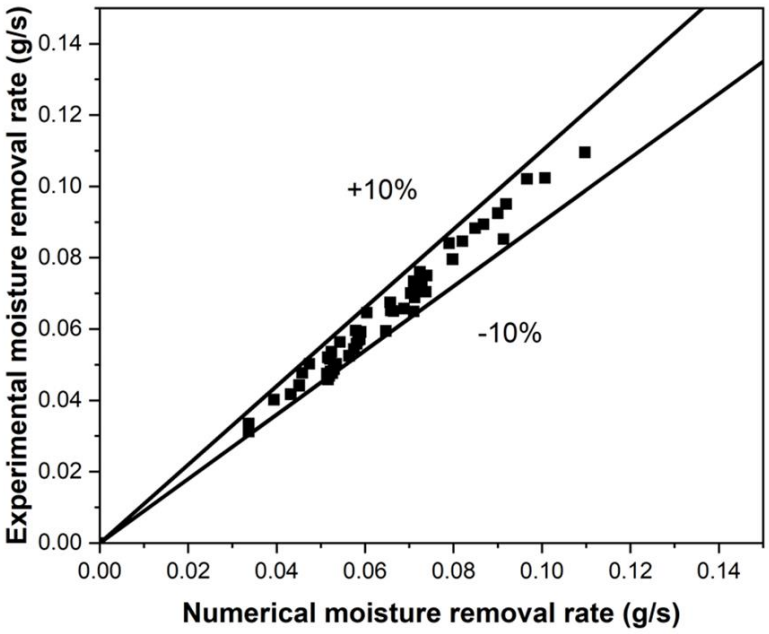

Figure 3-14 Comparison of moisture removal rate between numerical and experimental data

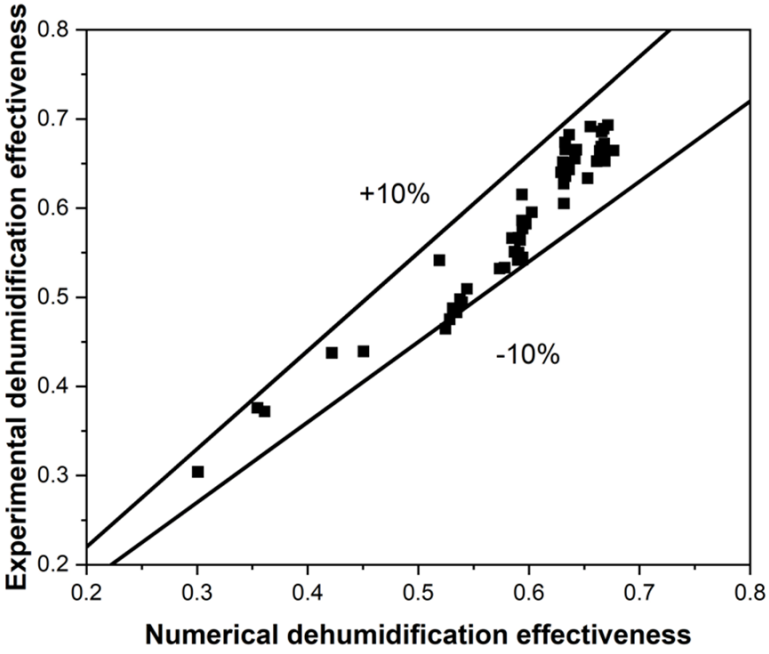

Figure 3-15 Comparison of dehumidification effectiveness between numerical and experimental data

3.6. Results and discussion

3.6.1. Equilibrium specific humidity of self-cooled desiccant solution

The equilibrium specific humidity of the desiccant solution is critical important for dehumidification performance since it represents the water vapour pressure, and the difference of surface vapour pressure is the main driving force for water content in the air to be absorbed by the desiccant solution. Normally, the concentration of lithium chloride is set from 30% to 40%. Based on previous research [60], the solubility of lithium chloride is reduced with the addition of ethanol. Therefore in this study, to avoid the problem of crystallization, the mass concentration of lithium chloride is between 28%, 31%, 34%, 37%, and the mass

concentrations of ethanol are set to 0%, 5% and 10%. Based on the NRTL method mentioned in Section 3.2.7, the relationship between the equilibrium specific humidity of the desiccant solution, temperature and mass concentration are shown in Fig. 3-16.

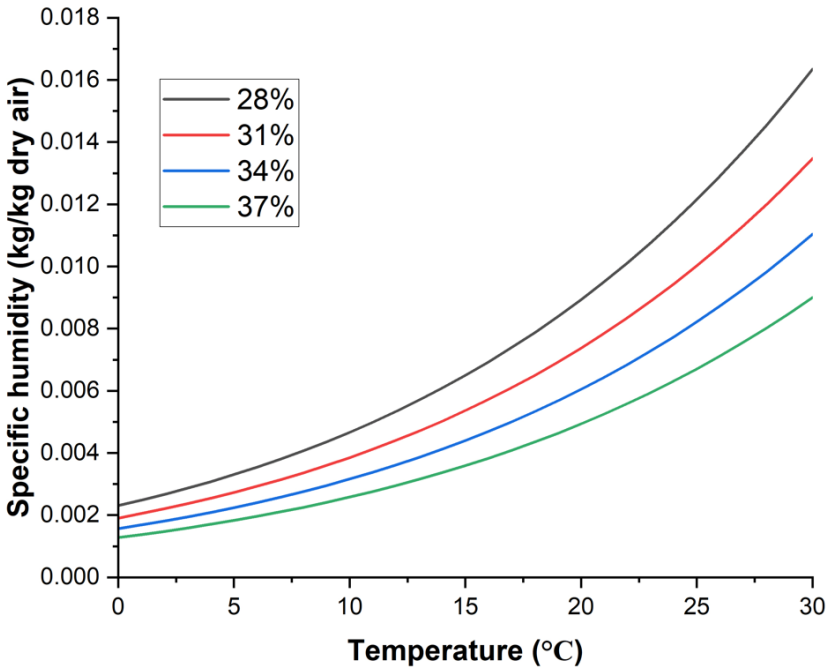

(a)

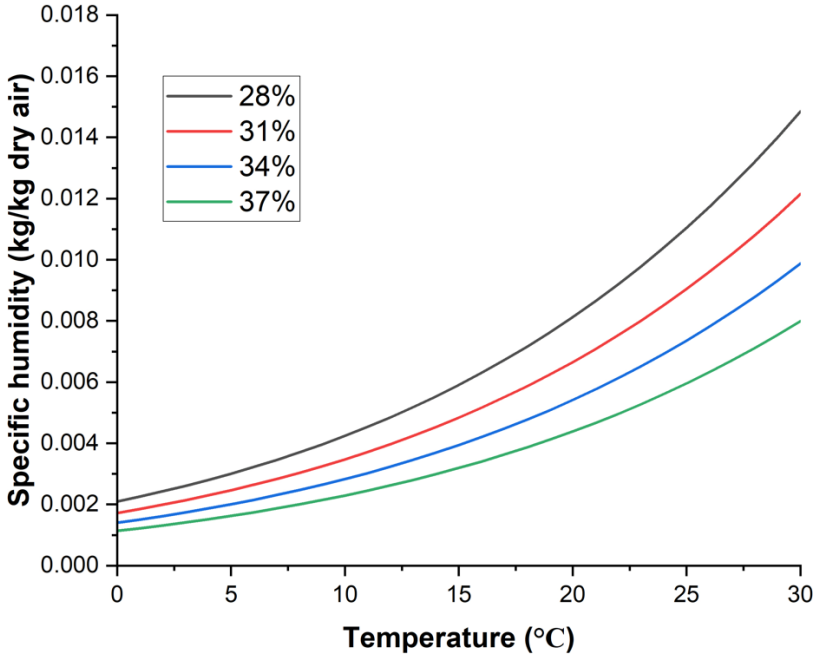

(b)

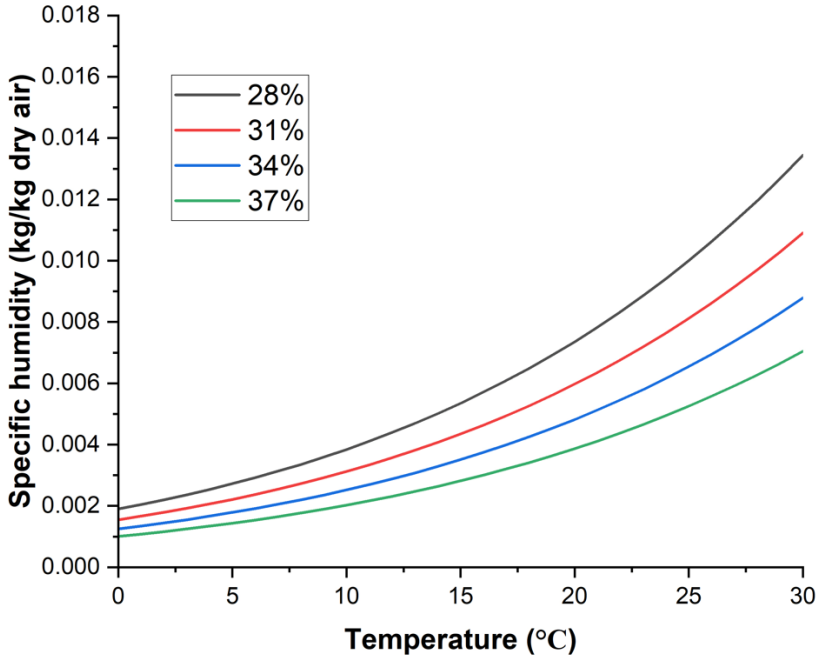

(c)

Figure 3-16 Specific humidity of desiccant solution at (a) $C_{eth} = 0\%$; (b) $C_{eth} = 5\%$; and (c) $C_{eth} = 10\%$

As shown in the figures above, the specific humidity of the self-cooled liquid desiccant increased with the increasing of solution temperature. For desiccant solution without adding ethanol, at $C_{LiCl} = 28\%$, the specific humidity of desiccant solution rises from 0.00231 to 0.01635 kg/kg if the solution temperature increases from 0 ℃ to 30 ℃. When $C_{LiCl} = 37\%$, the increasement of specific humidity is just at 0.00772 (from 0.00128 to 0.009) kg/kg. The results show that the solution temperature has more influence on the dehumidification capacity at lower concentration of lithium chloride. Meanwhile, the dehumidification capacity can also be improved with the increasing of LiCl mass concentration, since it can decrease the equilibrium specific humidity. For desiccant solution with 10% ethanol, when $T_{sol} = 28$ ℃, the specific humidity of desiccant solution are 0.0097, 0.00782 and 0.00628 kg/kg, respectively, under $C_{LiCl} = 31\%, 34\% \; and \; 37\%$. For the addition of ethanol into liquid desiccant solution, the dehumidification capacity can be enhanced while reducing the specific humidity. For example, under $T_{sol} = 28$ ℃ and $C_{LiCl} = 37\%$, the specific humidity decrease from 0.00801 to 0.00711 and 0.00628 kg/kg while the mass concentration of ethanol varies from 0% to 5% and 10%, respectively. As mentioned before, the activity of water in desiccant solution is reduced with the mixture of ethanol. Thus the surface vapour pressure of water is reduced, which represents that even without considering the evaporation of ethanol during the dehumidification process, the newly formed self-cooled liquid desiccant solution is able to improve the dehumidification performance compared with pure LiCl aqueous solution. It should be noted that both the reduction of the specific humidity of desiccant solution and the removal of latent heat from the evaporation of ethanol during the dehumidification process play a positive role in enhancing

the dehumidification performance. The results in the following sections do not distinguish these two factors separately.

3.6.2. Temperature and humidity fields

Fig. 3-17 shows the calculation results of air and solution conditions within the self-cooled membrane-based liquid desiccant dehumidifier based on the numerical model. The inlet conditions of process air temperature, humidity ratio, and mass flow rate are 28 ℃, 70% and 0.01 kg/s, respectively, while the inlet conditions of desiccant solution were set to be 20 ℃, 37% and 0.03 kg/s. The circulated air inlet temperature was 12 ℃ and mass flow rate is 0.03 kg/s. The inlet mass concentration of ethanol is set to be 10%. Since the process air was entering the dehumidifier from the left side while the desiccant solution flowed from top to bottom, it is obvious that the air temperature and humidity gradually decreased along its flow direction. The moisture content in air was absorbed by the desiccant solution while it flowed through the dehumidifier, the dehumidification ability of the desiccant solution was weakened. Therefore, the specific humidity of process air reaches its lowest point (0.00737 kg/kg) at the top right corner of the dehumidifier since it is closer to the inlet of desiccant solution. Similar to the process air temperature, the lowest air temperature is 20.87 ℃ at the top right corner since the solution temperature was increasing from top to bottom, as presented in Fig 3-16 (c). The desiccant solution has the highest value of 23.28 ℃ at the left bottom corner. This is because that the desiccant solution absorbed more water on the left side of the dehumidifier, resulting in more latent heat caused by the mass transfer of water from vapour to liquid being released into desiccant solution. Fig 3-16 (d) shows the change of

LiCl concentration during the dehumidification process. The result has been compared with using pure LiCl aqueous solution (0% ethanol), as presented in Fig. 3-18. If no ethanol is added to the desiccant solution, the mass concentration of LiCl gradually reduced along the flow direction of solution and reaches its lowest value at the left bottom corner. This is mainly because that the driving force of mass transfer of water is higher on the left side since the specific humidity of process air is the highest at its inlet condition. However, when ethanol is added into desiccant solution, the mass concentration of ethanol is not only affected by the absorption of water, but also related to the evaporation of ethanol. The LiCl concentration reduced at left side from top to bottom while it increasing at the right bottom corner. As mentioned above, more water is absorbed by the desiccant solution on the left side of the dehumidifier than on the right side, when the amount of evaporated ethanol is larger than the absorption of water, such unusual phenomena of LiCl concentration increasing during the dehumidification process has been obtained. With the evaporation of ethanol, the mass concentration of ethanol within the desiccant solution decreased from top to bottom. It reaches the lowest value at the left bottom corner due to the fact that the desiccation solution temperature is the highest at the left bottom corner. The higher the solution temperature, the greater the evaporation rate of ethanol. Figure 3-16 (f) shows that the temperature of circulated air increased from bottom to top, it is higher on the left side since the solution temperature is higher.

The results have shown that the temperature, humidity and concentration fields were not uniform. The driving force of heat and mass transfer processes is not

uniformly distributed within the air and solution channels, and inevitably, it reaches the maximum value at the inlet of the process air and desiccant solution.

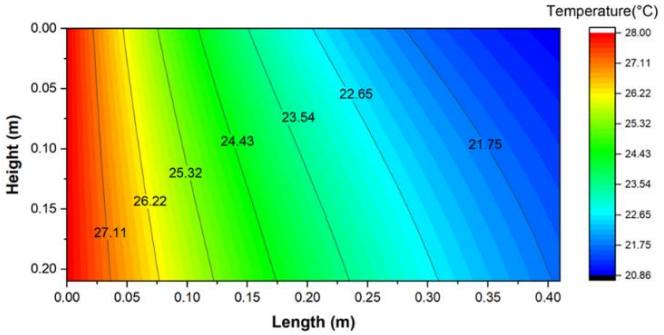

(a)

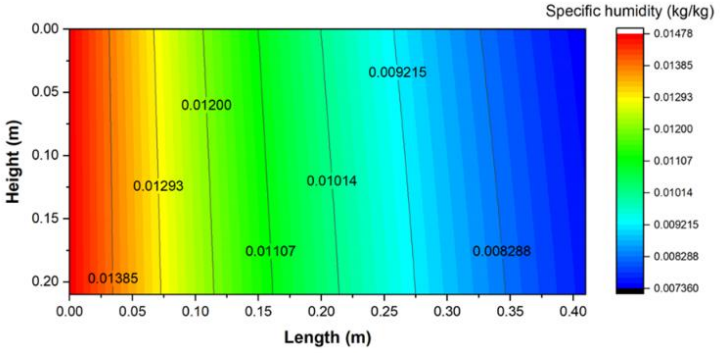

(b)

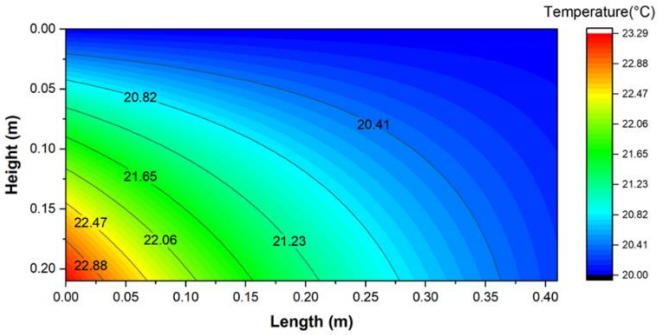

(c)

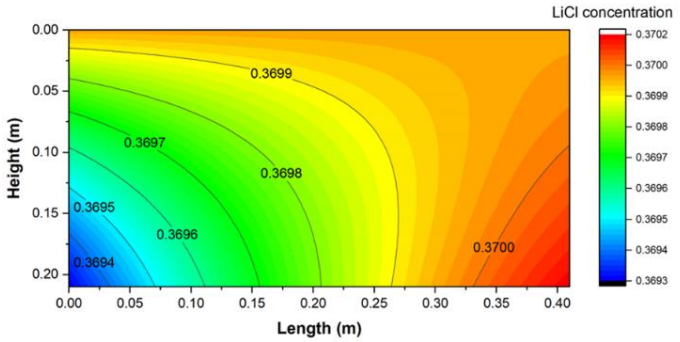

(d)

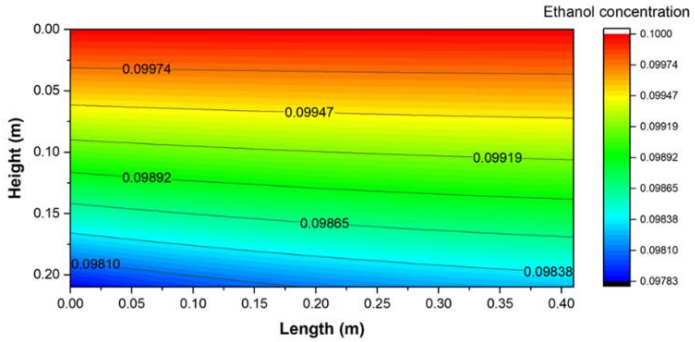

(e)

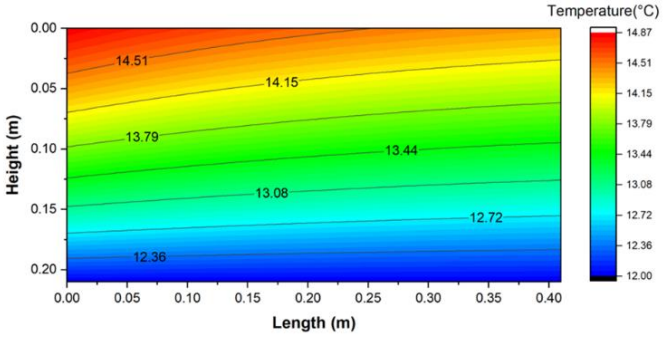

(f)

Figure 3-17 (a) Air temperature field; (b) Air specific humidity field; (c) Solution temperature field; (d) LiCl concentration field; (e) Ethanol concentration field; (f) Circulated air temperature field.

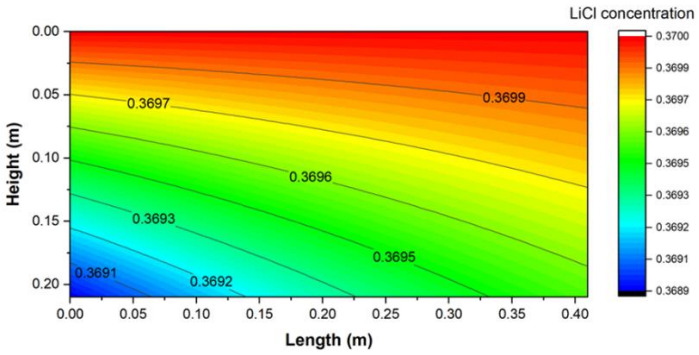

Figure 3-18 LiCl concentration field with 0% ethanol

3.6.3. Effects of process air conditions

3.6.3.1. Effect of process air temperature

To assess whether the dehumidification performance can be improved by the addition of ethanol, ethanol mass concentration of 0%, 5% and 10% have been tested during the dehumidification process. The effect of process air temperature on moisture removal rate is shown in Fig. 3-18. It is clear that both the experimental and numerical results indicate that the newly formed self-cooled liquid desiccant solution has a better dehumidification performance compared to conventional lithium chloride aqueous solution. The more ethanol added to the desiccant solution, the better the performance will be for both MRR and dehumidification effectiveness. Based on Fig. 3-19 (a), under the condition of 0%, 5% and 10% ethanol within desiccant solution, the MRR increased from 0.0337 to 0.0913 g/s, 0.0394 to 0.1007 g/s and 0.0451 to 0.1097 g/s, respectively, for air temperature ranging from 22 ℃ to 34 ℃. The effect of inlet air temperature on MRR are the same for desiccant solution adding different amount of ethanol. The MRR increased with the rise of inlet air temperature. This is because that the increase of air temperature at the same relative humidity lead to the increased of

air humidity ratio. The higher the air humidity ratio is, the greater the surface vapour pressure is. This leads to a larger vapour pressure difference between the process air and desiccant solution. Therefore, the mass transfer potential increases when the air temperature increases.

Fig. 3-19 (b) shows that the inlet air temperature has less impact on dehumidification effectiveness. For desiccant solution without ethanol, the dehumidification effectiveness varies from 60.26% to 59.06% when the air temperature rises from 22 ℃ to 34 ℃. While the dehumidification effectiveness changes from 67.65% to 66.4% for 10% ethanol. The temperature rises of process air leads to the increase of $W_{air,in}$ in Eq. $(3-91)$, thereby reducing the dehumidification effectiveness. The results have proved that the proposed self-cooled membrane-based liquid desiccant dehumidifier is able to maintain a high dehumidification performance even under high air temperature working condition.

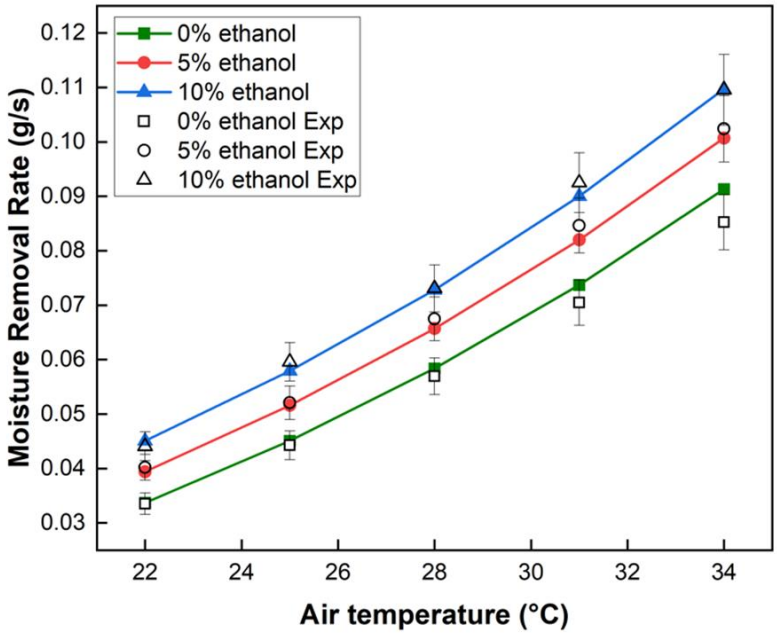

(a)

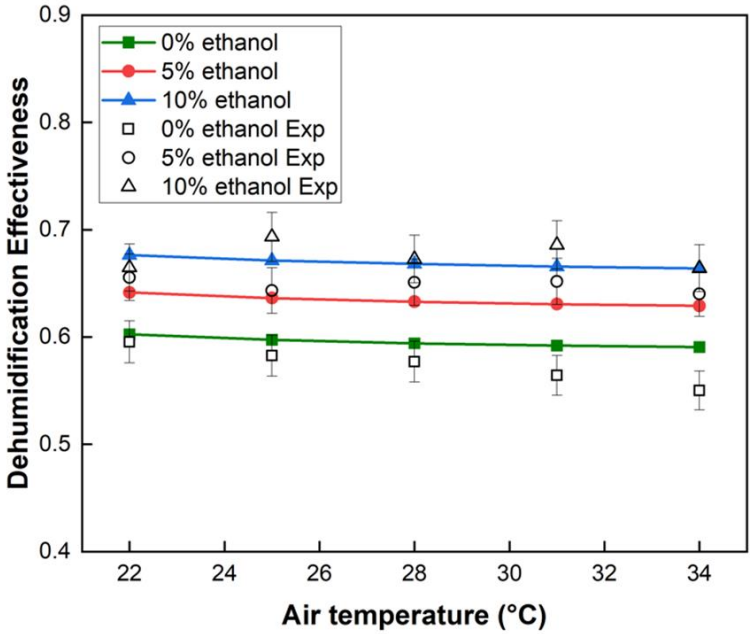

(b)

Figure 3-19 (a) Effect of inlet air temperature on moisture removal rate. (b) Effect of inlet air temperature on dehumidification effectiveness

3.6.3.2. Effect of process air humidity ratio

Inlet air relative humidity is another critical factor that affects the dehumidification performance. MRR and dehumidification effectiveness under different relative humidity are presented in Fig. 3-20 (a) and (b). The inlet air RH is changed while keeping the inlet air temperature at 28 ℃, air flow rate at 0.01 kg/s, solution temperature at 20 ℃, LiCl concentration at 37%, solution flow rate at 0.03 kg/s, circulated air inlet temperature at 12 ℃ and mass flow rate at 0.025 kg/s. Compared with conventional LiCl solution, when the inlet relative humidity is at 60%, the hybrid solution can improve the moisture removal rate up to 14.4% and 28.4%, respectively, by adding 5% and 10% ethanol. The moisture

removal rate increased with the increment of inlet air RH, while the reason is similar to the effect of inlet air temperature. The increase of relative humidity leads to a greater surface vapour pressure difference between the process air and desiccant solution. The maximum value of moisture removal rate under different ethanol concentrations are 0.0771, 0.079 and 0.0868 g/s for solutions with 0%, 5% and 10% ethanol, respectively, while the relative humidity reaches 80%.

On the contrary, as shown in Fig 3-19 (b), the dehumidification effectiveness is insensitive to the change in inlet air relative humidity. The variations of ε_{deh} from 60% to 80% inlet air humidity have the same trend under different ethanol mass concentrations. For 10% ethanol as an example, the ε_{deh} slightly decreased from 59.37% to 59.43%. The improvement of dehumidification effectiveness is about 6.5% and 12.3% for 5% and 10% ethanol, respectively. This indicates that the proposed self-cooled membrane-based liquid desiccant dehumidifier is capable of providing a good dehumidification performance under different weather conditions.

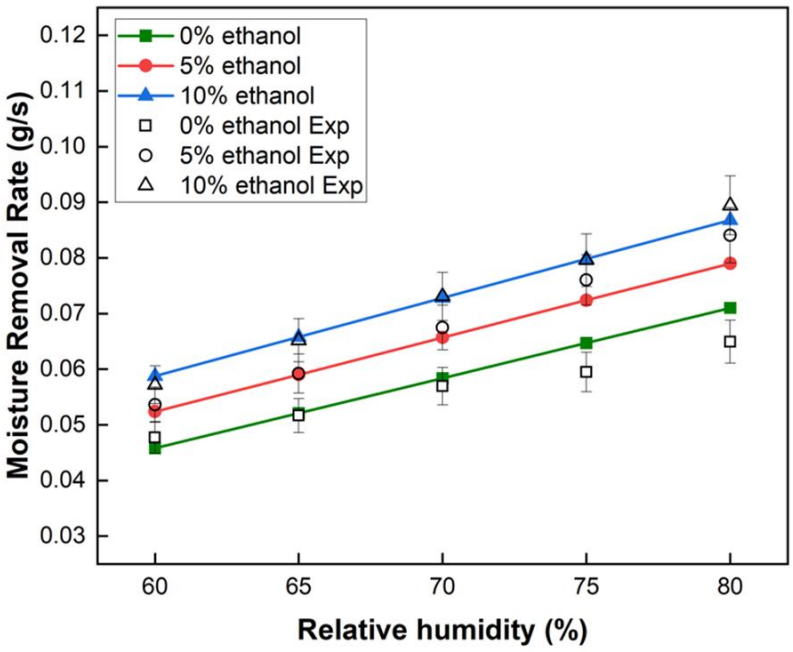

(a)

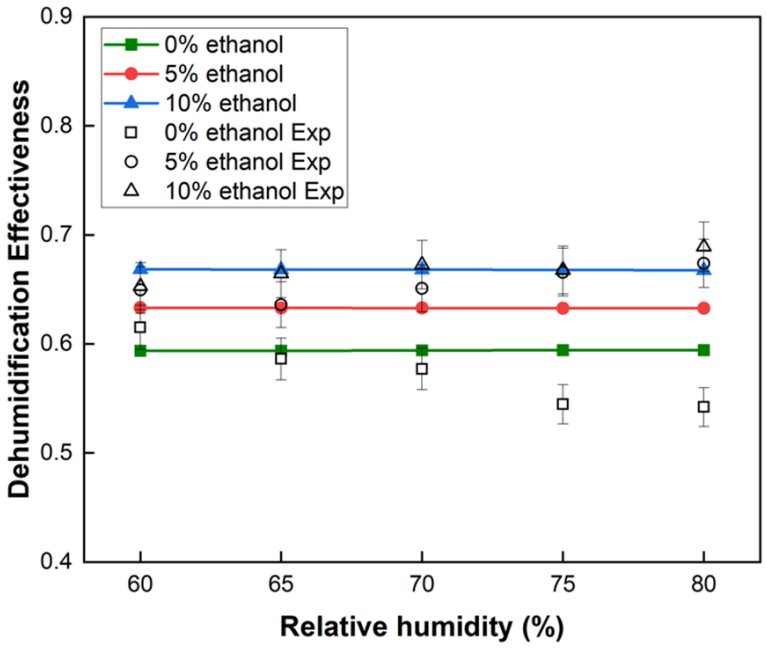

(b)

Figure 3-20 (a) Effect of inlet air relative humidity on moisture removal rate. (b) Effect of inlet air relative humidity on dehumidification effectiveness.

3.6.3.3. Effect of process air flow rate

The curves shown in Fig. 3-21 (a) and (b) describe the trends of moisture removal rate and dehumidification effectiveness with respect to the inlet air mass flow rate changes from 0.01 to 0.025 kg/s. For desiccant solution without adding ethanol, the MRR increased by 26.5% from 0.0584 to 0.0739 g/s, when inlet air flow rate rises from 0.01 to 0.025 kg/s. For desiccant solution with 5% and 10% ethanol, the MRR increased by 43.4% and 57.1%, respectively. It is obvious that the moisture removal rate increased with the increase of air inlet mass flow rate. This is because that the MRR is determined by the air flow rate and the air humidity ratio difference between the inlet and outlet, as shown in Eq. $(3-90)$. However, with the increase of air flow rate, the contact time between process air and desiccant solution is limited. The less time the process air stays inside the dehumidifier, the air outlet parameters are less likely to change, including the humidity ratio difference. This can also be potentially explained by the fact that the mass transfer unit between air and solution is reduced by increasing the air flow rate, and thus leads to the decrease in dehumidification effectiveness. For example, when $C_{eth} = 10\%$, ε_{deh} decreases by 46.92% from 66.81% to 35.46%, when m_{air} increases from 0.01 to 0.025 kg/s. The results have shown that the air flow rate has significant impact on moisture removal rates and dehumidification effectiveness. An operation condition with lower air flow rate is recommended due to the increase of number of heat and mass transfer units (NTU and NTU_m) between air and desiccant solution.

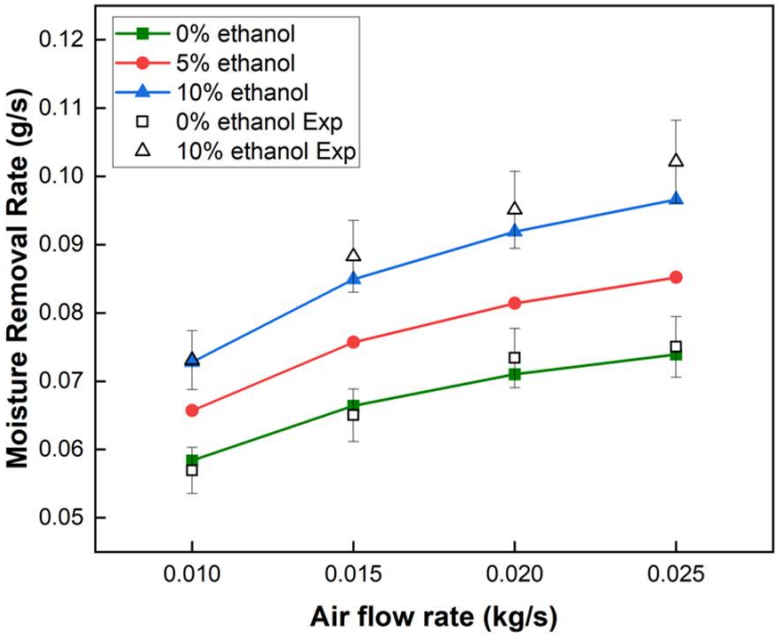

(a)

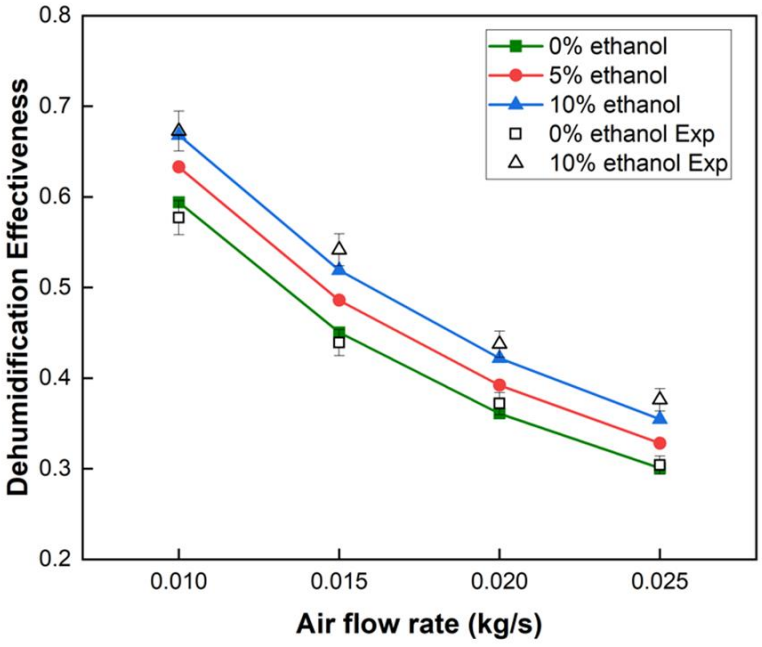

(b)

Figure 3-21 (a) Effect of process air flow rate on moisture removal rate. (b) Effect of inlet air flow rate on dehumidification effectiveness

3.6.4. Effects of solution properties

3.6.4.1. Effect of solution temperature

The desiccant solution temperature is another critical parameter affecting the dehumidification performance, since it is closely related to the surface vapour pressure. The variations of moisture removal rate and dehumidification effectiveness under different $T_{sol,in}$ are presented in Fig. 3-22 (a) and (b). The moisture removal rate reaches the maximum value of 0.0771 g/s when $T_{sol,in} =$ 17 ℃ and $C_{eth,in} = 10\%$, while its minimum value is 0.0387 g/s when $T_{sol,in} =$ 29 ℃ and $C_{eth,in} = 0\%$. For dehumidification effectiveness, it reaches the peak value of 68.96% when $T_{sol,in} = 29$ ℃ and $C_{eth,in} = 10\%$, while its minimum value is 59.31% when $T_{sol,in} = 17$ ℃ and $C_{eth,in} = 0$ %. The decrease of moisture removal rate is because that the driving force of mass transfer between process air and desiccant solution has been weakened, since the temperature rising of desiccant solution leads to a higher surface vapour pressure. On the contrary, the influence of solution inlet temperature is less pronounced on the dehumidification effectiveness, while it slightly increased from 59.31% to 61.72%, 63.15% to 65.56% and 66.65% to 68.96%, respectively, when the ethanol percentage is at 0%, 5% and 10%. This is due to the fact that the denominator ($W_{air,in} - W_{sol,in}$) in Eq. $(3-91)$ is reduced with the increase of solution temperature. Another potential explanation is that the rising of inlet solution temperature can enhance the evaporation of ethanol, which maintains a relatively low temperature of the desiccant solution during the dehumidification process, resulting in a better dehumidification effectiveness. For other studies

related to internally-cooled liquid desiccant dehumidifier, the lowest cooling water temperature is about 5 ℃ [147]. Since the dehumidifier is most commonly used in hot and humid areas, the locally supplied cold water may not reach such a low temperature. Taking the Mediterranean area as an example [148], the range of housing tap water is between 16℃ to 20℃, with an average temperature of 18℃ during summer cooling seasons. As shown in the Fig. 3-21, compared with conventional LiCl aqueous solution, adding 10% ethanol into desiccant solution can increase the moisture removal rate up to 44.7% at $T_{sol,in} = 29℃$, while the improvement of MRR is about 21.8% when inlet temperature at 17℃. The improvement of dehumidification performance by adding ethanol is more significant at a relatively high solution temperature. This study has proved that the proposed self-cooled liquid desiccant is capable of enhancing the dehumidification performance even under the condition that low temperature cooling water is not available.

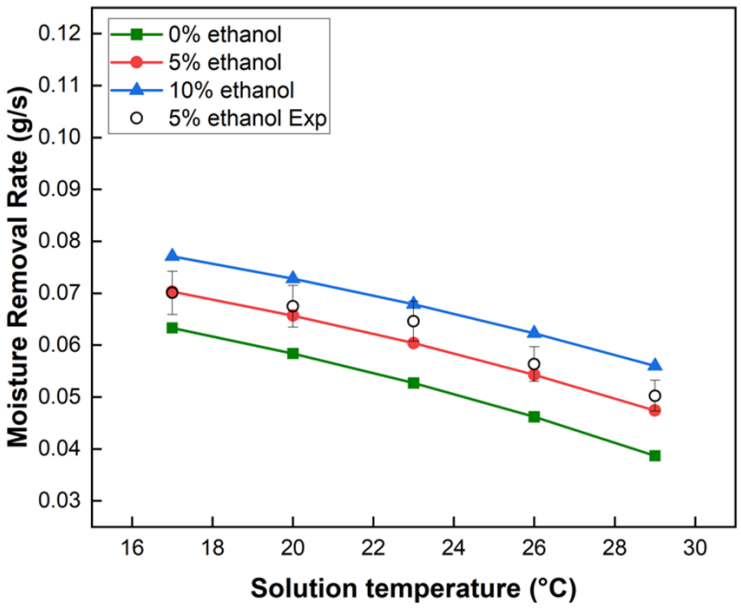

(a)

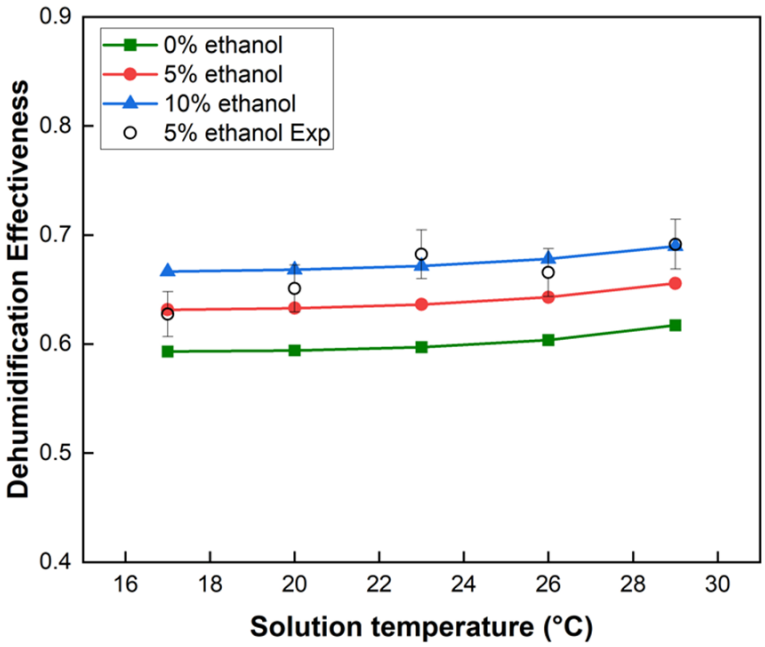

(b)

Figure 3-22 (a) Effect of inlet solution temperature on moisture removal rate.

(b) Effect of inlet solution temperature on dehumidification effectiveness

3.6.4.2. Effect of LiCl concentration

Fig. 3-23 (a) and (b) show the MRR and ε_{deh} under different concentrations of LiCl and ethanol. It is clear that as the concentration of LiCl increases, the moisture removal rate and dehumidification effectiveness tend to increase across all given ethanol percentages (0%, 5% and 10%). This indicates that the inlet mass concentration of LiCl plays a positive role in enhancing the dehumidification performance of the proposed dehumidifier. The reason is similar to the effect of desiccant solution temperature, increasing LiCl concentration will reduce the surface vapour pressure of solution, and thus enhancing the moisture absorption ability, which lead to a better dehumidification performance. For each LiCl concentration, both moisture removal rate and

effectiveness show a consistent increase with rising ethanol percentage. When there is no ethanol added to the desiccant solution, the moisture removal rate ranges from 0.00337 to 0.0584 g/s and ε_{deh} changes from 57.8% to 59.41% with the increase in LiCl concentration from 28% to 37%. At 5% ethanol, MRR varies from 0.0414 to 0.0657 g/s, and ε_{deh} from 62.37% to 63.29%, while for 10% ethanol, MRR ranges from 0.0492 to 0.0728 g/s, and dehumidification effectiveness is between 66.37% to 66.81%, respectively. While the moisture removal rate increases with the LiCl concentration, the magnitude of increase in dehumidification effectiveness is not as pronounced. This is because the increase of solution concentration will increase the inlet equilibrium specific humidity of solution, which makes the dehumidification effectiveness less sensitive to the solution temperature. The results have reaffirmed that the addition of ethanol positively impacts the dehumidification performance in both moisture removal rate and dehumidification effectiveness.

To sum up, both the moisture removal rate and dehumidification effectiveness show positive correlations with LiCl and ethanol concentrations. However, the rate of improvement in MRR is more significant compared to ε_{deh}. To ensure a better dehumidification performance, a higher concentration of LiCl and ethanol is suggested. It should also be noted that the desiccant solution with higher concentration for both LiCl and ethanol may lead to the problem of crystallization, further parametric design should be more careful to select the optimal solution concentration for the proposed self-cooled liquid desiccant dehumidifier.

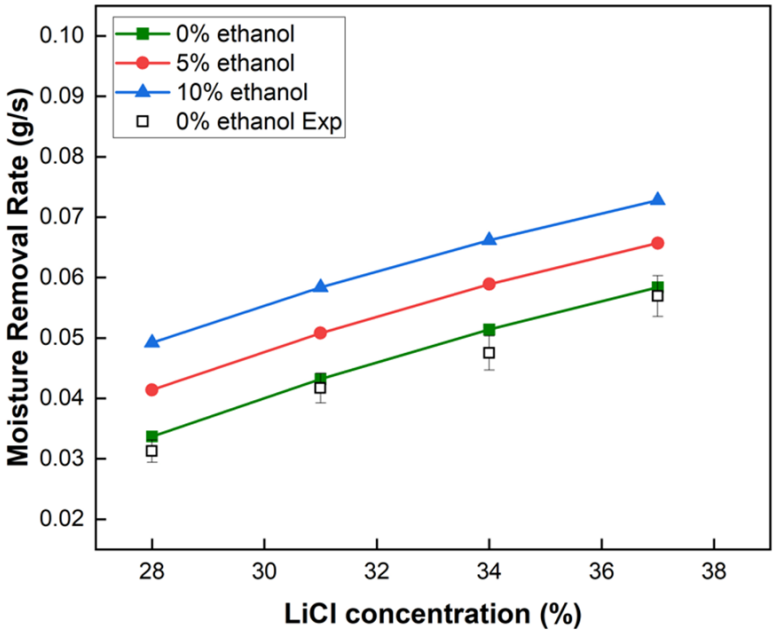

(a)

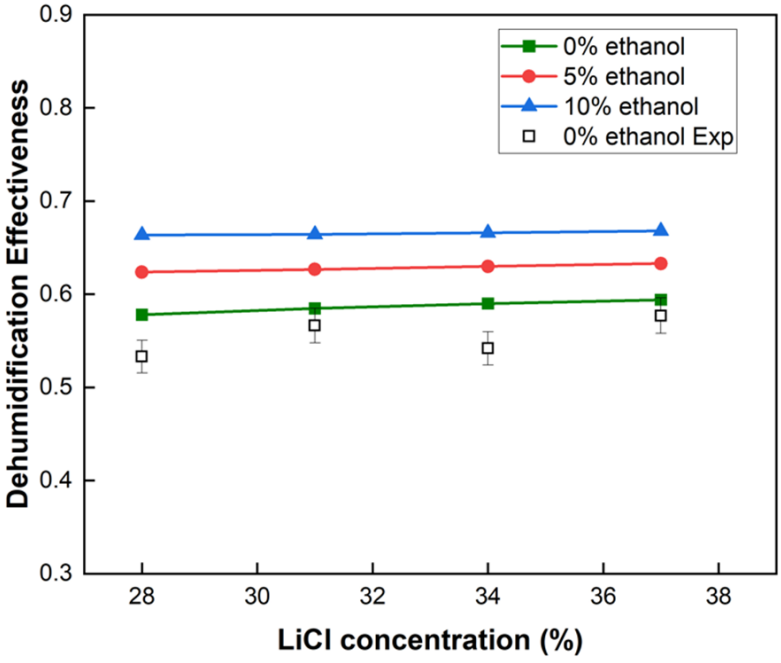

(b)

Figure 3-23 (a) Effect of inlet LiCl concentration on moisture removal rate. (b) Effect of inlet LiCl concentration on dehumidification effectiveness.

3.6.4.3. Effect of solution flow rate

In order to assess the impact of solution flow rate on dehumidification performance, both experimental and numerical tests were carried out for the ethanol concentration ratio in the range of 0% - 10% with the solution temperature at 20 ℃ an LiCl concentration at 37%, while the air flow rate was maintained at 0.01 kg/s. The influence of solution flow rate is shown in Fig. 3-24 (a) and (b). The maximum values of moisture removal rate and dehumidification effectiveness are 0.0728 g/s and 66.81% respectively when $C_{sol,in} = 10\%$ and $m_{sol} = 0.03\ kg/s$. The minimum values of moisture removal rate and dehumidification effectiveness are 0.0484 g/s and 49.26%, respectively. It is clear that the inlet mass flow rate of desiccant solution has significant influences on dehumidification performance. However, it can be found that when the solution flow rate exceeds 0.01 kg/s, the gradients of the changes become moderate and only a slight variation for both MRR and ε_{deh} is observed. During the parametric study of the effect of solution flow rate, the air flow rate is controlled to be 0.01 kg/s , thus the variation of the aforementioned dimensionless parameter m^* (mass flow rate ratio) changes from 0.25 to 3. Take desiccant solution with 10% ethanol as an example, the MRR increases by 11.64% and ε_{deh} increases by 9.18% when m^* rises from 0.25 to 1. While the MRR and ε_{deh} only increase by 3.79% and 3.04%, respectively, when m^* rises from 1 to 3. Similar trends have been found by other researches [149-151], all of their results indicate that the dehumidification performance can be improved with the increase of m^* when it is less than 1, and the performances start to remain constant when the mass flow rate ratio is higher than 1. As a result, to maintain a better

dehumidification performance while consuming less power for pump work, the proposed self-cooled liquid desiccant dehumidifier is suggested to operate under the condition that the mass flow rate of solution is closer to the process air flow rate for different ethanol percentages.

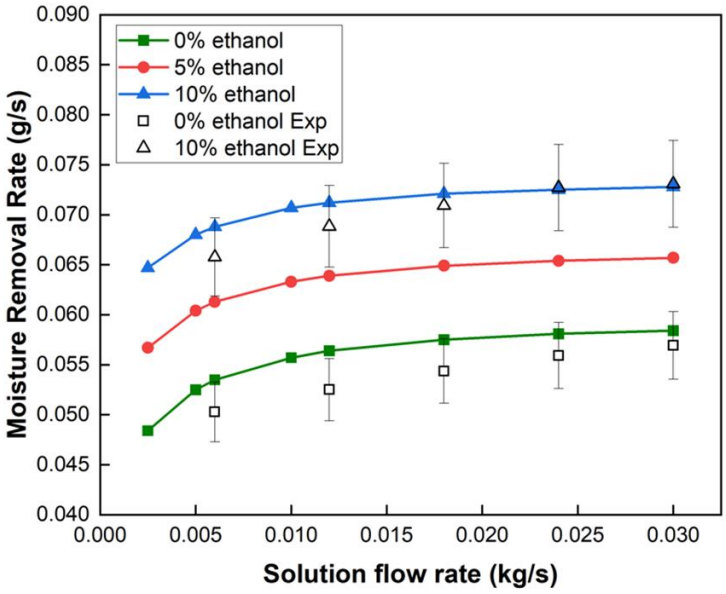

(a)

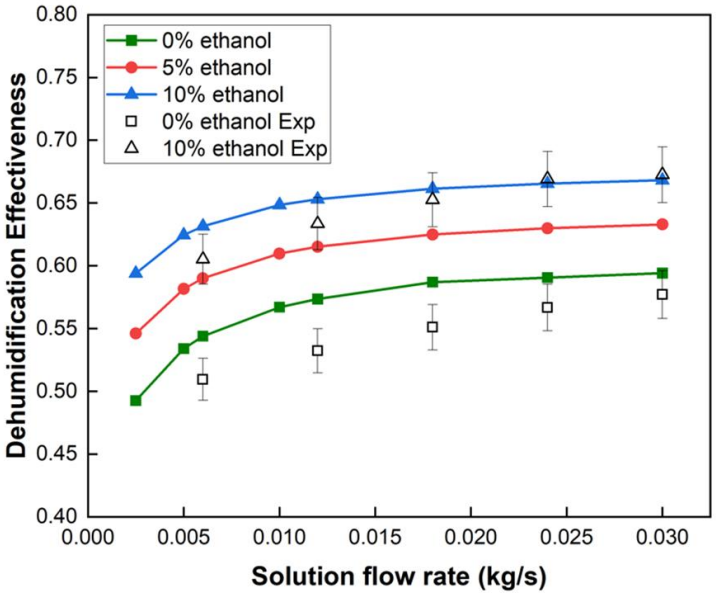

(b)

Figure 3-24 (a) Effect of solution mass flow rate on moisture removal rate. (b) Effect of solution mass flow rate on dehumidification effectiveness

3.6.5. Effects of circulated air conditions

3.6.5.1. Effect of circulated air temperature

The curves of circular air inlet temperature vary from 12 ℃ to 18 ℃ and reveal the impact on the moisture removal rate and dehumidification effectiveness as presented in Fig. 3-25. As shown in the figures, with the increase of the circulated air temperature, there is a marginal decrement in the moisture removal rate across all levels of ethanol concentration. Similarly, a decline is also observed in dehumidification effectiveness. This is potentially explained that the increase of circulated air temperature will lead to a higher solution temperature during the dehumidification performance. As mentioned above, since the solution temperature is closely related to the surface vapour pressure, the higher then desiccant solution temperature is, the lower the dehumidification performance will be. Moreover, the decline in moisture removal rate and dehumidification effectiveness with rising circulated air temperature, though consistent, is slight. Since the heat capacity of air is low, the cooling effect of circulated air is limited, which means that the variation of circulated inlet air temperature has less impact on solution temperature. Both the circulated air temperature and ethanol percentage play instrumental roles in dictating the dehumidification performance for both MRR and ε_{deh}. A cooler circulated inlet air temperature and a higher concentration of ethanol are marginally more favourable for optimizing the dehumidifier operations.

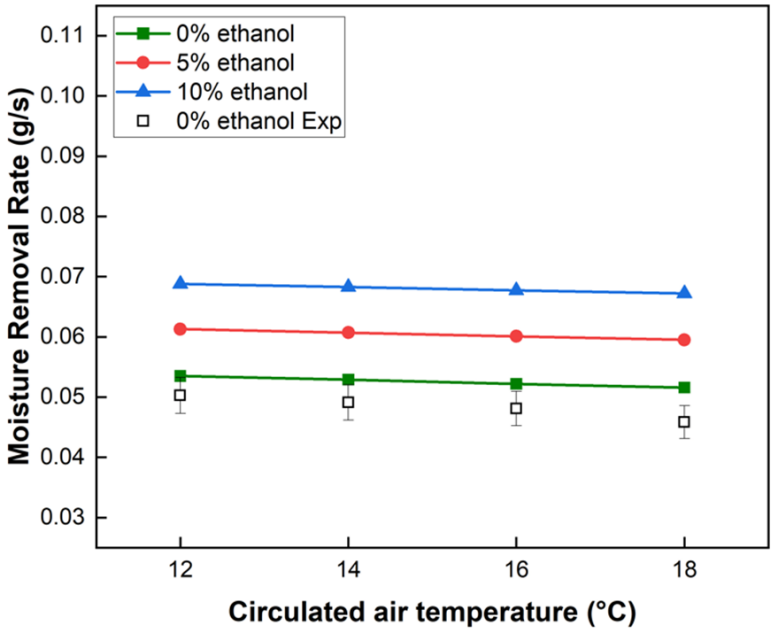

(a)

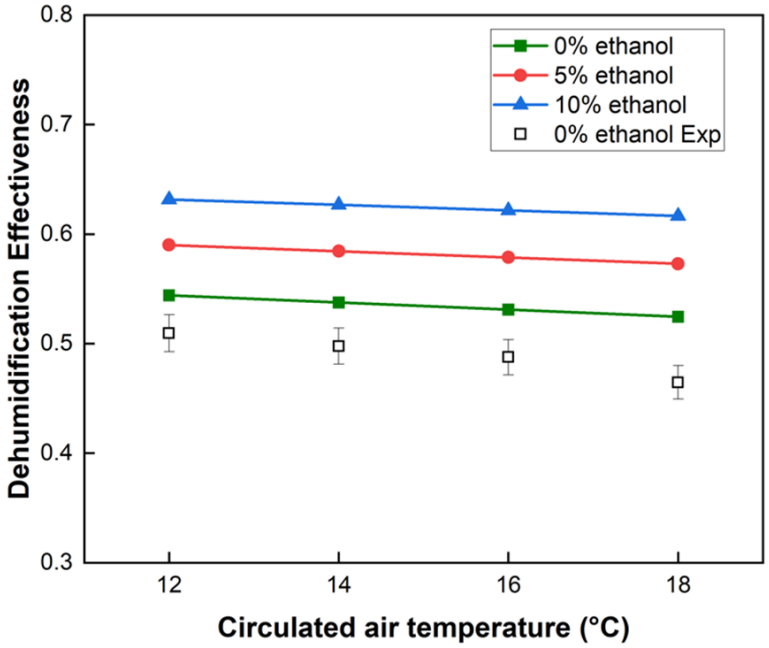

(b)

Figure 3-25 (a) Effect of inlet circulated air temperature on moisture removal rate. (b) Effect of inlet circulated air temperature on dehumidification effectiveness.

3.6.5.2. Effect of circulated air flow rate

The variations of the MRR and ε_{deh} with the circulated air flow rate are shown in Fig. 3-26, under the operation conditions with $T_{ca,in}$ at 12 ℃. The moisture removal rate increase from 0.0519 to 0.0535 g/s, 0.0593 to 0.0613 g/s and 0.0666 to 0.0688 g/s, respectively, when the mass concentration of ethanol changes from 0%, 5% and 10%. Increasing the circulated air flow rate through the solution channels can enhance the convection heat and mass transfer between desiccant solution and circulated air, resulting in a relatively low temperature of desiccant solution during the dehumidification process. The dehumidification effectiveness demonstrates a similar trend, it increases from 52.84% to 54.4%, 57.15% to 59% and 61.13% to 63.16% under different ethanol percentages, respectively. Although the increase in both moisture removal rate and dehumidification effectiveness with an elevated circulated air mass flow rate is moderate, further researches could be conducted by adjusting the geometry of the solution channel for circulated air. The parameter is limited by the dimensional design of this unique membrane-based dehumidifier. Therefore, it is evident that the dehumidification performance can be improved by increasing the circulated air flow rate and ethanol percentage.

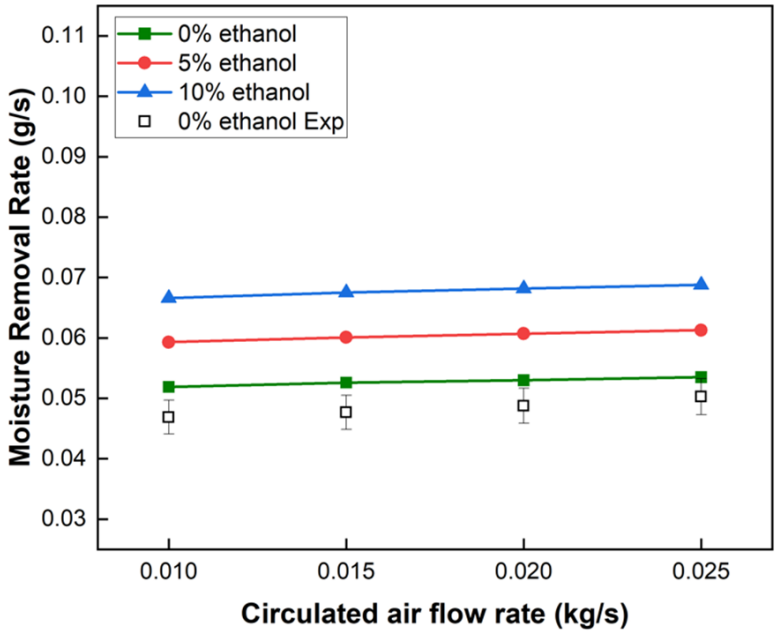

(a)

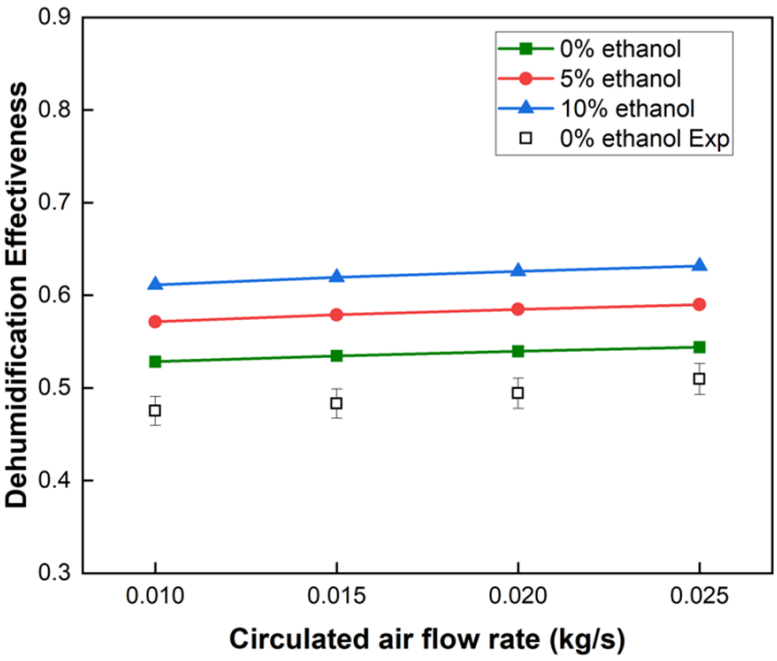

(b)

Figure 3-26 (a) Effect of circulated air flow rate on moisture removal rate. (b) Effect of circulated air flow rate on dehumidification effectiveness

3.7. Summary

In this section, a novel method of controlling the increase of desiccant solution temperature during the dehumidification process has been proposed. Vaporized coolant (ethanol) was added into lithium chloride aqueous solution to form a hybrid desiccant solution. The numerical model has been developed to evaluate the dehumidification performance of the self-cooled membrane-based liquid desiccant dehumidifier. The heat and mass transfer interactions among process air, desiccant solution and circulated air are investigated by generating the governing equations in Matlab using the finite difference method. As a newly formed hybrid desiccant solution, its thermodynamic parameters have been studied based on previous researches. The surface vapour pressure, the most critical parameter affecting the mass transfer process, has been solved by applying the NRTL method. The experimental tests have also been conducted to validate with the numerical results. The maximum discrepancies for MRR and dehumidification effectiveness are 11.2% and 11.4%, respectively.

A comprehensive parametric study has been conducted to assess the effects on the performance of the proposed self-cooled membrane-based liquid desiccant dehumidifier, the main parameters include: the air inlet temperature ($T_{air,in}$) and relative humidity ($RH_{air,in}$), air flow rate (m_{air}), solution inlet temperature ($T_{sol,in}$) and LiCl concentration ($C_{sol,in}$), solution flow rate (m_{sol}), circulated air temperature ($T_{ca,in}$) and mass flow rate (m_{sol}). All the results were evaluated under different ethanol concentrations. The main conclusions can be drawn as follows:

- The specific humidity of the novel self-cooled liquid desiccant solution can be reduced by decreasing its temperature, increasing the concentration of lithium chloride and adding more ethanol into the solution.
- The effects of inlet air temperature and relative humidity on dehumidification effectiveness are negligible. The proposed dehumidifier is capable of operating under high dehumidification performance in different weather conditions. Air flow rate is the most important parameter influencing the moisture removal rate and dehumidification effectiveness. Under $C_{eth} = 10\%$, ε_{deh} decreases by 46.92% from 66.81% to 35.46%, when m_{air} increases from 0.01 to 0.025 kg/s.
- The dehumidification effectiveness is also insensitive to inlet solution temperature and LiCl concentration. The results have shown that even if cold water is not easily available, adding ethanol can ensure that the dehumidifier can still be operated under a good dehumidification performance. A critical value of mass flow rate ratio has been discovered, it is suggested that the system operated at the critical condition when $m^* = 1$. The MRR increases by 11.64% and ε_{deh} increases by 9.18% when m^* rises from 0.25 to 1, while the MRR and ε_{deh} only increase by 3.79% and 3.04% when m^* varies from 1 to 3.
- Inlet circulated air temperature and its flow rate have no obvious influences on both MRR and ε_{deh} for inlet circulated air temperature and its flow rate. The effect of changing the solution channel geometry is suggested for future work.

- By adding different amount of ethanol into desiccant solution, the superior dehumidification performance has been verified. Under the same operation conditions, the increase of moisture removal rate can be up to 44.7%, by adding 10% ethanol compared with conventional liquid desiccant solution.

Overall, this section presented a progress in the field of developing a self-cooled membrane-based liquid desiccant dehumidifier. The aforementioned working principle of the self-cooled liquid desiccant solution is able to correspond to a competitive new dehumidification technology for the optimum design of dehumidification system in practice.

Section 4: Numerical and experimental analysis of a membrane-based liquid desiccant regenerator

4.1. Introduction

According to the literature review, most of the previous studies focused on the dehumidification performance. However, regenerator should also be considered as a critical part of the dehumidification system since the weak desiccant solution coming out from the dehumidifier has to be reconcentrated to realize the solution recycle. Meanwhile, as a newly formed self-cooled liquid desiccant solution, it is essential to compare its regeneration with conventional desiccant solution. Similarly to dehumidifier, the regeneration performance with different ethanol percentage has been evaluated by numerical model and experimental tests. Comprehensive parametric studies have been conducted to assess the effect of inlet air conditions (air temperature, relative humidity and flow rate) and inlet desiccant solution conditions (solution temperature, LiCl concentration and flow rate) on the performance of the membrane-based regenerator.

The structures of **Section 4** are: **Section 4.2** shows the numerical modelling method of the regenerator; **Section 4.3** introduces the experimental set-up in the laboratory; **Section 4.4** presents the regeneration performance indices; **Section 4.5** shows the validation of numerical model using the experimental results; **Section 4.6** reveals the effect of different parameters on the performance of the regenerator; **Section 4.7** is the main conclusion of this section.

4.2. Numerical modelling

4.2.1. Model description and assumptions

The coordinate structure of the proposed membrane-based regenerator used for numerical modelling is shown in Fig. 4-1. Compared with the dehumidifier, only diluted desiccant solution and process air interact with each other. There is no ethanol evaporation during the regeneration process since the air and solution channel are separated with semi-permeable membrane which only allows moisture to pass through. In the regenerator, the geometry of air and solution channels are the same as in dehumidifier. The hot and diluted desiccant solution flow through the solution channel, while the water content is absorbed by the process air within air channel. The air and solution are in cross-flow arrangement. One air channel and one neighbouring solution channel are selected as the calculating domain.

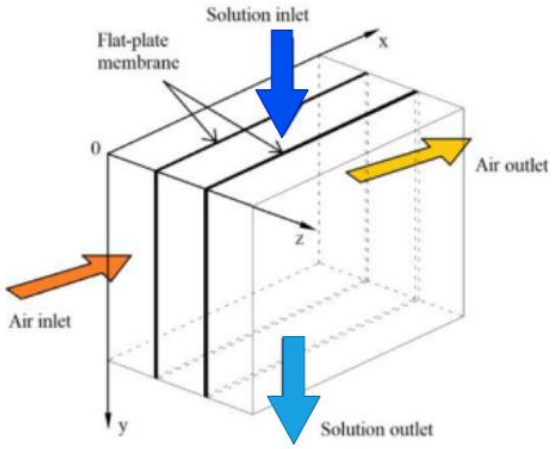

Figure 4-1 Structure of numerical modelling of regenerator

Several assumptions were made before establishing the numerical model of regenerator, which include:

- The regenerator is considered to be well insulated, no mass or heat transfer between the regenerator and outdoor environment.
- The processes of heat and mass transfer within the regenerator are in steady-state.
- Mass and heat transfer only take place on z direction and axial conduction is neglected.
- The air and solution streams on both solution channels and air channels are in laminar flow mode.
- All the fluids flow in air and solution channels are Newtonian and they are considered to maintain constant thermophysical properties (density, thermal conductivity, and specific heat capacity).
- All of the fluids are fully developed, and the entrance effects are neglected.
- The desiccant solution is considered to be evenly sprayed in regenerator, the heat and mass transfer interfaces are the same.

4.2.2. Governing equations

The process of heat and mass transfer in the membrane-based liquid desiccant regenerator can be simplified as a two-dimensional model, which is presented in Fig 4-2. The process air flow in x direction and the desiccant solution flow in y direction. The geometry of the regenerator is identical to the dehumidifier.

Further governing equations are generated based on the analyzation of the grid $dA = dx \times dy$.

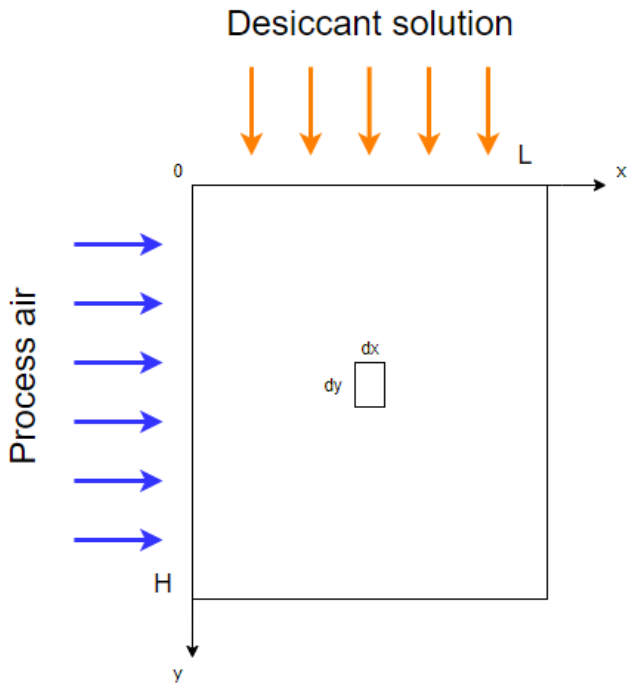

Figure 4-2 2D flow direction of the regenerator

The mass balance governing equation is developed based on the mass balance conservation of water content in the air channel and solution channel. The energy balance is developed based on the sensible heat transfer caused by temperature difference between two channels and latent heat transfer caused by water vapour evaporation, thus the mass and heat conservation and transfer equations are shown below:

Mass and heat conservation equations:

$$\frac{m_{air}}{H}\frac{dW_{air}}{dx} + \frac{m_{sol}}{L}\frac{dX_{sol}}{dy} = 0 \qquad (4-1)$$

$$\frac{m_{air}}{H}\frac{dh_{air}}{dx}+\frac{m_{sol}}{L}\frac{dh_{sol}}{dy}=0 \qquad (4-2)$$

Mass and heat transfer equations:

$$\frac{m_{air}}{H}\frac{dW_{air}}{dx}dxdy=U_m(W_{sol.mem}-W_{air})dxdy \qquad (4-3)$$

$$\frac{m_{air}}{H}\frac{dh_{air}}{dx}dxdy=\left[U_m h_{water}\left(W_{sol,mem}-W_{air}\right)+U(T_{sol}-T_{air})\right]dxdy \qquad (4-4)$$

By applying the same derivation process as shown in **Section 3.2.2**, the governing equations for X_{sol}, T_{air} and T_{sol} can thus be expressed as:

$$\frac{m_{sol}}{L}\frac{dX_{sol}}{dy}dxdy=-U_m\left(W_{sol,mem}-W_{air}\right)dxdy \qquad (4-5)$$

$$C_{p,air}\frac{m_{air}}{H}\frac{dT_{air}}{dx}dxdy=U(T_{sol}-T_{air})dxdy \qquad (4-6)$$

$$C_{p,sol}\frac{m_{sol}}{L}\frac{dT_{sol}}{dy}dxdy = -[r\cdot U_m\left(W_{sol,mem}-W_{air}\right)dxdy+U(T_{sol}-T_{air})]dxdy \qquad (4-7)$$

Overall, Eqs. $(4-3)$, $(4-5)$, $(4-6)$ and $(4-7)$ provide a comprehensive description of the heat and mass transfer with each elemental control volume in the regenerator. Further details of solving the governing equations have been presented in the following sections.

4.2.3. Boundary conditions

The boundary conditions for air channel:

$$W_{air} = W_{air,in}\ at\ x = 0 \qquad (4-8)$$

$$T_{air} = T_{air,in}\ at\ x = 0 \qquad (4-9)$$

The boundary conditions for solution channel:

$$X_{sol} = X_{sol,in}, at\ y = 0 \qquad (4-10)$$

$$T_{sol} = T_{sol.in}, at\ y = 0 \qquad (4-11)$$

To solve the governing equations between air channel and solution channel, mass and heat transfer boundary equations on membrane surface are shown as:

$$U_m\left(W_{air} - W_{sol,mem}\right) = \alpha_{m,sol}\left(C_{sol} - C_{sol,mem}\right) \qquad (4-12)$$

$$r \cdot U_m\left(W_{air} - W_{sol,mem}\right) + U\left(T_{air} - T_{sol,mem}\right) = \alpha_{sol}\left(T_{sol,mem} - T_{sol}\right) \qquad (4-13)$$

4.2.4. Normalization of governing equations

The governing equations are normalized as:

$$\frac{\partial {W_{air}}^*}{\partial x^*} = NTU_m\left({W_{sol,mem}}^* - {W_{air}}^*\right) \qquad (4-14)$$

$$\frac{\partial X_{sol}}{\partial y^*} = -NTU_m W_D \frac{1}{m^*}\left({W_{sol,mem}}^* - {W_{air}}^*\right) \qquad (4-15)$$

$$\frac{\partial {T_{air}}^*}{\partial x^*} = NTU({T_{sol}}^* - {T_{air}}^*) \qquad (4-16)$$

$$\frac{\partial {T_{sol}}^*}{\partial y^*} = -\left[NTU_m h^* Cr^* \left({W_{sol,mem}}^* - {W_{air}}^*\right) + NTUCr^* \left({T_{sol}}^* - {T_{air}}^*\right)\right] \quad (4-17)$$

4.2.5. Discretization of governing equations

The simplified governing equations are thus discretized by applying finite difference method using backward difference scheme:

$${W_{air(m,n+1)}}^* - {W_{air(m,n)}}^* = dx^* NTU_m \left[{W_{so,mem(m,n+1)}}^* - {W_{air(m,n+1)}}^*\right] \quad (4-18)$$

$$X_{sol(m+1,n)} - X_{sol(m,n)} = dy^* NTU_m W_D \frac{1}{m^*} \left[{W_{sol,mem(m+1,n)}}^* - {W_{air(m+1,n)}}^*\right] \quad (4-19)$$

$${T_{air(m,n+1)}}^* - {T_{air(m,n)}}^* = -dx^* NTU \left[{T_{sol(m,n+1)}}^* - {T_{air(m,n+1)}}^*\right] \quad (4-20)$$

$$\begin{aligned} {T_{sol(m+1,n)}}^* - {T_{sol(m,n)}}^* &= -\left[dy^* NTU_m h^* Cr^* \left({W_{sol,mem(m+1,n)}}^* - {W_{air(m+1,n)}}^*\right)\right. \\ &+ dy^* NTUCr^* \left({T_{sol(m+1,n)}}^*\right. \\ &\left. \left. - {T_{air(m+1,n)}}^*\right)\right] \end{aligned} \quad (4-21)$$

Where m and n are the grids number in x and y direction, respectively.

4.2.6. Thermodynamic parameters of air and desiccant solution

The calculation methods for air and desiccant solution properties have been shown in **Section 3.2.7**. It should be noted that comparing with the investigation of dehumidifier, the operation conditions for solution temperature and concentration are different. The equilibrium specific humidity of the proposed

self-cooled liquid desiccant solution under varies operation conditions for regenerator are calculated, the psychometric chart is present in Fig. 4-3.

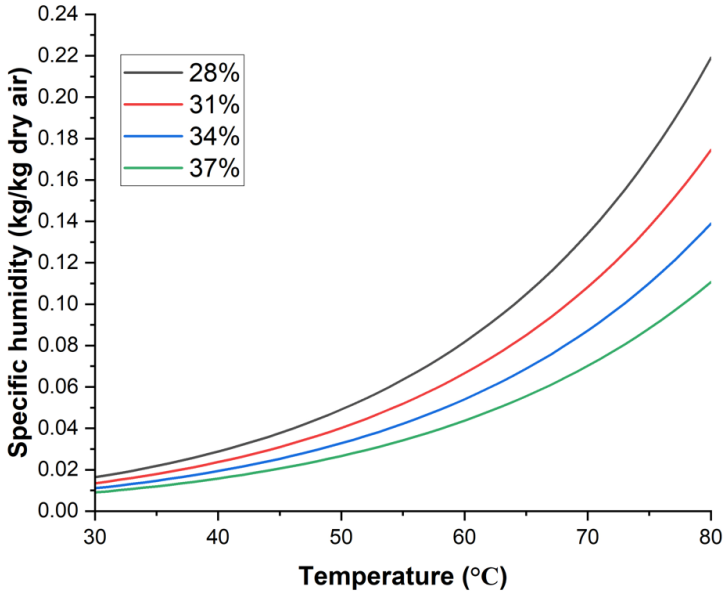

(a)

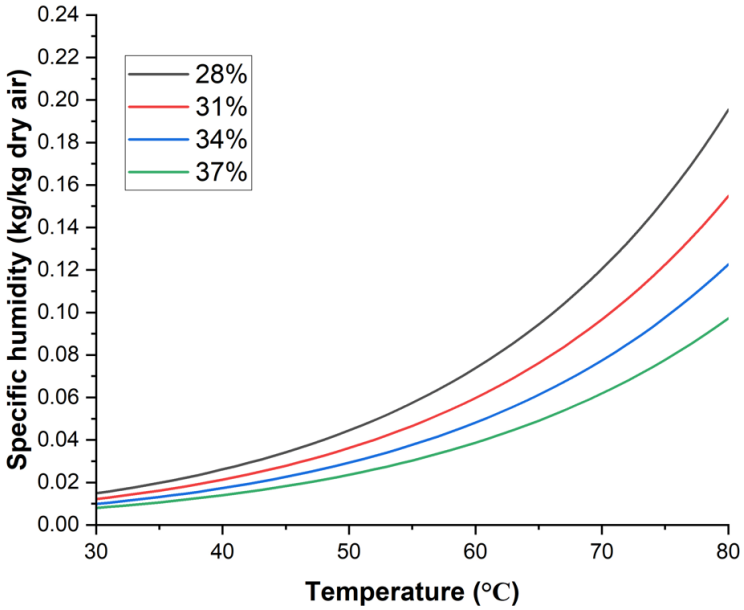

(b)

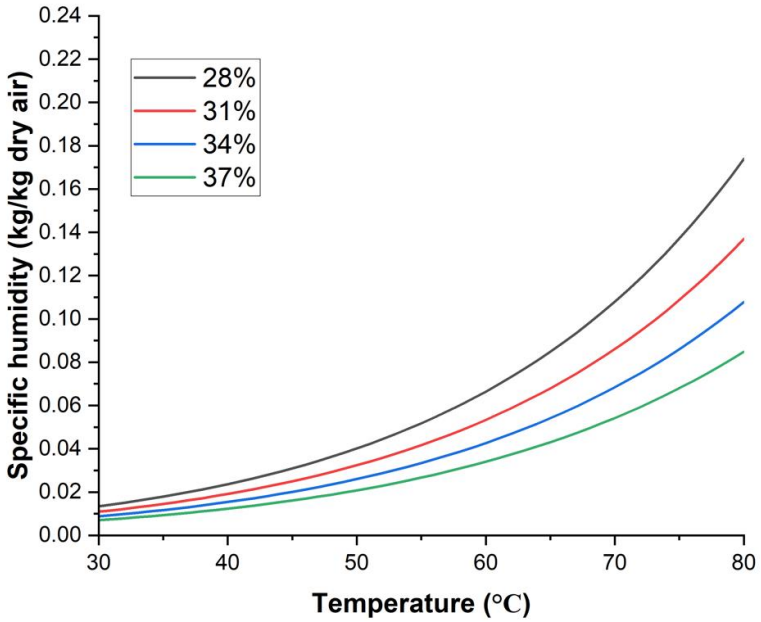

(c)

Figure 4-3 Specific humidity of desiccant solution for regenerator at (a) $C_{eth} = 0\%$; (b) $C_{eth} = 5\%$; and (c) $C_{eth} = 10\%$

4.2.7. Numerical solving scheme

Similarly to the dehumidifier, the governing equations of the membrane-based regenerator were solved iteratively in Matlab until they were converged. The simulation procedures are shown below:

1) Set the inlet conditions for air and diluted desiccant solution.
2) Assume the initial specific humidity of membrane surface is identical with the inlet equilibrium specific humidity of desiccant solution.
3) Solve the discrete governing equations to obtain T_{sol}, T_{air}, X_{sol} and W_{air} using the inlet conditions.

4) Based on the temperature and humidity fields for air and solution flows, solve the heat and mass transfer boundary conditions on the membrane surface to obtain the membrane surface temperature and concentration fields in the solution side ($T_{sol,mem}$ and $C_{sol,mem}$).
5) Calculate the membrane surface humidity field in the solution side ($W_{sol,mem}$) based on $T_{sol,mem}$ and $C_{sol,mem}$.
6) Adopt new $W_{sol,mem}$ as a default value and return to step 4 until $W_{sol,mem}$ is converged.
7) Apply the value obtained from last step and return to step 3 until the results are all converged.
8) Calculate the moisture addition rate and regeneration effectiveness based on the outlet conditions of the regenerator.

The solution procedure during the simulation process to solve the interacted governing equations is shown below:

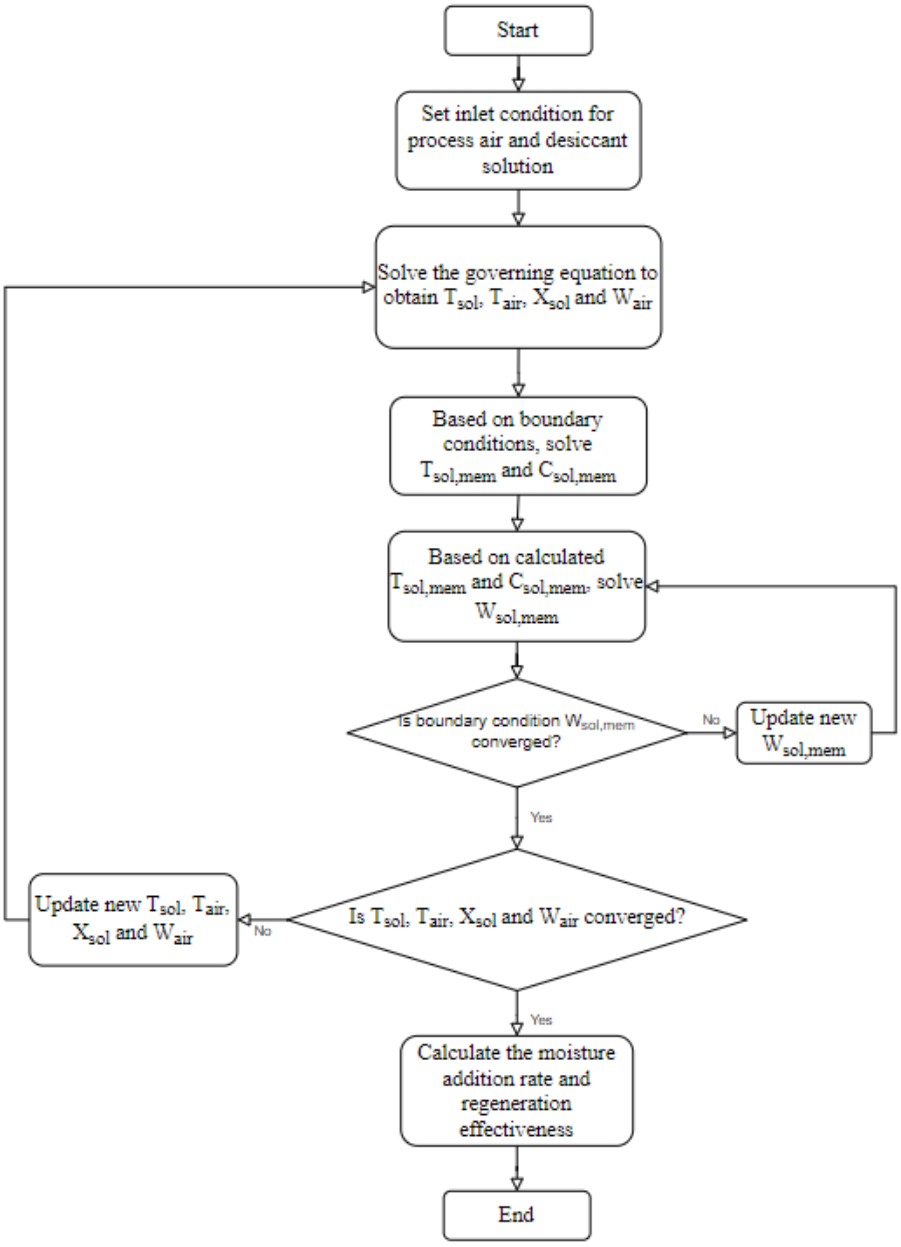

Figure 4-4 Flow chart of the solving procedure for regenerator

4.2.8. Mesh independent test

In order to guarantee the accuracy of the numerical model, several tests have been conducted with the mesh size of 30×60, 50×100 and 100×200. The simulation results under different mesh size is presented in Table 4-1. The inlet conditions of process air temperature, relative humidity and mass flow rate is 24 ℃, 40% and 0.01 kg/s, respectively, while the inlet conditions of desiccant solution were set to be 50 ℃, 37% and 0.03 kg/s. The inlet mass concentration of ethanol is set to be 10%. Since the variations of $T_{air,out}$ and $T_{sol,out}$ are 0.169% and 0.035%, respectively, when the mesh size changes from 30×60 to 100×200. It has been proved that the proposed numerical model to analyse the membrane-based regenerator is independent with its mesh size. To reduce the time consumption of the simulation process, mesh size of 50×100 is selected for further evaluation.

Table 4-1. Mesh independent test for regenerator

Mesh size	30×60	50×100	100×200
$T_{air,out}$ (℃)	45.618	45.662	45.695
$W_{air,out}$ (kg/kg)	0.0137	0.0137	0.0137
$T_{sol,out}$ (℃)	45.794	45.803	45.810
$C_{sol,out}$ (%)	37.09	37.09	37.09

4.3. Experiment set-up

The experimental test of the membrane-based liquid desiccant regenerator have been conducted using the test rigs in the laboratory as illustrated in **Section 3.3**. The geometry of the regenerator and the membranes within it were manufactured both to be the same as dehumidifier. The diluted desiccant solution coming out from dehumidifier will be heated by the hot water supply system with the water temperature range from 20℃ to 80℃. The hot water temperature is controlled by an electrical boiler (RM cylinders), while its flow rate is controlled by a liquid flow indicator (Paker). The details of the measurement instruments have been presented in **Section 3.3.3** and the uncertainty analysis method in Section **3.3.4**. Error bars with respective uncertainties are shown in the results and discussion sections.

4.4. Performance evaluation

To assess the regeneration performances under different operational condition, moisture addition rate (MAR) and regeneration effectiveness (ε_{reg}) are used in this study. The calculation methods for MAR [152] and ε_{reg} [153] are :

$$MAR = m_{air}\left(W_{air,out} - W_{air,in}\right) \qquad (4-22)$$

$$\varepsilon_{reg} = \frac{W_{air,out} - W_{air,in}}{W_{sol,in} - W_{air,in}} \qquad (4-23)$$

Where, m_{air} is the air flow rate of the regenerator (kg/s), $W_{air,in}$ and $W_{air,out}$ are the air inlet and outlet specific humidity (kg/kg), $W_{sol,in}$ is the solution inlet equilibrium specific humidity (kg/kg).

As it can be seen that the moisture addition rate reflects the amount of moisture absorbed by air from the weak desiccant solution. The regeneration effectiveness shows the ratio of the actual absorption of moisture content by air to the maximum moisture transfer. For conventional regeneration process using pure LiCl aqueous solution, different performance evaluation indices were used by other researchers [92, 154] such as moisture flux rate (MFR) and solution side effectiveness (ε_{sol}). Both of these performance evaluation indices need to measure the solution outlet concentration, and normally it is observed by measuring the outlet temperature and density of the desiccant solution. Since the main purpose of regenerator is to reconcentrate the desiccant solution, MFR and ε_{sol} are more directly reflecting the regeneration performance. However, with the addition of ethanol into desiccant solution, it is difficult to observed the outlet concentration of LiCl by simply measuring its temperature and density during the experimental tests. As a result, MAR and ε_{reg} are selected to assess the regeneration performance in this study.

4.5. Model validation

The experimental results have been used to validate the numerical model. Overall, 47 groups of the experimental tests under different operating conditions have been conducted to validate numerical results. The mass concentration of ethanol changes from 0% to 5% and 10%. The temperature of desiccant solution were varied from 45 ℃ to 65 ℃. The mass concentration of lithium chloride was within the range of 28% to 37%. The Based on the capacity of fans and solution pump, the range of mass flow rate of the air and desiccant solution were set to be the same as the inlet conditions of dehumidifier. To assess the regeneration

performance under different inlet air conditions, the air temperature and relative humidity of the return air before entering the membrane-based regenerator were in the range of $20-28$ ℃ and $30-50\%$, respectively. The comparison of moisture addition rate and regeneration effectiveness between the numerical results and experimental data were present in Fig. 4-5 and 4-6 below. It shows that all the deviation between numerical and experimental results were within 10%, which indicates that the numerical results are within the tolerance range of experimental data. The maximum discrepancies for moisture addition rate and regeneration effectiveness are 9.76% and 9.63%, respectively. As a result, the numerical results have been proved to have a good agreement with the experimental data which indicates that the proposed numerical model of the membrane-based liquid desiccant regenerator is valid to predict the regeneration performance.

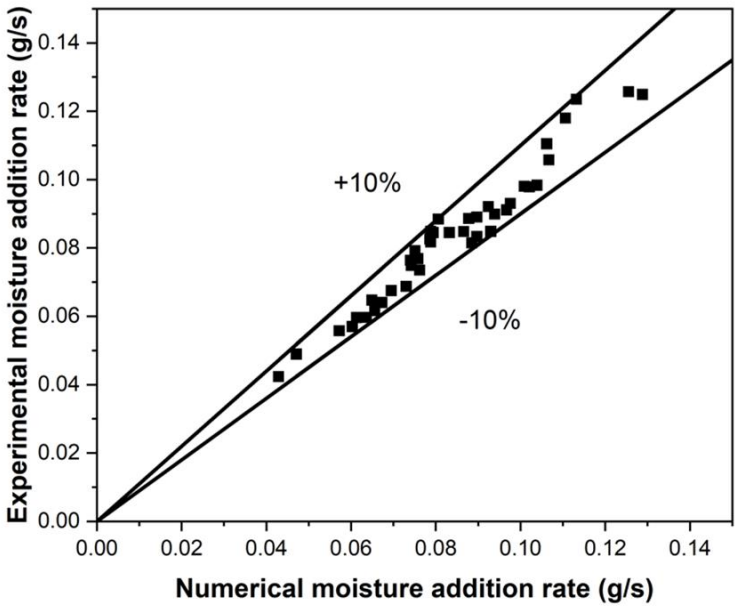

Figure 4-5 Comparison of moisture removal addition between numerical and experimental data

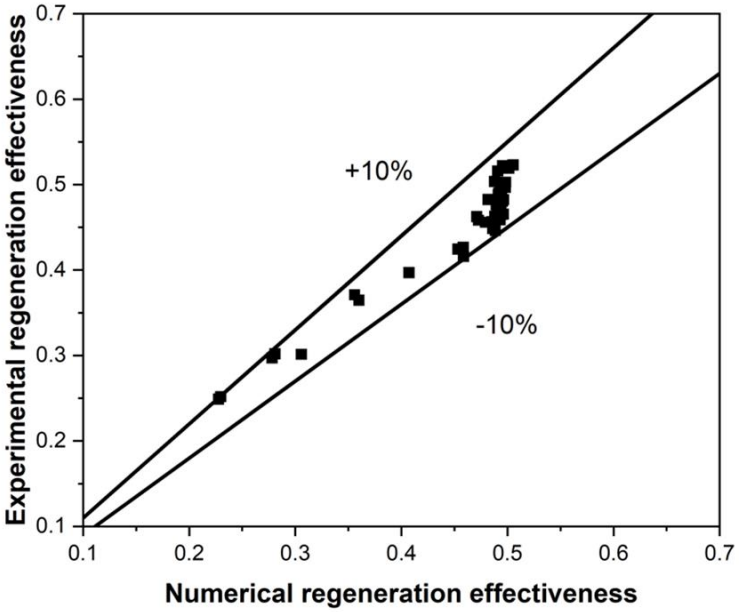

Figure 4-6 Comparison of regeneration effectiveness between numerical and experimental data

4.6. Results and discussion

4.6.1. Temperature and humidity field

After all the governing equations have been converged, the temperature, humidity and concentration fields of air and desiccant solution can be obtained under different operation conditions. Fig. 4-7 below shows the distributions of temperature and humidity filed in the air channel, and temperature and LiCl concentration filed in the solution channel. The inlet operation conditions of the air temperature, relative humidity and mass flow rate are set to be 24 ℃, 40% and 0.01 kg/s, respectively, while the inlet operation conditions of the solution temperature, LiCl concentration and mass flow rate are 50 ℃, 37% and 0.03 kg/s. It can be seen from Fig 4-7 (a) and (b) that both the air temperature and

humidity ratio reach the maximum values (47.17 ℃ and 0.01483 kg/kg, respectively) at the top right corner of the regenerator. This is because that the air is gradually heated by the hot solution along its flow direction inside the regenerator, and more moisture has been absorbed during the regeneration process. The air temperature and humidity are higher at top side since the desiccant solution has the highest temperature and lowest concentration at the top of the air channel, as shown in Fig 4-7 (c) and (d). A similar case can be found in the solution channel, where the solution reaches the lowest temperature (42.57 ℃) and the highest concentration (37.11%) at the left bottom corner. The results have indicated that the temperature and humidity fields are non-uniform two-dimensional profiles. The driving forces during the heat and mass process are also not uniform, and it reaches the highest value at the inlet of air and desiccant solution.

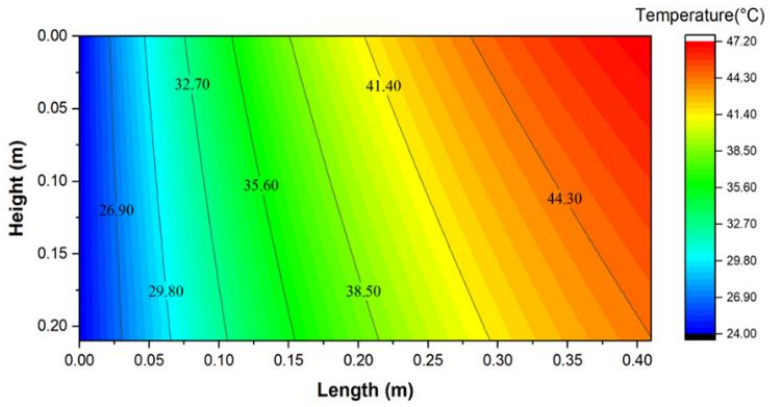

(a)

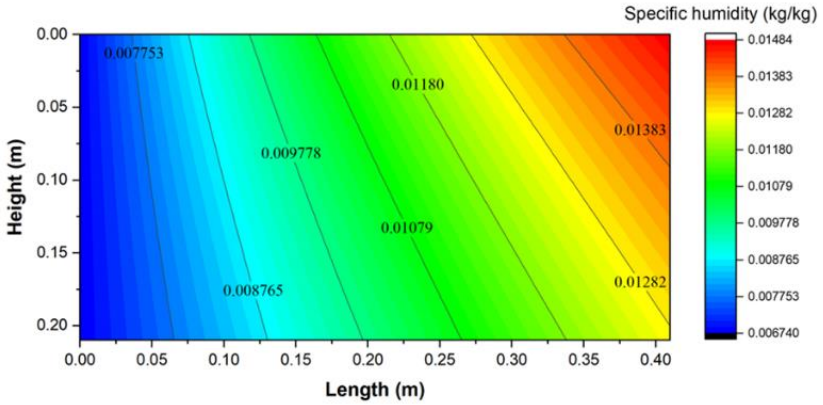

(b)

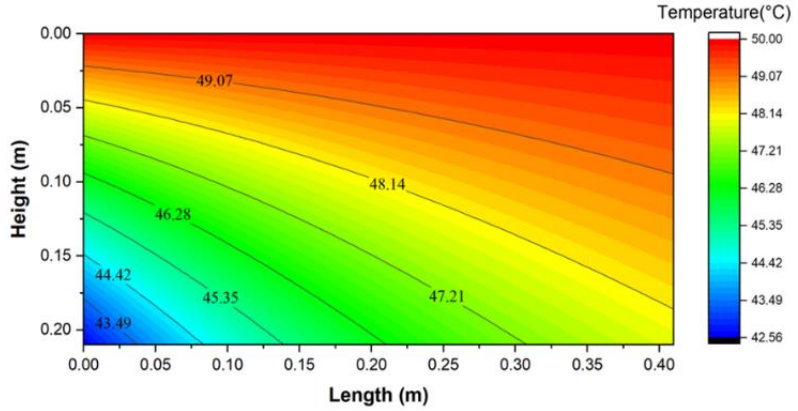

(c)

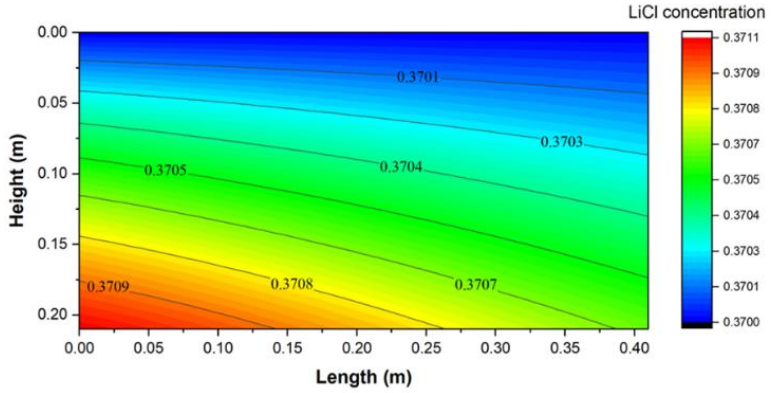

(d)

Figure 4-7(a) Air temperature field; (b) Air specific humidity field; (c) Solution temperature field; (d) LiCl concentration field.

4.6.2. Effects of air conditions

4.6.2.1. Effect of air temperature

The effect of the inlet air temperature on the regeneration performance under different ethanol concentrations have been presented in Fig 4-8 (a) and (b). The moisture addition rate reaches the maximum value of 0.1039 g/kg when $T_{air,in} = 20℃$ and $C_{eth} = 0\%$, while the minimum value is 0.0613 g/kg when $T_{air,in} = 28℃$ and $C_{eth} = 10\%$. The results have shown that the addition of ethanol will lead to a negative impact on the regeneration performance, since the surface vapour pressure of the desiccant solution is reduced with higher ethanol mass concentration, as shown in Section 4.2.6. By adding ethanol into desiccant solution, the driving force of moisture transfer between air and solution is weakened. For various inlet air temperatures under the same relative humidity (40%), the air humidity ratio will be increased with the increase of air temperature, which leads to a higher vapour pressure of air. Therefore, the amount of moisture been removed by the air during the regeneration process is reduced by increasing the inlet air temperature. Fig 4-8 (b) indicates that both the inlet air temperature and ethanol percentage have limited influence on regeneration effectiveness. For desiccant solution without ethanol, the regeneration effectiveness changes from 48.81% to 49.30% when the air temperature rises from 20 ℃ to 28 ℃. While the regeneration effectiveness varies from 49.38% to 49.64% for 10% ethanol. The increment of air temperature and ethanol mass concentration leads to the decrease of the denominator in Eq. ($4-23$), thereby increasing the regeneration effectiveness.

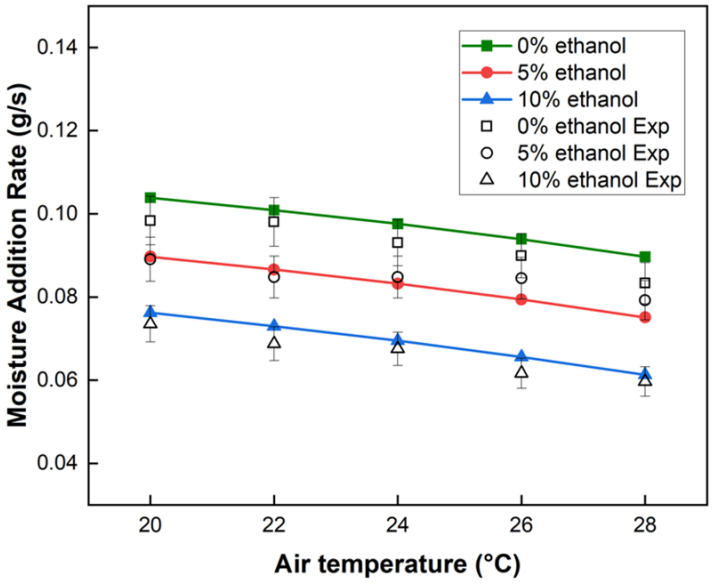

(a)

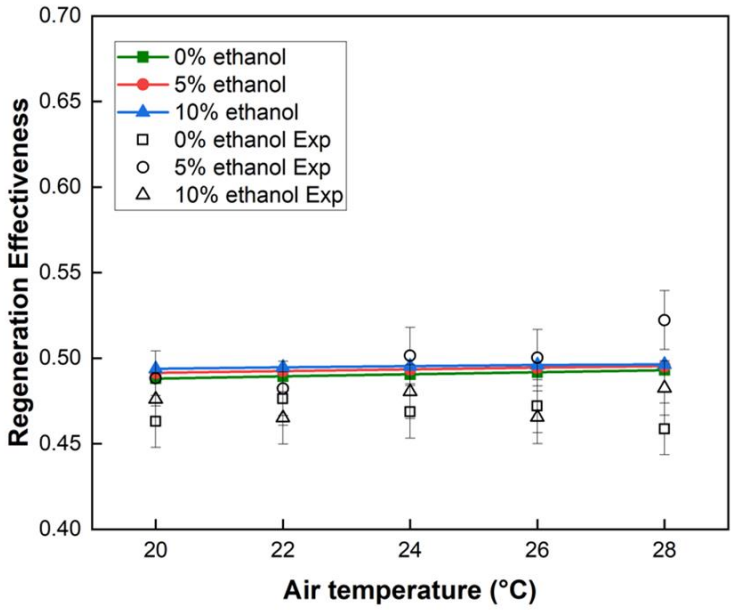

Figure 4-8 (a) Effect of inlet air temperature on moisture addition rate. (b) Effect of inlet air temperature on regeneration effectiveness

4.6.2.2. Effect of air relative humidity

Similarly to the inlet air temperature, the effect of the air relative humidity on the regeneration performance is identified. The air temperature and flow rate are set at 24 ℃ and 0.01 kg/s, respectively, while the solution temperature, LiCl concentration and flow rate are at 24 ℃, 37% and 0.03 kg/s. The regeneration performance, which includes moisture removal rate and regeneration effectiveness under different air relative humidity are presented in Fig. 4-9. For desiccant solution without adding ethanol, the moisture addition rate decreases by 17.06% from 0.1067 to 0.0885 g/kg, when the relative humidity rises from 30% to 50%. Moreover, by adding 5% and 10% ethanol into desiccant solution, the MAR decreased by 19.91% and 23.48% from 0.0924 to 0.074 g/kg and 0.0762 to 0.0613 g/kg, respectively. This is due to the decrease in water vapour partial pressure difference between air and solution. As shown in Fig. 4-9 (b), the impact of inlet air relative humidity and ethanol mass concentration on the regeneration effectiveness is almost negligible. For regenerators using conventional liquid desiccant solution, the same trend has been observed from previous studies [88]. As a result, the performance of the membrane-based regenerator can be improved by applying drier air to remove the moisture content.

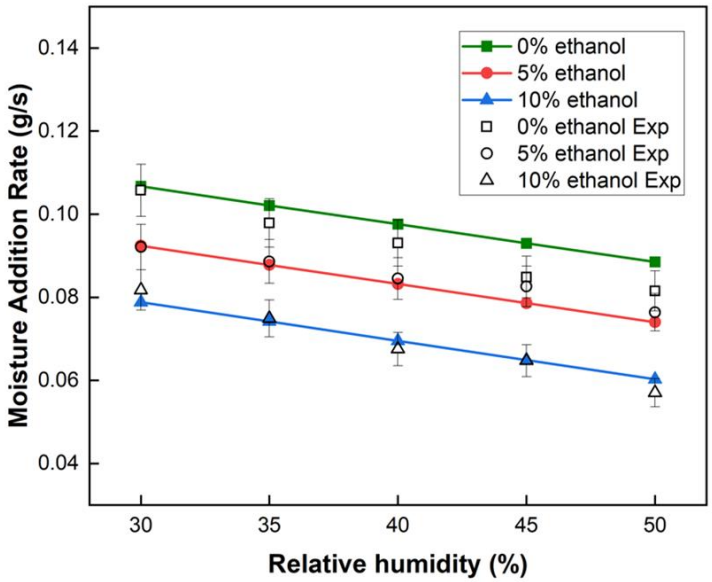

(a)

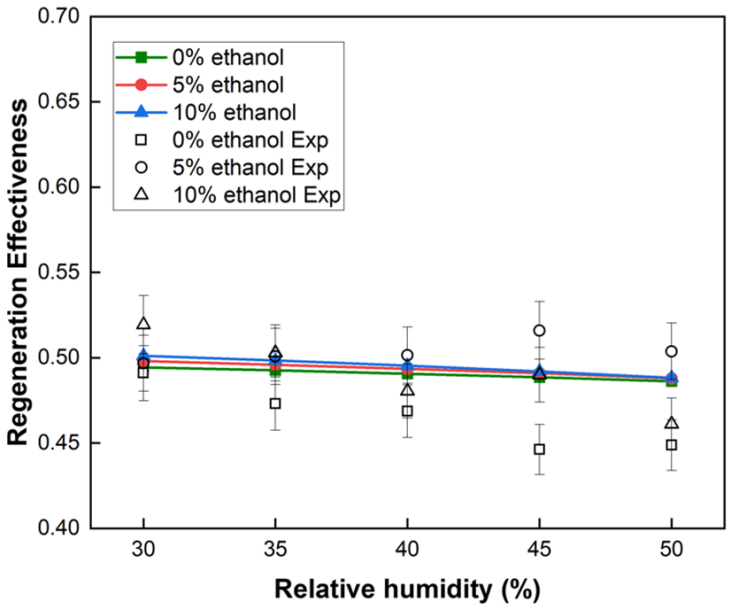

(b)

Figure 4-9 (a) Effect of inlet air relative humidity on moisture addition rate. (b) Effect of inlet air relative humidity on regeneration effectiveness

4.6.2.3. Effect of air flow rate

Fig. 4-10 (a) reveals that the moisture addition rate increases from 0.0976 to 0.1132 g/s as the air flow rate increases from 0.01 to 0.025 kg/s, when there is no ethanol added into desiccant solution. For $C_{eth} = 5\%$ and 10%, the moisture addition rate increase from 0.0832 to 0.0966 g/s and 0.0695 to 0.0806 g/s, respectively. The reason for this is that, with the addition of ethanol, the surface vapour pressure became smaller, and consequently reducing the main driving force ($W_{sol} - W_{air}$) of mass transfer process inside the regenerator. Besides, with the increase of air flow rate, the change of air humidity ratio is smaller in the air channel and the water vapour pressures maintains at relatively low value. As a result, the mass transfer between air and solution flow can be enhanced. However, the regeneration effectiveness is diminished since the difference between the inlet and out air humidity ratio is reduced. As presented in Fig. 4-10 (b), the regeneration effectiveness decreases by 53.63% from 49.54% to 22.97% when m_{air} increased from 0.01 to 0.025 kg/s at $C_{eth} = 10\%$. The results have proved that the air mass flow rate has a significant influence on the regeneration effectiveness, while the effect of ethanol mass concentration on the regeneration effectiveness can almost be neglected.

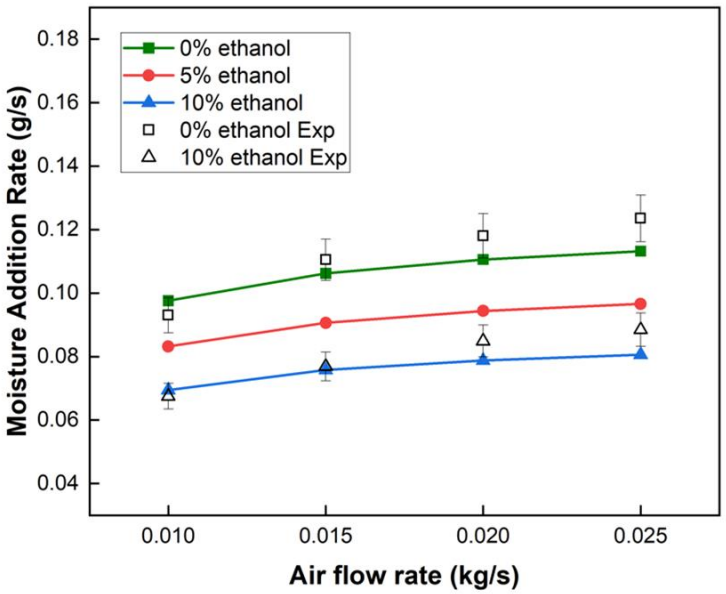

(a)

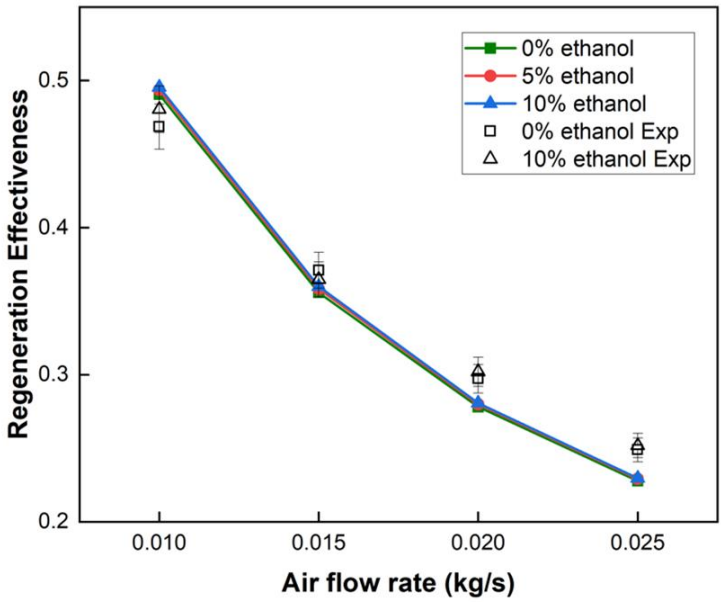

(b)

Figure 4-10 (a) Effect of inlet air flow rate on moisture addition rate. (b) Effect of inlet air flow rate on regeneration effectiveness

4.6.3. Effects of solution properties

4.6.3.1. Effect of solution temperature

The effect of solution inlet temperature on the moisture addition rate and regeneration effectiveness during the regeneration process are shown in Fig. 4-11. A significant increase in moisture addition rate with the increase of inlet solution temperature has been observed in Fig. 4-11 (a), under varying ethanol mass concentrations. This is due to the fact that the equilibrium surface vapour pressure of the desiccant solution is highly dependent on its temperature. As mentioned in **Section 4.2.6**, the higher the solution temperature is, the higher the vapour pressure will be. Thus, the vapour pressure difference between air and solution increases as the solution inlet temperature rises, which increases the potential for moisture transfer. It can be seen from Fig. 4-11 (b) that the regeneration effectiveness decreases with the solution inlet temperature and ethanol percentage. This is because the equilibrium specific humidity of desiccant solution increases and the denominator of Eq. $(4-23)$ increases significantly for a higher inlet solution temperature and ethanol mass concentration. It has also been found that the regeneration performances MAR and ε_{reg} are more sensitive to ethanol mass concentration when the inlet solution temperature is higher. For example, by adding 10% ethanol into desiccant solution, MAR decreases by 0.0224 g/s (from 0.0695 to 0.0471 g/s) at $T_{sol,in} = 45$℃, while MAR decreases by 0.0496 g/s at $T_{sol,in} = 65$℃. This is due to the fact that the ethanol mass concentration has a greater influence on solution equilibrium specific humidity at higher solution temperature.

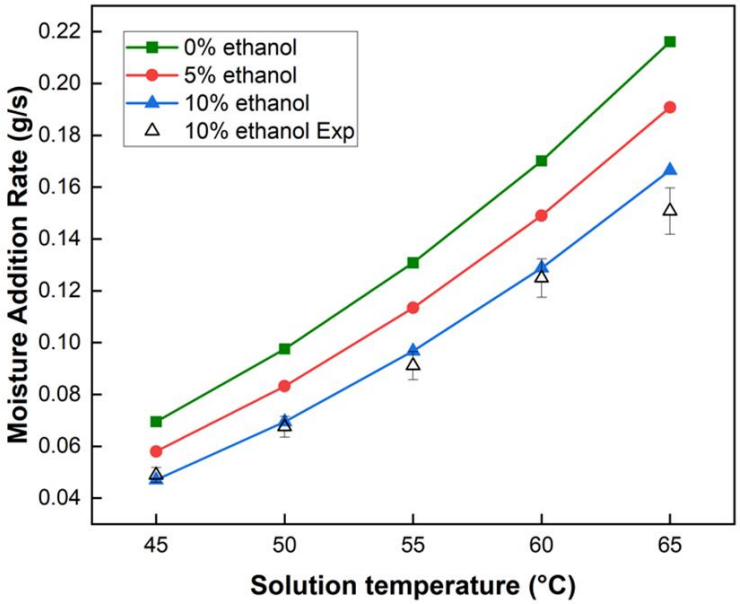

(a)

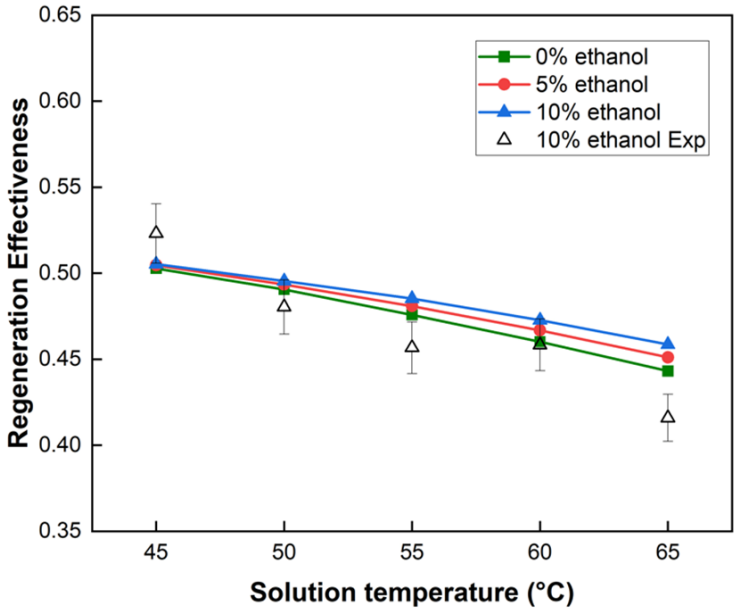

(b)

Figure 4-11 (a) Effect of solution temperature on moisture addition rate. (b) Effect of solution temperature on regeneration effectiveness

4.6.3.2. Effect of LiCl concentration

Fig. 4-12 illustrates the effect of solution concentration on regeneration performance. Similar to the dehumidifier, the LiCl concentration has a great impact on the regenerator since it is directly related to the equilibrium surface vapour pressure. Under the operation condition ($T_{air,in} = 24$ ℃, $RH_{air,in} = 40\%$, $m_{air,in} = 0.01\ kg/s$, $T_{sol.in} = 50$ ℃ and $m_{sol,in} = 0.03\ kg/s$), the MAR decrease from 0.1940 to 0.0976 g/s, 0.1753 to 0.0832 g/s and 0.1573 to 0.0695 g/s , respectively, at $C_{eth} = 0\%, 5\%\ and\ 10\%$. The increase of solution concentration would decrease the solution specific humidity and reduce the mass transfer potential, leading to the decrease in MAR as shown in Fig. 4-12 (a). On the contrary, the regeneration effectiveness can be improved slightly with the increase of inlet LiCl concentration. For example, under different ethanol concentrations (0%, 5% and 10%), the effectiveness changed by 7.05%, 6.13% and 5.11%, respectively, when C_{sol} rises from 28% to 37%. This is caused by the decrease of equilibrium humidity ratio $W_{sol,in}$ in Eq. $(4-23)$. Although the addition of ethanol can lead to a small improvement in regeneration effectiveness, the reduction in moisture addition rate is more significant. The results have shown that the newly formed self-cooled liquid desiccant solution has a negative impact on the regeneration performance, further studies on optimization design for the complete dehumidification system are required. Besides, as presented in Fig 4-12 (b), ε_{reg} is more sensitive to the variation of ethanol mass concentration when C_{sol} is lower.

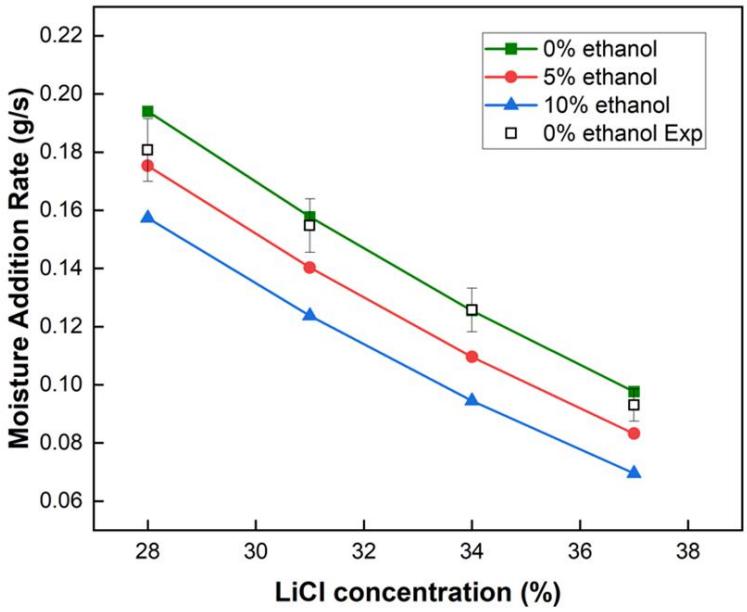

(a)

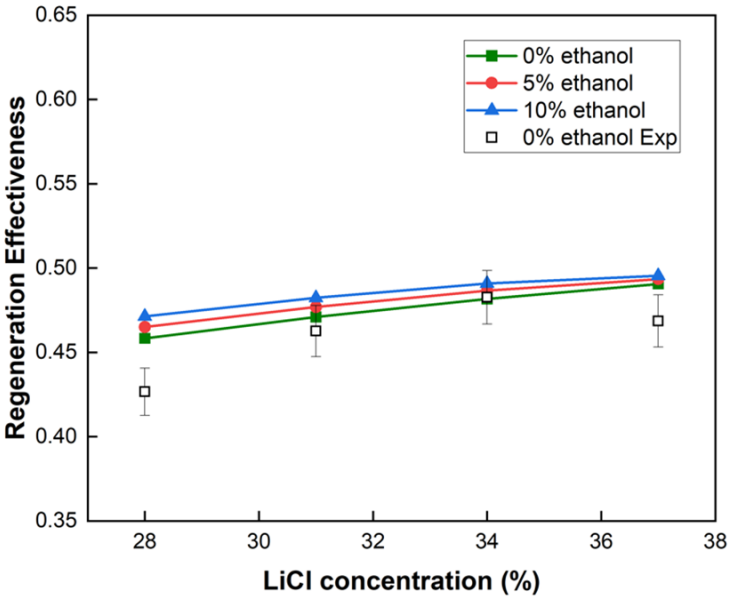

(b)

Figure 4-12 (a) Effect of LiCl concentration on moisture addition rate. (b) Effect of LiCl concentration on regeneration effectiveness

4.6.3.3. Effect of solution flow rate

Fig. 4-13 (a) reveals that the moisture addition rate, MAR, can be enhanced by the increase of solution inlet flow rate. A similar trend has been found when assessing the effect of solution flow rate on dehumidifier. This is because that a higher solution flow rate will increase the heat capacity rate and reduce the temperature decrease caused by the temperature difference and evaporation of water during the regeneration process. As a result, a higher vapour pressure difference between the air and desiccant solution would be maintained when the solution mass flow rate was higher, since the equilibrium specific humidity of the desiccant solution is higher at higher solution temperatures and constant LiCl concentration. The increase of solution flow rate in the regenerator will increase the moisture transfer potential between air and solution, and thus increase the regeneration performance. The moisture addition rate varies from 0.0887 to 0.0636 g/s when $m_{sol} = 0.0018\ kg/s$ and C_{eth} rises from 0% to 10%, while the variation of regeneration effectiveness is almost negligible (from 44.59% to 45.32%). It can also be seen that the gradients of the regeneration performance decrease with the increase of solution flow rate. For example, when $C_{eth} = 10\%$, the MAR and ε_{reg} are enhanced by 0.0266 g/s (from 0.0429 to 0.0695 g/s) and 18.96% (from 30.58% to 49.54%) when the solution mass flow rate changes from 0.006 to 0.03 kg/s. However, they only increase by 0.0061 g/s and 2.99%, respectively, when m_{sol} keep rising to 0.05 kg/s. Since the regenerator was operating under the condition of $m_{air} = 0.01\ kg/s$, a critical value of mass flow rate ratio ($m^* = 3$) for the membrane-based has been defined. The increase of regeneration performances becomes moderate when the mass flow rate ratio is

higher than 3. Therefore, the proposed membrane-based liquid desiccant regenerator is recommended to operate under the critical value of m^*.

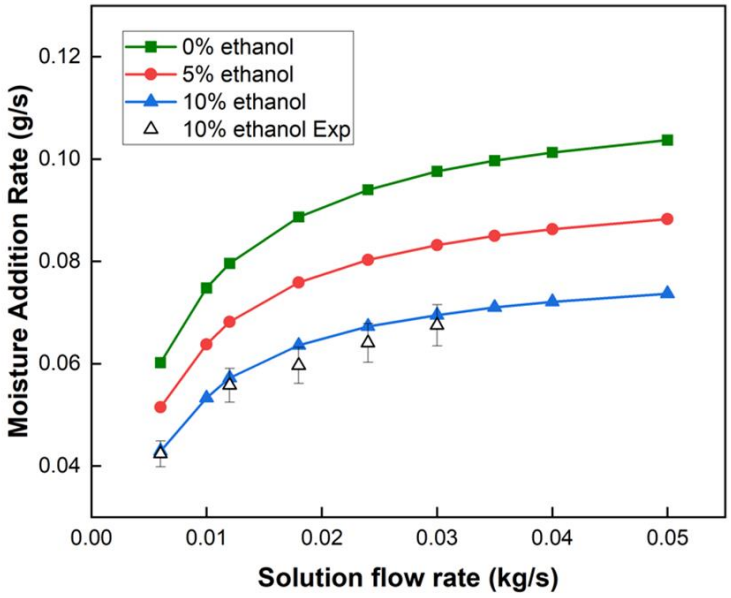

(a)

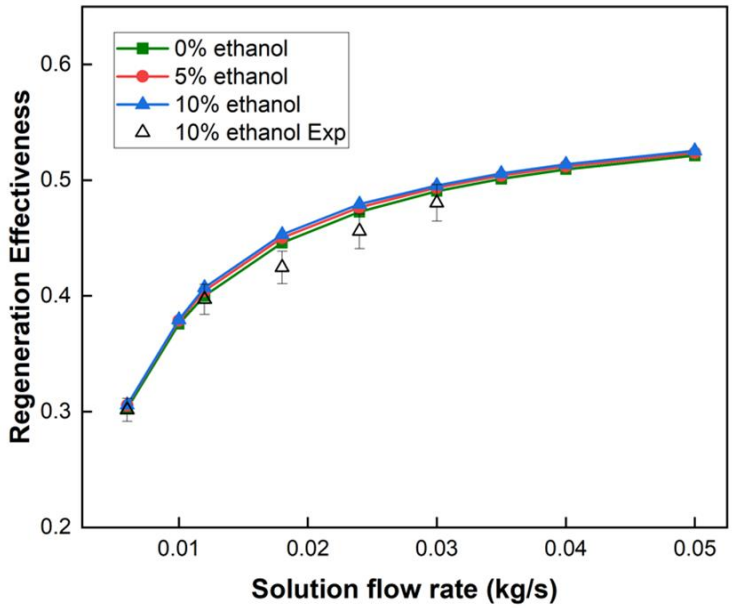

(b)

Figure 4-13 (a) Effect of solution flow rate on moisture addition rate. (b) Effect of solution flow rate on regeneration effectiveness

4.7. Summary

In this section, in order to reconcentrate the liquid desiccant coming out from the dehumidifier, a cross-flow membrane-based regenerator is used. The numerical model has been developed to evaluate the regeneration performance. The heat and mass transfer interactions between the process air and desiccant solution are investigated by generating the governing equations in Matlab using the finite difference method. The equilibrium specific humidity of the LiCl aqueous solution mixed with ethanol has been solved under the operation conditions of the regenerator. The experimental tests have also been conducted to validate with the numerical results. The maximum discrepancies for MAR and regeneration effectiveness are 9.76% and 9.63%, respectively.

A comprehensive parametric study has been conducted to assess the effects on the performance of the proposed membrane-based liquid desiccant regenerator, the key parameters include: the air inlet temperature ($T_{air,in}$) and relative humidity ($RH_{air,in}$), air flow rate (m_{air}), solution inlet temperature ($T_{sol,in}$), LiCl concentration ($C_{sol,in}$) and solution flow rate (m_{sol}). All the results were evaluated under different ethanol concentrations. The main conclusions are drawn below:

- The temperature and humidity fields of air and solution are not uniform during the regeneration process, since neither the heat transfer nor the mass transfer are uniform within the regenerator. The driving force of heat

and mass transfer reaches the maximum value at the inlet of air and desiccant solution.

- The influences of inlet air temperature and relative humidity on regeneration effectiveness are limited. The solution reconcentration ability can be enhanced by applying cooler and drier air. Air flow rate is an essential parameter affecting the regeneration performance, the regeneration effectiveness decreases by 53.63% from 49.54% to 22.97% when m_{air} increased from 0.01 to 0.025 kg/s at $C_{eth} = 10\%$.
- The regeneration performance can be improved with higher inlet solution temperature and lower LiCl concentration. It should be noted that adjusting the power output of the boiler and regulating the inlet solution temperature to enhance the desiccant regeneration performance is more effective and practical. The solution flow rate has a significant influence on the moisture transmission during the regeneration process. A critical value of m^* has been defined, and it is suggested that the regenerator is preferred to operate under the condition when the mass flow rate ratio is equal to 3.
- By adding evaporative coolant (ethanol) into desiccant solution, the moisture addition rate is significantly decreased with the increase of ethanol percentage. Although the regeneration effectiveness can be slightly improved with the addition of ethanol, it is clear that ethanol percentage has a certain inhibitory effect on the regeneration process of the desiccant solution. Further researches need to focus on the overall effect of adding ethanol on the liquid desiccant dehumidification

performance from a holistic system perspective, as presented in the next section.

Section 5: Performance assessment of a complete self-cooled membrane-based liquid desiccant dehumidification system

5.1. Introduction

The last two sections have investigated the performance of a single self-cooled liquid desiccant dehumidifier and membrane-based regenerator, respectively. The results have shown that although the addition of evaporative coolant (ethanol) into lithium chloride aqueous solution is capable of improving the dehumidification performance, it shows a negative impact on the regeneration of desiccant solution. To fully assess whether the proposed self-cooled liquid desiccant is able to improve the dehumidification performance from the system perspective, the complete self-cooled membrane-based liquid desiccant dehumidification system that include a dehumidifier, regenerator, cold and hot water supply is proposed. The desiccant solution is running through a close loop configuration, while there are external heat source (electrical boiler) and cooling source (tap water) to adjust the solution temperature before entering regenerator and dehumidifier, respectively. Both numerical model and experimental tests of the complete system have been conducted.

The structures of **Section 5** are: **Section 5.2** develops the numerical modelling of the complete dehumidification system; **Section 5.3** conducts the experimental set-up in the laboratory; **Section 5.4** shows the dehumidification system performance indices; **Section 5.5** validates the numerical data with the

experimental results; **Section 5.6** presents a comprehensive parametric study for the performance of the complete self-cooled liquid desiccant dehumidification system; **Section 5.7** is the main conclusion of this section.

5.2. Numerical modelling

5.2.1. Model description and assumptions

There are three main parts of the developed model for the complete dehumidification system, which include: dehumidifier, regenerator and heat exchangers. The concept diagram of the dehumidification system is shown in Fig. 5-1. The diluted desiccant solution coming out from dehumidifier is preheated by the hot concentrated solution coming out from regenerator at heat exchanger 1 to save the energy consumption of the boiler. The strong solution running through HX1 is then cooled by cold water at heat exchanger 2 before entering the dehumidifier. On contrast, the weak solution is heated by how water provide by the boiler at heat exchanger 3 before entering the regenerator.

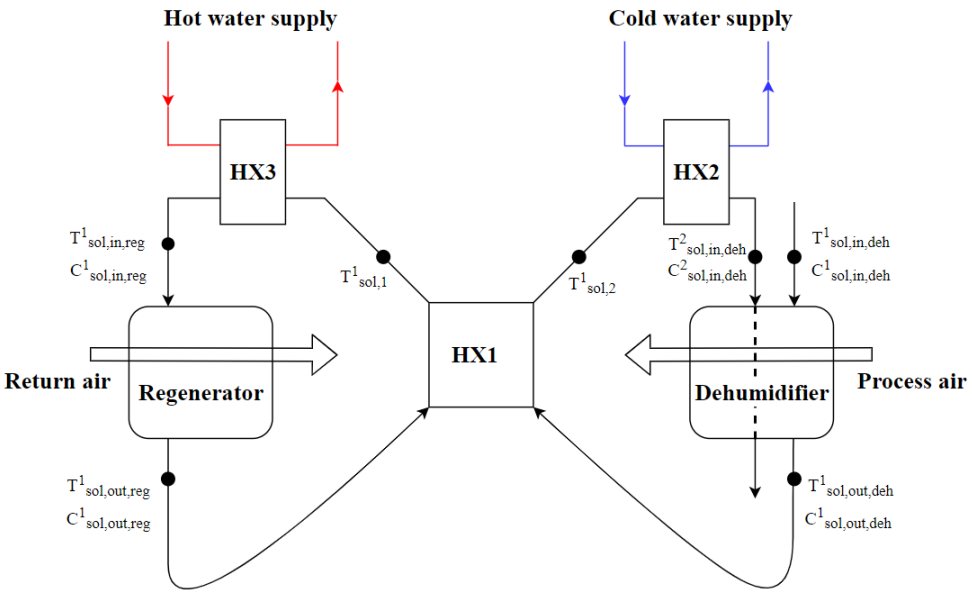

Figure 5-1 Modelling concept of the complete dehumidification system

Several assumptions were made before establishing the governing equations of the complete system, which include:

- All components, including the dehumidifier, regenerator, heat exchangers, ducts and pipes are considered to be well insulated, no mass or heat transfer between these components and surrounding environment.
- The processes of heat and mass transfer within the dehumidifier and regenerator are assumed to be steady-state.
- Mass and heat transfer only take place on z direction and axial conduction is neglected.
- The air and solution streams on both solution channels and air channels are laminar.
- All the fluids flow in air and solution channels are Newtonian and they are considered to maintain constant thermophysical properties (density, thermal conductivity, and specific heat capacity).

- All of the fluids in the system are fully developed, and the entrance effects are neglected.

5.2.2. Dehumidifier and regenerator

5.2.2.1. Governing equations

The heat and mass transfer processes of the proposed self-cooled liquid desiccant dehumidifier and membrane-based regenerator have been explained in Section 3 and Section 4, respectively. The governing equations for dehumidifier and regenerator are presented below.

For the dehumidifier:

$$\frac{m_{air}}{H}\frac{\partial W_{air}}{\partial x}dxdy = -U_m\left(W_{air} - W_{sol,mem}\right)dxdy \qquad (5-1)$$

$$\frac{m_{sol}}{L}\frac{\partial X_{sol}}{\partial y}dxdy = U_m\left(W_{air} - W_{sol,mem}\right)dxdy \qquad (5-2)$$

$$\frac{m_{air}}{H}\frac{\partial T_{air}}{\partial x}C_{p,air}dxdy = -U(T_{air} - T_{sol})dxdy \qquad (5-3)$$

$$C_{p,sol}\frac{m_{sol}}{L}\frac{\partial T_{sol}}{\partial y}dxdy = r \cdot U_m\left(W_{air} - W_{sol,mem}\right)dxdy + U(T_{air} - T_{sol})dxdy - U_{ca}(T_{sol} - T_{ca})dxdy - r_{eth} \cdot U_{m,eth}\left(W_{eth,sol} - W_{eth}\right) \qquad (5-4)$$

$$\frac{m_{sol}}{L}\frac{\partial C_{eth}}{\partial x}dxdy = -U_{m,eth}\left(W_{eth,sol} - W_{eth}\right)dxdy \qquad (5-5)$$

$$\frac{m_{ca}}{L}\frac{\partial T_{ca}}{\partial y}dxdy = -U_{ca}(T_{sol} - T_{ca})dxdy \qquad (5-6)$$

$$\frac{m_{ca}}{L}\frac{\partial W_{eth}}{\partial y}dxdy = -U_{m,eth}\left(W_{eth,sol} - W_{eth}\right)dxdy \qquad (5-7)$$

For the regenerator:

$$\frac{m_{air}}{H}\frac{dW_{air}}{dx}dxdy = U_m(W_{sol.mem} - W_{air})dxdy \quad (5-8)$$

$$\frac{m_{sol}}{L}\frac{dX_{sol}}{dy}dxdy = -U_m\left(W_{sol,mem} - W_{air}\right)dxdy \quad (5-9)$$

$$C_{p,air}\frac{m_{air}}{H}\frac{dT_{air}}{dx}dxdy = U(T_{sol} - T_{air})dxdy \quad (5-10)$$

$$C_{p,sol}\frac{m_{sol}}{L}\frac{dT_{sol}}{dy}dxdy = -[r \cdot U_m\left(W_{sol,mem} - W_{air}\right)dxdy + U(T_{sol} - T_{air})]dxdy \quad (5-11)$$

5.2.2.2. Boundary conditions

For the self-cooled liquid desiccant dehumidifier, the boundary conditions are:

$$W_{air} = W_{air,in}\ at\ x = 0 \quad (5-12)$$

$$T_{air} = T_{air,in}\ at\ x = 0 \quad (5-13)$$

$$X_{sol} = X_{sol,in}, at\ y = 0 \quad (5-14)$$

$$T_{sol} = T_{sol.in}, at\ y = 0 \quad (5-15)$$

$$C_{eth} = C_{eth,in}, at\ y = 0 \quad (5-16)$$

$$W_{eth} = W_{eth,in}\ at\ y = H \quad (5-17)$$

$$T_{ca} = T_{ca,in}, at\ y = H \quad (5-18)$$

For the membrane-based regenerator, the boundary conditions are:

$$W_{air} = W_{air,in}\ at\ x = 0 \quad (5-19)$$

$$T_{air} = T_{air,in}\ at\ x = 0 \quad (5-20)$$

$$X_{sol} = X_{sol,in}, at\ y = 0 \quad (5-21)$$

$$T_{sol} = T_{sol.in}, at\ y = 0 \quad (5-22)$$

To solve the governing equations between air channel and solution channel, mass and heat transfer boundary equations on membrane surface are shown as:

$$U_m(W_{air} - W_{sol,mem}) = \alpha_{m,sol}(C_{sol} - C_{sol,mem}) \quad (5-23)$$

$$r \cdot U_m(W_{air} - W_{sol,mem}) + U(T_{air} - T_{sol,mem}) = \alpha_{sol}(T_{sol,mem} - T_{sol}) \quad (5-24)$$

5.2.2.3. Normalization of governing equations

The normalized governing equations of dehumidifier and regenerator are summarized as:

$$\frac{\partial {W_{air}}^*}{\partial x^*} = -NTU_m({W_{air}}^* - {W_{sol,mem}}^*) \quad (5-25)$$

$$\frac{\partial {T_{air}}^*}{\partial x^*} = -NTU({T_{air}}^* - {T_{sol}}^*) \quad (5-26)$$

$$\frac{\partial {T_{sol}}^*}{\partial y^*} = NTU_m h^* Cr^*({W_{air}}^* - {W_{sol,mem}}^*) + NTUCr^*({T_{air}}^* - {T_{sol}}^*) - NTU_{m,ca} {h_e}^* {Cr_{ca}}^*({W_{eth,sol}}^* - {W_{eth}}^*) - NTU_{ca} {Cr_{ca}}^*({T_{sol}}^* - {T_{ca}}^*) \quad (5-27)$$

$$\frac{\partial X_{sol}}{\partial y^*} = NTU_m W_D \frac{1}{m^*}({W_{air}}^* - {W_{sol,mem}}^*) \quad (5-28)$$

$$\frac{\partial C_{eth}}{\partial y^*} = NTU_{m,ca} W_D \frac{1}{{m_{ca}}^*}({W_{eth,sol}}^* - {W_{eth}}^*) \quad (5-29)$$

$$\frac{\partial {T_{ca}}^*}{\partial y^*} = -NTU_{ca}({T_{sol}}^* - {T_{ca}}^*) \quad (5-30)$$

$$\frac{\partial {W_{eth}}^*}{\partial y^*} = -NTU_{m,ca}\left({W_{eth,sol}}^* - {W_{eth}}^*\right) \quad (5-31)$$

$$\frac{\partial {W_{air}}^*}{\partial x^*} = NTU_m\left({W_{sol,mem}}^* - {W_{air}}^*\right) \quad (5-32)$$

$$\frac{\partial X_{sol}}{\partial y^*} = -NTU_m W_D \frac{1}{m^*}\left({W_{sol,mem}}^* - {W_{air}}^*\right) \quad (5-33)$$

$$\frac{\partial {T_{air}}^*}{\partial x^*} = -NTU\left({T_{sol}}^* - {T_{air}}^*\right) \quad (5-34)$$

$$\frac{\partial {T_{sol}}^*}{\partial y^*} = -\left[NTU_m h^* Cr^*\left({W_{sol,mem}}^* - {W_{air}}^*\right) + NTUCr^*\left({T_{sol}}^* - {T_{air}}^*\right)\right] \quad (5-35)$$

5.2.2.4. Discretization of governing equations

To solve Eqs. $(5-25)-(5-35)$, finite difference method has been applied. The discretization equations are shown below:

$${W_{air(m,n+1)}}^* - {W_{air(m,n)}}^* = -dx^* NTU_m\left[{W_{air(m,n+1)}}^* - {W_{sol,mem(m,n+1)}}^*\right] \quad (5-36)$$

$${T_{air(m,n+1)}}^* - {T_{air(m,n)}}^* = -dx^* NTU\left[{T_{air(m,n+1)}}^* - {T_{sol(m,n+1)}}^*\right] \quad (5-37)$$

$${T_{sol(m+1,n)}}^* - {T_{sol(m,n)}}^* = dy^* NTU_m h^* Cr^*\left({W_{air(m+1,n)}}^* - {W_{sol,mem(m+1,n)}}^*\right) + dy^* NTUCr^*\left({T_{air(m+1,n)}}^* - {T_{sol(m+1,n)}}^*\right) - dy^* NTU_{m,ca} {h_e}^* Cr_{ca}^*\left({W_{eth,sol(m+1,n)}}^* - {W_{eth(m+1,n)}}^*\right) - dy^* NTU_{ca} Cr_{ca}^*\left({T_{sol(m+1,n)}}^* - {T_{ca(m+1,n)}}^*\right) \quad (5-38)$$

$$X_{sol(m+1,n)} - X_{sol(m,n)} = dy^* NTU_m W_D \frac{1}{m^*}\left[{W_{air(m+1,n)}}^* - {W_{sol,mem(m+1,n)}}^*\right] \quad (5-39)$$

$$C_{eth(m+1,n)} - C_{eth(m,n)} = dy^* NTU_{m,ca} W_D \frac{1}{m^*} \left[W_{eth,sol(m+1,n)}{}^* - W_{eth(m+1,n)}{}^* \right] \quad (5-40)$$

$$T_{ca(m+1,n)}{}^* - T_{ca(m,n)}{}^* = -dy^* NTU_{ca} \left[T_{sol(m+1,n)}{}^* - T_{ca(m+1,n)}{}^* \right] \quad (5-41)$$

$$W_{eth(m+1,n)}{}^* - W_{eth(m,n)}{}^* = -dy^* NTU_{m,ca} \left[W_{eth,sol(m+1,n)}{}^* - W_{eth(m+1,n)}{}^* \right] \quad (5-42)$$

$$W_{air(m,n+1)}{}^* - W_{air(m,n)}{}^* = dx^* NTU_m \left[W_{so,mem(m,n+1)}{}^* - W_{air(m,n+1)}{}^* \right] \quad (5-43)$$

$$X_{sol(m+1,n)} - X_{sol(m,n)} = dy^* NTU_m W_D \frac{1}{m^*} \left[W_{sol,mem(m+1,n)}{}^* - W_{air(m+1,n)}{}^* \right] \quad (5-44)$$

$$T_{air(m,n+1)}{}^* - T_{air(m,n)}{}^* = -dx^* NTU \left[T_{sol(m,n+1)}{}^* - T_{air(m,n+1)}{}^* \right] \quad (5-45)$$

$$\begin{aligned} T_{sol(m+1,n)}{}^* - T_{sol(m,n)}{}^* \\ = -\left[dy^* NTU_m h^* Cr^* \left(W_{sol,mem(m+1,n)}{}^* - W_{air(m+1,n)}{}^* \right) \right. \\ + dy^* NTU Cr^* \left(T_{sol(m+1,n)}{}^* \right. \\ \left. \left. - T_{air(m+1,n)}{}^* \right) \right] \end{aligned} \quad (5-46)$$

Where m and n are the grids number in x and y direction, respectively.

5.2.3. Heat exchanger

For the parallel-flow plat heat exchangers used in the dehumidification system, their effectiveness can be determined by the ratio of the actual heat transfer rate and the maximum heat transfer rate [137]:

$$\varepsilon = \frac{q}{q_{max}} = \frac{c_{p,h}\left(T_{h,in} - T_{h,out}\right)}{c_{min}\left(T_{h,in} - T_{c,in}\right)} = \frac{c_{p,c}\left(T_{c,out} - T_{c,in}\right)}{c_{min}\left(T_{h,in} - T_{c,in}\right)} \quad (5-47)$$

Where $c_{p,h}$ and $c_{p,c}$ are heat capacity rates of hot and cold fluid, respectively; $T_{h,in}$, $T_{h,out}$, $T_{c,in}$ and $T_{c,out}$ are temperatures of hot and cold fluids at inlets and outlets.

For HX1-HX3, their effectiveness are expressed as:

$$\varepsilon_1 = \frac{m_{sol}c_{p,sol}(T_{sol,out,reg} - T_{sol,2})}{m_{sol}c_{p,sol}(T_{sol,out,reg} - T_{sol,out,deh})}$$

$$= \frac{m_{sol}c_{p,sol}\left(T_{sol,1} - T_{sol,out,deh}\right)}{m_{sol}c_{p,sol}\left(T_{sol,out,reg} - T_{sol,out,deh}\right)} \quad (5-48)$$

$$\varepsilon_2 = \frac{m_{sol}c_{p,sol}\left(T_{sol,2} - T_{sol,out,deh}\right)}{\min\left(m_{sol}c_{p,sol}, m_{c,w}c_{p,w}\right)\left(T_{sol,2} - T_{c,w,in}\right)} \quad (5-49)$$

$$\varepsilon_3 = \frac{m_{sol}c_{p,sol}\left(T_{sol,in,reg} - T_{sol,1}\right)}{\min\left(m_{sol}c_{p,sol}, m_{h,w}c_{p,w}\right)\left(T_{h,w,in} - T_{sol,1}\right)} \quad (5-50)$$

Where subscripts deh and reg represent dehumidifier and regenerator, respectively; $T_{c,w,in}$ and $T_{h,w,in}$ are the inlet temperatures of cooling water from tap water and hot water from the boiler (℃); $T_{sol,1}$ and $T_{sol,2}$ are temperatures of strong and weak solution after HX1 (℃), respectively; $m_{c,w}$ and $m_{h,w}$ are mass flow rates of cold and hot water (kg/s), respectively.

5.2.4. Numerical solving scheme

The proposed numerical model of the dehumidification system is solved iteratively in Matlab until the required convergence has been accomplished. Detailed Matlab code is presented in appendix. The simulation procedures are shown below:

1) Set the initial inlet conditions of the process air, desiccant solution and

circulated air for dehumidifier.

2) Obtain the dehumidifier outlet solution temperature and concentration by solving Eqs. $(5-36)-(5-42)$.
3) Set the outlet solution temperature and concentration as the initial inlet conditions for regenerator.
4) Set the inlet conditions for both dehumidifier and regenerator.
5) Solve Eqs. $(5-36)-(5-42)$ to obtain T_{sol}, T_{ca}, T_{air}, X_{sol}, C_{eth}, W_{eth} and W_{air} for dehumidifier.
6) Solve Eqs. $(5-43)-(5-46)$ to obtain T_{sol}, T_{air}, X_{sol} and W_{air} for regenerator.
7) Based on the Eqs. $(5-23)$ and $(5-24)$, solve the heat and mass transfer boundary conditions on the membrane surface to obtain the membrane surface temperature and concentration fields in the solution side for both dehumidifier and regenerator.
8) Adopt new $W_{sol,mem,deh}$ and $W_{sol,mem,reg}$ as a default value and return to step 5 and 6 until they are converged.
9) Calculate the outlet conditions for dehumidifier and regenerator.
10) Based on the Eqs. $(5-48)-(5-50)$ and the result from last step, adopt new inlet conditions for dehumidifier and regenerator, return to step 4 until $T_{sol,in,deh}$, $C_{sol,in,deh}$, $T_{sol,in,reg}$ and $C_{sol,in,reg}$ are converged.
11) Calculate the effectiveness, cooling output and COP of the complete self-cooled membrane-based liquid desiccant dehumidification system.

The solution procedure during the simulation process to solve the interacted governing equations is presented in the flow chart Fig.5-2 below:

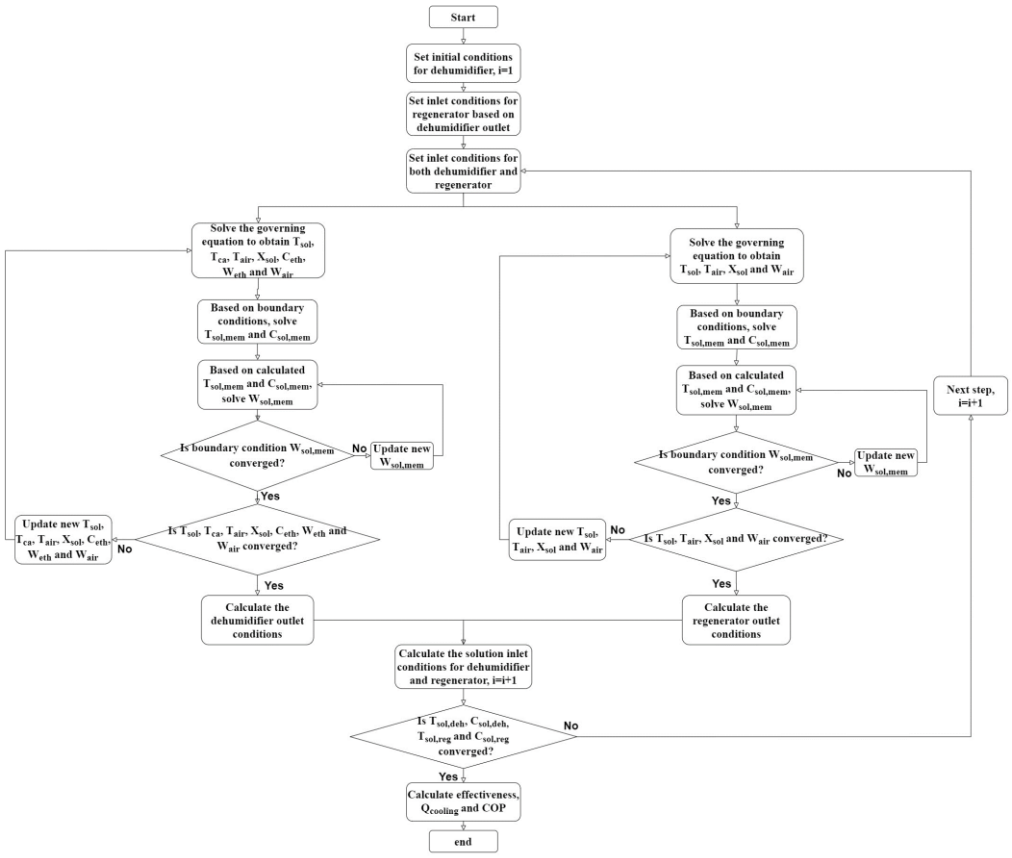

Figure 5-2 Flow chart of the solving procedure for the complete dehumidification system

5.3. Experimental set-up

The test rigs for the self-cooled membrane-based liquid desiccant dehumidification system has been established in the laboratory as depicted in Fig. 5-3. The comprehensive dehumidification system comprises of several components, including an air dehumidifier, a solution regenerator, a liquid to air heat exchanger and three liquid to liquid heat exchangers, a electrical boiler and a cold water supply unit. The hot and strong solution coming out from regenerator is pre-cooled by the cold solution coming out from dehumidifier. Then it is cooled by the tap water before entering the dehumidifier. The weak desiccant solution is

heated by hot water provided by the boiler after dehumidification process. The evaporated ethanol during the dehumidification process is condensed by the liquid to air heat exchanger on top of the dehumidifier. Two solution tank have been used to contain the solution coming out from dehumidifier and regenerator. Inlet air conditions of dehumidifier is controlled by the environmental chamber in the laboratory to simulate hot and humid weather conditions, while the indoor air is supplied to the regenerator to remove moisture from the diluted solution.

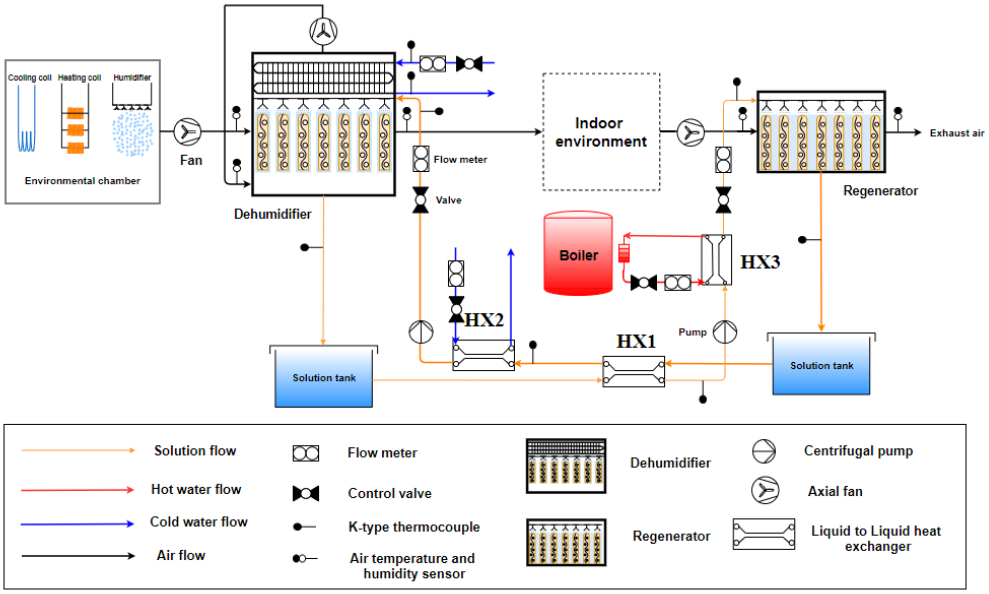

Figure 5-3 Schematic diagram of the dehumidification system

In terms of setting up the experimental tests, the air flow rates through the dehumidification system are controlled by two axial fans with speed controller, and it is measured by the Testo thermos-anemometer (0-10m/s) with an accuracy of 5%. The desiccant solution is driven by two 15W centrifugal magnetic pumps and the solution flow rate is controlled by the liquid flow indicator (1-15L/min) with an accuracy of 5%. The hot water comes from the boiler with a temperature range of 20℃ to 80℃, and the 12℃ cold water comes from the main supply pipe.

With an accuracy of 0.75%, K-type thermocouples (0-1100℃) are used to record the solution and water temperatures. The Sensiron Evaluation KIT, which has an accuracy of 3%, is used to measure the air temperature and relative humidity. All of the sensors are hooked up to a data logger (DT80) that can record data with an accuracy of 0.15%. Further details for the physical properties of the dehumidifier and regenerator are presented in Table 5-1 below.

Table 5-1 Physical properties of dehumidifier and regenerator

Properties	Symbol	Value	Unit
Length of dehumidifier/regenerator	L	0.41	m
Width of dehumidifier/regenerator	W	0.23	m
Width of dehumidifier/regenerator	H	0.21	m
Number of air channel	-	11	-
Number of solution channel	-	11	-
Thickness of air channel	d_{air}	0.0077	m
Thickness of solution channel	d_{sol}	0.0043	m
Thickness of membrane	δ_{mem}	0.0005	m
Membrane thermal conductivity	k_{mem}	0.3	W/mK
Membrane mass transfer conductivity	$k_{m,mem}$	3.87×10^{-6}	kg/ms

5.4. Performance evaluation

5.4.1. Effectiveness of the complete system

Effectiveness is a critical parameter to assess the performance of the heat and mass exchanger. The dehumidification and regeneration effectiveness have been determined and measured in previous sections. For a complete dehumidification system, the effectiveness can be divided into sensible and latent effectiveness, since the outdoor air has been cooled and dehumidified to provide for the indoor environment. The system sensible effectiveness is defined as the actual sensible heat transfer divided by the maximum possible sensible heat transfer between air and desiccant solution, while the system latent effectiveness is defined as the actual latent heat transfer over the maximum possible latent heat transfer. The expressions of the effectiveness for the complete system are [97]:

$$\varepsilon_{sen} = \frac{m_{air,deh} c_{p,air} \left(T_{air,in,deh} - T_{air,out,deh}\right)}{\min\left((mc_p)_{air,deh}, (mc_p)_{sol}\right) \left(T_{air,in,deh} - T_{air,in,reg}\right)} \qquad (5-51)$$

$$\varepsilon_{lat} = \frac{r \cdot m_{air,deh} \left(W_{air,in,deh} - W_{air,out,deh}\right)}{\min\left(r \cdot m_{air,deh}, r \cdot m_{sol}\right) \left(W_{air,in,deh} - W_{air,in,reg}\right)} \qquad (5-52)$$

5.4.2. Total cooling output

The total cooling output (Q_{tot}) (kW) is another important parameter to evaluate the system performance. Similar to the effectiveness, it is considered to be the sum of sensible cooling output and latent cooling output. The sensible cooling (Q_{sen}) and (Q_{lat}) latent cooling represent the reduction of air temperature and removal of air moisture, respectively.

$$Q_{tot} = Q_{sen} + Q_{lat} \quad (5-53)$$

$$Q_{sen} = m_{air,deh} c_{p,air} \left(T_{air,in,deh} - T_{air,out,deh}\right) \quad (5-54)$$

$$Q_{lat} = r \cdot m_{air,deh} \left(W_{air,in,deh} - W_{air,out,deh}\right) \quad (5-55)$$

5.4.3. Coefficient of performance

In order to evaluate the dehumidification system performance, coefficient of performance, COP can be expressed as [97]:

$$COP = \frac{Q_{tot}}{Q_{reg} + W_{fan} + W_{pump}} \quad (5-56)$$

Where Q_{reg} is the regeneration heat input (kW), which can be determined by:

$$Q_{reg} = m_{sol} c_{p,sol} \left(T_{sol,in,reg} - T_{sol,2}\right) \quad (5-57)$$

W_{fan} and W_{pump} are the fan and pump energy consumption (kW), which can be obtained by:

$$W_{fan} = \frac{W_{output,fan}}{\eta_{fan}} = \frac{Q_{fan} \Delta P_{air}}{\eta_{fan}} = \frac{m_{air} \Delta P_{air}}{\rho_{air} \eta_{fan}} \quad (5-58)$$

$$W_{pump} = \frac{W_{output,pump}}{\eta_{pump}} = \frac{Q_{pump} \Delta P_{sol}}{\eta_{pump}} = \frac{m_{sol} \Delta P_{sol}}{\rho_{sol} \eta_{pump}} \quad (5-59)$$

Where $W_{output,fan}$ and $W_{output,pump}$ are the useful power output applied to the air and solution by fan and pump (kW), respectively, η_{fan} and η_{pump} are the efficiency of fan and pump, Q_{fan} and Q_{pump} are the air and solution volumetric flow rate (m^3/s), ΔP_{air} and ΔP_{sol} are the total pressure drop of air and solution (Pa), which can be expressed as [97]:

$$\Delta P_{air} = \frac{1}{2}\rho_{air}{u_{air}}^2\left(\frac{A_{air}}{A_{duct}}\right)^2\left(\frac{A_{duct}}{A_{air}}-1\right)^2 \quad (5-60)$$

$$\Delta P_{sol} = \frac{1}{2}\rho_{sol}{u_{sol}}^2\left(\frac{A_{sol}}{A_{pipe}}\right)^2\left(\frac{A_{pipe}}{A_{sol}}-1\right)^2 \quad (5-61)$$

Where u_{air} and u_{sol} are the air and solution velocity ((m/s), respectively, A_{air} and A_{sol} are the air and solution flow area of the dehumidifier or regenerator (m^2), A_{duct} and A_{pipe} are the cross area of the duct and pipe, respectively (m^2).

5.5. Model validation

The experimental results have been used to validate the numerical model. Overall, 25 groups of the experimental tests under different operating conditions have been conducted to validate numerical results. The hot water temperature coming out from the boiler is set as 50 ℃, while the tap water temperature is 12 ℃. The hot and cold water flow rates are set to be 0.05 kg/s and 0.0833 kg/s, respectively. A comprehensive parametric study has been conducted to evaluate the performance of the complete dehumidification system, which include the effect of ethanol concentration, dehumidifier inlet air flow rate, regenerator inlet air flow rate, solution flow rate and LiCl concentration. The comparison of sensible and latent effectiveness between the numerical results and experimental data were present in Fig. 5-4 and 5-5 below. It indicates that almost all the deviation between numerical and experimental results were within 10%. The maximum discrepancies for sensible and latent effectiveness are 10.14% and 15.13%, respectively. It should be noted that the discrepancy of the complete system is higher than single dehumidifier or regenerator, which may cause by the incompletely condensation of ethanol during the experiment tests. Generally

speaking, the numerical results have been proved to have a good agreement with the experimental data which indicates that the proposed numerical model is valid to predict the performance of the complete self-cooled membrane-based liquid desiccant dehumidification system.

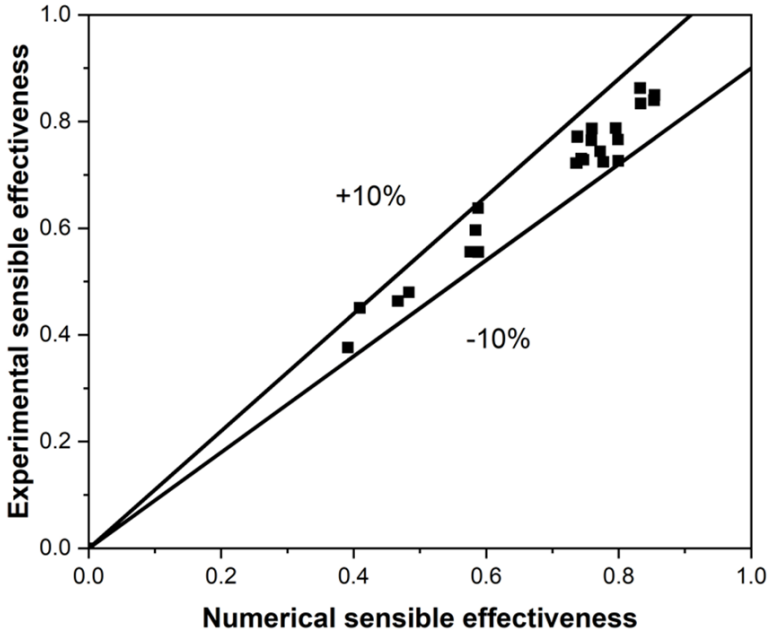

Figure 5-4 Comparison of sensible effectiveness between numerical and experimental data

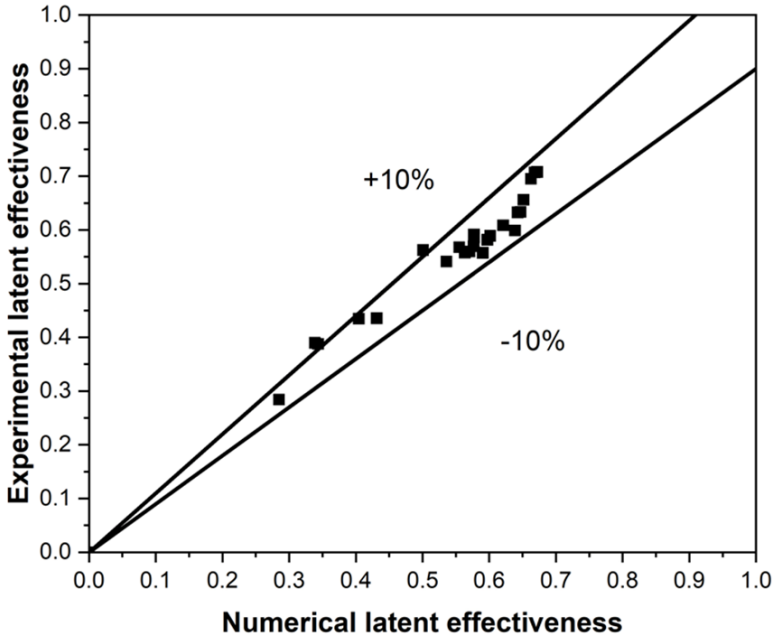

Figure 5-5 Comparison of latent effectiveness between numerical and experimental data

5.6. Results and discussion

5.6.1. Effect of evaporative coolant

Based on previous sections, the results have proved that the addition of ethanol can improve the dehumidification process, but reduce the regeneration performance. In order to assess whether the newly formed self-cooled liquid desiccant solution is able to improve the dehumidification performance from the complete system perspective, the variations of the dehumidification system performance including the effectiveness, total cooling output and COP under different ethanol mass concentrations are presented in Figs. 5-6 – 5-8. The inlet air temperature and relative humidity of dehumidifier are 30 ℃ and 80%, respectively, while the return air from indoor environment 24℃ and 40%. The

inlet solution temperature and LiCl concentration are set to be 20℃ and 37%. It can be observed from Fig. 5-6 that the sensible effectiveness almost remains constant while the latent effectiveness increases from 57.65% to 65.14% when 10% ethanol is added into desiccant solution. This is because the addition of ethanol reduces the equilibrium vapour pressure of the desiccant solution, and the evaporation of ethanol during the dehumidification process can restrain the temperature rise of solution, therefore enhancing the dehumidification abilities. Although the evaporation of ethanol is able to remove the latent heat gain from desiccant solution, more latent heat is released into air and solution with the increase of ethanol concentrations. As a result, no obvious improvement of system sensible effectiveness has been obtained by using the proposed self-cooled liquid desiccant solution.

Apart from the system effectiveness, it is of our interest to evaluate the energy performance of the complete dehumidification system as well. As illustrated in Fig. 5-6, the latent cooling output is significantly higher than the sensible cooling output under all circumstances. The results have shown that Q_{lat} is the majority of the total cooling output for the proposed self-cooled membrane-based liquid desiccant dehumidification system. When ethanol concentration changes from 0% to 10%, the sensible cooling output decreases from 0.0961 kW to 0.0951 kW, while the latent cooling output increases from 0.207 kW to 0.2475 kW. As discussed previously, although the moisture removal potential of the dehumidification system is improved, the addition of ethanol has a limited impact on the sensible cooling output. For a complete dehumidification system in reality, the process air coming out from the dehumidifier is considered to be pre-cooled

and significant sensible cooling source is required after dehumidification [155] to meet the needs of indoor thermal comfort. A similar trend can be observed from the variations of COP with different ethanol concentrations in Fig. 5-8. By adding 10% of ethanol into desiccant solution, the COP increases by 21.98% from 0.6511 to 0.7942. The improvement of COP is caused not only by the increase of total cooling output, but also by the decrease of solution specific heat capacity, which can slightly reduce the regeneration heat input of the boiler. Even though the influence of ethanol on system sensible effectiveness and cooling output are negligible, the significant improvement of latent effectiveness, cooling output and COP have shown that the proposed self-cooled liquid desiccant is able to enhance the performance of the complete dehumidification system compared with pure LiCl aqueous solution.

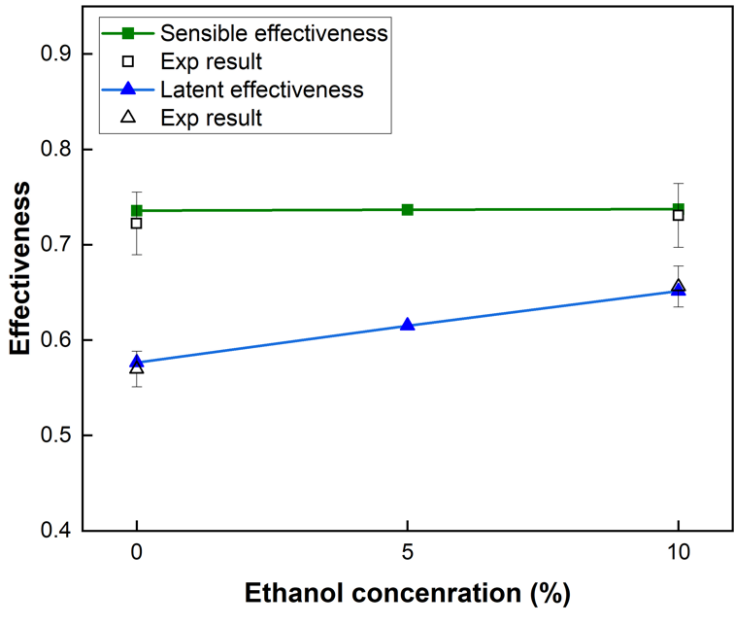

Figure 5-6 System effectiveness variations under different ethanol concentrations

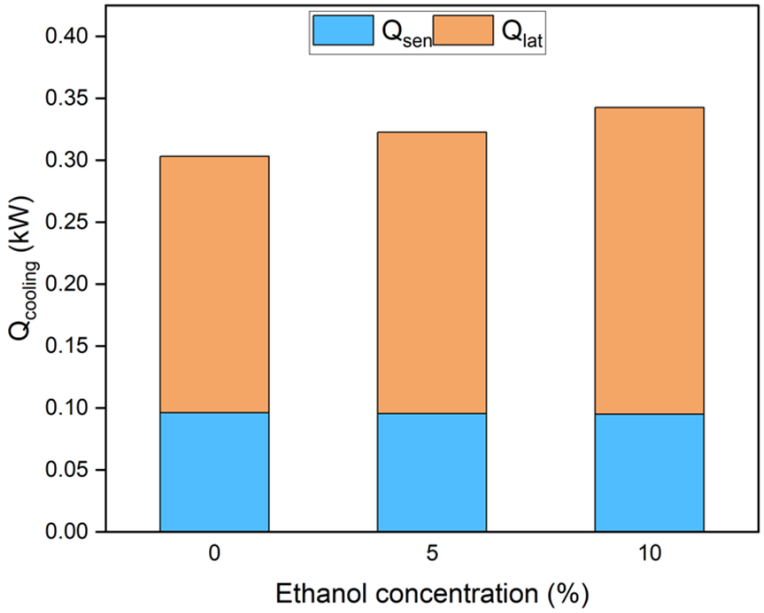

Figure 5-7 Total cooling output variations under different ethanol concentrations

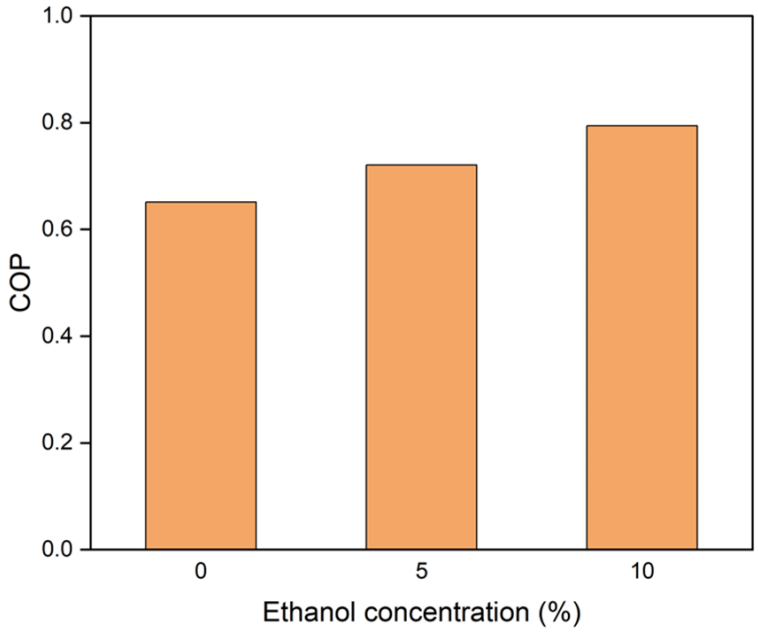

Figure 5-8 COP variations under different ethanol concentrations

5.6.2. Effect of dehumidifier air flow rate

The influence of dehumidifier air flow rate has been assessed in this study since it is closely related to the number of heat transfer unit (NTU) between air and desiccant solution. According to previous research on the dehumidification system [97], NTU is believed to have the most significant impact on dehumidification performance. Based on Eq. $(3-39)$, as a given dehumidification system with the fixed size and properties of the dehumidifier and regenerator, NTU can only be adjusted by changing the air flow rate through dehumidifier. As shown in Figs. 5-9 and 5-10, The variations of ε_{sen} and ε_{lat} under different air flow rates of dehumidifier have been plotted. Both sensible and latent effectiveness decrease with the increase of $m_{air,deh}$. For example, when no ethanol is added to desiccant solution, ε_{sen} decreases from 73.57% to 40.93%, while ε_{lat} decreases from 57.65% to 28.47% when the air mass flow rate within the dehumidifier rises from 0.01 to 0.025 kg/s. When $C_{eth} = 10\%$, ε_{sen} and ε_{lat} decrease from 74.36% to 39.13% and 65.14% to 33.86%, respectively. It is also noticed that the sensible effectiveness is not always higher, while the latent effectiveness is always higher for the proposed self-cooled liquid desiccant solution compared with conventional LiCl aqueous solution. The increase of air mass flow rate will reduce the time of process air staying in the dehumidifier, which makes the difference between inlet and outlet air conditions become smaller. The reduction of $(T_{air,out,deh} - T_{air,in,deh})$ and $(W_{air,out,deh} - W_{air,in,deh})$ will lead to the decrease of both sensible and latent effectiveness of the complete dehumidification system.

The total cooling output for both Q_{sen} and Q_{lat} under different dehumidifier air flow rates has been presented in Fig. 5-11. It is clear that Q_{lat} is much higher than Q_{sen} since the main purpose of the dehumidification system is to remove the moisture content. For instance, under $m_{air,deh} = 0.02\ kg/s$ and $C_{eth} = 0\%$, the sensible cooling output is 0.1218 kW while the latent cooling output is 0.2446 kW, which is two times greater than the sensible cooling output. It should be noted that the addition of ethanol will reduce the sensible cooling output. For example, when $m_{air,deh} = 0.015\ kg/s$, under $C_{eth} = 0\%$ and 10%, the sensible cooling output decreases from 0.1121 kW to 0.1086 kW, while the latent cooling output increases from 0.2308 kW to 0.2846 kW. Moreover, under all ethanol concentrations, the sensible, latent and total cooling output increase significantly with the increase of dehumidifier air flow rate. For $C_{eth} = 10\%$, Q_{sen} increases from 0.0951 kW to 0.1209 kW, Q_{lat} increases from 0.2475 kW to 0.3197 kW and Q_{tot} increases from 0.3426 kW to 0.4406 kW, when $m_{air,deh}$ increases from 0.01 to 0.025 kg/s. The results have proved that the increase of dehumidifier air mass flow rate is able to increase the amount of both sensible and latent cooling output for the process air. A similar trend can be obtained from the variations of COP, as shown in Fig. 5-12. When $m_{air,deh}$ varies from 0.01 to 0.025 kg/s, the coefficient of performance increases from 0.6511 to 0.8584 and 0.7942 to 1.0789, respectively, for desiccant solution with 0% and 10% ethanol concentrations. As a result, although the system sensible and latent effectiveness are reduced with the increase of dehumidifier air flow rate, both cooling output and COP can be improved.

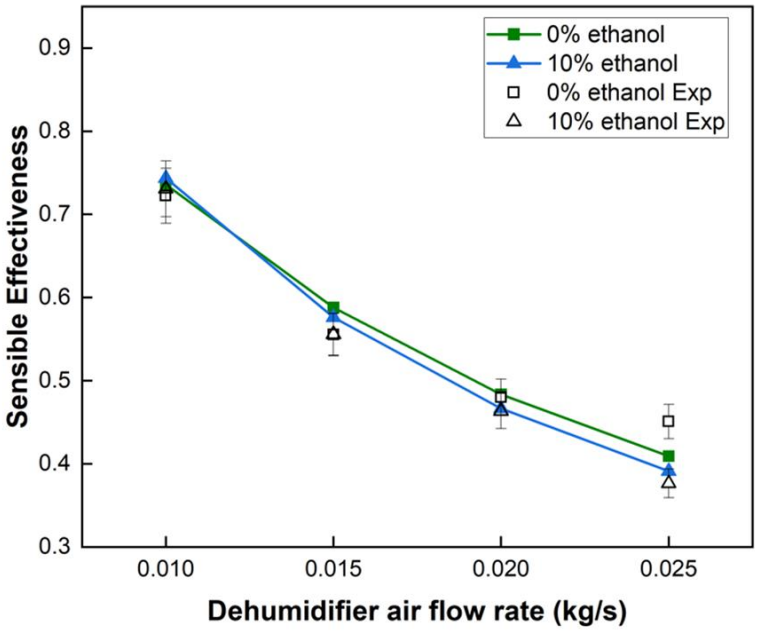

Figure 5-9 Sensible effectiveness variations under different dehumidifier air flow rates

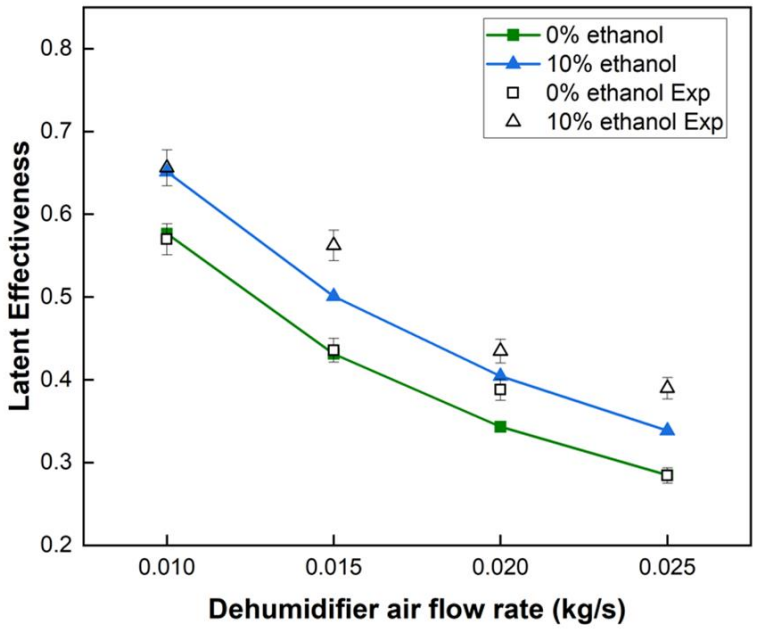

Figure 5-10 Latent effectiveness variations under different dehumidifier air flow rates

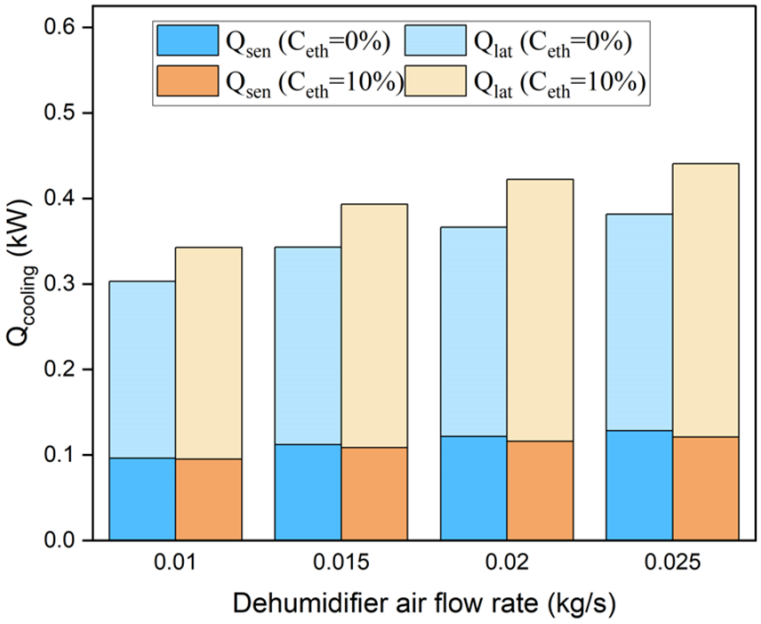

Figure 5-11 Total cooling output variations under different dehumidifier air flow rates

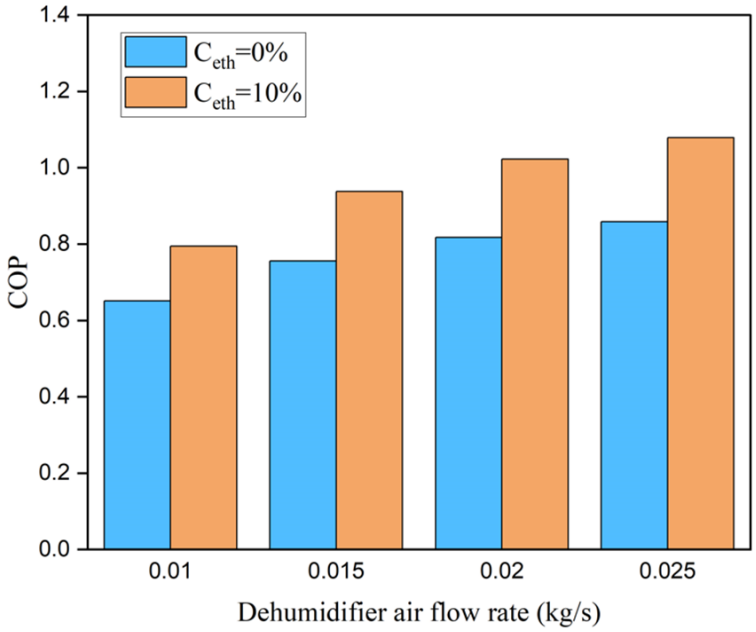

Figure 5-12 COP variations under different dehumidifier air flow rates

5.6.3. Effect of regenerator air flow rate

Similar to the effect of $m_{air,deh}$, the influences of the regenerator air flow rate are evaluated in this section. The variations of sensible and latent effectiveness under different ethanol concentrations are presented in Figs. 5-13 and 5-14 respectively. As illustrated in the figures, the influence of the regenerator air flow rate is less noticeable compared to the dehumidifier air flow rate. Under $C_{eth} = 0\%$, ε_{sen} increases from 73.57% to 73.76% while ε_{lat} increases from 57.65% to 57.72%, when the air flow rate increases from 0.01 kg/s to 0.025 kg/s. Under $C_{eth} = 10\%$, ε_{sen} increases from 74.36% to 74.56% while ε_{lat} increases from 65.14% to 65.19%. Based on previous study [92], the air flow rate is supposed to have a considerable influence on the sensible and latent performance of the regenerator. This can be explained by the difference between evaluating the regenerator effectiveness and system effectiveness. The main interest in the proposed self-cooled liquid desiccant dehumidification system is the amount of sensible and latent cooling output which can be achieved for a conditioned space after the dehumidification process. As a result, adjusting the air flow rate of regeneration has no obvious impact on the improvement of the dehumidification system's sensible and latent effectiveness.

Moreover, the variations of Q_{tot} and COP with $m_{air,reg}$ under different ethanol mass concentrations are plotted in Figs. 5-15 and 5-16. Since the air flow rate in dehumidifier remain constant, it is clear that the variations of Q_{sen} and Q_{lat} are supposed to have the same trend compared to ε_{sen} and ε_{lat}. The influence of $m_{air,reg}$ on system cooling output is almost negligible. For example, the sensible and latent cooling output vary from 0.0951 kW to 0.0968 kW and 0.2475 kW to

0.2482 kW, respectively, when 10% ethanol is added into solution. It can be noticed that the latent cooling output is considerably higher than sensible cooling output, and Q_{tot} slightly increases from 0.3426 kW to 0.3450 kW, when the air flow rate increases from 0.01 kg/s to 0.025 kg/s. On the contrary, the regenerator air flow rate has a negative influence on the system COP for both desiccant solutions with and without ethanol. For $C_{eth} = 0\%$, with the increase of $m_{air,reg}$ from 0.01 kg/s to 0.025 kg/s, COP decreases by 8.26% from 0.6511 to 0.5973. For $C_{eth} = 10\%$, COP decreases by 8.97% from 0.7942 to 0.723. This is due to the fact that the increase of air flow rate will lead to higher fan power of regenerator. Another possible explanation is that the increase of $m_{air,reg}$ will reduce the solution temperature coming out from the regenerator, which can reduce the heat exchange occurs in HX1. Thus the diluted desiccant solution will be pre-heated to a relatively low temperature, and a higher amount of heat input Q_{reg} is required from the electrical boiler.

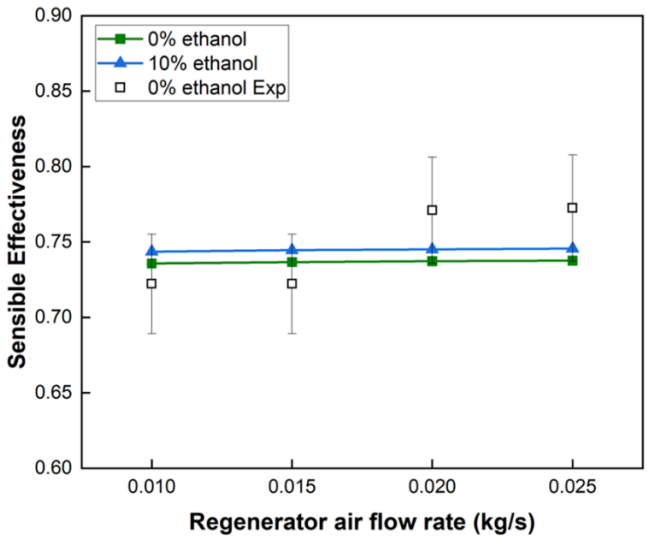

Figure 5-13 Sensible effectiveness variations under different regenerator air flow rates

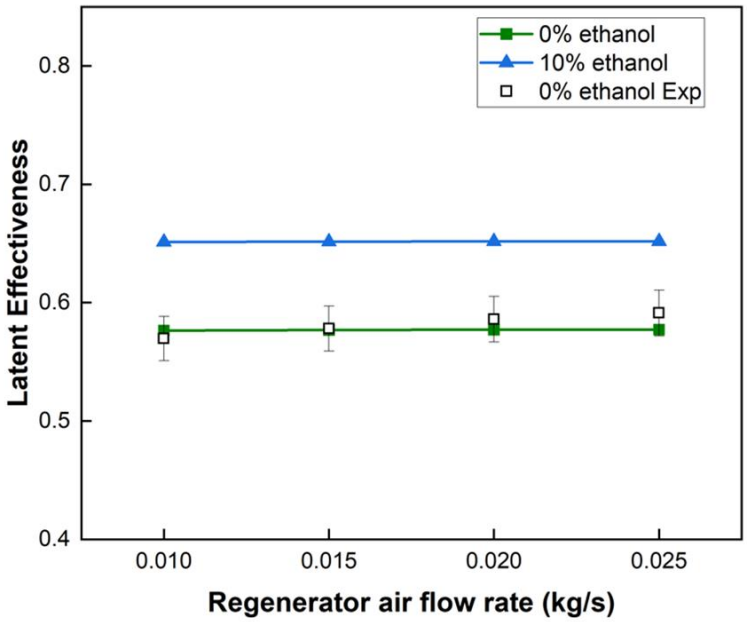

Figure 5-14 Latent effectiveness variations under different regenerator air flow rates

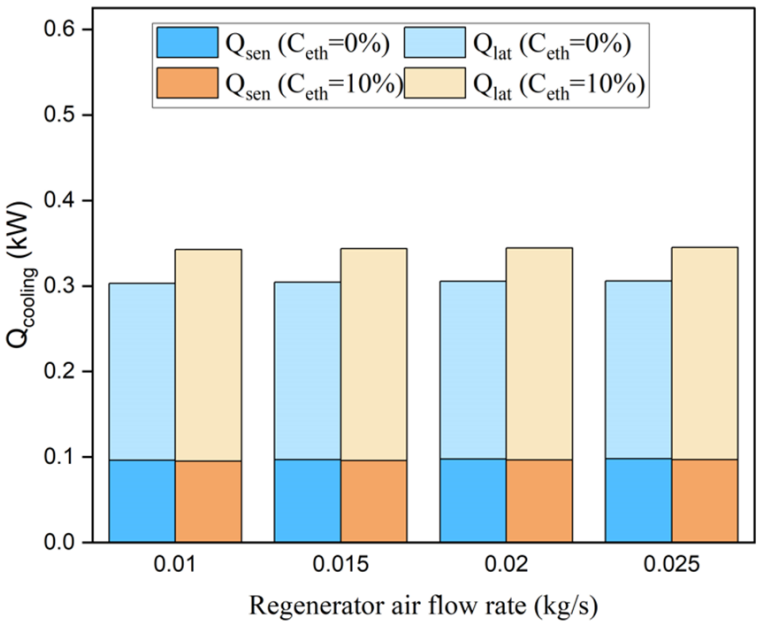

Figure 5-15 Total cooling output variations under different regenerator air flow rates

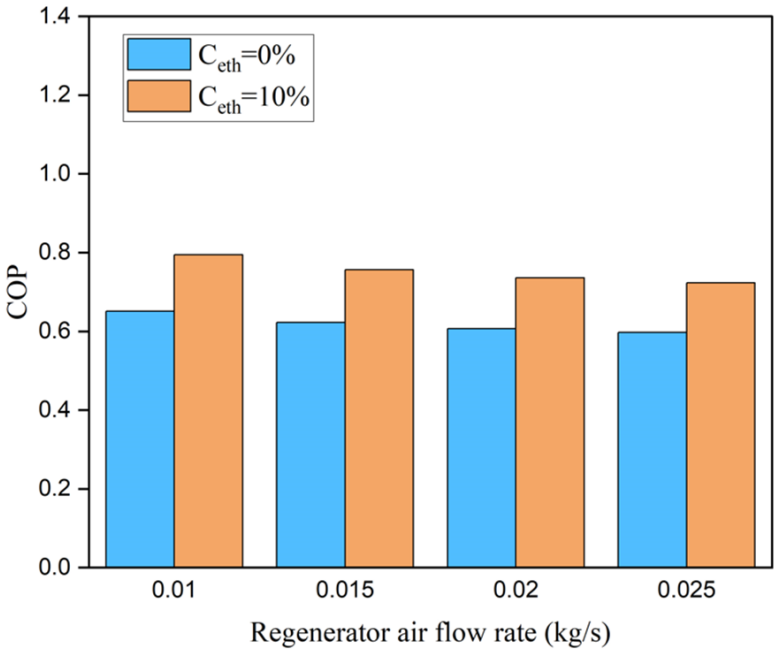

Figure 5-16 COP variations under different regenerator air flow rates

5.6.4. Effect of solution flow rate

The solution mass flow rate is another critical factor affecting the dehumidification system performance. For the complete system, the desiccant solution run through it within a closed loop. To address the effect of m_{sol}, the air flow rates through the dehumidifier and regenerator are set to be the same and constant. This is also reasonable in practice that the flow rates of supply air and exhaled air should be balanced to maintain indoor thermal comfort and the performance of building occupants [156]. The effect of solution flow rate on sensible and latent effectiveness under different ethanol concentrations are shown in Figs 5-17 and 5-18. It can be found that the solution flow rate has a significant influence on the system sensible effectiveness, while the influence of C_{eth} is limited. When there is 10% of ethanol in desiccant solution, ε_{sen} increases by 45.19% from 58.77% to 85.33% while the solution mass flow rate increases from

0.006 kg/s to 0.03 kg/s. The effect of m_{sol} on the system latent effectiveness is less significant than that of the sensible effectiveness, and the gradients of variation become moderate with the increase of solution mass flow rate. Under $C_{eth} = 0\%$, the latent effectiveness increases from 53.59% to 60.14% when m_{sol} changes from 0.006 kg/s to 0.03 kg/s. Similarly, under $C_{eth} = 10\%$, the latent effectiveness increases from 62.08% to 67.18%. The results have shown that the addition of ethanol into LiCl aqueous solution is a suitable way to improve the dehumidification performance, especially for latent effectiveness.

Similar to previous sections, the latent cooling capacity occupies the majority portion of the total cooling output, as shown in Fig. 5-19. The variation of Q_{sen} and Q_{lat} with solution flow rates flow the same trend of ε_{sen} and ε_{lat}, respectively. For example, under $C_{eth} = 10\%$, a noticeable increase of sensible cooling output by 53.04% from 0.0739 kW to 0.1131 kW, while the latent cooling output only increase by 9.01% from 0.2354 kW to 0.2566 kW as m_{sol} increases from 0.006 kg/s to 0.03 kg/s. Although the total cooling capacity can be improved with the increase of solution flow rate in the dehumidification system, a dramatic reduction in system COP can be observed in Fig. 5-20. When pure LiCl aqueous solution is used as desiccant solution, COP decreases by 67.56% from 1.0057 to 0.3263, for solution flow rate increases from 0.006 kg/s to 0.03 kg/s. When the proposed self-cooled desiccant solution is used, COP decreases by 69.52% from 1.2676 to 0.3864. By increasing the desiccant solution flow rate within the dehumidification system, the pump power assumption can be increased significantly. Moreover, the regeneration heat input from the electrical boiler is directly related to the solution mass flow as shown in Eq. (5-57). To sum up,

when the air flow rate has been determined by the building operator, there is no benefit to running the dehumidification system under a high solution flow rate condition. Although the system effectiveness and cooling output can be improved, the high solution flow rate will consume more pump energy and regeneration heat input, which would drag down the system COP.

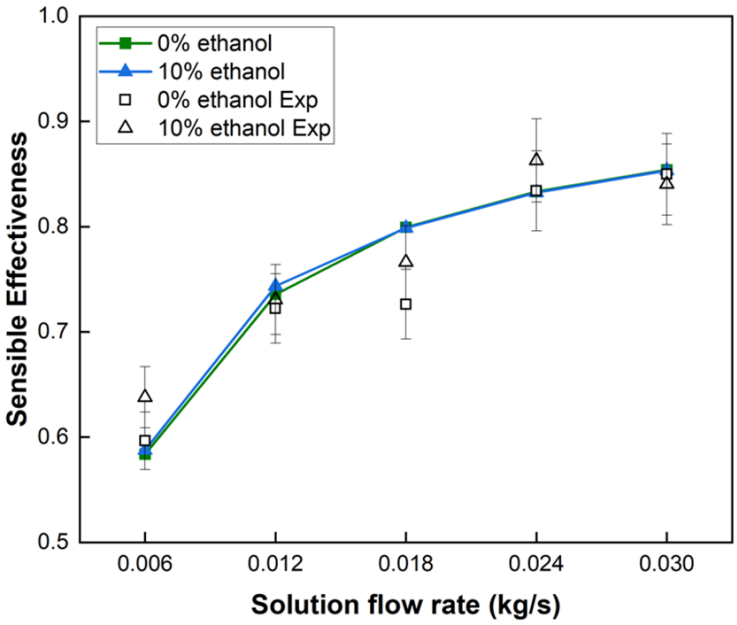

Figure 5-17 Sensible effectiveness variations under different solution flow rates

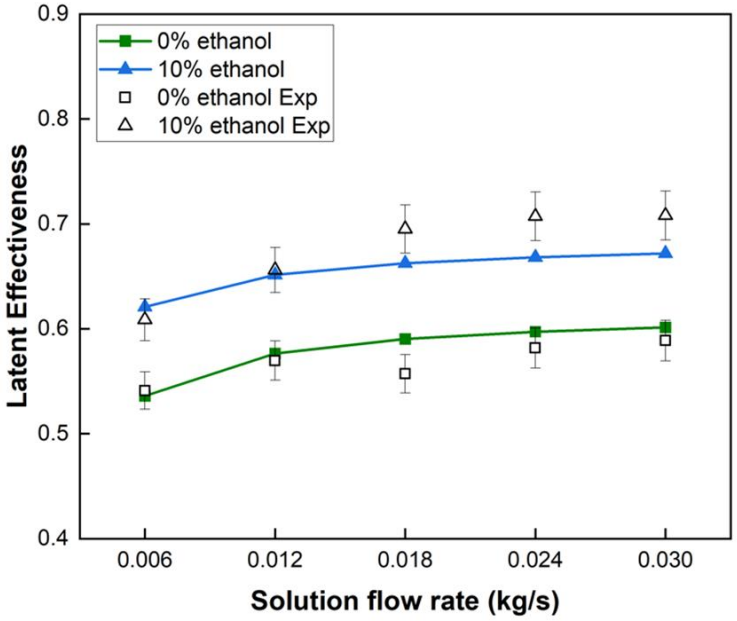

Figure 5-18 Latent effectiveness variations under different solution flow rates

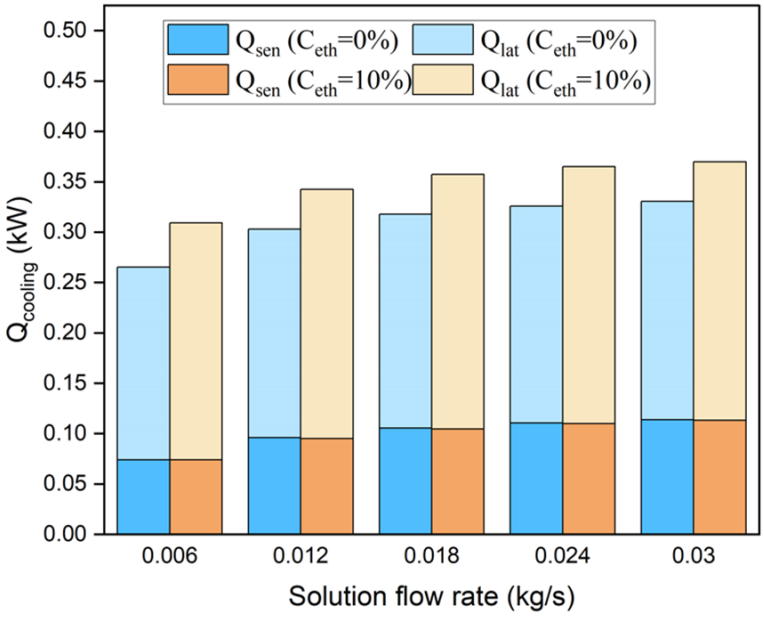

Figure 5-19 Total cooling output variations under different solution flow rates

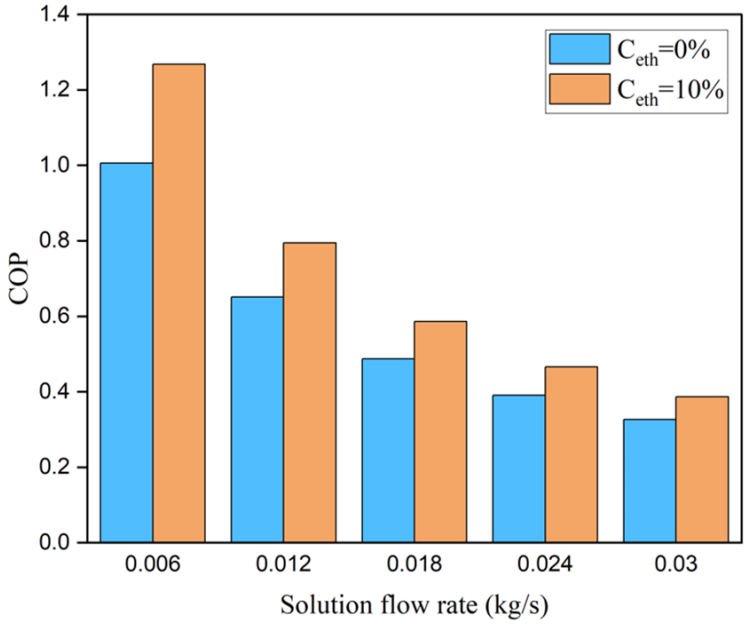

Figure 5-20 COP variations under different solution flow rates

5.6.5. Effect of solution concentration

The influence of the LiCl concentration on the complete dehumidification system performance are evaluated in this section. The variations of the system effectiveness (sensible and latent) when the solution flow rate is 0.012 kg/s have been presented in Figs. 5-21 and 5-22. By increasing the LiCl concentration from 28% to 37%, the system sensible effectiveness decreases from 77.19% to 73.57% and 79.54% to 74.36%, respectively, when C_{eth} = 0% and 10%. While the system latent effectiveness increases from 55.5% to 57.65% and 63.86% to 65.14% under different ethanol concentrations. By adding more LiCl into desiccant solution, the equilibrium surface vapour pressure can be reduced, which will improve the moisture absorption potential and thus enhance the latent effectiveness. In the meantime, with more moisture content in the process air being absorbed by the desiccant solution, more latent heat is released into the

dehumidifier during the heat and mass transfer process. Therefore, a negative impact has been observed between solution concentration and sensible effectiveness. It should also be noted that with a lower amount of LiCl concentration, the influence of ethanol on sensible effectiveness becomes more obvious.

Fig. 5-23 illustrates the variation of system cooling capacity with C_{sol} under different ethanol mass concentrations. Since the air and solution flow rates remain constant, the changes of the sensible and latent cooling output is directly related to ε_{sen} and ε_{lat}. Therefore, Q_{sen} is reduced with the increase of LiCl concentration, while Q_{lat} can be improved. For example, under $C_{eth} = 10\%$, the sensible cooling output slightly decreases by 10.87% from 0.1067 kW to 0.0951 kW, while the latent cooling output increases by 23.44% from 0.2005 kW to 0.2475 kW. As a result, the total cooling output can be improved from 0.3072 kW to 0.3426 kW. Similar trend is obtained for the system COP in Fig. 5-24. For $C_{eth} = 0\%$, with the increase of C_{sol} from 28% to 37%, COP increases from 0.4808 to 0.6511. For $C_{eth} = 10\%$, COP increases by 32.94% from 0.5974 to 0.7942. In real applications, the increase of desiccant solution concentration is more practical and suitable to improve the performance of the complete dehumidification system. However, it should be noted that high concentrated solution may lead to further problems such as crystallization, membrane blocking and high pumping pressure. As a result, the operation condition of the dehumidification system using high solution concentration should be more careful to avoid crystallization.

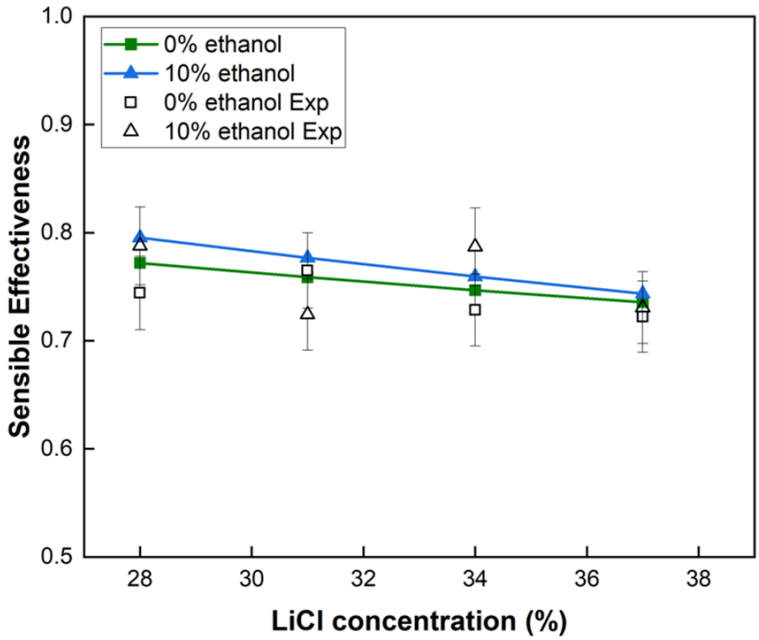

Figure 5-21 Sensible effectiveness variations under different solution concentrations

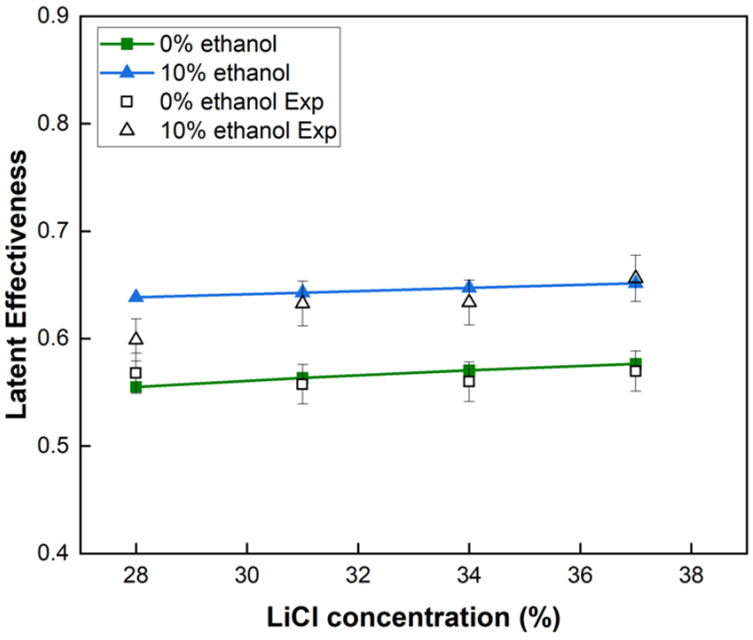

Figure 5-22 Latent effectiveness variations under different solution concentrations

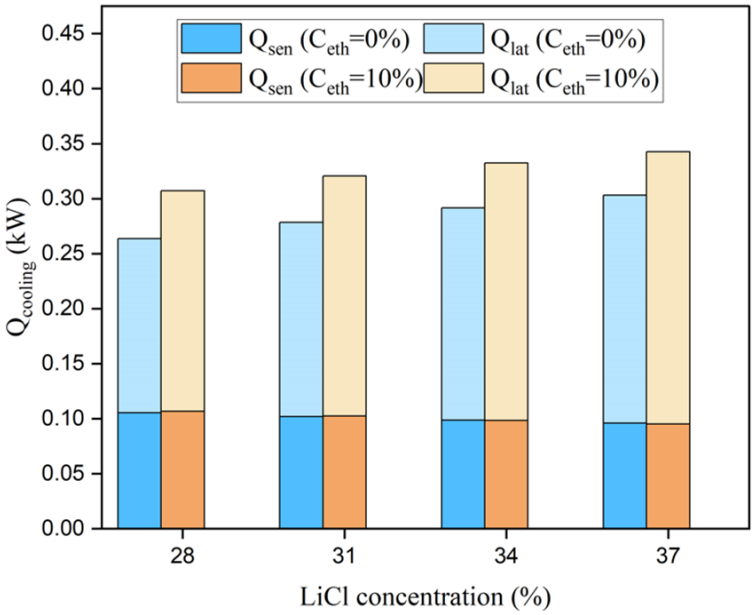

Figure 5-23 Total cooling output variations under different solution concentrations

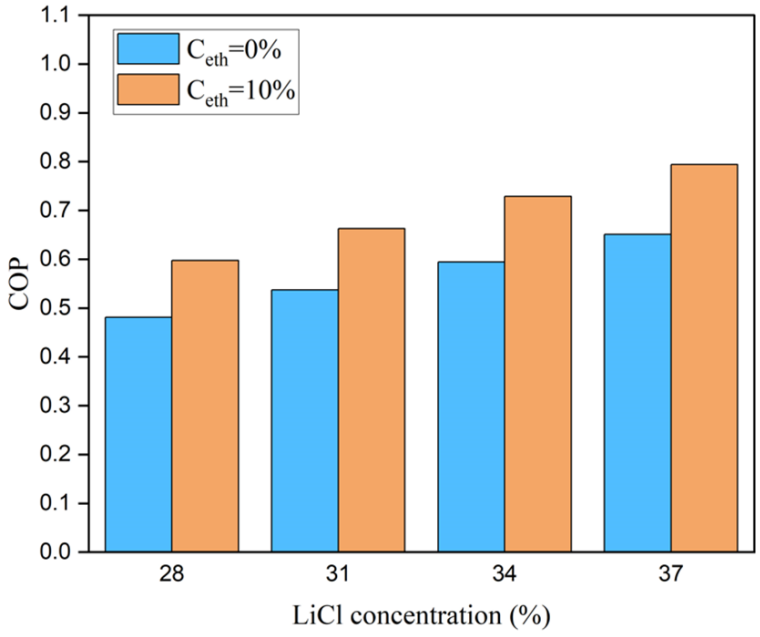

Figure 5-24 COP variations under different solution flow rates

5.7. Summary

In this section, a novel self-cooled membrane-based liquid desiccant dehumidification system which includes the dehumidifier, regenerator, heat exchangers, cold and hot water supply units have been proposed and fully investigated. Heat and mass transfer during the dehumidification and regeneration processes are evaluated by generating the numerical models in Matlab. Experimental tests have also been conducted and good agreement has been found between numerical data and experimental results. The performance of the dehumidification system is assessed by the system sensible and latent effectiveness, and its energy performance is evaluated by the total cooling output and COP. The influence of the newly formed self-cooled liquid desiccant on system performance is investigated by adjusting the ethanol mass concentrations. The influences of other main operating parameters such as the inlet air flow rate of dehumidifier and regenerator, solution flow rate and LiCl concentration have been investigated. The main conclusions of the section are presented as follows:

- The proposed self-cooled liquid desiccant solution has been proved to have the ability to increase the dehumidification performance comparing with the conventional LiCl aqueous solution. Although the sensible effectiveness and cooling output can barely be affected with the addition of ethanol, given the same operation conditions. The latent cooling output increases by 19.57% from 0.207 kW to 0.2475 kW, while the system COP can be increased by 21.98%, respectively, when the ethanol concentration varies from 0% to 10%.

- The sensible and latent effectiveness can reach up to 74.36% and 65.14%, respectively, by reducing the dehumidifier air flow rate to 0.01 kg/s. However, the system cooling output and COP are improved from 0.3426 kW to 0.4406 kW and 0.7942 to 1.0789, respectively, when $m_{air,deh}$ increases from 0.01 to 0.025 kg/s.
- The influences of regenerator air flow rate on the dehumidification system effectiveness and cooling output are negligible. The latent cooling output is around 2 times higher than the sensible cooling output. With the increase of $m_{air,reg}$ from 0.01 kg/s to 0.025 kg/s, COP decreases by 8.26% from 0.6511 to 0.5973.
- The sensible effectiveness is more sensitive to the solution flow rate, ε_{sen} increases from 58.77% to 85.33% when the solution mass flow rate increases from 0.006 kg/s to 0.03 kg/s. Although increasing the solution flow rate in the closed loop can increase the system effectiveness and colling output, COP can be dramatically decreased from 1.2676 to 0.3864.
- All of the dehumidification performance indices are improved with higher amount of solution concentration. The system COP can reach up to 0.7942 when $C_{sol} = 37\%$ and $C_{eth} = 10\%$. The problem of crystallization should be concerned in real applications.

Section 6: Conclusion and future work

The proposed self-cooled liquid desiccant dehumidification system offers better thermal and energy performance compared to conventional air humidity control unit. The aim of this thesis is to develop a novel self-cooled membrane-based liquid desiccant dehumidification system by combining the membrane-based air to liquid contactors with self-cooled liquid desiccant solution. The primary components including the dehumidifier and regenerator, and the complete system have been studied through simulation models and experimental works. According to numerical and experimental results, this research has proved the feasibility of adding ethanol into LiCl aqueous solution and its potential to enhance the dehumidification performance. The working hypothesis of the self-cooled liquid desiccant dehumidification can correspond to a competitive novel technique for air humidity control. A comprehensive conclusion summarizes the main findings of this thesis and relevant recommendations for future works.

6.1. Main conclusions

The aforementioned five sections have achieved the main purpose of this research by reaching the thesis objectives. The main findings of this thesis are listed below.

1) The first objective: 'Literature review on previous studies and researches related to liquid desiccant dehumidification technologies' has been accomplished in Section 2. After a comprehensive literature review of liquid desiccant dehumidifier, regenerator, complete dehumidification system and numerical modelling methods, it has been found that although the internally-cooled dehumidifier can enhance the dehumidification

performance, it suffers from complex structure design and high maintenance cost. The novel concept of self-cooled liquid desiccant solution can simplify the structure but may lead to the pollution of air that supplies to the indoor environment. Therefore, this research has firstly proposed the idea of combining membrane-based air-liquid contactor with self-cooled liquid desiccant solution to restrain the solution temperature rise, reduce maintenance cost and prevent air pollution from evaporative coolant at the same time. There are only a few numerical models developed to analyse the heat and mass transfer within dehumidifier with internally-cooling coil, and so far to the author's knowledge, none of the cooling medium involves phase change during the dehumidification process. Furthermore, no previous research has been reported on the performance of the self-cooled liquid desiccant solution nor the energy performance evaluation of the complete self-cooled liquid desiccant dehumidification system.

2) The second objective: 'Numerical and experimental analyses of the self-cooled membrane-based dehumidifier under different operating conditions and performance evaluation based on simulation and experimental results' has been accomplished in Section 3. The numerical model was developed by finite difference method and the equilibrium vapour pressure of self-cooled desiccant was solved by non-random two liquid method (NRTL). It is found that the addition of ethanol into desiccant solution can enhance the moisture removal rate and dehumidification effectiveness of dehumidifier by 44.7% and 21.8%, respectively. The air and solution mass flow rates are the most critical

parameters affecting the dehumidifier effectiveness. The variation of dehumidifier performance became less rapidly when mass flow rate ratio is higher than 1. The dehumidification performance can be improved by decreasing the inlet solution temperature and increasing the LiCl concentration, while it is insensitive to circulated air inlet temperature and flow rate. The results have also proved that the proposed self-cooled liquid desiccant dehumidifier can operate effectively under hot and humid weather conditions.

3) The third objective: 'Numerical and experimental analyses of the membrane-based regenerator under different operating conditions and performance evaluation based on simulation and experimental results' has been achieved in Section 4 by numerical modelling using finite difference method and experimental tests. The membrane-based regenerator has identical structure as the dehumidifier, but the heat and mass transfer is in opposite directions and different operation conditions. It is found that the newly formed self-cooled liquid desiccant leads to a negative impact on the moisture addition rate. Similarly to dehumidifier, the air and solution flow rates have the most significant influences on the regeneration effectiveness, ε_{reg}, can be decreased by 53.63% with the increase of air flow rate, while there is hardly benefit to the regeneration performance by increasing the mass flow rate ratio to be higher than 3. Although the influences of air temperature and relative humidity on regenerator effectiveness are less significant, cooler and drier air is recommended to enhance the reconnection potential of the regenerator. In real application, the solution inlet concentration is generally determined by the outlet

condition of dehumidifier, which is difficult to control, adjusting the solution inlet temperature is considered to be more practical to enhance the regeneration performance.

4) The forth objective: 'Developing a complete self-cooled membrane-based dehumidification system by combining the dehumidifier, regenerator and external heating and cooling medium, and investigating the system performance based on numerical and experimental results' has been achieved in Section 5. Based on the simulation results and experimental data for the complete self-cooled dehumidification system, it is found that the latent cooling output and COP can be improved by 19.57% and 21.98%, respectively, compared to pure LiCl aqueous solution. The sensible and latent effectiveness of the dehumidification system are more sensitive to dehumidifier air flow rate and solution flow rate, while the effects of regenerator air flow rate and LiCl concentration are relatively weak. As an air humidity control unit, the latent cooling output is normally two times higher than sensible cooling output under all operating conditions. Increasing the dehumidifier air flow rate can enhance the system total cooling output and COP, while increasing regenerator air flow rate could slightly reduce COP, for example, the system COP decrease by 8.26% when regeneration air flow rate changes from 0.01 kg/s to 0.025 kg/s. The total cooling output can be slightly improved by the increase of solution flow rate, but COP is dramatically reduced by 69.52% when solution flow rate varies from 0.01 kg/s to 0.025 kg/s, this is due to the increase of regeneration heat input from the boiler. The improvement of dehumidification energy performance by

increasing the solution concentration is more practical, however, the problem of crystallization should be more concerned especially for the proposed self-cooled liquid desiccant, since the addition of ethanol could reduce the solubility of lithium chloride.

6.2. Recommendation for future work

According to the main results conducted from the previous section, several recommendations for future work of the self-cooled membrane-based liquid desiccant dehumidification system have been proposed and listed below:

1) As a newly formed liquid desiccant solution, the thermophysical properties such as density, thermal conductivity and surface vapour pressure were determined based on references. Further experimental tests could be conducted to validate the properties of liquid desiccant mixed with evaporative coolant.
2) During previous chapters, a comprehensive parametric evaluation has been carried out for dehumidifier, regenerator and the entire dehumidification system, which include the effect of air and solution properties, mass flow rate and circulated air conditions. However, due to the limitation of fundings and research time, several critical parameters have not been investigated, including the structure of dehumidifier and regenerator, different types of membrane materials and other coolants. Since the main purpose of this research is to develop a membrane-based liquid desiccant dehumidification system using self-cooled liquid desiccant solution, it is recommended that future work can focus more on

evaluating different types of coolants that can be added into desiccant solution such as PCM.

3) For the proposed self-cooled liquid desiccant dehumidifier, the ethanol vapour was recovered through a fin type air-liquid heat exchanger. However, it should be treated more strictly to avoid the pollution of ethanol gas since it can cause intoxication in humans. The recovery of ethanol vapour could be redesigned in the future, for example using glycerol absorption cycle system.
4) Due to the limitations of testing time and rigs, only the inlet and outlet data were collected during the experiment. Although the temperature and concentration field have been conducted by numerical modelling, there is no experimental data to validate the accuracy of temperature and concentration field within dehumidifier and regenerator. Future experimental work could place the sensor inside the air and solution channels.
5) The numerical modelling is established based on the conservation of mass and energy using finite difference method. To fully understand the working principle of dehumidifier and regenerator, velocity and pressure profile should be taken into consideration. Navier-Stokes equations could be established and solved by CFD simulation software.
6) An electrical boiler was used in this project to supply hot water for regeneration. To increase the energy efficiency, the self-cooled liquid desiccant dehumidification system can be integrating with low-grade energy sources such as solar energy or ground source heat pump.

7) At last, the application of the proposed self-cooled membrane-based liquid desiccant dehumidification system could be tested by integrating with real buildings under hot and humid weather conditions either experimentally or numerically. The energy, carbon and economic performance could be further evaluated.

Reference list

[1] Y. Lin, J. Wang, W. Yang, L. Tian, and C. Candido, "A systematic review on COVID-19 related research in HVAC system and indoor environment," *Energy and Built Environment,* 2023/08/02/ 2023, doi: https://doi.org/10.1016/j.enbenv.2023.07.009.

[2] W. H. Organization, "Addressing violence against children, women and older people during the COVID-19 pandemic: key actions, 17 June 2020," JSTOR, 2020.

[3] G. Q. Sun *et al.*, "Transmission dynamics of COVID-19 in Wuhan, China: effects of lockdown and medical resources," *Nonlinear Dynamics,* Article vol. 101, no. 3, pp. 1981-1993, 2020, doi: 10.1007/s11071-020-05770-9.

[4] M. Kipp, "Impact of the covid-19 pandemic on the acceptance and use of an e-learning platform," *International Journal of Environmental Research and Public Health,* Article vol. 18, no. 21, 2021, Art no. 11372, doi: 10.3390/ijerph182111372.

[5] J. Molloy, T. Schatzmann, B. Schoeman, C. Tchervenkov, B. Hintermann, and K. W. Axhausen, "Observed impacts of the Covid-19 first wave on travel behaviour in Switzerland based on a large GPS panel," *Transport Policy,* vol. 104, pp. 43-51, 2021/04/01/ 2021, doi: https://doi.org/10.1016/j.tranpol.2021.01.009.

[6] "World Economic Outlook, April 2020: The Great Lockdown," ed: Bernan Associates, 2020.

[7] IMF, "Policy response to Covid-19 Policy Tracker," 2020.

[8] L. Micheli, Á. F. Solas, A. Soria-Moya, F. Almonacid, and E. F. Fernández, "Short-term impact of the COVID-19 lockdown on the energy and economic performance of photovoltaics in the Spanish electricity sector," *Journal of Cleaner Production,* vol. 308, p. 127045, 2021/07/25/ 2021, doi: https://doi.org/10.1016/j.jclepro.2021.127045.

[9] L. Cozzi *et al.*, "World energy outlook 2020," *International Energy Agency: Paris, France,* pp. 1-461, 2020.

[10] I. MacLeay, K. Harris, and A. Annut, *Digest of United KingdomEnergy Statistics 2011*. A National Statistics publication 2011.

[11] J. Mayernik, O. o. E. Efficiency, and E. Renewable. *Buildings Energy Data Book*, National Renewable Energy Laboratory, 2015/06/11. [Online]. Available: https://data.openei.org/submissions/

[12] G. Gausden, "Home electricity consumption now peaks at 1pm while smart meter data suggests people are having early nights AND late mornings," *Article in This is Money,* 2020.

[13] Savills, "COVID-19 restrictions changing the daily patterns of energy consumption," ed, 2020.

[14] "Energy Commission Releases New Data on How COVID-19 is Impacting the Energy Sector, California Energy Commission (2020)," ed. https://www.energy.ca.gov/news/2020-05/energy-commission-releases-new-data-how-covid-19-impacting-energy-sector, 2020.

[15] C. Global, ""Willis Carrier – 1876–1902"," ed, 2021.

[16] A. M. Elsaid and M. S. Ahmed, "Indoor Air Quality Strategies for Air-Conditioning and Ventilation Systems with the Spread of the Global Coronavirus (COVID-19) Epidemic: Improvements and Recommendations," *Environmental Research,* vol. 199, p. 111314, 2021/08/01/ 2021, doi: https://doi.org/10.1016/j.envres.2021.111314.
[17] (2020). *REHVA COVID-19 guidance document*.
[18] ASHRAE, *Building Readiness*. 2020.
[19] ASC, *Guidelines for office buildings to deal with "new coronavirus" operational management emergency measures*. 2020.
[20] SHASE, *Operation of air-conditioning equipment and other facilities as SARS-CoV-2 infectious disease control*. 2020.
[21] CCIAQ, *Addressing COVID-19 in Buildings*. 2020.
[22] L. Z. Zhang and J. L. Niu, "Indoor humidity behaviors associated with decoupled cooling in hot and humid climates," *Building and Environment,* vol. 38, no. 1, pp. 99-107, 2003/01/01/ 2003, doi: https://doi.org/10.1016/S0360-1323(02)00018-5.
[23] R. American Society of Heating and E. Air-Conditioning, *ASHRAE standard 55-04: Thermal environmental conditions for human occupancy*. Atlanta, Ga. : The Society, [2004] ©2004, 2004.
[24] R. G. Nevins, "Temperature-Humidity Chart for Themal Comfort of Seated Persons," *Ashrae Transactions,* vol. 72, pp. 283-291, 1966.
[25] A. Baughman and E. A. Arens, "Indoor humidity and human health--Part I: Literature review of health effects of humidity-influenced indoor pollutants," 1996.
[26] E. Chartered Institution of Building Services, *Environmental design : CIBSE guide A*, 7th ed. London: CIBSE London (in eng), 2006.
[27] L. Pérez-Lombard, J. Ortiz, and C. Pout, "A review on buildings energy consumption information," *Energy and Buildings,* vol. 40, no. 3, pp. 394-398, 2008/01/01/ 2008, doi: https://doi.org/10.1016/j.enbuild.2007.03.007.
[28] C. F. A. Afonso, "Recent advances in building air conditioning systems," *Applied Thermal Engineering,* vol. 26, no. 16, pp. 1961-1971, 2006/11/01/ 2006, doi: https://doi.org/10.1016/j.applthermaleng.2006.01.016.
[29] X. Liu, Z. Li, and T. Zhang, "Liquid desiccant dehumidification," *China Architecture and Building Press, Beijing,* 2014.
[30] H.-X. Fu and X.-H. Liu, "Review of the impact of liquid desiccant dehumidification on indoor air quality," *Building and Environment,* vol. 116, pp. 158-172, 2017/05/01/ 2017, doi: https://doi.org/10.1016/j.buildenv.2017.02.014.
[31] Z. Weirong, Q. Kaiyang, L. Xiaohua, and C. Xiaomin, "Pilot study of the impact of liquid desiccant dehumidification on IAQ," *Hv & Ac,* vol. 11, p. 28, 2004.
[32] (2003). *Test of whether Lithium Bromide and Lithium Chloride Mixed Solution Kills SARS Virus*.
[33] M. M. Rafique, P. Gandhidasan, and H. M. S. Bahaidarah, "Liquid desiccant materials and dehumidifiers – A review," *Renewable and Sustainable Energy Reviews,* vol. 56, pp. 179-195, 2016/04/01/ 2016, doi: https://doi.org/10.1016/j.rser.2015.11.061.

[34] Y. H. Zurigat, M. K. Abu-Arabi, and S. A. Abdul-Wahab, "Air dehumidification by triethylene glycol desiccant in a packed column," *Energy Conversion and Management,* vol. 45, no. 1, pp. 141-155, 2004/01/01/ 2004, doi: https://doi.org/10.1016/S0196-8904(03)00109-2.

[35] T.-W. Chung, "Predictions of moisture removal efficiencies for packed-bed dehumidification systems," *Gas Separation & Purification,* vol. 8, no. 4, pp. 265-268, 1994/01/01/ 1994, doi: https://doi.org/10.1016/0950-4214(94)80007-3.

[36] D. Babakhani and M. Soleymani, "An analytical solution for air dehumidification by liquid desiccant in a packed column," *International Communications in Heat and Mass Transfer,* vol. 36, no. 9, pp. 969-977, 2009/11/01/ 2009, doi: https://doi.org/10.1016/j.icheatmasstransfer.2009.06.002.

[37] G. A. Longo and A. Gasparella, "Experimental Analysis on Chemical Dehumidification of Air by Liquid Desiccant and Desiccant Regeneration in a Packed Tower," *Journal of Solar Energy Engineering,* vol. 126, no. 1, pp. 587-591, 2004, doi: 10.1115/1.1637642.

[38] D. Pietruschka, U. Eicker, M. Huber, and J. Schumacher, "Experimental performance analysis and modelling of liquid desiccant cooling systems for air conditioning in residential buildings," *International Journal of Refrigeration,* vol. 29, no. 1, pp. 110-124, 2006/01/01/ 2006, doi: https://doi.org/10.1016/j.ijrefrig.2005.05.012.

[39] L. Zhang, E. Hihara, F. Matsuoka, and C. Dang, "Experimental analysis of mass transfer in adiabatic structured packing dehumidifier/regenerator with liquid desiccant," *International Journal of Heat and Mass Transfer,* vol. 53, no. 13, pp. 2856-2863, 2010/06/01/ 2010, doi: https://doi.org/10.1016/j.ijheatmasstransfer.2010.02.012.

[40] W. Z. Gao, J. H. Liu, Y. P. Cheng, and X. L. Zhang, "Experimental investigation on the heat and mass transfer between air and liquid desiccant in a cross-flow dehumidifier," *Renewable Energy,* vol. 37, no. 1, pp. 117-123, 2012/01/01/ 2012, doi: https://doi.org/10.1016/j.renene.2011.06.006.

[41] A. M. Radhwan, H. N. Gari, and M. M. Elsayed, "Parametric study of a packed bed dehumidifier/regenerator using CaCl2 liquid desiccant," *Renewable Energy,* vol. 3, no. 1, pp. 49-60, 1993/02/01/ 1993, doi: https://doi.org/10.1016/0960-1481(93)90130-9.

[42] N. Fumo and D. Y. Goswami, "Study of an aqueous lithium chloride desiccant system: air dehumidification and desiccant regeneration," *Solar Energy,* vol. 72, no. 4, pp. 351-361, 2002/04/01/ 2002, doi: https://doi.org/10.1016/S0038-092X(02)00013-0.

[43] L.-Z. Zhang, *Total heat recovery heat and moisture recovery from ventilation air*. New York : Nova Science Publishers, c2008., 2008.

[44] J.-I. Yoon, T.-T. Phan, C.-G. Moon, and P. Bansal, "Numerical study on heat and mass transfer characteristic of plate absorber," *Applied Thermal Engineering,* vol. 25, no. 14, pp. 2219-2235, 2005/10/01/ 2005, doi: https://doi.org/10.1016/j.applthermaleng.2005.01.004.

[45] W. Kessling, E. Laevemann, and C. Kapfhammer, "ENERGY STORAGE FOR DESICCANT COOLING SYSTEMS COMPONENT

DEVELOPMENT," *Solar Energy,* vol. 64, no. 4, pp. 209-221, 1998/12/01/ 1998, doi: https://doi.org/10.1016/S0038-092X(98)00081-4.
[46] Y. Yin, X. Zhang, G. Wang, and L. Luo, "Experimental study on a new internally cooled/heated dehumidifier/regenerator of liquid desiccant systems," *International Journal of Refrigeration,* vol. 31, no. 5, pp. 857-866, 2008/08/01/ 2008, doi: https://doi.org/10.1016/j.ijrefrig.2007.10.004.
[47] J. Liu, T. Zhang, X. Liu, and J. Jiang, "Experimental analysis of an internally-cooled/heated liquid desiccant dehumidifier/regenerator made of thermally conductive plastic," *Energy and Buildings,* vol. 99, pp. 75-86, 2015/07/15/ 2015, doi: https://doi.org/10.1016/j.enbuild.2015.04.023.
[48] L. Chen, Z. Li, and Z.-Y. Guo, "Experimental investigation of plastic finned-tube heat exchangers, with emphasis on material thermal conductivity," *Experimental Thermal and Fluid Science,* vol. 33, no. 5, pp. 922-928, 2009/07/01/ 2009, doi: https://doi.org/10.1016/j.expthermflusci.2009.04.001.
[49] T. Zhang, X. Liu, J. Jiang, X. Chang, and Y. Jiang, "Experimental analysis of an internally-cooled liquid desiccant dehumidifier," *Building and Environment,* vol. 63, pp. 1-10, 2013/05/01/ 2013, doi: https://doi.org/10.1016/j.buildenv.2013.01.007.
[50] N. Giannetti, S. Yamaguchi, and K. Saito, "Wetting behavior of a liquid film on an internally-cooled desiccant contactor," *International Journal of Heat and Mass Transfer,* vol. 101, pp. 958-969, 2016/10/01/ 2016, doi: https://doi.org/10.1016/j.ijheatmasstransfer.2016.05.128.
[51] P. Bansal, S. Jain, and C. Moon, "Performance comparison of an adiabatic and an internally cooled structured packed-bed dehumidifier," *Applied Thermal Engineering,* vol. 31, no. 1, pp. 14-19, 2011/01/01/ 2011, doi: https://doi.org/10.1016/j.applthermaleng.2010.06.026.
[52] W. Y. Saman and S. Alizadeh, "An experimental study of a cross-flow type plate heat exchanger for dehumidification/cooling," *Solar Energy,* vol. 73, no. 1, pp. 59-71, 2002/07/01/ 2002, doi: https://doi.org/10.1016/S0038-092X(01)00078-0.
[53] X. Cheng, D. Peng, Y. Yin, S. Xu, and D. Luo, "Experimental study and performance analysis on a new dehumidifier with outside evaporative cooling," *Building and Environment,* vol. 148, pp. 200-211, 2019/01/15/ 2019, doi: https://doi.org/10.1016/j.buildenv.2018.11.006.
[54] S. Yamaguchi, J. Jeong, K. Saito, H. Miyauchi, and M. Harada, "Hybrid liquid desiccant air-conditioning system: Experiments and simulations," *Applied Thermal Engineering,* vol. 31, no. 17, pp. 3741-3747, 2011/12/01/ 2011, doi: https://doi.org/10.1016/j.applthermaleng.2011.04.009.
[55] J. Liu, T. Zhang, and X. Liu, "Model-based investigation of a heat pump driven, internally cooled liquid desiccant dehumidification system," *Building and Environment,* vol. 143, pp. 431-442, 2018/10/01/ 2018, doi: https://doi.org/10.1016/j.buildenv.2018.07.027.
[56] T. W. Chung and H. Wu, "Comparison between spray towers with and without fin coils for air dehumidification using triethylene glycol solutions and development of the mass-transfer correlations," *Industrial and Engineering Chemistry Research,* Article vol. 39, no. 6, pp. 2076-2084, 2000, doi: 10.1021/ie990630d.

[57] H. Ren, Z. Ma, and S. Gschwander, "Characterisation and evaluation of a new phase change enhanced working solution for liquid desiccant cooling systems," *Applied Thermal Engineering,* vol. 150, pp. 1197-1205, 2019/03/05/ 2019, doi: https://doi.org/10.1016/j.applthermaleng.2019.01.096.

[58] Z. Lu, X. Niu, J. Zhou, and Y. Yin, "Experimental study of the surface vapor pressure of a microencapsulated phase change material slurry liquid desiccant within the entire temperature range of a dehumidification system," *Energy and Buildings,* vol. 277, p. 112586, 2022.

[59] H. Dong *et al.*, "Experimental study on the liquid desiccant dehumidification performance of microencapsulated phase change materials slurry," *Energy,* vol. 239, 2022, doi: 10.1016/j.energy.2021.122212.

[60] W. Lun, K. Li, B. Liu, H. Zhang, Y. Yang, and C. Yang, "Experimental analysis of a novel internally-cooled dehumidifier with self-cooled liquid desiccant," *Building and Environment,* vol. 141, pp. 117-126, 2018, doi: 10.1016/j.buildenv.2018.05.055.

[61] S.-M. Huang and L.-Z. Zhang, "Researches and trends in membrane-based liquid desiccant air dehumidification," *Renewable and Sustainable Energy Reviews,* vol. 28, pp. 425-440, 2013/12/01/ 2013, doi: https://doi.org/10.1016/j.rser.2013.08.005.

[62] S.-M. Huang, L.-Z. Zhang, K. Tang, and L.-X. Pei, "Fluid flow and heat mass transfer in membrane parallel-plates channels used for liquid desiccant air dehumidification," *International Journal of Heat and Mass Transfer,* vol. 55, no. 9, pp. 2571-2580, 2012/04/01/ 2012, doi: https://doi.org/10.1016/j.ijheatmasstransfer.2012.01.003.

[63] L.-Z. Zhang, "Heat and mass transfer in a cross-flow membrane-based enthalpy exchanger under naturally formed boundary conditions," *International Journal of Heat and Mass Transfer,* vol. 50, no. 1, pp. 151-162, 2007/01/01/ 2007, doi: https://doi.org/10.1016/j.ijheatmasstransfer.2006.06.025.

[64] K. Mahmud, G. I. Mahmood, C. J. Simonson, and R. W. Besant, "Performance testing of a counter-cross-flow run-around membrane energy exchanger (RAMEE) system for HVAC applications," *Energy and Buildings,* vol. 42, no. 7, pp. 1139-1147, 2010/07/01/ 2010, doi: https://doi.org/10.1016/j.enbuild.2010.02.005.

[65] A. Vali, C. J. Simonson, R. W. Besant, and G. Mahmood, "Numerical model and effectiveness correlations for a run-around heat recovery system with combined counter and cross flow exchangers," *International Journal of Heat and Mass Transfer,* vol. 52, no. 25, pp. 5827-5840, 2009/12/01/ 2009, doi: https://doi.org/10.1016/j.ijheatmasstransfer.2009.07.020.

[66] M. D. Larson, C. J. Simonson, R. W. Besant, and P. W. Gibson, "The elastic and moisture transfer properties of polyethylene and polypropylene membranes for use in liquid-to-air energy exchangers," *Journal of Membrane Science,* vol. 302, no. 1, pp. 136-149, 2007/09/15/ 2007, doi: https://doi.org/10.1016/j.memsci.2007.06.050.

[67] M. Seyed-Ahmadi, B. Erb, C. J. Simonson, and R. W. Besant, "Transient behavior of run-around heat and moisture exchanger system. Part I:

Model formulation and verification," *International Journal of Heat and Mass Transfer,* vol. 52, no. 25, pp. 6000-6011, 2009/12/01/ 2009, doi: https://doi.org/10.1016/j.ijheatmasstransfer.2009.07.012.

[68] M. Seyed-Ahmadi, B. Erb, C. J. Simonson, and R. W. Besant, "Transient behavior of run-around heat and moisture exchanger system. Part II: Sensitivity studies for a range of initial conditions," *International Journal of Heat and Mass Transfer,* vol. 52, no. 25, pp. 6012-6020, 2009/12/01/ 2009, doi: https://doi.org/10.1016/j.ijheatmasstransfer.2009.06.037.

[69] A. Mansourizadeh and A. F. Ismail, "Hollow fiber gas–liquid membrane contactors for acid gas capture: A review," *Journal of Hazardous Materials,* vol. 171, no. 1, pp. 38-53, 2009/11/15/ 2009, doi: https://doi.org/10.1016/j.jhazmat.2009.06.026.

[70] S. Bergero and A. Chiari, "Experimental and theoretical analysis of air humidification/dehumidification processes using hydrophobic capillary contactors," *Applied Thermal Engineering,* vol. 21, no. 11, pp. 1119-1135, 2001/08/01/ 2001, doi: https://doi.org/10.1016/S1359-4311(00)00107-1.

[71] L.-Z. Zhang, "An Analytical Solution to Heat and Mass Transfer in Hollow Fiber Membrane Contactors for Liquid Desiccant Air Dehumidification," *Journal of Heat Transfer,* vol. 133, no. 9, 2011, doi: 10.1115/1.4003900.

[72] L.-Z. Zhang, S.-M. Huang, J.-H. Chi, and L.-X. Pei, "Conjugate heat and mass transfer in a hollow fiber membrane module for liquid desiccant air dehumidification: A free surface model approach," *International Journal of Heat and Mass Transfer,* vol. 55, no. 13, pp. 3789-3799, 2012/06/01/ 2012, doi: https://doi.org/10.1016/j.ijheatmasstransfer.2012.03.034.

[73] S.-M. Huang, L.-Z. Zhang, K. Tang, and L.-X. Pei, "Turbulent Heat and Mass Transfer Across a Hollow Fiber Membrane Tube Bank in Liquid Desiccant Air Dehumidification," *Journal of Heat Transfer,* vol. 134, no. 8, 2012, doi: 10.1115/1.4006208.

[74] X. Chen *et al.*, "Performance analysis and design implementation of a novel polymer hollow fiber liquid desiccant dehumidifier with aqueous potassium formate," *Thermal Science and Engineering Progress,* vol. 13, p. 100366, 2019/10/01/ 2019, doi: https://doi.org/10.1016/j.tsep.2019.100366.

[75] M. Conde-Petit, R. Weber, and V. Dorer, "Open absorption system for cooling and air conditioning using membrane contactors-Final report," 2008.

[76] S.-M. Huang, M. Yang, and X. Yang, "Performance analysis of a quasi-counter flow parallel-plate membrane contactor used for liquid desiccant air dehumidification," *Applied Thermal Engineering,* vol. 63, no. 1, pp. 323-332, 2014/02/05/ 2014, doi: https://doi.org/10.1016/j.applthermaleng.2013.11.027.

[77] M. R. H. Abdel-Salam, R. W. Besant, and C. J. Simonson, "Design and testing of a novel 3-fluid liquid-to-air membrane energy exchanger (3-fluid LAMEE)," *International Journal of Heat and Mass Transfer,* vol. 92, pp. 312-329, 2016/01/01/ 2016, doi: https://doi.org/10.1016/j.ijheatmasstransfer.2015.08.075.

[78] D. Qiu *et al.*, "Laminar flow and heat transfer in an internally-cooled hexagonal parallel-plate membrane channel (IHPMC)," *Applied Thermal*

Engineering, vol. 124, pp. 767-780, 2017/09/01/ 2017, doi: https://doi.org/10.1016/j.applthermaleng.2017.06.079.

[79] L.-Z. Zhang, "Heat and mass transfer in a quasi-counter flow membrane-based total heat exchanger," *International Journal of Heat and Mass Transfer,* vol. 53, no. 23, pp. 5478-5486, 2010/11/01/ 2010, doi: https://doi.org/10.1016/j.ijheatmasstransfer.2010.07.009.

[80] G. A. Longo and A. Gasparella, "Experimental analysis on desiccant regeneration in a packed column with structured and random packing," *Solar Energy,* vol. 83, no. 4, pp. 511-521, 2009/04/01/ 2009, doi: https://doi.org/10.1016/j.solener.2008.08.016.

[81] X. Y. Chen, Z. Li, Y. Jiang, and K. Y. Qu, "Field study on independent dehumidification air-conditioning system - I: Performance of liquid desiccant dehumidification system," *ASHRAE Transactions,* vol. 111, pp. 271-276, 01/01 2005.

[82] X. H. Liu, Y. Jiang, X. M. Chang, and X. Q. Yi, "Experimental investigation of the heat and mass transfer between air and liquid desiccant in a cross-flow regenerator," *Renewable Energy,* vol. 32, no. 10, pp. 1623-1636, 2007/08/01/ 2007, doi: https://doi.org/10.1016/j.renene.2006.07.002.

[83] S. Shen, W. Cai, X. Wang, Q. Wu, and H. Yon, "Investigation of liquid desiccant regenerator with heat recovery heat pipe system," *Energy and Buildings,* vol. 146, pp. 353-363, 2017/07/01/ 2017, doi: https://doi.org/10.1016/j.enbuild.2017.04.057.

[84] S. Shen, W. Cai, X. Wang, Q. Wu, and H. Yon, "Investigation of liquid desiccant regenerator with fixed-plate heat recovery system," *Energy,* vol. 137, pp. 172-182, 2017/10/15/ 2017, doi: https://doi.org/10.1016/j.energy.2017.07.024.

[85] Q. Cheng and X. Zhang, "Review of solar regeneration methods for liquid desiccant air-conditioning system," *Energy and Buildings,* vol. 67, pp. 426-433, 2013/12/01/ 2013, doi: https://doi.org/10.1016/j.enbuild.2013.08.053.

[86] A. S. Alosaimy and A. M. Hamed, "Theoretical and experimental investigation on the application of solar water heater coupled with air humidifier for regeneration of liquid desiccant," *Energy,* vol. 36, no. 7, pp. 3992-4001, 2011/07/01/ 2011, doi: https://doi.org/10.1016/j.energy.2011.05.002.

[87] Q. Cheng, Y. Xu, and X.-S. Zhang, "Experimental investigation of an electrodialysis regenerator for liquid desiccant," *Energy and Buildings,* vol. 67, pp. 419-425, 2013/12/01/ 2013, doi: https://doi.org/10.1016/j.enbuild.2013.08.052.

[88] G. Ge, D. Ghadiri Moghaddam, A. H. Abdel-Salam, R. W. Besant, and C. J. Simonson, "Comparison of experimental data and a model for heat and mass transfer performance of a liquid-to-air membrane energy exchanger (LAMEE) when used for air dehumidification and salt solution regeneration," *International Journal of Heat and Mass Transfer,* vol. 68, pp. 119-131, 2014/01/01/ 2014, doi: https://doi.org/10.1016/j.ijheatmasstransfer.2013.09.016.

[89] D. G. Moghaddam, P. LePoudre, G. Ge, R. W. Besant, and C. J. Simonson, "Small-scale single-panel liquid-to-air membrane energy exchanger

(LAMEE) test facility development, commissioning and evaluating the steady-state performance," *Energy and Buildings,* vol. 66, pp. 424-436, 2013/11/01/ 2013, doi: https://doi.org/10.1016/j.enbuild.2013.07.017.

[90] H. C. Duong, F. I. Hai, A. Al-Jubainawi, Z. Ma, T. He, and L. D. Nghiem, "Liquid desiccant lithium chloride regeneration by membrane distillation for air conditioning," *Separation and Purification Technology,* vol. 177, pp. 121-128, 2017/04/28/ 2017, doi: https://doi.org/10.1016/j.seppur.2016.12.031.

[91] N. Datta, A. Chakraborty, S. M. Ali, and F. H. Choo, "Experimental investigation of multi-effect regenerator for desiccant dehumidifier: Effects of various regeneration temperatures and solution flow rates on system performances," *International Journal of Refrigeration,* vol. 76, pp. 7-18, 2017/04/01/ 2017, doi: https://doi.org/10.1016/j.ijrefrig.2017.01.019.

[92] H. Bai, J. Zhu, Z. Chen, J. Chu, and Y. Liu, "Performance evaluation of a membrane-based flat-plate heat and mass exchanger used for liquid desiccant regeneration," *Applied Thermal Engineering,* vol. 139, pp. 569-584, 2018/07/05/ 2018, doi: https://doi.org/10.1016/j.applthermaleng.2018.05.011.

[93] A. London and W. Kays, "The liquid-coupled indirect-transfer regenerator for gas-turbine plants," *Transactions of the American Society of Mechanical Engineers,* vol. 73, no. 5, pp. 529-540, 1951.

[94] B. Forsyth and R. Besant, "The design of a run-around heat recovery system," *ASHRAE transactions,* vol. 94, pp. 511-531, 1988.

[95] H. Fan, C. J. Simonson, R. W. Besant, and W. Shang, "Performance of a Run-Around System for HVAC Heat and Moisture Transfer Applications Using Cross-Flow Plate Exchangers Coupled with Aqueous Lithium Bromide," *HVAC&R Research,* vol. 12, no. 2, pp. 313-336, 2006/04/01 2006, doi: 10.1080/10789669.2006.10391181.

[96] H. B. Hemingson, C. J. Simonson, and R. W. Besant, "Steady-state performance of a run-around membrane energy exchanger (RAMEE) for a range of outdoor air conditions," *International Journal of Heat and Mass Transfer,* vol. 54, no. 9, pp. 1814-1824, 2011/04/01/ 2011, doi: https://doi.org/10.1016/j.ijheatmasstransfer.2010.12.036.

[97] H. Bai, J. Zhu, X. Chen, J. Chu, Y. Cui, and Y. Yan, "Steady-state performance evaluation and energy assessment of a complete membrane-based liquid desiccant dehumidification system," *Applied Energy,* vol. 258, p. 114082, 2020/01/15/ 2020, doi: https://doi.org/10.1016/j.apenergy.2019.114082.

[98] H. Patel, G. Ge, M. R. H. Abdel-Salam, A. H. Abdel-Salam, R. W. Besant, and C. J. Simonson, "Contaminant transfer in run-around membrane energy exchangers," *Energy and Buildings,* vol. 70, pp. 94-105, 2014/02/01/ 2014, doi: https://doi.org/10.1016/j.enbuild.2013.11.013.

[99] T. Zhang, X. Liu, and Y. Jiang, "Performance optimization of heat pump driven liquid desiccant dehumidification systems," *Energy and Buildings,* vol. 52, pp. 132-144, 2012/09/01/ 2012, doi: https://doi.org/10.1016/j.enbuild.2012.06.002.

[100] J. Liu, X. Liu, and T. Zhang, "Performance of heat pump driven internally cooled liquid desiccant dehumidification system," *Energy Conversion*

and Management, vol. 205, p. 112447, 2020/02/01/ 2020, doi: https://doi.org/10.1016/j.enconman.2019.112447.

[101] Q. Zhang, X. Liu, T. Zhang, and Y. Xie, "Performance optimization of a heat pump driven liquid desiccant dehumidification system using exergy analysis," *Energy,* vol. 204, p. 117891, 2020/08/01/ 2020, doi: https://doi.org/10.1016/j.energy.2020.117891.

[102] L. C. S. Mesquita, S. J. Harrison, and D. Thomey, "Modeling of heat and mass transfer in parallel plate liquid-desiccant dehumidifiers," *Solar Energy,* vol. 80, no. 11, pp. 1475-1482, 2006/11/01/ 2006, doi: https://doi.org/10.1016/j.solener.2006.03.003.

[103] S. Jain, P. L. Dhar, and S. C. Kaushik, "Experimental studies on the dehumidifier and regenerator of a liquid desiccant cooling system," *Applied Thermal Engineering,* vol. 20, no. 3, pp. 253-267, 2000/02/01/ 2000, doi: https://doi.org/10.1016/S1359-4311(99)00030-7.

[104] T. Wen and L. Lu, "Numerical and experimental study on internally cooled liquid desiccant dehumidification concerning film shrinkage shape and vapor condensation," *International Journal of Thermal Sciences,* vol. 136, pp. 316-327, 2019/02/01/ 2019, doi: https://doi.org/10.1016/j.ijthermalsci.2018.10.046.

[105] A. Y. Khan and H. D. Ball, "Development of a generalized model for performance evaluation of packed-type liquid sorbent dehumidifiers and regenerators," in *ASHRAE Transactions*, 1992, vol. 98, pt 1 ed., pp. 525-533. [Online]. Available: https://www.scopus.com/inward/record.uri?eid=2-s2.0-0026961341&partnerID=40&md5=4d8845004579d99772330452d5781ba6. [Online]. Available: https://www.scopus.com/inward/record.uri?eid=2-s2.0-0026961341&partnerID=40&md5=4d8845004579d99772330452d5781ba6

[106] X. H. Liu, K. Y. Qu, and Y. Jiang, "Empirical correlations to predict the performance of the dehumidifier using liquid desiccant in heat and mass transfer," *Renewable Energy,* vol. 31, no. 10, pp. 1627-1639, 2006/08/01/ 2006, doi: https://doi.org/10.1016/j.renene.2005.08.029.

[107] P. Gandhidasan, "A simplified model for air dehumidification with liquid desiccant," *Solar Energy,* vol. 76, no. 4, pp. 409-416, 2004/04/01/ 2004, doi: https://doi.org/10.1016/j.solener.2003.10.001.

[108] X. Y. Chen, Z. Li, Y. Jiang, and K. Y. Qu, "Analytical solution of adiabatic heat and mass transfer process in packed-type liquid desiccant equipment and its application," *Solar Energy,* vol. 80, no. 11, pp. 1509-1516, 2006/11/01/ 2006, doi: https://doi.org/10.1016/j.solener.2005.12.002.

[109] R. Chengqin, J. Yi, and Z. Yianpin, "Simplified analysis of coupled heat and mass transfer processes in packed bed liquid desiccant-air contact system," *Solar Energy,* vol. 80, no. 1, pp. 121-131, 2006/01/01/ 2006, doi: https://doi.org/10.1016/j.solener.2005.01.007.

[110] D. Babakhani and M. Soleymani, "Simplified analysis of heat and mass transfer model in liquid desiccant regeneration process," *Journal of the Taiwan Institute of Chemical Engineers,* vol. 41, no. 3, pp. 259-267, 2010.

[111] D. Babakhani, "Developing an Application Analytical Solution of Adiabatic Heat and Mass Transfer Processes in a Liquid Desiccant Dehumidifier/Regenerator," *Chemical Engineering & Technology,* vol. 32, no. 12, pp. 1875-1884, 2009, doi: https://doi.org/10.1002/ceat.200900290.
[112] X. Wang, W. Cai, J. Lu, Y. Sun, and X. Ding, "A hybrid dehumidifier model for real-time performance monitoring, control and optimization in liquid desiccant dehumidification system," *Applied Energy,* vol. 111, pp. 449-455, 2013/11/01/ 2013, doi: https://doi.org/10.1016/j.apenergy.2013.05.026.
[113] J.-Y. Park and J.-W. Jeong, "A Simplified Model for Predicting Dehumidification Effectiveness of a Liquid Desiccant System," in *AEI 2013*, pp. 516-523.
[114] D. I. Stevens, J. E. Braun, and S. A. Klein, "An effectiveness model of liquid-desiccant system heat/mass exchangers," *Solar Energy,* vol. 42, no. 6, pp. 449-455, 1989/01/01/ 1989, doi: https://doi.org/10.1016/0038-092X(89)90045-5.
[115] J. Braun, "Methodologies for the design and control of chilled water systems," *Ph. D. Thesis, University of Wisconsin-Madison,* 1988.
[116] M. Sadasivam and A. R. Balakrishnan, "Effectiveness-NTU method for design of packed bed liquid desiccant dehumidifiers," *Chemical Engineering Research and Design,* Article vol. 70, no. A6, pp. 572-577, 1992. [Online]. Available: https://www.scopus.com/inward/record.uri?eid=2-s2.0-0026947324&partnerID=40&md5=f9ede05e2d50f5fa7e201c64fc56a001.
[117] H. Jaber and R. L. Webb, "Design of Cooling Towers by the Effectiveness-NTU Method," *Journal of Heat Transfer,* vol. 111, no. 4, pp. 837-843, 1989, doi: 10.1115/1.3250794.
[118] R. K. Shah and D. P. Sekulic, *Fundamentals of Heat Exchanger Design*. Wiley, 2003.
[119] M. Nasif, G. Morrison, and M. Behnia, "Heat and Mass Transfer in Air to Air Enthalpy Heat Exchangers," 01/01 2005.
[120] L. Z. Zhang and J. L. Niu, "Effectiveness Correlations for Heat and Moisture Transfer Processes in an Enthalpy Exchanger With Membrane Cores," *Journal of Heat Transfer,* vol. 124, no. 5, pp. 922-929, 2002, doi: 10.1115/1.1469524.
[121] L.-Z. Zhang, "An analytical solution for heat mass transfer in a hollow fiber membrane based air-to-air heat mass exchanger," *Journal of Membrane Science,* vol. 360, no. 1, pp. 217-225, 2010/09/15/ 2010, doi: https://doi.org/10.1016/j.memsci.2010.05.015.
[122] G. Ge, D. Ghadiri Moghaddam, R. Namvar, C. J. Simonson, and R. W. Besant, "Analytical model based performance evaluation, sizing and coupling flow optimization of liquid desiccant run-around membrane energy exchanger systems," *Energy and Buildings,* vol. 62, pp. 248-257, 2013/07/01/ 2013, doi: https://doi.org/10.1016/j.enbuild.2013.03.017.
[123] H. M. Factor and G. Grossman, "A packed bed dehumidifier/regenerator for solar air conditioning with liquid desiccants," *Solar Energy,* vol. 24,

no. 6, pp. 541-550, 1980/01/01/ 1980, doi: https://doi.org/10.1016/0038-092X(80)90353-9.

[124] Y. Luo, H. Yang, L. Lu, and R. Qi, "A review of the mathematical models for predicting the heat and mass transfer process in the liquid desiccant dehumidifier," *Renewable and Sustainable Energy Reviews,* vol. 31, pp. 587-599, 2014/03/01/ 2014, doi: https://doi.org/10.1016/j.rser.2013.12.009.

[125] P. Gandhidasan, M. R. Ullah, and C. F. Kettleborough, "Analysis of Heat and Mass Transfer Between a Desiccant-Air System in a Packed Tower," *Journal of Solar Energy Engineering,* vol. 109, no. 2, pp. 89-93, 1987, doi: 10.1115/1.3268198.

[126] V. O¨berg and D. Y. Goswami, "Experimental Study of the Heat and Mass Transfer in a Packed Bed Liquid Desiccant Air Dehumidifier," *Journal of Solar Energy Engineering,* vol. 120, no. 4, pp. 289-297, 1998, doi: 10.1115/1.2888133.

[127] X. H. Liu, Y. Jiang, and K. Y. Qu, "Heat and mass transfer model of cross flow liquid desiccant air dehumidifier/regenerator," *Energy Conversion and Management,* vol. 48, no. 2, pp. 546-554, 2007/02/01/ 2007, doi: https://doi.org/10.1016/j.enconman.2006.06.002.

[128] A. Y. Khan and J. L. Martinez, "Modelling and parametric analysis of heat and mass transfer performance of a hybrid liquid desiccant absorber," *Energy Conversion and Management,* vol. 39, no. 10, pp. 1095-1112, 1998/07/01/ 1998, doi: https://doi.org/10.1016/S0196-8904(97)00032-0.

[129] C. Q. Ren, M. Tu, and H. H. Wang, "An analytical model for heat and mass transfer processes in internally cooled or heated liquid desiccant–air contact units," *International Journal of Heat and Mass Transfer,* vol. 50, no. 17, pp. 3545-3555, 2007/08/01/ 2007, doi: https://doi.org/10.1016/j.ijheatmasstransfer.2006.12.034.

[130] X. H. Liu, X. M. Chang, J. J. Xia, and Y. Jiang, "Performance analysis on the internally cooled dehumidifier using liquid desiccant," *Building and Environment,* vol. 44, no. 2, pp. 299-308, 2009/02/01/ 2009, doi: https://doi.org/10.1016/j.buildenv.2008.03.009.

[131] D. Ghadiri Moghaddam, A. Oghabi, G. Ge, R. W. Besant, and C. J. Simonson, "Numerical model of a small-scale liquid-to-air membrane energy exchanger: Parametric study of membrane resistance and air side convective heat transfer coefficient," *Applied Thermal Engineering,* vol. 61, no. 2, pp. 245-258, 2013/11/03/ 2013, doi: https://doi.org/10.1016/j.applthermaleng.2013.07.017.

[132] A. Vali, G. Ge, R. W. Besant, and C. J. Simonson, "Numerical modeling of fluid flow and coupled heat and mass transfer in a counter-cross-flow parallel-plate liquid-to-air membrane energy exchanger," *International Journal of Heat and Mass Transfer,* vol. 89, pp. 1258-1276, 2015/10/01/ 2015, doi: https://doi.org/10.1016/j.ijheatmasstransfer.2015.06.043.

[133] F. P. Incropera, D. P. DeWitt, T. L. Bergman, and A. S. Lavine, *Fundamentals of heat and mass transfer*. Wiley New York, 1996.

[134] K. Qu, G. Barreto, M. Iten, Y. Wang, and S. Riffat, "Energy and thermal performance of optimised hollow fibre liquid desiccant cooling and dehumidification systems in mediterranean regions: Modelling,

validation and case study," *Energy,* vol. 263, p. 125852, 2023/01/15/ 2023, doi: https://doi.org/10.1016/j.energy.2022.125852.
[135] S.-M. Huang, L.-Z. Zhang, and M. Yang, "Conjugate heat and mass transfer in membrane parallel-plates ducts for liquid desiccant air dehumidification: Effects of the developing entrances," *Journal of Membrane Science,* vol. 437, pp. 82-89, 2013/06/15/ 2013, doi: https://doi.org/10.1016/j.memsci.2013.02.048.
[136] D. P. D. Frank P. Incropera, Teodore L. Bergman, Adrienne S. Lavine, *Fundamentals of Heat and Mass Transfer*, Sixth ed. 2007.
[137] D. P. D. Frank P. Incropera, Teodore L. Bergman, Adrienne S. Lavine, *Principles of heat and mass transfer*. Hoboken, NJ:Wiley, 2013.
[138] R. American Society of Heating, A.-C. Engineers, and Ashrae, *2013 ASHRAE Handbook: Fundamentals*. ASHRAE, 2013.
[139] C.-C. Chen, H. I. Britt, J. F. Boston, and L. B. Evans, "Local composition model for excess Gibbs energy of electrolyte systems. Part I: Single solvent, single completely dissociated electrolyte systems," *AIChE Journal,* vol. 28, no. 4, pp. 588-596, 1982, doi: https://doi.org/10.1002/aic.690280410.
[140] J. A. Dean and N. A. Lange, *Lange's Handbook of Chemistry* (no. v. 15). McGraw-Hill, 1999.
[141] B. Mock, L. B. Evans, and C.-C. Chen, "Thermodynamic representation of phase equilibria of mixed-solvent electrolyte systems," *AIChE Journal,* vol. 32, no. 10, pp. 1655-1664, 1986, doi: https://doi.org/10.1002/aic.690321009.
[142] M. R. Conde, "Properties of aqueous solutions of lithium and calcium chlorides: formulations for use in air conditioning equipment design," *International Journal of Thermal Sciences,* vol. 43, no. 4, pp. 367-382, 2004/04/01/ 2004, doi: https://doi.org/10.1016/j.ijthermalsci.2003.09.003.
[143] M. Lapuerta, J. P. Hernández, and J. R. Agudelo, "An equation for the estimation of alcohol-air diffusion coefficients for modelling evaporation losses in fuel systems," *Applied Thermal Engineering,* vol. 73, no. 1, pp. 539-548, 2014/12/05/ 2014, doi: https://doi.org/10.1016/j.applthermaleng.2014.08.009.
[144] L. Mei and Y. J. Dai, "A technical review on use of liquid-desiccant dehumidification for air-conditioning application," *Renewable and Sustainable Energy Reviews,* vol. 12, no. 3, pp. 662-689, 2008/04/01/ 2008, doi: https://doi.org/10.1016/j.rser.2006.10.006.
[145] S. Liu, "A novel heat recovery/desiccant cooling system," Citeseer, 2008.
[146] S. Bell, "Measurement good practice guide no. 11. A beginner's guide to uncertainty of measurement," *Institute of Measurement & Control,* 1999.
[147] A. Y. Khan, "Cooling and dehumidification performance analysis of internally-cooled liquid desiccant absorbers," *Applied Thermal Engineering,* vol. 18, no. 5, pp. 265-281, 1998/01/30/ 1998, doi: https://doi.org/10.1016/S1359-4311(97)00074-4.
[148] C. Agudelo-Vera *et al.*, "Drinking Water Temperature around the Globe: Understanding, Policies, Challenges and Opportunities," *Water,* vol. 12, no. 4, p. 1049, 2020. [Online]. Available: https://www.mdpi.com/2073-4441/12/4/1049.

[149] H. Fan, C. J. Simonson, R. W. Besant, and W. Shang, "Performance of a run-around system for HVAC heat and moisture transfer applications using cross-flow plate exchangers coupled with aqueous lithium bromide," *HVAC and R Research,* Article vol. 12, no. 2, pp. 313-336, 2006, doi: 10.1080/10789669.2006.10391181.
[150] H. Fan, "Modeling a run-around heat and moisture recovery system," MSc, Department of Mechanical Engineering, College of Engineering, , University of Saskatchewan, Saskatoon, Saskatchewan, Canada, 2005.
[151] H. Bai, J. Zhu, Z. Chen, L. Ma, R. Wang, and T. Li, "Performance testing of a cross-flow membrane-based liquid desiccant dehumidification system," *Applied Thermal Engineering,* vol. 119, pp. 119-131, 2017/06/05/ 2017, doi: https://doi.org/10.1016/j.applthermaleng.2017.03.058.
[152] Z. Chen, J. Zhu, and H. Bai, "Performance assessment of a membrane liquid desiccant dehumidification cooling system based on experimental investigations," *Energy and Buildings,* Article vol. 139, pp. 665-679, 2017, doi: 10.1016/j.enbuild.2017.01.046.
[153] H. Lim, S.-J. Lee, Y. Su, and J.-W. Jeong, "Experimental study and prediction model of a liquid desiccant unit for humidification during the heating season," *Journal of Building Engineering,* vol. 45, p. 103549, 2022/01/01/ 2022, doi: https://doi.org/10.1016/j.jobe.2021.103549.
[154] D. G. Moghaddam, R. W. Besant, and C. J. Simonson, "Solution-side effectiveness for a liquid-to-air membrane energy exchanger used as a dehumidifier/regenerator," *Applied energy,* vol. 113, pp. 872-882, 2014.
[155] J. Burch, J. Woods, E. Kozubal, and A. Boranian, "Zero Energy Communities with Central Solar Plants using Liquid Desiccants and Local Storage," *Energy Procedia,* vol. 30, pp. 55-64, 2012/01/01/ 2012, doi: https://doi.org/10.1016/j.egypro.2012.11.008.
[156] R. American Society of Heating and A.-C. Engineers, *2017 ASHRAE Handbook: Fundamentals*. American Society of Heating, Refrigerating and Air-Conditioning Engineers, 2017.

Appendices

Appendix A: Normalization procedures for governing equations

For dehumidifier:

The governing equation of heat transfer for the process air is :

$$\left(\frac{\dot{m}_{air}}{H}\cdot\frac{\partial T_{air}}{\partial x}\cdot c_{p,air}\right)dxdy = -U(T_{air}-T_{sol})dxdy$$

Then the governing equation can be derived as:

$$\frac{1}{LH}\left(mc_p\right)_{air}\frac{\partial {T_{air}}^*}{\partial x^*} = -U({T_{air}}^* - {T_{sol}}^*)$$

Times $\frac{LH}{\left(mc_p\right)_{air}}$ for both sides,

$$\frac{\partial {T_{air}}^*}{\partial x^*} = -NTU({T_{air}}^* - {T_{sol}}^*)$$

The governing equation of mass transfer for the process air is:

$$\left(\frac{\dot{m}_{air}}{H}\frac{\partial W_{air}}{\partial x}\right)dxdy = -U_m\left(W_{air}-W_{sol,mem}\right)dxdy$$

Then the governing equation can be derived as:

$$\frac{\dot{m}_{air}}{LH}\frac{\partial {W_{air}}^*}{\partial x^*} = -U_m\cdot({W_{air}}^* - {W_{sol,mem}}^*)$$

Times $\frac{LH}{m_{air}}$ for both sides,

$$\frac{\partial {W_{air}}^*}{\partial x^*} = -NTU_m({W_{air}}^* - {W_{sol,mem}}^*)$$

The heat transfer governing equation of desiccant solution is:

$$C_{p,sol}\frac{m_{sol}}{L}\frac{\partial T_{sol}}{\partial y}dxdy = r\cdot U_m\left(W_{air}-W_{sol,mem}\right)dxdy + U(T_{air}-T_{sol})dxdy - U_{ca}(T_{sol}-T_{ca})dxdy - r_{eth}\cdot U_{m,eth}\left(W_{eth,sol}-W_{eth}\right)dxdy$$

Then the governing equation can be derived as:

$$C_{p,sol}\frac{m_{sol}}{LH}\frac{\partial T_{sol}}{\partial y^*} = r\cdot U_m\left({W_{air}}^*-{W_{sol,mem}}^*\right)\left(W_{sol,in}-W_{air,in}\right) + U({T_{air}}^*-{T_{sol}}^*)\left(T_{sol,in}-T_{air,in}\right) - U_{ca}({T_{sol}}^*-{T_{ca}}^*)\left(T_{sol,in}-T_{air,in}\right) - r_{eth}\cdot U_{m,eth}\left(W_{eth,sol}-W_{eth}\right)\left(W_{sol,in}-W_{air,in}\right)$$

Times $\frac{LH}{(mc_p)_{sol}(T_{sol,in}-T_{air,in})}$ for both sides,

Since:

$$Cr^* = \frac{(\dot{m}\,c_p)_{sol}}{\dot{m}_{air}c_{p,air}}$$

$${Cr_{ca}}^* = \frac{(\dot{m}\,c_p)_{sol}}{\dot{m}_{ca}c_{p,air}}$$

$$h^* = \frac{\omega_{\mathrm{sol,in}}-\omega_{\mathrm{air,in}}}{\mathrm{T_{sol,in}}-\mathrm{T_{air,in}}}\times\frac{r}{c_{p,air}}$$

$${h_e}^* = \frac{\omega_{\mathrm{sol,in}}-\omega_{\mathrm{air,in}}}{\mathrm{T_{sol,in}}-\mathrm{T_{air,in}}}\times\frac{r_{eth}}{c_{p,air}}$$

The governing equation can be normalized as:

$$\frac{\partial {T_{sol}}^*}{\partial y^*} = NTU_m h^* Cr^*\left({W_{air}}^*-{W_{sol,mem}}^*\right) + NTUCr^*({T_{air}}^*-{T_{sol}}^*) - NTU_{m,ca}{h_e}^*{Cr_{ca}}^*\left({W_{eth,sol}}^*-{W_{eth}}^*\right) - NTU_{ca}{Cr_{ca}}^*({T_{sol}}^*-{T_{ca}}^*)$$

The governing equation of mass transfer of water for solution is:

$$(\frac{m_{sol}}{L}\frac{\partial X_{sol}}{\partial y})dxdy = U_m(W_{air} - W_{sol,mem})dxdy$$

Then the governing equation can be derived as:

$$\frac{m_{sol}}{LH}\frac{\partial X_{sol}}{\partial y^*} = U_m({W_{air}}^* - {W_{sol,mem}}^*)\left(W_{sol,in} - W_{air,in}\right)$$

Times $\frac{LH}{m_{sol}}$ for both sides,

$$\frac{\partial X_{sol}}{\partial y^*} = NTU_m W_D \frac{1}{m^*}\left({W_{air}}^* - {W_{sol,mem}}^*\right)$$

The governing equation of mass transfer of ethanol for solution is:

$$\frac{m_{sol}}{L}\frac{\partial C_{eth}}{\partial x}dxdy = -U_{m,eth}\left(W_{eth,sol} - W_{eth}\right)dxdy$$

Then the governing equation can be derived as:

$$\frac{m_{sol}}{LH}\frac{\partial C_{eth}}{\partial x^*} = -U_{m,eth}\left({W_{eth,sol}}^* - {W_{eth}}^*\right)\left(W_{sol,in} - W_{air,in}\right)$$

Times $\frac{LH}{m_{sol}}$ for both sides,

$$\frac{\partial C_{eth}}{\partial y^*} = NTU_{m,ca} W_D \frac{1}{{m_{ca}}^*}\left({W_{eth,sol}}^* - {W_{eth}}^*\right)$$

The governing equation of heat transfer for circulated air is:

$$\frac{m_{ca}}{L}\frac{\partial T_{ca}}{\partial y}dxdy = -U_{ca}(T_{sol} - T_{ca})dxdy$$

Then the governing equation can be derived as:

$$\frac{m_{ca}}{LH}\frac{\partial T_{ca}}{\partial y^*} = -U_{ca}({T_{sol}}^* - {T_{ca}}^*)\left(T_{sol,in} - T_{air,in}\right)$$

Times $\frac{LH}{m_{sol}(T_{sol,in} - T_{air,in})}$ for both sides,

$$\frac{\partial {T_{ca}}^*}{\partial y^*} = -NTU_{ca}({T_{sol}}^* - {T_{ca}}^*)$$

The governing equation of mass transfer of ethanol for circulated air is:

$$\frac{m_{ca}}{L}\frac{\partial W_{eth}}{\partial y}dxdy = -U_{m,eth}\left(W_{eth,sol} - W_{eth}\right)dxdy$$

Then the governing equation can be derived as:

$$\frac{m_{ca}}{LH}\frac{\partial W_{eth}}{\partial y^*} = -U_{m,eth}\left({W_{eth,sol}}^* - {W_{eth}}^*\right)\left(W_{sol,in} - W_{air,in}\right)$$

Times $\frac{LH}{m_{sol}\left(W_{sol,in} - W_{air,in}\right)}$ for both sides,

$$\frac{\partial {W_{eth}}^*}{\partial y^*} = -NTU_{m,ca}\left({W_{eth,sol}}^* - {W_{eth}}^*\right)$$

For regenerator:

The governing equation of mass transfer for the air is:

$$\left(\frac{\dot{m}_{air}}{H} \cdot \frac{\partial W_{air}}{\partial x}\right)dxdy + U_m \cdot \left(W_{air} - W_{sol,mem}\right)dxdy = 0$$

Then the governing equation can be derived as:

$$\frac{\dot{m}_{air}}{LH} \cdot \frac{\partial {W_{air}}^*}{\partial x^*} = -U_m \cdot ({W_{air}}^* - {W_{sol,mem}}^*)$$

Times $\frac{LH}{m_{air}}$ for both sides,

$$\frac{\partial {W_{air}}^*}{\partial x^*} = -NTU_m({W_{air}}^* - {W_{sol,mem}}^*)$$

The governing equation of mass transfer for the solution is:

$$\frac{m_{sol}}{L}\frac{dX_{sol}}{dy}dxdy = -U_m\left(W_{sol,mem} - W_{air}\right)dxdy$$

Then the governing equation can be derived as:

$$\frac{m_{sol}}{LH}\frac{dX_{sol}}{dy^*} = -U_m\left({W_{sol,mem}}^* - {W_{air}}^*\right)\left(W_{sol,in} - W_{air,in}\right)$$

Times $\frac{LH}{m_{sol}}$ for both sides,

$$\frac{\partial X_{sol}}{\partial y^*} = -NTU_m W_D \frac{1}{m^*}\left({W_{sol,mem}}^* - {W_{air}}^*\right)$$

The governing equation of heat transfer for the air is:

$$C_{p,air}\frac{m_{air}}{H}\frac{dT_{air}}{dx}dxdy = U(T_{sol} - T_{air})dxdy$$

Then the governing equation can be derived as:

$$C_{p,air}\frac{m_{air}}{LH}\frac{d{T_{air}}^*}{dx^*} = U({T_{sol}}^* - {T_{air}}^*)$$

Times $\frac{LH}{m_{air}}$ for both sides,

$$\frac{\partial {T_{air}}^*}{\partial x^*} = -NTU({T_{sol}}^* - {T_{air}}^*)$$

The governing equation of heat transfer for the solution is:

$$C_{p,sol}\frac{m_{sol}}{L}\frac{dT_{sol}}{dy}dxdy = -[r \cdot U_m\left(W_{sol,mem} - W_{air}\right)dxdy + U(T_{sol} - T_{air})]dxdy$$

Then the governing equation can be derived as:

$$C_{p,sol}\frac{m_{sol}}{LH}\frac{\partial T_{sol}}{\partial y^*} = -[r \cdot U_m\left({W_{air}}^* - {W_{sol,mem}}^*\right)\left(W_{sol,in} - W_{air,in}\right) + U({T_{air}}^* - {T_{sol}}^*)\left(T_{sol,in} - T_{air,in}\right)]$$

Times $\frac{LH}{(mc_p)_{sol}(T_{sol,in} - T_{air,in})}$ for both sides,

$$\frac{\partial {T_{sol}}^*}{\partial y^*} = -\left[NTU_m h^* Cr^*\left({W_{sol,mem}}^* - {W_{air}}^*\right) + NTUCr^*({T_{sol}}^* - {T_{air}}^*)\right]$$

Appendix B: Matlab code for air humidity and solution equilibrium humidity

Air specific humidity:

```
function W_air_in=humidityratio_air(T_air_in,RH_air_in)

W_air_in=((6.112*exp((17.67*T_air_in)/(T_air_in+243.5))*RH_air_in*2.16
74)/(273.15+T_air_in))/(1.29*1000)
```

Solution equilibrium specific humidity:

```
function W_sol = calculate_W_sol(T_sol_in, C_sol_in, C_e_sol_in)
    % Constants
    tau_LiCl_e = -13.548; % LiCl electrolyte relaxation time
    tau_e_LiCl = 24.659; % other electrolyte relaxation time
    tau_LiCl_w = -5.902; % LiCl solvent relaxation time
    tau_e_w = 0.4472; % other electrolyte solvent relaxation time
    tau_w_LiCl = 13.592; % solvent-LiCl relaxation time
    tau_w_e = 1.4623; % solvent-other electrolyte relaxation time
    P_atm = 101325; % atmospheric pressure

    m_w = 1 - C_sol_in - C_e_sol_in;

    x_LiCl = (C_sol_in ./ 42.39) ./ ((C_sol_in ./ 42.39) +
(C_e_sol_in ./ 46) + (m_w ./ 18)); % mol fraction of LiCl

    x_Li = (C_sol_in ./ 42.39) ./ (2 * (C_sol_in ./ 42.39) +
(C_e_sol_in ./ 46) + (m_w ./ 18));
    x_e = (C_e_sol_in ./ 46) ./ (2 * (C_sol_in ./ 42.39) +
(C_e_sol_in ./ 46) + (m_w ./ 18)); % mol fraction of ethanol
    x_w = 1 - x_e - x_Li .* 2; % mol fraction of water

    A = exp(-0.053 * tau_LiCl_e);
    A_prime = exp(-0.053 * tau_e_LiCl);
    B = exp(-0.2 * tau_LiCl_w);
    B_prime = exp(-0.2 * tau_w_LiCl);
    C = exp(-0.3 * tau_e_w);
    C_prime = exp(-0.3 * tau_w_e);

    first_term = (2 * B * x_Li .* tau_LiCl_w + C * x_e .* tau_e_w) ./
(x_Li .* (2 * B - 2) + x_e .* (C - 1) + 1);
    second_term = (2 * B_prime * x_Li .* (x_Li .* tau_w_LiCl + A_prime
* x_e .* (tau_w_LiCl - tau_e_LiCl))) ./ (x_Li .* (1 - 2 * B_prime) +
x_e .* (A_prime - B_prime) + B_prime).^2;
    third_term = ((x_Li .* 2 + x_e - 1) .* (2 * B * x_Li .* tau_LiCl_w
+ C * x_e .* tau_e_w)) ./ (x_Li .* (2 * B - 2) + x_e .* (C - 1) +
1).^2;
    fourth_term = (C_prime * x_e .* (2 * A * x_Li .* (tau_w_e -
tau_LiCl_e) + x_e .* tau_w_e)) ./ (x_Li .* (2 * A - 2 * C_prime) +
x_e .* (1 - C_prime) + C_prime).^2;
```

```
    f_w = exp(first_term + second_term + third_term + fourth_term);
    a_w = x_w.*f_w;

    % Intermediate variables
    P_w = 133.322 * 10 .^ (8.07131 - (1730.63 ./ (233.426 +
T_sol_in)));
    P_sol = a_w.*P_w;
    W_sol = P_sol./(P_atm - P_sol);
end
function W_e_sol = calculate_W_e_sol(T_sol_in, C_sol_in, C_e_sol_in)
    % Constants
    tau_LiCl_e = -13.548; % LiCl electrolyte relaxation time
    tau_e_LiCl = 24.659; % other electrolyte relaxation time
    tau_LiCl_w = -5.902; % LiCl solvent relaxation time
    tau_e_w = 0.4472; % other electrolyte solvent relaxation time
    tau_w_LiCl = 13.592; % solvent-LiCl relaxation time
    tau_w_e = 1.4623; % solvent-other electrolyte relaxation time
    P_atm = 101325; % atmospheric pressure

    m_w = 1 - C_sol_in - C_e_sol_in;

    x_LiCl = (C_sol_in ./ 42.39) ./ ((C_sol_in ./ 42.39) +
(C_e_sol_in ./ 46) + (m_w ./ 18)); % mol fraction of LiCl

    x_Li = (C_sol_in ./ 42.39) ./ (2 * (C_sol_in ./ 42.39) +
(C_e_sol_in ./ 46) + (m_w ./ 18));
    x_e = (C_e_sol_in ./ 46) ./ (2 * (C_sol_in ./ 42.39) +
(C_e_sol_in ./ 46) + (m_w ./ 18)); % mol fraction of ethanol
    x_w = 1 - x_e - x_Li .* 2; % mol fraction of water

    A = exp(-0.053 * tau_LiCl_e);
    A_prime = exp(-0.053 * tau_e_LiCl);
    B = exp(-0.2 * tau_LiCl_w);
    B_prime = exp(-0.2 * tau_w_LiCl);
    C = exp(-0.3 * tau_e_w);
    C_prime = exp(-0.3 * tau_w_e);

    first_term = (2 * B * x_Li .* tau_LiCl_w + C * x_e .* tau_e_w) ./
(x_Li .* (2 * B - 2) + x_e .* (C - 1) + 1);
    second_term = (2 * B_prime * x_Li .* (x_Li .* tau_w_LiCl + A_prime
* x_e .* (tau_w_LiCl - tau_e_LiCl))) ./ (x_Li .* (1 - 2 * B_prime) +
x_e .* (A_prime - B_prime) + B_prime).^2;
    third_term = ((x_Li .* 2 + x_e - 1) .* (2 * B * x_Li .* tau_LiCl_w
+ C * x_e .* tau_e_w)) ./ (x_Li .* (2 * B - 2) + x_e .* (C - 1) +
1).^2;
    fourth_term = (C_prime * x_e .* (2 * A * x_Li .* (tau_w_e -
tau_LiCl_e) + x_e .* tau_w_e)) ./ (x_Li .* (2 * A - 2 * C_prime) +
x_e .* (1 - C_prime) + C_prime).^2;

    f_w = exp(first_term + second_term + third_term + fourth_term);
    a_e = 10*x_e.*f_w;

    % Intermediate variables
    P_e = 133.322 * 10 .^ (8.04494 - (1554.3 ./ (222.65 + T_sol_in)));
    P_sol = a_e.*P_e;
    W_e_sol = P_sol./(P_atm - P_sol);
end
```

Appendix C: Matlab code for the self-cooled membrane-based liquid desiccant dehumidifier

```
clear

%inlet conditions
T_sol_in=20; % Solution inlet temperature (C)
T_air_in=28; % Air inlet temperature (C)
C_sol_in=0.37; % Solution inlet concentration of LiCl
C_e_sol_in=0.1; % Ethanol initial content in solution (kg/kg)
X_sol_in=(1-C_sol_in-C_e_sol_in)/C_sol_in; % Solution desiccant
concentration (kg/kg)
X_e_sol_in=C_e_sol_in/C_sol_in;
RH_air_in=70; % Air inlet humidity (kg/kg)
W_air_in=humidityratio_air(T_air_in,RH_air_in); % Air inlet humidity
ratio (kg/kg)


m_air=0.01; % Air mass flow rate (kg/s)
m_sol=0.03; % Solution mass flow rate (kg/s)
m_e=m_sol; % Ethanol mass flow rate (kg/s)
m_ca=0.025; % Circulated air mass flow rate (kg/s)
m=m_sol./m_air; % m is the mass flow rate of air over mass flow rate
% solution
m_star=1/m;
M_ca=m_ca./m_sol;
rou_air=1.29; % Air density (kg/m3)
rou_LiCl=1254; % Solution density (kg/m3)
rou_e=789; % Ethanol density (kg/m3)
rou_sol=(1-C_e_sol_in)*rou_LiCl+C_e_sol_in*rou_e;
T_ca_in=12; % Circulated air inlet temperature (C)

W_e_ca_in=0;
W_sol_in=calculate_W_sol(T_sol_in, C_sol_in, C_e_sol_in); % Solution
inlet humidity (kg/kg)
W_e_sol_in=calculate_W_e_sol(T_sol_in, C_sol_in, C_e_sol_in); %
Solution inlet ethanol (kg/kg)
W0=W_sol_in-W_air_in; % Humidity difference

% Geometry
number_of_channels=11; % Number of membrane channel
L=0.41; % Channel length(m)
W=0.23; % Channel width (m)
H=0.21; % Channel height (m)
d_air=7.7e-3; % Air channel thickness (m)
d_sol=4.3e-3; % Solution channel thickness (m)
D_air=4*H*d_air/(2*(H+d_air)); % Air channel hydrolic diameter (m)
D_sol=4*H*d_sol/(2*(H+d_sol)); % Solution channel hydrolic diameter
(m)
A=L*H*(number_of_channels*2-1); % Total contactor area (m2)

% Membrane properties
k_mem=0.3; % Membrane conductivity (W/mK)
d_mem=0.0005; % Membrane thickness (m)
```

```
k_mmem=3.87e-6;% Membrane mass conductivity (kg/ms)

% Heat transfer coefficient
k_sol=0.564; % Solution desiccant conductivity (W/mK)
Nu_sol=7.74; % Solution side Nu
k_ethanol=0.167; % Solution ethanol conductivity (W/mK)
h_sol=(Nu_sol*k_sol)/D_sol; % Solution side heat transfer coefficient
(W/m2K)
k_air=0.03; % Air conductivity (W/mK)
Nu_air=6.58; % Air side Nu
h_air=(Nu_air*k_air)/D_air; % Air side heat transfer coefficient
(W/m2K)

h_ethanol=(Nu_sol*k_ethanol)/D_sol; % Ethanol side heat transfer
coefficient (W/m2K)
h_cir_air=(Nu_air*k_air)/D_sol; % Circulated air side heat transfer
coefficient (W/m2K)

% Mass trasnfer coefficient
D_va=2.46e-5; % Air side diffusivity (m2/s)
D_e=1.264e-5;
D_ms=0.892e-2; % Solution side diffusivity (m2/s)
D_me=9.29e-6; % Solution side ethanol diffusivity (m2/s)
Sh=7.74; % Air side Sh
Sh_sol=7.74; % Solution side side Sh
Sh_e=2.517;
h_vm=((Sh*D_va/D_air))*rou_air; % Air side mass transfer coefficient
(kg/m2K)
h_m_sol=((Sh_sol*D_ms)/D_sol)*rou_sol; % Solution side mass transfer
coefficient
h_m_e=((Sh_sol*D_me)/D_sol)*rou_e; % Solution side ethanol mass
transfer coefficient (kg/m2K)
h_m_ca=((Sh_e*D_e/D_sol))*rou_air; % Circulated air side mass transfer
coefficient (kg/m2K)
% Heat capacity
cp_LiCl=3.2; % Solution heat capacity (kJ/kgK)
cp_air=1.02; % Air heat capacity (kJ/kgK)
cp_ca=cp_air; % Circulated air heat capacity (kJ/kgK)
cp_el=2.46; % Ethanol heat capacity in liquid (kJ/kgK)
cp_eg=1.6; % Ethanol heat capacity in gas (kJ/kgK
cp_sol=(1-C_e_sol_in)*cp_LiCl+C_e_sol_in*cp_el;
Y=(m_sol*cp_sol)/(m_air*cp_air); % Thermal capaicty ration between
solution and process air
Y_star=1/Y;
Y_el=(m_e*cp_el)/(m_air*cp_air); % Thermal capaicty ration between
ethanol(in liquid) and circulated air
Y_eg=(m_ca*cp_air)/(m_sol*cp_sol); % Thermal capaicty ration between
circulated air and ethanol(gas)
h_fg=2450; % Water evaporation latent heat (kJ/kg)
h_fge=846; % Ethanol condensation latent heat (kJ/kg)
% NTUm
U_m=((1/h_vm)+(d_mem/k_mmem))^-1; % Overall mass transfer coefficient
between process air side and solution side (kg/m2s)
U_me=(1/h_m_ca)^-1; % Overall mass transfer coefficient betweeen
solution ethanol side and circulated air side(kg/m2s)
NTU_m=((U_m*A)/m_air)*(1+2*C_e_sol_in/0.9532);
NTU_m_e=(U_me*A)/m_ca;
NTU_m_sol=(h_m_sol*A)/m_air;
```

```
% NTU
U=((1/h_air)+(d_mem/k_mem)+(1/h_sol))^-1; % Overall heat transfer
coefficient between process air side and solution side (W/m2K)
U_ca=(1/h_sol+1/h_cir_air)^-1; % Overall heat transfer coefficient
betweeen solution ethanol side and circulated air side(W/m2K)
NTU=(U*A)/(m_air*cp_air*1000);
NTU_ca=NTU_m_e;
NTU_sol=(h_sol*A)/(m_air*cp_air*1000);
% Matrixing
N=50; % Number of grid in y direction
M=100; % Number of grid in x direction
dx=1/(M-1); % Grid length in x direction
dy=1/(N-1); % Grid length in y direction
z=ones(N,M);
error1=10;error2=10;error3=10;error4=10;error5=10;error6=10;error7=10;
error8=10;error9=10;
% Assign initial value
T_air=T_air_in*z; % Air inlet temperature
T_sol=T_sol_in*z; % Solution inlet temperature
W_air=W_air_in*z; % Air inlet humidity ratio

X_sol=X_sol_in*z; % Solution inlet mass ratio
T_sol_mem=T_sol_in*z; %solution membrane temperature
W_sol_mem=W_sol_in*z; % Solution membrane humidity ratio
W_e_sol=W_e_sol_in*z; % Solution inlet ethanol content
T_ca=T_ca_in*z; % Circulated inlet air temperature
W_e_ca=W_e_ca_in*z; % Circulated inlet ethanol content
X_e_sol=X_e_sol_in*z;
C_e_sol=C_e_sol_in*z;

% Normalization

W_norm_air=(W_air-W_air_in)/W0;
W_norm_e_ca=(W_e_ca-W_air_in)/W0;
W_norm_e_sol=(W_e_sol-W_air_in)/W0;
T_norm_air=(T_air-T_air_in)/(T_sol_in-T_air_in);
T_norm_sol=(T_sol-T_air_in)/(T_sol_in-T_air_in);
T_norm_ca=(T_ca-T_air_in)/(T_sol_in-T_air_in);
T_norm_sol_mem=(T_sol_mem-T_air_in)/(T_sol_in-T_air_in);
W_norm_sol_mem=(W_sol_mem-W_air_in)/W0;
H_p=(W_sol_in-W_air_in)/(T_sol_in-T_air_in)*(h_fg/cp_air);
H_pe=(W_sol_in-W_air_in)/(T_sol_in-T_air_in)*(h_fge/cp_air);

% Start the loop
while (error1>1e-10)||(error2>1e-10)||(error3>1e-10)||(error4>1e-
10)||(error5>1e-10)||(error6>1e-10)||(error7>1e-10)

  % Solution side mass equation
  X_sol_f=X_sol;
  for a=1:N-1
   for b=1:M
       X_sol(1,b)=X_sol_in; % boundary condition

X_sol(a+1,b)=(X_sol(a,b)+dy*m_star*W0*NTU_m*(1+X_e_sol(a+1,b))*((W_nor
m_air(a+1,b))-W_norm_sol_mem(a+1,b))).*(1-
dy*m_star*W0*NTU_m*(W_norm_air(a+1,b)-W_norm_sol_mem(a+1,b)));
   end
  end
```

```
  error1=sum(sum(abs(X_sol-X_sol_f)./(X_sol)));
  C_sol=1./(1+X_sol+X_e_sol);
  % Solution side energy equation
  T_sol_f=T_sol;
  for c=1:N-1
   for d=1:M
      T_norm_sol(1,d)=1; % boundary condition

T_norm_sol(c+1,d)=(T_norm_sol(c,d)+(dy*NTU*Y_star*(T_norm_air(c+1,d)))
+(dy*NTU_m*Y_star*H_p*(W_norm_air(c+1,d)-W_norm_sol_mem(c+1,d)))-
(dy*NTU_m_e*Y_eg*H_pe*(W_norm_e_sol(c+1,d)-
W_norm_e_ca(c+1,d)))+dy*NTU_ca*Y_eg*T_norm_ca(c+1,d))./(1+dy*NTU*Y_sta
r+dy*NTU_ca*Y_eg);
   end
  end
  T_sol=T_norm_sol*(T_sol_in-T_air_in)+T_air_in;
  error2=sum(sum(abs(T_sol-T_sol_f)./(T_sol)));

  % Solution side ethanol mass equation
  X_e_sol_f=X_e_sol;
  for e=1:N-1
    for f=1:M
       X_e_sol(1,f)=X_e_sol_in; % boundary condition

X_e_sol(e+1,f)=(X_e_sol(e,f)-
dy*M_ca*W0*NTU_m_e*(1+X_sol(e+1,f))*((W_norm_e_sol(e+1,f))-
W_norm_e_ca(e+1,f)))./(1+dy*M_ca*W0*NTU_m_e*(W_norm_e_sol(e+1,f)-
W_norm_e_ca(e+1,f)));
    end
  end
  error3=sum(sum(abs(X_e_sol-X_e_sol_f)./(X_e_sol)));
  C_e_sol= X_e_sol./(1+X_sol+X_e_sol);


  % Air side mass equation
  W_air_f=W_air;
  for g=1:N
     for h=1:M-1
       W_norm_air(g,1)=0; % boundary condition

W_norm_air(g,h+1)=(W_norm_air(g,h)+dx*NTU_m*W_norm_sol_mem(g,h+1))./(1
+dx*NTU_m);
     end
  end
  W_air=W_norm_air*W0+W_air_in;
  error4=sum(sum(abs(W_air-W_air_f)./(W_air)));

  % Air side energy equation
  T_air_f=T_air;
  for i=1:N
      for j=1:M-1
 T_norm_air(i,1)=0; % boundary condition

T_norm_air(i,j+1)=(T_norm_air(i,j)+dx*NTU*T_norm_sol(i,j+1))./(1+dx*NT
U);
      end
  end
 T_air=T_norm_air*(T_sol_in-T_air_in)+T_air_in;
```

```
 error5=sum(sum(abs(T_air-T_air_f)./(T_air)));

    % Circulated air ethanol mass equation
    W_e_ca_f=W_e_ca;
    for k=2:N
        for l=1:M
            W_norm_e_ca(N,l)=(W_e_ca_in-W_air_in)/W0; %boundary
condition

 W_norm_e_ca(k-1,l)=(W_norm_e_ca(k,l)+dy*NTU_m_e*(W_norm_e_sol(k-
1,l)))./(1+dy*NTU_m_e);
        end
    end
    W_e_ca=(W_norm_e_ca*W0)+W_air_in;
    error6=sum(sum(abs(W_e_ca-W_e_ca_f)./(W_e_ca)));

    % Circulated air energy equation
    T_ca_f=T_ca;
    for m_=2:N
        for n=1:M
            T_norm_ca(N,n)=(T_ca_in-T_air_in)/(T_sol_in-
T_air_in); %boundary condition

            T_norm_ca(m_-
1,n)=(T_norm_ca(m_,n)+dy*NTU_ca*(T_norm_sol(m_-1,n)))./(1+dy*NTU_ca);
        end
    end
    T_ca=T_norm_ca*(T_sol_in-T_air_in)+T_air_in;
    error7=sum(sum(abs(T_ca-T_ca_f)./(T_ca)));

         error8=10;
    while(error8>1e-10)
        W_norm_e_sol_f=W_norm_e_sol;

        W_e_sol=calculate_W_e_sol(T_sol,C_sol,C_e_sol);
        W_norm_e_sol=(W_e_sol-W_air_in)/W0;
        error8=sum(sum(abs(W_norm_e_sol-
W_norm_e_sol_f)./(W_norm_e_sol)));
    end


 error9=10;
 while (error9>1e-10)
 W_norm_sol_mem_f=W_norm_sol_mem;
 C_sol_mem=C_sol-((NTU_m*W0*(W_norm_air-
W_norm_sol_mem))./(NTU_m_sol)); % solve membrane mass equation
 T_norm_sol_mem=(NTU*T_norm_air+NTU_m*H_p*(W_norm_air-
W_norm_sol_mem)+NTU_sol*T_norm_sol)./(NTU_sol+NTU);
 T_sol_mem=T_norm_sol_mem*(T_sol_in-T_air_in)+T_air_in;

 % obtain new membrane humidityratio
 W_sol_mem=calculate_W_sol(T_sol_mem, C_sol_mem,C_e_sol);
 W_norm_sol_mem=(W_sol_mem-W_air_in)/W0;

 error9=sum(sum(abs(W_norm_sol_mem-
W_norm_sol_mem_f)./(W_norm_sol_mem)));
 end
end
```

```
T_air_out=mean(T_air(:,M));
W_air_out=mean(W_air(:,M));
T_sol_out=mean(T_sol(N,:));
X_sol_out=mean(X_sol(N,:));
C_sol_out=mean(C_sol(N,:));

W_e_sol_out=mean(W_e_sol(:,M));
W_e_ca_out=mean(W_e_ca(1,:));
T_ca_out=mean(T_ca(1,:));
effec_sen_air=(T_air_in-T_air_out)/(T_air_in-T_sol_in);
effec_lat_air=(W_air_in-W_air_out)/(W_air_in-W_sol_in);
effec_tot_air=(effec_sen_air+H_p*effec_lat_air)/(1+H_p);

MRR=1000*m_air*(W_air_in-W_air_out);
```

Appendix D: Matlab code for the membrane-based liquid desiccant regenerator

```
clear

%inlet conditions
T_sol_in=50;   %solution inlet temperature (C) (input value)
C_sol_in=0.37; %solution inlet mass concentration (%) (input value)
C_e_sol_in=0.1; % Ethanol initial content in solution (kg/kg)
X_sol_in=(1-C_e_sol_in-C_sol_in)/C_sol_in;  %solution inlet mass ratio
between water and salt (%)
W_sol_in=calculate_W_sol(T_sol_in, C_sol_in, C_e_sol_in); % Solution
inlet humidity (kg/kg)

T_air_in=24;   %air inlet temperature (C) (input value)
RH_air_in=40;  %air inlet relative humidity (%)  (input value)
W_air_in=humidityratio_air(T_air_in,RH_air_in);  %air inlet humidity
ratio (kg/kg)


m_air=0.01;  %inlet air mass flow rate(kg/s)
m_sol=0.03;  %inlet solution mass flow rate
m_mass_flow_ratio=m_sol/m_air;   %solution mass flow rate over air
mass flow rate (input value)
m_star=1/m_mass_flow_ratio;            %air mass flow rate over
solution mass flow rate

rou_air=1.29;  %air density (kg/m3)01
rou_sol=1247;  %solution density (kg/m3)


%geometric peroperties
number_of_channels=11;  %number of channels
L=0.41;     %length of dehumidfiier unit (m)
H=0.21;     %height of dehumidifier unit (m)
d_air=7.7e-3;   %air channel thickness (m)
d_sol=4.3e-3;   %solution channel thickness (m)
L_air=(4*d_air*H)/(2*(d_air+H));  %air channel hydrolic diameter (m)
L_sol=(4*d_sol*H)/(2*(d_sol+H));  %solution channel hydrolic diameter
(m)
A=L*H*(number_of_channels*2-1);   %total heat and mass transfer area
(m2)


%heat transfer coefficients
Nu_air=6.58;  %air side Nusselt number
k_air=0.03;   %air side heat conductivity (W/mK)
h_air=(Nu_air*k_air)/L_air;  %air side convective heat transfer
coefficient (W/m2K)

Nu_sol=7.74;  %solution side Nusselt number
k_sol=0.53;   %solution side heat conductivity (W/mK)
h_sol=(Nu_sol*k_sol)/L_sol;  %solution side convective heat transfer
coefficient (W/m2K)
```

```
%mass transfer coefficient
Sh_air=6.7;     %air side Sherwood number
D_air=2.46e-5;  %air side diffusivity
h_m_air=((Sh_air*D_air)/L_air)*rou_air;   %air side convective mass
transfer coefficient (kg/m2K)

Sh_sol=6.7;     %solution side Sherwood number ??
D_sol=0.892e-2;  %solution side diffusivity ??
h_m_sol=((Sh_sol*D_sol)/L_sol)*rou_sol;   %solution side convective
mass transfer coefficnet (kg/m2K)


%membrane properties
delta_mem=0.0005;   %membrane thickness (m)
k_mem=0.3;           %membrane heat conductivity (W/mK)
k_m_mem=3.87e-6;     %membrane mass conductivity (kg/mK)

%other peroperties
cp_air=1.02;                %air specific heat capacity (kJ/kgK)
cp_sol=3.2;                 %solution specific capacity (kJ/kgK)
h_fg=2450;                  %condensation heat of water (J/kg)
Cr=m_star*(cp_air/cp_sol);   %thermal capacity ratio

%NTU and NTUm
U=(1/h_air+delta_mem/k_mem+1/h_sol)^-1; %overall heat transfer
coefficient (W/m2K)
U_m=(delta_mem/k_m_mem+1/h_m_air)^-1;   %overall mass transfer
coefficient (kg/m2s)
NTU=(U*A)/(m_air*1000*cp_air);    %NTU

NTU_m=(U_m*A)/m_air;                    %NTUm
NTU_sol=(h_sol*A)/(m_air*cp_air*1000);  %solution side NTU
NTU_m_sol=(h_m_sol*A)/m_air;            %solution side NTUm


m_salt=m_sol/(1+X_sol_in);              %salt mass flow rate (kg/s)

%matrixing and assign initial values
n=30;   %number of grids in y direction
m=60;  %number of grids in x direction
dx=1/(m-1); %grid length in x direction
dy=1/(n-1); %grid length in y direction

z=ones(n,m);
error1=10;error2=10;error3=10;error4=10;error5=10;

T_air=T_air_in*z;     %assign initial values for air inlet temperature
T_sol=T_sol_in*z;     %assign initial values for solution inlet
temperature
W_air=W_air_in*z;     %assign initial values for air inlet humidity
ratio
X_sol=X_sol_in*z;     %assign initial values for solution inlet mass
ratio
W_sol_mem=W_sol_in*z; %assign initial values for solution membrane
humidity ratio
```

```
W0=W_sol_in-W_air_in;                                        %define the
dimentionless parameter W0
T_non_air=(T_air-T_air_in)/(T_sol_in-
T_air_in);            %normalization of air temperature
T_non_sol=(T_sol-T_air_in)/(T_sol_in-
T_air_in);            %normalization of solution temperature
W_non_air=(W_air-
W_air_in)/W0;                              %normalization of air
humidity ratio
W_non_sol_mem=(W_sol_mem-
W_air_in)/W0;                      %normalization of solution membrane
humidity ratio
h=((W_sol_in-W_air_in)/(T_sol_in-
T_air_in))*(h_fg/cp_air); %normalization of h*


%start the loop
while (error1>1e-10)||(error2>1e-10)||(error3>1e-10)||(error4>1e-10)


%the solution side mass equation
 X_sol_f=X_sol;
 for a=1:n-1
    for b=1:m
        X_sol(1,b)=X_sol_in;  %boundary condition

X_sol(a+1,b)=(X_sol(a,b)+dy*m_star*W0*NTU_m*((W_non_air(a+1,b))-
W_non_sol_mem(a+1,b))./(1-dy*m_star*W0*NTU_m*(W_non_air(a+1,b)-
W_non_sol_mem(a+1,b)));
    end
 end
 error1=sum(sum(abs(X_sol-X_sol_f)./(X_sol)));
 C_sol=(1-C_e_sol_in)./(1+X_sol);


 %the solution side energy equation
 T_sol_f=T_sol;
 for c=1:n-1
     for d=1:m
         T_non_sol(1,d)=1;   %boudary condition

T_non_sol(c+1,d)=(T_non_sol(c,d)+dy*NTU_m*h*Cr*(W_non_air(c+1,d)-
W_non_sol_mem(c+1,d))+dy*Cr*NTU*T_non_air(c+1,d))/(1+dy*NTU*Cr);
     end
 end
 T_sol=T_non_sol*(T_sol_in-T_air_in)+T_air_in;
 error2=sum(sum(abs(T_sol-T_sol_f)./(T_sol)));


 %the air side mass equation
 W_air_f=W_air;
 for e_=1:n
     for f=1:m-1
         W_non_air(e_,1)=0;   %boundary condition

W_non_air(e_,f+1)=(W_non_air(e_,f)+dx*NTU_m*W_non_sol_mem(e_,f+1))./(1
+dx*NTU_m);
     end
```

```
 end
 W_air=W_non_air*W0+W_air_in;
 error3=sum(sum(abs(W_air-W_air_f)./(W_air)));


 %the air side energy equation
 T_air_f=T_air;
 for g=1:n
     for h_=1:m-1
         T_non_air(g,1)=0;    %boundary condition

T_non_air(g,h_+1)=(T_non_air(g,h_)+dx*NTU*T_non_sol(g,h_+1))./(1+dx*NT
U);
     end
 end
 T_air=T_non_air*(T_sol_in-T_air_in)+T_air_in;
 error4=sum(sum(abs(T_air-T_air_f)./(T_air)));

 error5=10;


         while (error5>1e-10)

             W_non_sol_mem_f=W_non_sol_mem;
             C_sol_mem=C_sol-((NTU_m*W0*(W_non_air-
W_non_sol_mem))./(NTU_m_sol));  %solve membrane mass equation
             T_non_sol_mem=(NTU*T_non_air+NTU_m*h*(W_non_air-
W_non_sol_mem)+NTU_sol*T_non_sol)./(NTU_sol+NTU);
             T_sol_mem=T_non_sol_mem*(T_sol_in-T_air_in)+T_air_in;

             %obtain the new membrane humidity ratio
            W_sol_mem=calculate_W_sol(T_sol_mem, C_sol_mem,
C_e_sol_in);
             W_non_sol_mem=(W_sol_mem-W_air_in)/W0;

             error5=sum(sum(abs(W_non_sol_mem-
W_non_sol_mem_f)./(W_non_sol_mem)));

         end
end

T_air_out=mean(T_air(:,m));
W_air_out=mean(W_air(:,m));
T_sol_out=mean(T_sol(n,:));
X_sol_out=mean(X_sol(n,:));
C_sol_out=(1-C_e_sol_in)./(1+X_sol_out);


effec_sen_air=(T_air_in-T_air_out)/(T_air_in-
T_sol_in);      %calculate the air side sensible effectiveness
effec_lat_air=(W_air_in-W_air_out)/(W_air_in-
W_sol_in);      %calcualte the air side latent effectiveness
effec_tot_air=(effec_sen_air+h*effec_lat_air)/(1+h);         %calculat
e the air side total effectiveness

effec_sen_sol=(m_sol*cp_sol*(T_sol_out-T_sol_in)-
m_salt*h_fg*(X_sol_out-X_sol_in))/(m_air*cp_air*(T_air_in-
T_sol_in));  %calculate the solution side sensible effectiveness
```

```
effec_lat_sol=(m_salt*h_fg*(X_sol_out-
X_sol_in))/(m_air*h_fg*(W_air_in-
W_sol_in));                                    %calculate the
solution side latent effectiveness
effec_tot_sol=(m_sol*cp_sol*(T_sol_out-
T_sol_in))/(m_air*cp_air*(T_air_in-T_sol_in)+m_air*h_fg*(W_air_in-
W_sol_in));    %calculate the solution side total effectiveness


MAR=1000*m_air*(W_air_out-W_air_in);
```

Appendix E: Matlab code for the complete self-cooled membrane-based liquid desiccant dehumidification system

```
clear

% inlet conditions in dehumidifier and regenerator
T_air_in_de(1)=30; %air inlet temperature in dehumidifier (C)
RH_air_in_de(1)=80;
W_air_in_de(1)=humidityratio_air(T_air_in_de(1),RH_air_in_de(1)); %air
inlet specific humidity in dehumidifier (kg/kg)
T_air_in_re(1)=24; %air inlet temperature in regenerator (C)
RH_air_in_re(1)=40;
W_air_in_re(1)=humidityratio_air(T_air_in_re(1),RH_air_in_re(1)); %air
inlet specific humidity in regenerator (kg/kg)
T_sol_in_de(1)=20; %solution inlet temperature in dehumidifier (C)
C_sol_in_de(1)=0.37; %solution inlet mass concentration in
dehumidifier
C_e_sol_in_de(1)=0.1;
T_sol_in_re(1)=45; %solution inlet temperature in regenerator (C)
C_sol_in_re(1)=0.37; %solution inlet mass concentration in regenerator
(%)
C_e_sol_in_re(1)=C_e_sol_in_de(1);
T_ca_in(1)=12; % Circulated air inlet temperature (C)
W_e_ca_in(1)=0;
m_ca=0.025;

%basic inlet conditions
m_sol_de=0.012; %assign solution mass flow rate in dehumidifier (kg/s)
m_sol_re=m_sol_de; %assign solution mass flow rate in regenerator
(kg/s)
m_air_de=0.01;
m_air_re=0.01;

%basic inlet conditions
rou_air=1.29; %air density (kg/m3)
rou_LiCl=1247; %solution density (kg/m3)
rou_e=789; % Ethanol density (kg/m3)
rou_sol=(1-C_e_sol_in_de(1))*rou_LiCl+C_e_sol_in_de(1)*rou_e;

cp_air=1.02; %air specific heat capacity (kJ/kgK)
cp_LiCl=3.2; %solution specific heat capacity (kJ/kgK)
cp_el=2.46; % Ethanol heat capacity in liquid (kJ/kgK)
cp_sol=(1-C_e_sol_in_de(1))*cp_LiCl+C_e_sol_in_de(1)*cp_el;
cp_water=4.187; %water specific heat capacity (KJ/kgK)
h_fg=2450; %condensation heat of water (J/kg)
h_fge=846; % Ethanol condensation latent heat (kJ/kg)
A=1.8081; %total heat and mass transfer area (m2)

%heat and mass transfer coefficient
L_air=0.0149; %air channel hydrolic diameter (m)
```

```
L_sol=0.0084; %solution channel hydrolic diameter (m)
Nu_air=6.58; %air side Nusselt number
k_air=0.03; %air side heat conductivity (W/mK)
h_air=(Nu_air*k_air)/L_air; %air side convective heat transfer
coefficient (W/m2K)
Nu_sol=7.74; %solution side Nusselt number
k_sol=0.53; %solution side heat conductivity (W/mK)
h_sol=(Nu_sol*k_sol)/L_sol; %solution side convective heat transfer
coefficient (W/m2K)
Sh_air=7.74; %air side Sherwood number
D_air=2.46e-5; %air side diffusivity
h_m_air=((Sh_air*D_air)/L_air)*rou_air; %air side convective mass
transfer coefficient (kg/m2K)
Sh_sol=7.74; %solution side Sherwood number
D_sol=0.892e-2; %solution side diffusivity
h_m_sol=((Sh_sol*D_sol)/L_sol)*rou_sol; %solution side convective mass
transfer coefficnet (kg/m2K)

h_cir_air=(Nu_air*k_air)/D_sol; % Circulated air side heat transfer
coefficient (W/m2K)

D_e=1.264e-5;
D_ms=0.892e-2; % Solution side diffusivity (m2/s)
D_me=9.29e-6; % Solution side ethanol diffusivity (m2/s)

Sh_e=2.517;

h_m_e=((Sh_sol*D_me)/D_sol)*rou_e; % Solution side ethanol mass
transfer coefficient (kg/m2K)
h_m_ca=((Sh_e*D_e/D_sol))*rou_air; % Circulated air side mass transfer
coefficient (kg/m2K)

%membrane properties
delta_mem=0.0005; %membrane thickness (m)
k_mem=0.3; %membrane heat conductivity (W/mK)
k_m_mem=3.87e-6; %membrane mass conductivity (kg/mK)

%NTU and NTUm; m_air and m_sol;m* and Cr*
U=(1/h_air+delta_mem/k_mem+1/h_sol)^-1; %overall heat transfer
coefficient (W/m2K)
U_m=(delta_mem/k_m_mem+1/h_m_air)^-1; %overall mass transfer
coefficient (kg/m2s)

NTU_de=(U*A)/(m_air_de*cp_air*1000);
NTU_re=(U*A)/(m_air_re*cp_air*1000);
NTU_m_de=((U_m*A)/m_air_de)*(1+2*C_e_sol_in_de(1)/0.9532); %NTUm in
dehumidifier
NTU_m_re=(U_m*A)/m_air_re; %NTUm in regenerator
NTU_sol_de=(h_sol*A)/(m_air_de*cp_air*1000); %solution side NTU in
dehumidifier
NTU_sol_re=(h_sol*A)/(m_air_re*cp_air*1000); %solution side NTU in
regenerator
NTU_m_sol_de=(h_m_sol*A)/m_air_de; %solution side NTUm in dehumidifier
NTU_m_sol_re=(h_m_sol*A)/m_air_re; %solution side NTUm in regenerator
m_mass_flow_ratio_de=m_sol_de/m_air_de;
m_mass_flow_ratio_re=m_sol_re/m_air_re;
m_star_de=1/m_mass_flow_ratio_de;
m_star_re=1/m_mass_flow_ratio_re;
```

```
M_ca=m_ca./m_sol_de;
Cr_de=m_star_de*(cp_air/cp_sol); %thermal capacity ratio in
dehumidifier
Cr_re=m_star_re*(cp_air/cp_sol); %thermal capacity ratio in
regenerator
Y_eg=(m_ca*cp_air)/(m_sol_de*cp_sol); % Thermal capaicty ration
between circulated air and ethanol(gas)

U_me=(1/h_m_ca)^-1; % Overall mass transfer coefficient betweeen
solution ethanol side and circulated air side(kg/m2s)
NTU_m_e=(U_me*A)/m_ca;
U_ca=(1/h_sol+1/h_cir_air)^-1; % Overall heat transfer coefficient
betweeen solution ethanol side and circulated air side(W/m2K)
NTU_ca=NTU_m_e;

n=30; %number of grids in y direction
m=60; %number of grids in x direction
dx=1/(m-1); %grid length in x direction
dy=1/(n-1); %grid length in y direction
z=ones(n,m); %define the matrix

%three heat exchangers,boiler and coolin water simulation
effect_1=0.7; %effectiveness of heat exchanger 1(solution exchanger)
effect_2=0.7; %effectiveness of heat exchanger 2(cooling water)
effect_3=0.7; %effectiveness of heat exchanger 3(hot water)
T_coldwater_in=12; %cold water inlet temperature (C)
m_coldwater=0.08333; %cold water mass flow rate (kg/s)
T_hotwater_in=50; %hot water inlet temperature (C)
m_hotwater=0.05; %hot water mass flow rate (kg/s)

%start the loop
%matrixing and assign initial values

error_C_de=10;error_C_re=10;error_T_de=10;error_T_re=10;

i=1;

while
(error_C_de>0.05)||(error_C_re>0.05)||(error_T_de>0.05)||(error_T_re>0
.05)

error1=10;error2=10;error3=10;error4=10;error5=10;error6=10;error7=10;
error8=10;error9=10;error10=10;error11=10;error12=10;error13=10;error1
4=10;

W_air_in_de(i)=W_air_in_de(1); %air inlet humidity ratio in
dehumidifier (kg/kg)
W_air_in_re(i)=W_air_in_re(1); %air inlet humidity ratio in
regenerator (kg/kg)
W_e_ca_in(i)=W_e_ca_in(1);
T_ca_in(i)=T_ca_in(1);
C_e_sol_in_de(i)=C_e_sol_in_de(1);
C_e_sol_in_re(i)=C_e_sol_in_re(1);
X_sol_in_de(i)=(1-C_sol_in_de(i)-
C_e_sol_in_de(i))/C_sol_in_de(i); %solution inlet mass ratio between
water and salt in dehumidifier (%)

X_e_sol_in_de(i)=C_e_sol_in_de(i)/C_sol_in_de(i);
```

```
X_sol_in_re(i)=(1-C_sol_in_re(i)-
C_e_sol_in_re(i))/C_sol_in_re(i); %solution inlet mass ratio between
water and salt in dehumidifier (%)

W_sol_in_de(i)=calculate_W_sol(T_sol_in_de(i),C_sol_in_de(i),C_e_sol_i
n_de(i)); %solution inlet humidity ratio in dehumidifier (kg/kg)
W_sol_in_re(i)=calculate_W_sol(T_sol_in_re(i),C_sol_in_re(i),C_e_sol_i
n_re(i)); %solution inlet humidity ratio in dehumidifier (kg/kg)
W_e_sol_in(i)=calculate_W_e_sol(T_sol_in_de(i), C_sol_in_de(i),
C_e_sol_in_de(i)); % Solution inlet ethanol (kg/kg)



T_air_de=T_air_in_de(i)*z; %assign initial values for air inlet
temperature in dehumidifier
T_air_re=T_air_in_re(i)*z; %assign initial values for air inlet
temperature in regenerator
T_sol_de=T_sol_in_de(i)*z; %assign initial values for solution inlet
temperature in dehumidifier
T_sol_re=T_sol_in_re(i)*z; %assign initial values for solution inlet
temperature in regenerator
W_air_de=W_air_in_de(i)*z; %assign initial values for air inlet
humidity ratio in dehumidifier
W_air_re=W_air_in_re(i)*z; %assign initial values for air inlet
humidity ratio in regenerator
X_sol_de=X_sol_in_de(i)*z; %assign initial values for solution inlet
mass ratio in dehumidifier
X_sol_re=X_sol_in_re(i)*z; %assign initial values for solution inlet
mass ratio in dehumidifier
W_sol_mem_de=W_sol_in_de(i)*z; %assign initial values for solution
membrane humidity ratio in dehumidifier
W_sol_mem_re=W_sol_in_re(i)*z; %assign initial values for solution
membrane humidity ratio in regenerator
C_e_sol_de=C_e_sol_in_de(i)*z;
C_e_sol_re=C_e_sol_in_re(i)*z;
X_e_sol_de=X_e_sol_in_de(i)*z;

W_e_sol=W_e_sol_in(i)*z;
W_e_ca=W_e_ca_in(i)*z;
T_ca=T_ca_in(i)*z;


%normalization
W0_de=W_sol_in_de(i)-W_air_in_de(i); %define the dimentionless
parameter W0 in dehumidifier
W0_re=W_sol_in_re(i)-W_air_in_re(i); %define the dimentionless
parameter W0 in regenerator
T_non_air_de=(T_air_de-T_air_in_de(i))/(T_sol_in_de(i)-
T_air_in_de(i)); %normalization of air temperature in dehumidifier
T_non_air_re=(T_air_re-T_air_in_re(i))/(T_sol_in_re(i)-
T_air_in_re(i)); %normalization of air temperature in regenerator
T_non_sol_de=(T_sol_de-T_air_in_de(i))/(T_sol_in_de(i)-
T_air_in_de(i)); %normalization of solution temperature in
dehumidifier
T_non_sol_re=(T_sol_re-T_air_in_re(i))/(T_sol_in_re(i)-
T_air_in_re(i)); %normalization of solution temperature in regenerator
W_non_air_de=(W_air_de-W_air_in_de(i))/W0_de; %normal ization of air
humidity ratio in dehumidifier
```

```
W_non_air_re=(W_air_re-W_air_in_re(i))/W0_re; %normal ization of air
humidity ratio in regenerator
W_non_sol_mem_de=(W_sol_mem_de-W_air_in_de(i))/W0_de; %normalization
of solution membrane humidity ratio in dehumidifier
W_non_sol_mem_re=(W_sol_mem_re-W_air_in_re(i))/W0_re; %normalization
of solution membrane humidity ratio in regenerator
h_de=((W_sol_in_de(i)-W_air_in_de(i))/(T_sol_in_de(i)-
T_air_in_de(i)))*(h_fg/cp_air); %normalization of h* in dehumidifier
h_re=((W_sol_in_re(i)-W_air_in_re(i))/(T_sol_in_re(i)-
T_air_in_re(i)))*(h_fg/cp_air); %normalization of h* in regenerator
H_pe=(W_sol_in_de(i)-W_air_in_de(i))/(T_sol_in_de(i)-
T_air_in_de(i))*(h_fge/cp_air);


W_non_e_ca=(W_e_ca-W_air_in_de(i))/W0_de;
W_non_e_sol=(W_e_sol-W_air_in_de(i))/W0_de;
T_non_ca=(T_ca-T_air_in_de(i))/(T_sol_in_re(i)-T_air_in_de(i));

%solve heat and mass transfer in dehumidifier
while (error1>1e-10)||(error2>1e-10)||(error3>1e-10)||(error4>1e-
10)||(error11>1e-10)||(error12>1e-10)||(error13>1e-10)
%the solution side mass equation in dehumidifier
X_sol_f_de=X_sol_de;
for a=1:n-1
for b=1:m
X_sol_de(1,b)=X_sol_in_de(i); %boundary condition
X_sol_de(a+1,b)=(X_sol_de(a,b)+dy*m_star_de*W0_de*NTU_m_de*((W_non_air
_de(a+1,b))-W_non_sol_mem_de(a+1,b)))./(1-
dy*m_star_de*W0_de*NTU_m_de*(W_non_air_de(a+1,b)-
W_non_sol_mem_de(a+1,b)));
end
end
error1=sum(sum(abs(X_sol_de-X_sol_f_de)./(X_sol_de)));
C_sol_de=1./(1+X_sol_de+X_e_sol_de);

%the solution side energy equation in dehumidifier
T_sol_f_de=T_sol_de;
for c=1:n-1
for d=1:m
T_non_sol_de(1,d)=1; %boudary condition
T_non_sol_de(c+1,d)=(T_non_sol_de(c,d)+(dy*NTU_de*Cr_de*(T_non_air_de(
c+1,d)))+(dy*NTU_m_de*Cr_de*h_de*(W_non_air_de(c+1,d)-
W_non_sol_mem_de(c+1,d)))-(dy*NTU_m_e*Y_eg*H_pe*(W_non_e_sol(c+1,d)-
W_non_e_ca(c+1,d)))+dy*NTU_ca*Y_eg*T_non_ca(c+1,d))./(1+dy*NTU_de*Cr_d
e+dy*NTU_ca*Y_eg);
end
end
T_sol_de=T_non_sol_de*(T_sol_in_de(i)-T_air_in_de(i))+T_air_in_de(i);
error2=sum(sum(abs(T_sol_de-T_sol_f_de)./(T_sol_de)));

%the air side mass equation in dehumidifier
W_air_f_de=W_air_de;
for e_=1:n
for f=1:m-1
W_non_air_de(e_,1)=0; %boundary condition
W_non_air_de(e_,f+1)=(W_non_air_de(e_,f)+dx*NTU_m_de*W_non_sol_mem_de(
e_,f+ 1))./(1+dx*NTU_m_de);
end
```

```
end
W_air_de=W_non_air_de*W0_de+W_air_in_de(i);
error3=sum(sum(abs(W_air_de-W_air_f_de)./(W_air_de)));

%the air side energy equation in dehumidifier
T_air_f_de=T_air_de;
for g=1:n
for h_=1:m-1
T_non_air_de(g,1)=0; %boundary condition
T_non_air_de(g,h_+1)=(T_non_air_de(g,h_)+dx*NTU_de*T_non_sol_de(g,h_+1
)).(1+dx*NTU_de);
end
end
T_air_de=T_non_air_de*(T_sol_in_de(i)-T_air_in_de(i))+T_air_in_de(i);
error4=sum(sum(abs(T_air_de-T_air_f_de)./(T_air_de)));

  % Solution side ethanol mass equation
  X_e_sol_f_de=X_e_sol_de;
  for j=1:n-1
    for k=1:m
       X_e_sol_de(1,k)=X_e_sol_in_de(i); % boundary condition

X_e_sol_de(j+1,k)=(X_e_sol_de(j,k)-
dy*M_ca*W0_de*NTU_m_e*(1+X_sol_de(j+1,k))*((W_non_e_sol(j+1,k))-
W_non_e_ca(j+1,k))).(1+dy*M_ca*W0_de*NTU_m_e*(W_non_e_sol(j+1,k)-
W_non_e_ca(j+1,k)));
    end
  end
  error11=sum(sum(abs(X_e_sol_de-X_e_sol_f_de)./(X_e_sol_de)));
  C_e_sol_de= X_e_sol_de./(1+X_sol_de+X_e_sol_de);

    % Circulated air ethanol mass equation
    W_e_ca_f=W_e_ca;
    for N=2:n
        for l=1:m
            W_non_e_ca(n,l)=(W_e_ca_in(i)-
W_air_in_de(i))/W0_de; %boundary condition

 W_non_e_ca(N-1,l)=(W_non_e_ca(N,l)+dy*NTU_m_e*(W_non_e_sol(N-
1,l))).(1+dy*NTU_m_e);
        end
    end
    W_e_ca=(W_non_e_ca*W0_de)+W_air_in_de(i);
    error12=sum(sum(abs(W_e_ca-W_e_ca_f)./(W_e_ca)));

 % Circulated air energy equation
    T_ca_f=T_ca;
    for o=2:n
        for p=1:m
            T_non_ca(n,p)=(T_ca_in(i)-T_air_in_de(i))/(T_sol_in_de(i)-
T_air_in_de(i)); %boundary condition

            T_non_ca(o-
1,p)=(T_non_ca(o,p)+dy*NTU_ca*(T_non_sol_de(o,p))).(1+dy*NTU_ca);
        end
    end
    T_ca=T_non_ca*(T_sol_in_de(i)-T_air_in_de(i))+T_air_in_de(i);
    error13=sum(sum(abs(T_ca-T_ca_f)./(T_ca)));
```

```
            error14=10;
    while(error14>1e-10)
        W_non_e_sol_f=W_non_e_sol;

        W_e_sol=calculate_W_e_sol(T_sol_de,C_sol_de,C_e_sol_de);
        W_non_e_sol=(W_e_sol-W_air_in_de(i))/W0_de;
        error14=sum(sum(abs(W_non_e_sol-
W_non_e_sol_f)./(W_non_e_sol)));
    end

error5=10;
while (error5>1e-10)
W_non_sol_mem_f_de=W_non_sol_mem_de;
C_sol_mem_de=C_sol_de-((NTU_m_de*W0_de*(W_non_air_de-
W_non_sol_mem_de))./(NTU_m_sol_de)); %solve membrane mass equation in
dehumidifier
T_non_sol_mem_de=(NTU_de*T_non_air_de+NTU_m_de*h_de*(W_non_air_de-
W_non_sol_mem_de)+NTU_sol_de*T_non_sol_de)./(NTU_sol_de+NTU_de);
T_sol_mem_de=T_non_sol_mem_de*(T_sol_in_de(i)-
T_air_in_de(i))+T_air_in_de(i);
%obtain the new membrane humidity ratio in dehumidifier
W_sol_mem_de=calculate_W_sol(T_sol_mem_de,C_sol_mem_de,C_e_sol_de);
W_non_sol_mem_de=(W_sol_mem_de-W_air_in_de(i))/W0_de;
error5=sum(sum(abs(W_non_sol_mem_de-
W_non_sol_mem_f_de)./(W_non_sol_mem_de)));
end
end
T_air_out_de(i)=mean(T_air_de(:,m)); %calculate the air outlet
temperature in dehumidifier
W_air_out_de(i)=mean(W_air_de(:,m)); %calculate the air outlet
humidity ratio in dehumidifier
T_sol_out_de(i)=mean(T_sol_de(n,:)); %calculate the solution outlet
temperature in dehumidifier
X_sol_out_de(i)=mean(X_sol_de(n,:)); %calculate the solution outlet
mass ratio in dehumidifier
X_e_sol_out_de(i)=mean(X_e_sol_de(n,:));
C_sol_out_de(i)=1/(1+X_e_sol_out_de(i)+X_sol_out_de(i)); %calculate
the solution outlet concentration in dehumidifier

while (error6>1e-10)||(error7>1e-10)||(error8>1e-10)||(error9>1e-10)
%the solution side mass equation in regenerator
X_sol_f_re=X_sol_re;
for a=1:n-1
for b=1:m
X_sol_re(1,b)=X_sol_in_re(i); %boundary condition
X_sol_re(a+1,b)=(X_sol_re(a,b)+dy*m_star_re*W0_re*NTU_m_re*((W_non_air
_re(a +1,b))-W_non_sol_mem_re(a+1,b)))./(1-
dy*m_star_re*W0_re*NTU_m_re*(W_non_air_re(a+1,b)-
W_non_sol_mem_re(a+1,b)));
end
end
error6=sum(sum(abs(X_sol_re-X_sol_f_re)./(X_sol_re)));
C_sol_re=(1-C_e_sol_re)./(1+X_sol_re);

%the solution side energy equation in regenerator
T_sol_f_re=T_sol_re;
for c=1:n-1
```

```
for d=1:m
T_non_sol_re(1,d)=1; %boudary condition
T_non_sol_re(c+1,d)=(T_non_sol_re(c,d)+dy*NTU_m_re*h_re*Cr_re*(W_non_a
ir_re (c+1,d)-
W_non_sol_mem_re(c+1,d))+dy*Cr_re*NTU_re*T_non_air_re(c+1,d))/(1+dy*NT
U_re*Cr_re);
end
end
T_sol_re=T_non_sol_re*(T_sol_in_re(i)-T_air_in_re(i))+T_air_in_re(i);
error7=sum(sum(abs(T_sol_re-T_sol_f_re)./(T_sol_re)));

%the air side mass equation in regenerator
W_air_f_re=W_air_re;
for e_=1:n
for f=1:m-1
W_non_air_re(e_,1)=0; %boundary condition
W_non_air_re(e_,f+1)=(W_non_air_re(e_,f)+dx*NTU_m_re*W_non_sol_mem_re(
e_,f+ 1))./(1+dx*NTU_m_re);
end
end
W_air_re=W_non_air_re*W0_re+W_air_in_re(i);
error8=sum(sum(abs(W_air_re-W_air_f_re)./(W_air_re)));

%the air side energy equation in regenerator
T_air_f_re=T_air_re;
for g=1:n
for h_=1:m-1
T_non_air_re(g,1)=0; %boundary condition
T_non_air_re(g,h_+1)=(T_non_air_re(g,h_)+dx*NTU_re*T_non_sol_re(g,h_+1
))./( 1+dx*NTU_re);
end
end
T_air_re=T_non_air_re*(T_sol_in_re(i)-T_air_in_re(i))+T_air_in_re(i);
error9=sum(sum(abs(T_air_re-T_air_f_re)./(T_air_re)));

error10=10;

while (error10>1e-10)
W_non_sol_mem_f_re=W_non_sol_mem_re;
C_sol_mem_re=C_sol_re-((NTU_m_re*W0_re*(W_non_air_re-
W_non_sol_mem_re))./(NTU_m_sol_re)); %solve membrane mass equation in
regenerator
T_non_sol_mem_re=(NTU_re*T_non_air_re+NTU_m_re*h_re*(W_non_air_re-
W_non_sol_mem_re)+NTU_sol_re*T_non_sol_re)./(NTU_sol_re+NTU_re);
T_sol_mem_re=T_non_sol_mem_re*(T_sol_in_re(i)-
T_air_in_re(i))+T_air_in_re(i);

%obtain the new membrane humidity ratio in dehumidifier
W_sol_mem_re=calculate_W_sol(T_sol_mem_re,C_sol_mem_re,C_e_sol_re);
W_non_sol_mem_re=(W_sol_mem_re-W_air_in_re(i))/W0_re;
error10=sum(sum(abs(W_non_sol_mem_re-
W_non_sol_mem_f_re)./(W_non_sol_mem_re)));
end
end

T_air_out_re(i)=mean(T_air_re(:,m)); %calculate the air outlet
temperature in regenerator
```

```
W_air_out_re(i)=mean(W_air_re(:,m)); %calculate the air humidiity
ratio in regenerator
T_sol_out_re(i)=mean(T_sol_re(n,:)); %calculate the solution outlet
temperature in regenerator
X_sol_out_re(i)=mean(X_sol_re(n,:)); %calculate the solution outlet
mass ratio in regenerator
C_sol_out_re(i)=(1-C_e_sol_in_re(i))./(1+X_sol_out_re(i)); %calculate
the solution outlet concentration in regenerator

T1(i)=T_sol_out_re(i)-
((effect_1*min(m_sol_de*cp_sol,m_sol_re*cp_sol)*(T_sol_out_re(i)-
T_sol_out_de(i)))/(m_sol_de*cp_sol));
T2(i)=((effect_1*min(m_sol_de*cp_sol,m_sol_re*cp_sol)*(T_sol_out_re(i)
-T_sol_out_de(i)))/(m_sol_re*cp_sol))+T_sol_out_de(i);
T_sol_in_de(i+1)=T1(i)-
((effect_2*min(m_sol_de*cp_sol,m_coldwater*cp_water)*(T1(i)-
T_coldwater_in))/(m_sol_de*cp_sol));
C_sol_in_de(i+1)=C_sol_out_re(i); %assign new solution inlet
concentration in dehumidifier
T_sol_in_re(i+1)=((effect_3*min(m_sol_re*cp_sol,m_hotwater*cp_water)*(
T_hotwater_in-T2(i)))/(m_sol_re*cp_sol))+T2(i);
C_sol_in_re(i+1)=C_sol_out_de(i);
T_air_in_de(i+1)=T_air_in_de(i); %assign new air inlet temperature in
dehumidifier
T_air_in_re(i+1)=T_air_in_re(i); %assign new air inlet temperature in
regenerator
W_air_in_de(i+1)=W_air_in_de(i); %calculate new air inlet humidity
ratio in dehumidifier (kg/kg)
W_air_in_re(i+1)=W_air_in_de(i); %calculate new air inlet humidity
ratio in regenerator (kg/kg)
C_e_sol_in_de(i+1)=C_e_sol_in_de(i);
C_e_sol_in_re(i+1)=C_e_sol_in_re(i);
X_sol_in_de(i+1)=(1-C_sol_in_de(i+1)-
C_e_sol_in_de(i+1))/(C_sol_in_de(i+1)); %calculate new solution inlet
mass ratio between water and salt in regenerator (%)
X_sol_in_re(i+1)=(1-C_sol_in_re(i+1)-
C_e_sol_in_re(i+1))/(C_sol_in_re(i+1)); %calculate new solution inlet
mass ratio between water and salt in dehumidifier (%)

W_sol_in_de(i+1)=calculate_W_sol(T_sol_in_de(i+1),C_sol_in_de(i+1),C_e
_sol_in_de(i)); %calculate new solution inlet humidity ratio in
dehumidifier (kg/kg)
W_sol_in_re(i+1)=calculate_W_sol(T_sol_in_re(i+1),C_sol_in_re(i+1),C_e
_sol_in_re(i)); %calculate new solution inlet humidity ratio in
dehumidifier (kg/kg)

error_T_de=abs(T_sol_in_de(i+1)-T_sol_in_de(i));
error_T_re=abs(T_sol_in_re(i+1)-T_sol_in_re(i));
error_C_de=abs(C_sol_in_de(i+1)-C_sol_in_de(i));
error_C_re=abs(C_sol_in_re(i+1)-C_sol_in_re(i));

i=i+1;

end

m_salt_re=m_sol_re./(1+X_sol_in_re(1));
```

```
Result_effect_sen=(T_air_in_de-T_air_out_de(i-1))/(T_air_in_de-
T_sol_in_de);
Result_effect_lat=(W_air_in_de-W_air_out_de(i-1))/(W_air_in_de-
W_sol_in_de);

MRR=m_air_de*(W_air_in_de(1)-W_air_out_de(i-1));
MAD=m_salt_re*(X_sol_in_re(1)-X_sol_out_re(i-1));
MFR_de=MRR/(U_m*A);
MFR_re=MAD/(U_m*A);

Result_Q_sen=m_air_de*cp_air*(T_air_in_de-T_air_out_de(i-1));
Result_Q_lat=m_air_de*h_fg*(W_air_in_de-W_air_out_de(i-1));
Q_reg=m_sol_de*cp_sol*(T_sol_in_re(i-1)-T2(i-1));
Result_COP=(Result_Q_sen+Result_Q_lat)/Q_reg;
```

Appendix F: Calculation of Re number

The Reynold number can be determined by:

$$Re = \frac{ud_h}{v}$$

For the process air, the mass flow rate ratio is within 0.01 kg/s to 0.025 kg/s, the Reynold number varies from 437 to 1092, which is less than 2300.

For the desiccant solution, the mass flow rate ratio is within 0.01 kg/s to 0.05 kg/s, Reynold number varies from 19.4 to 96.9, which is also less than 2300.